The Pennsylvania State University

The Graduate School

Department of Chemical Engineering

PROTEIN SEPARATION USING AFFINITY ULTRAFILTRATION WITH SMALL CHARGED LIGANDS

A Thesis in

Chemical Engineering

by

Suma Rao

Submitted in Partial Fulfillment
of the Requirements
for the Degree of

Doctor of Philosophy

May 2007

The thesis of Suma Rao was reviewed and approved* by the following:

Andrew L. Zydney
Professor of Chemical Engineering
Head of the Department of Chemical Engineering
Thesis Advisor
Chair of Committee

Arnold A. Fontaine
Senior Scientist Applied Research Laboratory
Professor of Bioengineering

Themis Matsoukas
Associate Professor of Chemical Engineering

Darrell Velegol
Associate Professor of Chemical Engineering

*Signatures are on file in the Graduate School

ABSTRACT

There is a critical need to develop new technologies that provide high resolution protein purification at a price, scale, and throughput needed for the production of high value protein products. Affinity chromatography can provide very high selectivity, but throughput is often reduced by mass transfer limitations. Affinity ultrafiltration is a potentially attractive alternative, but the high cost and practical limitations of the large macroligands used in previous studies has limited the viability of this technique. The overall objective of this work was to demonstrate the feasibility of affinity ultrafiltration using small charged affinity ligands, with the change in protein charge exploited for high resolution separation using an electrically charged membrane.

Experiments were performed using a model system of bovine serum albumin and ovalbumin with the dye Cibacron Blue chosen as the charged affinity ligand. The equilibrium binding characteristics between the two proteins and Cibacron Blue were evaluated using a simple ultrafiltration technique over a wide range of solution conditions. Protein filtration experiments were performed to evaluate the affects of Cibacron Blue on protein transmission using essentially neutral and negatively-charged versions of a composite regenerated cellulose membrane. The addition of only 1 g/L of Cibacron Blue to an 8 g/L BSA solution reduced the BSA sieving coefficient through the negatively-charged membrane by more than two orders of magnitude, with this effect being largely eliminated at high salt and with the neutral membrane. Protein sieving data were in good agreement with model calculations based on the partitioning of a charged sphere in a charged pore accounting for the change in net protein charge due to ligand

binding and the increase in solution ionic strength due to the free ligand in solution. These results clearly demonstrate that the addition of small charged ligands can be used to control protein transmission during ultrafiltration.

The high affinity of BSA for Cibacron Blue was exploited to enhance the selectivity for the separation of BSA from ovalbumin. The membrane selectivity was a complex function of the solution conditions, Cibacron Blue concentration, and membrane charge. The addition of Cibacron Blue caused a 30-fold increase in selectivity due to the strong electrostatic repulsion of the highly charged BSA-Cibacron Blue complex. Protein separations were accomplished using a diafiltration process, giving a BSA product with a purification factor of more than 90-fold and a yield greater than 90%. An ovalbumin product was generated in the filtrate with a purification factor of over 10 and a yield of nearly 100%. Subsequent experiments used a tangential flow filtration device that was linearly scalable to commercial manufacturing operations, demonstrating that this process should be feasible even at large scale. The results clearly demonstrate the ability to use small charged affinity ligands with bio-specific binding characteristics to achieve high selectivity protein separations by high performance tangential flow filtration.

TABLE OF CONTENTS

LIST OF FIGURES

LIST OF TABLES

ACKNOWLEDGEMENTS

I would like to thank Dr Zydney for giving me the opportunity to work with him and for all his insight and guidance during the course of my Ph.D. at Penn State. I would also like to thank him for giving me the opportunity to intern at Amgen.

I would also like to take this opportunity to thank the entire Zydney group for all their help and friendship over the years. I would especially like to thank David Bohonak for taking the time during the first few years of graduate school to help me conduct experiments and also for giving me insights into life here in the United States. I would also like to thank Kimberly Ager and Benjamin Smith for being such great undergraduate researchers to work with and for many fun times both in lab and otherwise.

None of this would have been possible without the constant support and encouragement of my parents. I thank them both for everything they have done for me. I also would like to thank Amma for always making the time to listen to whatever it was that I had to say. My sister Anuradha and Paul have always been there for me and I am indebted to them for all they have done for me over the years. I would like to thank Anuradha for having been such a constant source of inspiration. I would also like to thank Siddhartha and Ashwini for being the best friends I could ever hope to have in life. I am really blessed to have you all in my life.

Chapter 1

INTRODUCTION

1.1 Biotechnology

Recent developments in molecular biology, and in particular the area of genetic engineering, has lead to the rapid growth of the biotechnology industry over the past 2 decades. Biotechnology refers to any technological application that uses biological systems, in particular metabolic processes of plant, animal, or microbial cells, to make or modify products or to convert undesirable material to less toxic or dangerous forms.

Biotechnology is used widely in both the food and pharmaceutical industries; the discussion in this Chapter will focus on the use of biotechnology for the production of recombinant protein products. A large number of different product classes have been developed including interferons, interleukins, thrombolytic or anticoagulating blood factors, growth factors, enzymes, and monoclonal antibodies. These proteins have been shown to have therapeutic benefits for a wide range of diseases such as AIDS, different types of cancer, infectious diseases, diabetes, etc. Table 1.1 gives a list of the potential applications of some of the currently available recombinant protein products.

Table **1.1**: Representative biotechnology products and their therapeutic indications. Adapted from Walsh and Headon (1994)

Product	Disease Treated
Recombinant insulin	Diabetes
Urokinase	Blood clots
Erythropoietins	Anaemia
Human growth hormone	Cancer, AIDS and growth deficiency in children
Monoclonal antibodies	Cancer and rheumatoid arthritis
Epidermal growth factor	Burns
Orthoclone	Kidney transplant
Tissue plasminogen activator	Heart attacks and strokes
Protein C	Hip surgery, protein C deficiency
Interferons (α, β and γ)	Cancer, allergies, asthma, AIDS, arthritis and infectious diseases
Platelet-derived growth factor	Ulcers
Tumor necrosis factor	Cancer
Superoxide dismutase	Prevention of oxygen toxicity

There are currently more than 150 biopharmaceutical based therapeutics in the market, with 32 of these being approved in the past three and a half years alone. Figure 1.1 (adapted from Walsh, 2006) gives the number of biologicals in discovery phase with the corresponding target disease. It is estimated that 2,500 biotechnology based drugs are currently in the discovery phase with over 1600 of these in clinical trials and another 900 in preclinical phase. These figures translate to a market size of an estimated $ 33 billion in 2004 with a projected increase to approximately $ 70 billion by 2010. The projected sales of monoclonal antibodies alone are expected to rise to more than $ 16 billion by 2008. Figure 1.2 (adapted from Lawrence, 2005) gives an estimate of the sales in billions of dollars per year with the solid line being the estimated research and development spending for the same time period.

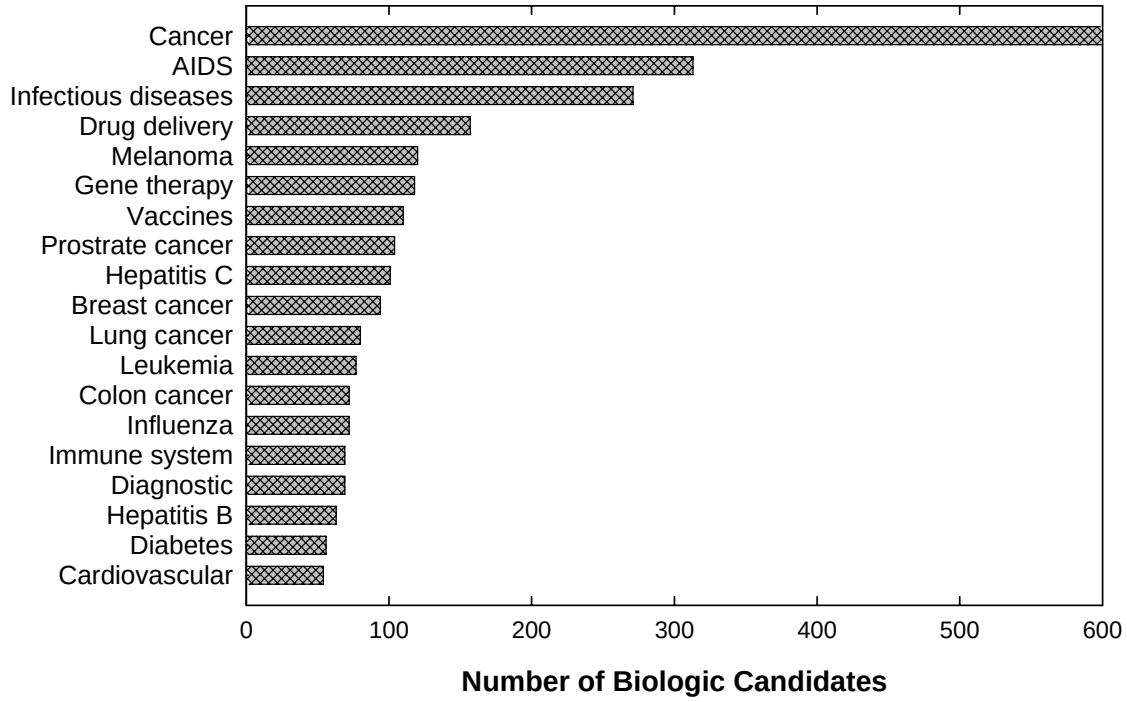

Figure **1.1**: Biopharmaceuticals in the pipeline (adapted from Walsh, 2006)

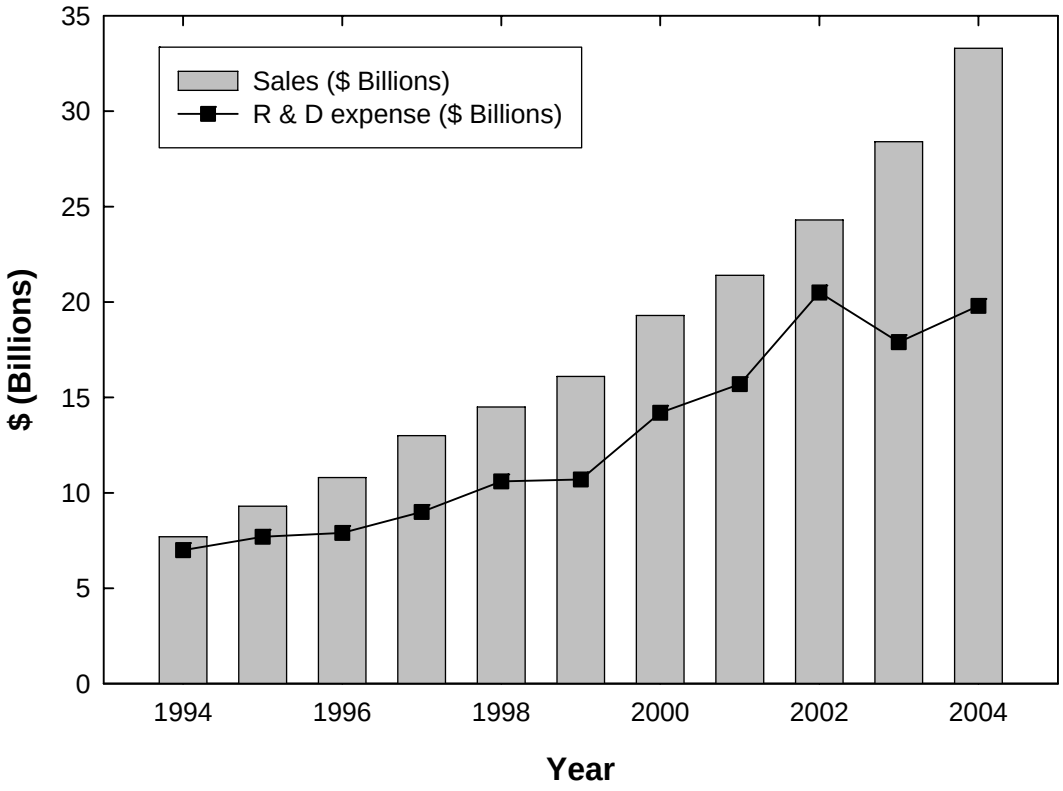

Figure **1.2**: Biotech sales revenue and research and development expenditure (Adapted from Lawrence (2005)

The large majority of these proteins are produced in either *Escherichia coli* or mammalian cell lines. Of the 31 drugs approved since 2003, 17 are produced in mammalian cell lines, mostly using Chinese Hamster Ovary (CHO) cells, and 9 were produced in *E. coli*. There is also the possibility of producing recombinant proteins in yeast, insect, and plant cells. Yeast cells are primarily used in the production of enzymes, with titers of up to 15 g/L (Werten et al., 1999). Meripase, which is produced by

Meristem Therapeutics in France, is a recombinant gastric lipase produced in transgenic corn and used to counter lipid malabsorption caused by cystic fibrosis and chronic pancreatitis. Zhu et al. (2005) were able to produce functional human monoclonal antibodies at levels of 3 mg in chicken eggs. Ivarie (2006) hypothesized that a single hen could produce up to 300 g of recombinant material annually.

Continual advances in cell culture technology have caused dramatic increases in the titer of recombinant proteins, with values close to 5 g / L or higher regularly obtained in current cell cultures. This is almost an order of magnitude larger than product titers just a decade ago (Butler, 2005). Regardless of the method of manufacture, the protein product is initially obtained as part of a complex mixture with a wide range of undesired proteinacious material, cell debris, and DNA. Since most therapeutic proteins are given by injection, the final protein product needs to be provided in an extremely pure form. The FDA (Food and Drug Administration) currently recommends that the final concentration of host cell proteins be reduced to less than 10 ppm that there is less than 1 virus per million doses, and there is less than 10 ng of DNA per dose of drug.

These requirements are currently met using a series of downstream purification steps each targeted at different classes of impurities. For example, monoclonal antibodies using purified using centrifugation (or microfiltration) for harvest, protein A affinity chromatography as an initial capture step, followed by one or more additional chromatographic steps, normally ion-exchange and / or hydrophobic interaction chromatography. pH inactivation and virus filtration are commonly used for virus deactivation and removal, respectively. Blanch and Clark (1997) estimated that downstream purification can amount to as much as 80 - 90 % of the total cost of

manufacture. Ladisch (2001) reported the purification costs to be approximately 50 - 60 % of the total. Irrespective of the details of these numbers, there is clearly a need to develop new technologies that can provide the necessary purification at the desired scale, purity, throughput, and overall economics needed for the production of high value therapeutic protein products.

1.2 Affinity Chromatography

Affinity chromatography is one of the most important and powerful techniques available for the purification of high value proteins (Dordick, 1991; Clonis and Labrou, 1994). A wide range of affinity ligands are available for use in affinity separations. Bio-affinity ligands are of biological origin and have specific affinity to the product of interest (Hage, 1999). Typical ligands include enzymes, antibodies, lectins, carbohydrates, and the avidin/biotin system. Immunoaffinity columns with either immobilized Protein A, or in some cases Protein G, are widely used for the purification of a variety of monoclonal antibodies for both therapeutic and diagnostic applications (Haber, 1992; Hage, 1998). Immobilized metal-ion affinity chromatography (IMAC) uses divalent metal ions to form co-ordination complexes with histidine surface groups on proteins. Recombinant proteins with histidine tags are readily purified using IMAC (Porath, 1988; 1992), although this approach is rarely used for therapeutics since the histidine tag would need to be cleaved as part of the downstream process. Synthetic compounds such as dyes and other biomimetic molecules are also used as affinity ligands. Immobilized Cibacron Blue

F3GA has been used to recover and purify a number of plasma proteins, kinases, dehydogensases, and interferons (Clonis, 1990).

Despite the enormous potential of affinity chromatography, there are a number of challenges associated with the use of this technology, particularly for large scale commercial applications. In particular, chromatographic separations often suffer from significant mass transfer limitations. In order to achieve the high capacities needed for large-scale commercial processes, affinity ligands are typically immobilized within highly porous beads. Thus, the protein of interest needs to diffuse into the narrow pores within the support matrix, and this step can often be a limiting factor in the design of these processes. A large amount of research has focused on overcoming these internal mass transfer limitations, and this work has led to the development of chromatographic resins that contain both macropores and micropores (Afeyan et. al., 1990), affinity membranes that exploit convective flow (Klein, 1991; Knudsen, 2001; Ghosh, 2002), and macroporous monoliths with highly ordered pore structures (del Valle., 2003; Podgornik, 2003; Leinweber, 2003; Branovic, 2003). However, these novel support structures remain expensive and can often be difficult to implement at large scale.

In addition to mass transfer limitations, ligand immobilization on solid supports often reduces the accessibility of the binding site. For example, Jankowski et al. (1976) found minimal binding of leukocyte interferon to Cibacron Blue F3GA when the ligand was immobilized directly to an agarose matrix, in contrast to the relatively strong binding observed with free Cibacron Blue. Naumann et al. (1989) showed that the addition of a spacer arm could increase the binding of lactate dehydogenase to several immobilized dye ligands. The accessibility of binding sites on large protein ligands also depends on

the orientation of the immobilized ligand. Butterfield et al. (2001) demonstrated that a higher binding activity can often be achieved by site-directed immobilization, although this required site-directed mutagenesis of the protein ligand prior to immobilization.

Chromatographic processes can only achieve high degrees of purification if there is minimal non-specific binding of impurities to the resin. Agarose resins are very attractive in many applications since this highly hydrophilic material shows relatively little non-specific protein adsorption. However agarose is compressible, limiting the allowable operating pressure, and thus flow rate, in the chromatographic columns. Other researchers have looked at a variety of techniques for chemically modifying the base resin to reduce non-specific binding. For example, Mislovicova et al. (1995) were able to significantly reduce non-specific binding to a polyhydroxyethyl methacrylate support by filling the macropores with a dextran gel. High-performance incompressible particles made of silica can potentially be used for affinity separations by chemically masking the silanol groups (Clonis, 1990). However the performance and cost effectiveness of these materials is often inadequate for large-scale commercial applications.

In addition to the above concerns, large proteinaceous ligands often loose binding activity over time due to conformational changes and these ligands are also susceptible to leaching. For example, ligands immobilized using cyanogen bromide are susceptible to leaching at high pH because the iso-urea bond can be cleaved by hydrolysis (Mohan and Lyddiatt, 1997). Fuglistaller (1989) demonstrated that there was small but detectable leaching of Protein A from eight different commercially available chromatography columns. This leached Protein A is eluted with the protein product and must be removed as part of the subsequent downstream process.

1.3 Affinity Ultrafiltration

Affinity ultrafiltration is one method to potentially eliminate many of the disadvantages of affinity chromatography while still maintaining the selectivity of the affinity process. In contrast to affinity chromatography, the product and the ligand in affinity ultrafiltration are allowed to interact in free solution, which eliminates any concerns about mass transfer limitations or ligand inaccessibility. The process involves four steps: (1) the ligand and the protein are allowed to equilibrate in free solution, (2) the bound product is separated from the other impurities by filtration through a membrane that retains the protein-ligand complex, (3) the product is separated from the ligand, typically by the addition of salt, change in pH, or by the use of an appropriate displacer, and (4) the free ligand is separated and recovered from the unbound product.

The first initial work on affinity ultrafiltration was done by Mattiason and Ramstorp (1983) and Adamiski-Medda et al. (1981). Mattainson and Ramstrop (1983) purified concanavalin from crude jack bean extract using residues on the membrane of heat killed *Saccharomyces cerevisae* as a natural macroligand. Adamiski-Medda et al. (1981) used p-aminobenzamidine linked to dextran as a synthetic ligand to partially separate trypsin from chymotrypsin. Subsequent studies examined the separation of trypsin from chymotrypsin using a high molecular weight polymer bearing m-aminobenzamide (Luong et al., 1987), the isolation of urokinase using N-acryloyl-m-aminobenzamide copolymerized with acrylamide (Male et al., 1980), the isolation of human serum albumin from lysozyme using Cibacron Blue bound to agarose (Herrak and Merrill, 1989), and the recovery of bovine serum albumin using highly substituted blue

sepharose (He et al., 1998). Affinity ultrafiltration has also been used to separate chiral molecules using a stereoselective macroligand, e.g. the optical resolution of tryptophan using bovine serum albumin (Poncet et al., 1997; Higuchi et al., 1994; Romero and Zydney, 2001) and the chiral purification of ibuprofen using human serum albumin (Itoh, 1997). Table 1.2 summarizes the characteristics of a number of various ultrafiltration systems that have been used for protein purification.

In all of these prior applications of affinity ultrafiltration, the separation was accomplished with the use of a very large ligand relative to the size of the product to facilitate the retention of the product-ligand complex in the ultrafiltration step. However, these large ligands are typically quite expensive, which severely limits the overall economics of the process. In addition, systems employing small ligands bound to large carriers, for example Cibacron Blue bound to agarose, can suffer from many of the challenges faced with chromatographic resins including limited ligand accessibility and ligand leaching. The net result is that there are currently no large-scale commercial applications of affinity ultrafiltration for the purification of high value protein products.

It would be much more attractive to perform the affinity ultrafiltration using small soluble ligands since this would eliminate the mass transfer, steric accessibility, and leaching issues that often limit applications of affinity chromatography using packed columns. However, the product–ligand complex formed using a small ligand would be only slightly larger than the product itself, which would appear to eliminate the possibility of obtaining high product selectivity during the ultrafiltration step.

Table 1.2: Summary of affinity ultrafiltration systems for protein purification (adapted from Galaev et al., 2001)

Carrier	Size	Ligand	Target Protein
Soluble macroligands			
Poly(acrylamide)	MW > 100,000 Da	m-aminobenzamidine	Trypsin
Poly(acrylamide)	MW > 100,000 Da	m-aminobenzamidine	Urokinase
Dextran	MW 2,000,000 Da	Protein A	IgG
Dextran	MW 2,000,000 Da	p-amino-benzamidine	Trypsin
Insoluble macroligands			
Silica nanoparticles	12 nm	Cibacron Blue	Alcohol dehydrogenase
Liposomes	27 nm	Biotin	Avadin
Polystyrene core-shell latex particles	0.25-0.4 μm	Cibacron Blue	BSA
Saccharomyces cerevisiae cells	5 μm	Surface carbohydrate groups	Concanavalin A
Starch granules	1-10 μm	Cibacron Blue	Alcohol dehydrogenase
Sepharose beads	11-15 μm	Cibacron Blue	HSA
Sepharose beads	45-165 μm	Cibacron Blue	HSA
Sepharose beads	45-165 μm	Cibacron Blue	Lysozyme
Sepharose beads	45-165 μm	Concanavalin A	Horse radish peroxidase
Agarose beads	45-165 μm	Protein A	IgG
Sepharose beads	45-165 μm	Heparin	Lactoferrin

1.4 Membrane Separations

Traditionally, membrane systems have been thought to be purely sized based separation process requiring at least a factor of 10 difference in size between the product and impurity in order to achieve significant separation. Hence, the use of membrane systems in the biotechnology industry has been limited primarily to applications involving very large differences in size such as buffer exchange, protein concentration, initial clarification of cell culture media, and in sterile filtration.

Recent experimental evidence has conclusively shown that high resolution protein separations can be achieved by exploiting electrostatic interactions in addition to size differences in membrane systems. For example, Pujar and Zydney (1994) showed that the transmission of BSA through a 100 kD membrane could be decreased by two orders of magnitude just by lowering the solution ionic strength from 150 mM to 1.5 mM. This dramatic increase in protein retention was due to the increase in electrostatic shielding at high salt concentrations. Burns and Zydney (1999) demonstrated that the sieving coefficient of several proteins was reduced by more than an order of magnitude when the solution pH was shifted approximately two pH units away from the protein isoelectric point due to an increase in protein charge at pH both above and below the isoelectric point.

These electrostatic interactions can be exploited for protein separations through the use of a relatively new membrane technology called high performance tangential flow filtration or HPTFF (van Reis et al., 1997). HPTFF is able to achieve the high selectivities required for protein purification by combing several key strategies, including

the adjustment of solution pH and ionic strength to exploit different electrostatic interactions between the product / impurities and the membrane. For example, Saksena and Zydney (1994) demonstrated that the selectivity for separating bovine serum albumin (BSA) from immunoglobulin G using a 100 kD molecular weight cut off polyethersulfone membrane could be increased 25-fold by switching the pH from 7.0 to 4.8 and lowering the NaCl concentration, conditions which enhanced the electrostatic exclusion of the charged immunoglobulins from the membrane pores. van Reis et al. (1999) were able to achieve 900-fold purification at more than 90% yield for the separation of an antigen binding fragment of a monoclonal antibody from BSA using a single membrane step, even though BSA and the antigen binding fragment have very similar molecular weights. In this case the high purification was achieved using an electrically charged membrane in conjunction with the appropriate solution conditions to enhance the electrostatic repulsion of the desired product from the membrane. However these HPTFF processes all exploit a substantial difference in the electrical charge of the product and impurity, which could significantly limit the applicability of this new technology.

1.5 Thesis Program

The overall goal of this thesis was to demonstrate the feasibility of using affinity ultrafiltration for high resolution protein separations but with small charged affinity ligands, with the change in electrical charge of the protein-ligand complex allowing effective separation of the product from impurities. The specific aims included:

(1) Evaluating the binding interactions between the small affinity ligand and two model proteins over a range of buffer conditions and in the presence of specific displacement agents

(2) Evaluating the effects of the affinity ligand concentration on protein transmission using both electrically neutral and charged ultrafiltration membranes

(3) Developing a theoretical analysis of the effects of ligand binding on protein charge accounting for charge regulation phenomenon and on protein transmission accounting for electrostatic interactions between the protein and membrane

(4) Designing and optimizing a diafiltration process for affinity ultrafiltration using small charged affinity ligands

(5) Providing a framework for the development of new affinity ultrafiltration processes for protein separations using small charged ligands and HPTFF.

Chapter 2 provides a brief review of the available theoretical models used to describe solute transport in membrane systems, including both bulk and membrane transport phenomena. This general framework was subsequently applied to analyze data for protein transport in membrane filtration and to examine the effects of key process variables on the system performance.

Chapter 3 provides a description of the apparatus, materials, and methods used in the general experimental studies performed in this thesis. Additional details on more specialized experiments are provided in the appropriate chapters.

Chapter 4 presents experimental data for the binding interactions between the small charged affinity ligand Cibacron Blue and the model proteins BSA and ovalbumin. Data were obtained over a range of solution conditions and in the presence of a displacement agent to facilitate the disassociation of the protein ligand complex. Theoretical calculations were performed to evaluate the net electrical charge on the protein-ligand complex taking into account the effects of charge regulation and the binding of the negatively-charged dye.

Chapter 5 examines the effects of a small charged ligand on protein transport. Experiments were performed using both neutral and charged modified versions of the Ultracel composite regenerated cellulose membranes. The data were analyzed using available theoretical models to determine the critical factors determining the rate of protein transmission in this system. Model simulations were also performed to obtain additional insights into the effect of the equilibrium binding parameters on protein transport.

Chapter 6 presents the methodology used to determine the best separation conditions for the affinity ultrafiltration process, including the appropriate values of the membrane surface charge density, the affinity ligand concentration, and the solution pH and ionic strength. The feasibility of the protein separations was demonstrated using a small stirred ultrafiltration cell. The results were analyzed in terms of the trade-off between the product yield and purification factor.

Chapter 7 examines the use of tangential flow filtration (HPTFF) in combination with the small charged affinity ligands for protein purification. Experiments were performed in a laboratory scale tangential flow filtration device that is linearly scalable to

commercial manufacturing. Data were obtained over a range of feed flow rate and filtrate flux to determine the appropriate conditions for the protein separation. A two stage diafiltration separation process was designed and implemented, with the protein separation accomplished in the first stage while the ligand recovery was performed in the second stage. The results clearly demonstrate the capability of using affinity ultrafiltration with small charged affinity ligands for protein separations.

Chapter 8 summarizes the major findings of this thesis and makes recommendations for future work to further understand the behavior and to facilitate the development of affinity ultrafiltration using small charged affinity ligands.

Chapter 2

BACKGROUND

2.1 Introduction

This chapter provides a brief review of the theoretical models that have been developed to describe protein transport in membrane systems, with a particular emphasis on the theoretical description of the effects of electrostatic interactions on protein partitioning and transport in narrow pores. These phenomena are of interest in a number of applications including chromatography, gel-based capillary electrophoresis, and membrane separations. Much of this discussion is based on the presentations in the theses by Menon (1999) and Burns (2000).

2.2 Bulk Mass Transport

The overall performance of any membrane device is determined by the rate of solute transport through the membrane in combination with the rate of transport from the bulk solution to the surface of the membrane. During filtration, the pressure driven flow through the membrane convectively transports solutes towards the upstream surface of the membrane as shown in Figure 2.1. If the membrane is partially (or completely) retentive to the solute, the solute molecules will begin to accumulate on the upper surface of the membrane, a phenomenon called concentration polarization. Polarization causes the protein concentration to vary from a value of C_b in the bulk solution to a much greater value at the membrane surface (C_w), over a distance equal to the concentration

polarization boundary layer thickness δ. The increase in concentration in the solution immediately upstream of the membrane can significantly alter protein transmission due to the increase in the concentration gradient across the membrane. In addition, the osmotic pressure associated with this high protein concentration can reduce the effective pressure driving force, thereby reducing the solvent flux. The high protein concentration at the membrane surface can also increase membrane fouling leading to irreversible changes in the membrane properties.

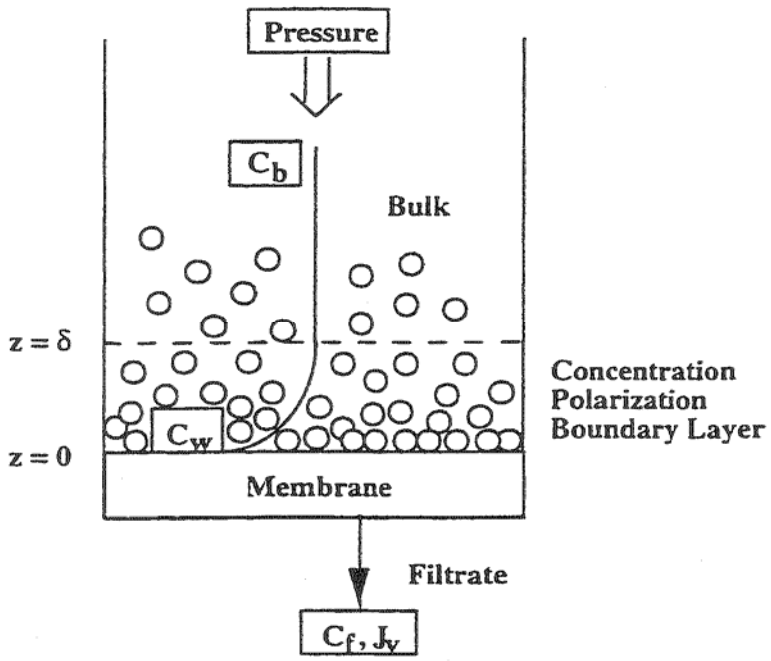

Figure **2.1**: Concentration polarization during membrane filtration

2.2.1 Stagnant Film Model

The stagnant film model is the most commonly used approach to describe concentration polarization in membrane systems. This model provides an approximate analysis of mass transfer within the concentration polarization boundary layer neglecting, many of the complexities associated with the detailed fluid flow characteristics in the particular module as well as the coupling between mass and momentum transport. The net solute flux towards the membrane (N_s) has two contributions – one from convection and one from diffusion back into the bulk solution:

$$N_s = -J_v C_s - D_\infty \frac{dC_s}{dz} \qquad (2.1)$$

where C_s is the local solute concentration at a height z above the membrane surface, D_∞ is the free solution diffusivity, and J_v is the filtrate flux, which is taken to be a positive quantity even though the flow is in the negative z-direction. In the stagnant film model, the protein flux towards the membrane is assumed to be constant throughout the boundary layer and equal to the solute flux through the membrane:

$$N_S = -J_v C_f \qquad (2.2)$$

where C_f is the protein concentration in the filtrate solution. Equation (2.1) is integrated across the concentration boundary layer (from $C_s = C_w$ at $z = 0$ and $C_s = C_b$ at $z = \delta$) giving the following expression for filtrate flux:

$$J_v = k \ln\left(\frac{C_w - C_f}{C_b - C_f}\right) \qquad (2.3)$$

where k, the mass transfer coefficient in the particular membrane device, has been set equal to the ratio of the free solution diffusivity (D_∞) to the boundary layer thickness (δ). Equation (2.3) is the classical form of the stagnant film model. It relates the filtrate flux to the product of the mass transfer coefficient and an appropriate concentration driving force, with the latter expressed in terms of the solute concentrations in the bulk solution (C_b), at the membrane surface (C_w), and in the filtrate solution (C_f).

Although Equation (2.3) is approximate, it has been extensively used to analyze both solute and solvent transport in membrane systems. The mass transfer coefficient is a function of both the solute diffusivity and the device hydrodynamics. The mass transfer coefficient can, at least in principle, be obtained by solving the appropriate mass transfer equations for the system geometry of interest. However, it is often difficult to develop complete solutions to the governing equations because of the complexities of the fluid flow within typical membrane devices. Hence, empirical or semi-empirical correlations are typically developed from experimental data or from analogies with corresponding heat and mass transfer problems.

Most of the experimental studies performed in this thesis were conducted in a stirred ultrafiltration cell. Smith et al. (1968) developed the following correlation for the average mass transfer coefficient for laminar flow (Re<32,000) above a stirred surface based on data for the rate of dissolution of benzoic acid:

$$Sh = \chi(\mathrm{Re})^{0.567}(Sc)^{0.33} \qquad (2.4)$$

where Sh is the Sherwood number, $Sh = kb/D_\infty$, Re is the Reynolds number, $Re = \omega b^2/\upsilon$, Sc is the Schmidt number, $Sc = \upsilon/D_\infty$, b is the radius of the stirred cell, ω is the stirring speed, and ν is the kinematic viscosity. The coefficient, χ, is a function of the actual system geometry (Smith et al., 1968) and possibly the membrane porosity (Malone and Anderson, 1977). The value of χ for the Amicon 8010 stirred cell used in this thesis, which has a diameter of 2.5 cm, was evaluated by Opong and Zydney (1991) as $\chi = 0.23$ based on data for the filtrate flux of bovine serum albumin (BSA) solutions through fully retentive polyethersulfone membranes using different stirring speeds and bulk protein concentrations.

The mass transfer coefficient is a function of the protein diffusion coefficient, which depends on both the solution pH and the ionic strength due to the effects of electrostatic interactions on protein-protein interactions. Table 2.1 shows experimental results for the diffusion coefficient of BSA obtained from quasi-elastic light scattering by Doherty and Banedek (1974) in different ionic strength solutions. The data were all obtained under conditions where BSA had a net charge of approximately -10 electronic charges. The increase in the diffusivity at low ionic strengths is due to the strong repulsive interactions between BSA molecules under these conditions.

The third column in Table 2.1 shows the BSA mass transfer coefficient calculated from the diffusivity values using Equation (2.4). The calculated mass transfer coefficients decrease by a factor of 3 as the salt concentration was increased from 1.5 to

150 mM due to the change in the intermolecular interactions. The final column of Table 2.1 give the values of the BSA mass transfer coefficient evaluated by Pujar (1996) from filtrate flux data obtained in a stirred ultrafiltration cell using a fully retentive 30 kD molecular weight cut off membranes. These experimental results show a much weaker dependence on the solution ionic strength than is predicted by Equation (2.4), which is likely due to the effects of concentration polarization in the highly concentrated layer that exists immediately adjacent to the membrane surface.

Table **2.1**: BSA diffusivity and bulk mass transfer coefficient at different ionic strengths (Adapted from Pujar, 1996)

Ionic Strength (mM)	Diffusivity (m^2/s x 10^{11}) (Doherty and Benedek, 1974)	k_{BSA} from Diffusivity Data (μm/s)	k_{BSA} from Filtration Data (μm/s) (Pujar,1996)
150	6	4.8	4.8
50	8.5	6.1	–
15	13	7.9	5.5
5	22	11.3	–
1.5	28	13.5	8.5

The diffusion coefficients for other proteins examined in this thesis were calculated from the correlation developed by Young et. al. (1980):

$$D_\infty = 8.34 \times 10^{-8} \left(\frac{T}{\eta M^{1/3}} \right) \qquad (2.5)$$

where D_∞ is in cm/s^2, η is the solution viscosity in cP, T is the absolute temperature, and M is the molecular weight of the protein in g/mol. Equation (2.5) is valid only for infinitely dilute solutions since it neglects any protein-protein interactions and hence it predicts that D_∞ is essentially independent of solution ionic strength.

The development of the stagnant film implicitly assumes that the transport properties, both the solute diffusivity and the solution viscosity, are independent of the solute concentration and thus constant throughout the boundary layer. Although more advanced models are available that account for the concentration dependence of the solute diffusivity, at least in an approximate fashion, these models have not been widely used in the analysis of filtration data largely because of the lack of available data on the concentration-dependence of the protein diffusion coefficient over the full range of concentrations from C_b to C_w.

2.3 Membrane Transport

Solute transport through semipermeable membranes can be analyzed using a number of different approaches. The Kedem-Katchalasky analysis and the Stefan-Maxwell multicomponent diffusion analysis were both developed from the principles of irreversible thermodynamics. The solvent and solute fluxes are related to the concentration and pressure gradients by a set of phenomenological coefficients, accounting for the inherent coupling between solute and solvent transport. However, the phenomenological coefficients have to be determined experimentally, and there is no explicit dependence of the parameters on the membrane pore size or surface charge

characteristics, severely limiting the usefulness of these approaches for describing the affects of electrostatic interactions on solute transport.

An alternative approach for describing solute and solvent transport is based on the application of appropriate hydrodynamic models. In this case the equations of motion are solved to describe the transport of a well-defined solute moving through a well-defined pore, typically a long cylindrical capillary. These models treat the solvent as a continuum and are thus physically limited to situations where the radius of the pore (r_p) and the radius of the solute (r_s) are both significantly larger than the size of the solvent molecules. The pore length is typically assumed to be much greater than the pore radius so that entrance and exit effects can be neglected. Hydrodynamic models are also easily extended to include the effects of a pore size distribution (by integration over a range of pore sizes) as well as the effects of electrostatic interactions. The analysis of membrane transport phenomena in this thesis makes extensive use of available hydrodynamic models; the key features of these models are described in the following sections.

2.3.1 Solvent Transport

The hydraulic permeability (L_p) provides a measure of the rate of solvent transport through a membrane:

$$L_p = \frac{\eta J_v}{\Delta P} \qquad (2.6)$$

where J_v is the solvent flux (volumetric solvent flow rate normalized by the membrane area), η is the solvent viscosity, and ΔP is the applied transmembrane pressure difference.

For laminar flow through a membrane composed of a parallel array of uniform cylindrical uncharged pores of radius r_p and length δ_m, the hydraulic permeability can be evaluated assuming Hagen-Poiseuille flow as:

$$L_p = \frac{N\pi r_p^4}{8\delta_m} \qquad (2.7)$$

where N is the number of pores per unit area of the membrane. Equation (2.7) neglects end-effects, which is valid for most ultrafiltration membranes where the ratio of pore radius to length is typically less than 0.01. The effects of electrical stresses on solvent transport through electrically charged pores is discussed in the next section.

2.3.1.1 Solvent Transport through a Charged Membrane

The rate of solvent transport is also dependent on the membrane surface charge and solution ionic strength due to electrokinetic effects as described by the electrical stresses in the Navier-Stokes equations. The presence of a net surface charge on the pore wall causes an accumulation of counterions in the region immediately adjacent to the pore wall; this region is typically referred to as the electrical double layer. Application of a pressure drop across the membrane causes a transient accumulation of counterions at the downstream surface of the membrane, leading to the development of an induced electrical (or streaming) potential. At steady state, the streaming potential generates a back conductive ion transport that is just sufficient to balance the convective ion flux, resulting in a situation in which there is no net current flow through the pore.

The induced streaming potential reduces the magnitude of the solvent flux due to the net force on the fluid exerted by the action of the electric field on the ions (often referred to as electroosmosis). The one-dimensional momentum equation for flow through a cylindrical pore is thus written as (Newmann, 1991):

$$\frac{\eta}{r}\frac{d}{dr}\left(r\frac{dv_z}{dr}\right)+\rho_e E_z-\frac{dP}{dz}=0 \qquad (2.8)$$

where v_z is the axial velocity, η is the solution viscosity, ρ_e is the local charge density in the electrolyte solution, E_z is the axial electric field, and dP/dz is the pressure gradient. The electrical potential gradient satisfies Poisson's equation in cylindrical co-ordinates and can be written as:

$$\frac{1}{r}\frac{\partial}{\partial r}\left(r\frac{\partial\phi}{\partial r}\right)=-\frac{\rho_e}{\varepsilon_o\varepsilon_r} \qquad (2.9)$$

where ε_o is the permittivity of free space, ε_r is the dielectric constant of the medium. The term $d^2\phi/dz^2$ is equal to zero since the electrical potential in a long uniform pore is a linear function of z. The local charge density is evaluated in terms of the local concentrations of all the ions in solution as:

$$\rho_e=F\sum_i z_i C_i \qquad (2.10)$$

where F is the Faraday's constant and z_i and C_i are the ion valence and concentration, respectively.

The velocity profile is evaluated by integrating Equation (2.8) in the radial direction, with the local charge density given by Equation (2.10), and applying the

boundary conditions that $v_z = 0$ at $r = r_p$ and that v_z and ϕ are finite at $r = 0$ (Newman, 1991) to give:

$$v_z = E_z \frac{\varepsilon_o \varepsilon_r}{\eta}\left(\phi - \phi_{r=r_p}\right) - \frac{dP}{dz}\frac{r_p^2 - r^2}{4\eta} \qquad \textbf{(2.11)}$$

where $\phi_{r=r_p}$ is the electrical potential at the surface of the pore. The radial dependence of the electrostatic potential is evaluated by first recognizing that the net ion flux in the radial direction is zero.

$$N_i = D_i \frac{\partial C_i}{\partial r} + u_i z_i F E_r = 0 \qquad \textbf{(2.12)}$$

where E_r is the radial electric field ($-\frac{\partial \phi}{\partial r}$) and u_i is the ion mobility (given by $u_i = D_i/RT$). Eqaution (2.12) is integrated in the radial direction over the radius of the pore yielding the Boltzman distribution:

$$C_i = C_i^0 \exp\left[-\frac{z_i F}{RT}\left(\phi - \phi_{r=0}\right)\right] = C_i^0\left[1 - \frac{z_i F}{RT}\left(\phi - \phi_{r=0}\right)\right] \qquad \textbf{(2.13)}$$

where the second expression is valid only for low potentials (the Debye Huckel approximation) since it accounts for only the first terms in the Taylor series expansion for the exponentials. Equation (2.13) is substituted into Equation (2.9), with the resulting second order differential equation solved using a constant surface charge density boundary condition yielding:

$$\left(\phi - \phi_{r=0}\right) = \frac{q_p}{\varepsilon_0 \varepsilon_r \kappa}\frac{\left[I_0(\kappa r) - 1\right]}{I_1(\kappa r_p)} \qquad \textbf{(2.14)}$$

where I_0 and I_1 are modified Bessel functions of the first kind, q_p is the surface charge density of the pore, and κ is the inverse Debye length which is given by:

$$\kappa^{-1} = \left[\frac{F^2}{\varepsilon_o \varepsilon_r RT} \sum_i \left(z_i^2 C_i^0 \right) \right] \tag{2.15}$$

For an uncharged pore, the fluid velocity has a parabolic profile with the maximum at the pore centerline where $v_z = (dP/dz)\, r_m^2/4\eta$. The radial dependence of velocity in a charged pore is more complex because of the presence of the counter-electroosmotic flow which acts in the opposite direction to the pressure driven flow. The average fluid velocity through the pore is evaluated by integrating Equation (2.11) over the pore radius to give:

$$\langle V \rangle = \frac{\Delta P}{\delta_m} \frac{r_p^2}{8\eta} - E_z \frac{q_p I_2(\kappa r_p)}{\kappa \eta I_1(\kappa r_p)} \tag{2.16}$$

where I_2 is the modified Bessel function of the first kind. The counter-electroosmotic flow is represented by the second term in Equation (2.16) and always acts in the direction opposite to the pressure-driven flow, irrespective of the polarity of the membrane surface charge.

The magnitude of the streaming potential can be evaluated directly from the constraint that there is no net electrical current flow through the pore. The current is given by the sum of the convective and conductive contributions (the diffusive contribution is zero since the ion concentration gradient in the axial direction is assumed to be negligible):

$$I = 2\pi \int_0^{r_p} i_z r dr = \int_0^{r_p} v_z \rho_e r dr + E_z \int_0^{r_p} \Lambda r dr \qquad (2.17)$$

where Λ is the local conductivity:

$$\Lambda = F^2 \sum_i z_i^2 u_i C_i \qquad (2.18)$$

Equation (2.17) also ignores any electrical conduction through the membrane polymer. The induced electrical field (E_z) associated with the streaming potential is evaluated by setting the net electrical current I to be equal to zero which gives the following after some manipulation (Newman, 1991):

$$E_z = \frac{\Delta P}{\delta_m} \frac{q_p}{\Lambda_{eff} \kappa \mu} \frac{I_2(\kappa r_p)}{I_1(\kappa r_p)} \qquad (2.19)$$

where Λ_{eff} is the effective conductivity of the electrolyte solution as accounting for the change in ion concentrations caused by the partitioning into the charged pore:

$$\Lambda_{eff} = \Lambda_{avg} + \frac{q_p^2}{\eta} \left[1 - \frac{I_0(\kappa r_p) I_2(\kappa r_p)}{I_1^2(\kappa r_p)} \right] \qquad (2.20)$$

where

$$\Lambda_{avg} = \Lambda^0 \left(1 + \frac{q_p F}{\kappa \varepsilon_o \varepsilon_r RT} \left[\frac{2}{\kappa r_m} - \frac{1}{I_1(\kappa r_p)} \right] \frac{\sum_i z_i^3 u_i C_i^0}{\sum_i z_i^2 u_i C_i^0} \right) \qquad (2.21)$$

with Λ^0 the conductivity at the pore centerline. The bracketed terms in Equation (2.21) account for the radial variation of the solute conductivity within the pore.

2.3.2 Solute Transport

The rate of solute transport in fluid filled pores can be evaluated by equating the gradient in the chemical potential of the solute ($-\nabla\mu_s$) to the hydrodynamic drag force acting on a solute within the pore (Anderson and Quinn, 1974; Deen 1987):

$$-\nabla\mu_s = f_\infty K(U - GV) \tag{2.22}$$

where f_∞ is the friction coefficient of the solute in the bulk solution and U and V are the solute and solvent velocity, respectively, both evaluated relative to a fixed coordinate system relative with respect to the pore walls. The lag coefficient (G) and the enhanced drag coefficient (K) account for hydrodynamic interactions between the solute and pore walls and are complex functions of the pore and solute size, the position of the solute in the pore, and the presence of any long range electrostatic interactions.

The gradient in the solute chemical potential arises from both chemical and electrochemical contributions:

$$-\nabla\mu_s = RT\nabla \ln C_s + \nabla\Phi_\psi \tag{2.23}$$

where C_s is the concentration of solute in the pore at a radial position r and axial position z and $\nabla\Phi_\psi$ is the electrical potential energy of the solute. Equation (2.23) assumes that the solute activity coefficient is unity; thus, it neglects the effects of solute-solute interactions within the pore, limiting its applicability to dilute solutions. Equation (2.23) is substituted into Equation (2.22), which is then solved for the solute flux:

$$N_s = UC_s = -K^{-1}D_\infty \nabla C_s + GVC_s - K^{-1}D_\infty \frac{C_s}{RT}\nabla\Phi_\psi \tag{2.24}$$

where $D_\infty = RT/f_\infty$ is the free solute diffusivity at infinite dilution. The three terms in Equation (2.24) represent the diffusive, convective, and electrophoretic contributions to the solute flux. This equation provides a general description of the solute flux accounting for the hydrodynamic interactions with system boundaries as discussed by Pujar and Zydney (1994).

Since our primary interest is in the overall solute flux through the pore, Equation (2.24) is integrated over the pore cross section:

$$\langle N_s \rangle = \frac{\int_0^1 N_s \beta d\beta}{\int_0^1 \beta d\beta} = 2\int_0^{1-\lambda} N_s \beta d\beta \qquad (2.25)$$

where β is the dimensionless radial position in the pore ($\beta = r/r_p$). The upper limit in the last integral is set at $\beta = 1-\lambda$ with $\lambda = r_s/r_p$ where r_s is the radius of the solute. This properly accounts for the steric exclusion of the spherical solute from the annular region within one solute radius of the pore wall. Equation (2.24) is substituted into Equation (2.25) to yield:

$$\langle N_s \rangle = -2D_\infty \int_0^{1-\lambda} K^{-1} \frac{\partial C_s}{\partial z} \beta d\beta - 2D_\infty \int_0^{1-\lambda} K^{-1} C_s \frac{1}{RT} \frac{\partial \Phi_\psi}{\partial z} \beta d\beta + 2\int_0^{1-\lambda} G C_s V \beta d\beta \qquad (2.26)$$

The radial variation of the solute concentration within the pore is described by a Boltzmann (equilibrium) distribution:

$$C_s(\beta) = C_s(\beta = 0)\exp\left[-\frac{\psi(\beta) - \psi(\beta = 0)}{kT}\right] \qquad (2.27)$$

where $\psi(\beta = 0)$ and $C_s(\beta = 0)$ are the potential energy of interaction and the solute concentration, respectively, at the centerline of the pore. Equation (2.27) can also be obtained by integrating Equation (2.24) over r with V = 0 and $N_s = 0$ in the radial direction. Deen (1987) has provided an excellent review of the previous theoretical and experimental work on solute transport in liquid-filled pores.

Substitution of Equation (2.27) to (2.26) yields:

$$\langle N_s \rangle = K_c \langle V \rangle \langle C_s \rangle - K_d D_\infty \frac{d\langle C_s \rangle}{dz} \qquad (2.28)$$

where it has been assumed that the electropherotic contribution is negligible. This effect is discussed in more detail by Pujar and Zydney (1994). The coefficients K_c and K_d account for the hindrance to convective and diffusive transport, respectively, and are given by:

$$K_c = \frac{\int_0^{1-\lambda} GV\exp\left(\frac{-\psi}{kT}\right)\beta d\beta}{\left[\int_0^{1-\lambda}\exp\left(\frac{-\psi}{kT}\right)\beta d\beta\right]\left[2\int_0^1 V\beta d\beta\right]} \qquad (2.29)$$

$$K_d = \frac{\int_0^{1-\lambda} K^{-1} \exp\left(\frac{-\psi}{kT}\right) \beta d\beta}{\int_0^{1-\lambda} \exp\left(\frac{-\psi}{kT}\right) \beta d\beta} \tag{2.30}$$

The evaluation of the hindrance factors is discussed in the next section.

In order to relate the solute concentration at the upstream and downstream surfaces of the membrane, Equation (2.28) is integrated across the pore length. Appropriate boundary conditions at the upper (z = 0) and lower (z = δ_m) surfaces are developed by assuming that the solute concentrations across the membrane-solute interface are in equilibrium (Deen, 1987). Results are expressed in terms of the equilibrium partition coefficient (ϕ):

$$\phi = \frac{\langle C_s \rangle_{z=0}}{C_w} = \frac{\langle C_s \rangle_{z=\delta_m}}{C_f} = 2\int \exp\left(\frac{-\psi}{kT}\right) \beta d\beta \tag{2.31}$$

which is equal to the ratio of the average solute concentration in the pore to that in the bulk solution at the upper and lower surfaces of the membrane. For purely steric (hard sphere) interactions, $\psi(\beta) = 0$ in the region $\beta < 1-\lambda$ and Equation (2.31) becomes:

$$\phi = (1-\lambda)^2 \tag{2.32}$$

The solute flux through the pore is thus given as (Anderson and Quinn, 1974; Opong and Zydney, 1991):

$$\langle N_s \rangle = S_\infty C_w \langle V \rangle \frac{\left[1 - \left(\frac{C_f}{C_w}\right) \exp(-Pe_m)\right]}{\left[1 - \exp(-Pe_m)\right]} \tag{2.33}$$

where

$$S_\infty = \phi K_c = 4\int_0^{1-\lambda} G(1-\beta)^2 \exp\left[\frac{-\psi}{kT}\right]\beta d\beta \qquad (2.34)$$

$$Pe_m = \left(\frac{K_c}{K_d}\right)\left(\frac{\langle V\rangle \delta_m}{D_\infty}\right) = \left(\frac{S_\infty}{\phi K_d}\right)\left(\frac{\langle V\rangle \delta_m}{D_\infty}\right) \qquad (2.35)$$

$$\langle V\rangle = \frac{-r_p^2}{8\eta}\frac{dP}{dz} \qquad (2.37)$$

$$\frac{D_{eff}}{D_\infty} = \phi K_d = 2\int_0^{1-\lambda} K^{-1} \exp\left(\frac{-\psi}{kT}\right)\beta d\beta \qquad (2.36)$$

S_∞ is the asymptotic sieving coefficient and describes the purely convective contribution to the solute flux, i.e., $N_s = S_\infty \langle V \rangle C_w$ in the limit of very high fluid velocity. D_{eff} is the effective solute diffusion coefficient in the membrane and describes the rate of solute transport in the limit of $\langle V \rangle = 0$. Pe_m is the membrane Peclet number and describes the relative contributions of convective to diffusive transport through the pore.

Equation (2.33) can be rewritten in terms of the actual membrane sieving coefficient, S_a, which is defined as the ratio of the solute concentration in the filtrate C_f solution downstream of the membrane to the solute concentration in the solution just upstream of the membrane, C_w (Opong and Zydney, 1991):

$$S_a = \frac{C_f}{C_w} = \frac{S_\infty \exp(Pe_m)}{S_\infty + \exp(Pe_m) - 1} \qquad (2.38)$$

where Equation (2.38) is developed by setting the solute flux equal to the product of the filtration velocity and the filtrate concentration. Thus, a complete description of solute transport (sieving) during membrane filtration requires the knowledge of two parameters: the asymptotic membrane sieving coefficient, S_∞, and the membrane Peclet number, Pe_m, with the latter depending on both the filtration velocity and the effective diffusion coefficient through the membrane.

Figure (2.2) shows a typical plot of the actual sieving coefficient as a function of the membrane Peclet number for different values of S_∞. The actual sieving coefficient decreases with increasing values of Pe_m, approaching a constant asymptotic value at high Peclet numbers where $S_a = S_\infty$. At low Peclet numbers, $Pe_m \rightarrow 0$, Equation (2.38) predicts that the actual sieving coefficient will be equal to one, regardless of the value of S_∞, assuming that the membrane is at least partially permeable to the solute, i.e. $S_\infty > 0$. Under these conditions solute transport is governed by diffusion, which tends to equalize the solute concentrations on both sides of the membrane causing the sieving coefficient to approach a value of one.

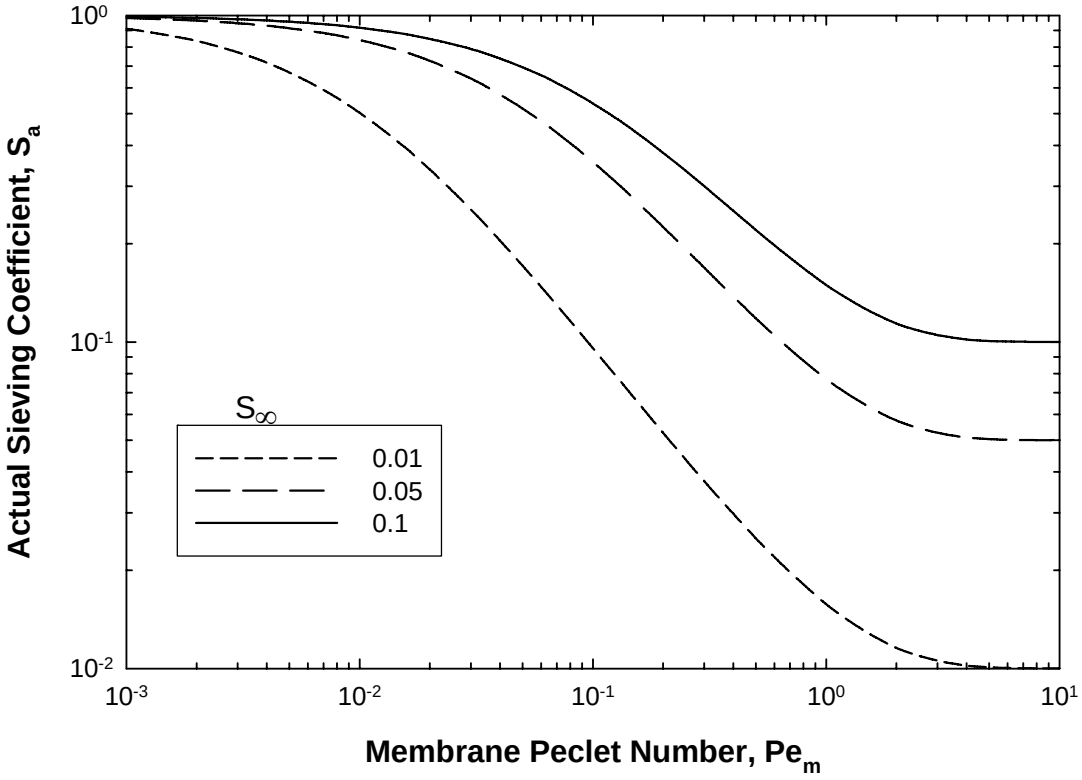

Figure **2.2**: Actual sieving coefficient as a function of the membrane Peclet number

2.3.2.1 Transport Parameters: Hydrodynamic Contribution

The lag coefficient [G(λ,β)] and the enhanced drag coefficient [K(λ,β)] can both be evaluated by solving the governing Navier-Stokes equation for the motion of an isolated sphere in a long cylindrical pore. Since detailed analytical expressions for G and K^{-1} for arbitrary radial positions are currently unavailable, Equations (2.29) and (2.30) are typically evaluated using the centerline approximation (Deen, 1987) in which the

$$K_c = \left(2 - (1-\lambda)^2\right) G(\lambda,0) \qquad (2.39)$$

hindrance coefficients are assumed to be constant at their centerline values giving:

$$K_d = K^{-1}(\lambda,0) \qquad (2.40)$$

Bungay and Brenner (1973) developed expressions for G(λ, 0) and K^{-1} (λ, 0) for uncharged spheres in uncharged cylindrical pores that are valid for all values of λ, the ratio of solute to pore radius, using matched asymptotic expansions for both small and close-fitting spheres. Details of the calculations are available elsewhere (Bungay and Brenner, 1973; Deen, 1987; Pujar, 1996), with the final results given as:

$$K^{-1}(\lambda,0) = \left(\frac{6\pi}{K_t}\right) \qquad (2.41)$$

$$G(\lambda,0) = \frac{K_s}{2K_t} \qquad (2.42)$$

The hydrodynamic functions K_s and K_t are expressed as expansions in λ:

$$\begin{bmatrix} K_t \\ K_s \end{bmatrix} = \frac{9}{4}\pi^2\sqrt{2}(1-\lambda)^{-5/2}\left[1+\sum_{n=1}^{2}\begin{pmatrix} a_n \\ b_n \end{pmatrix}(1-\lambda)^n\right]+\sum_{n=0}^{4}\begin{pmatrix} a_{n+3} \\ b_{n+3} \end{pmatrix}\lambda^n \qquad (2.43)$$

with the coefficients a_n and b_n given in the Table 2.2. Equations (2.41) and (2.42) are in good agreement with more rigorous analyses of hindered transport valid for $\lambda < 0.1$ (Brenner and Gaydos, 1977) and $\lambda > 0.9$ (Mavrovouniotis and Brenner, 1988) developed by explicitly averaging the local solute concentrations in the pore over the radial direction.

Table 2.2: Expansion Coefficients for hydrodynamic functions K_t and K_s in Equation (2.29)

Subscript n	a_n	b_n
1	-73/60	7/60
2	77239/50400	-2227/50400
3	-22.5083	4.0180
4	-5.6117	-3.9788
5	-0.3363	-1.9215
6	-1.216	4.392
7	1.647	5.006

Figure 2.3 shows a plot of the hydrodynamic functions G and K^{-1} as function of the ratio of solute to pore radii. Both G and K^{-1} decrease as λ increases due to the increased hydrodynamic interactions with the pore wall. As $\lambda \rightarrow 1$, $K^{-1} \rightarrow 0$ since the drag on the solute becomes infinitely large. In contrast, the convective coefficient, G, approaches a value of 0.5 when $\lambda \rightarrow 1$ because the sphere moves like a piston under these conditions with a velocity equal to exactly one-half the centerline velocity due to the parabolic velocity profile in the pore.

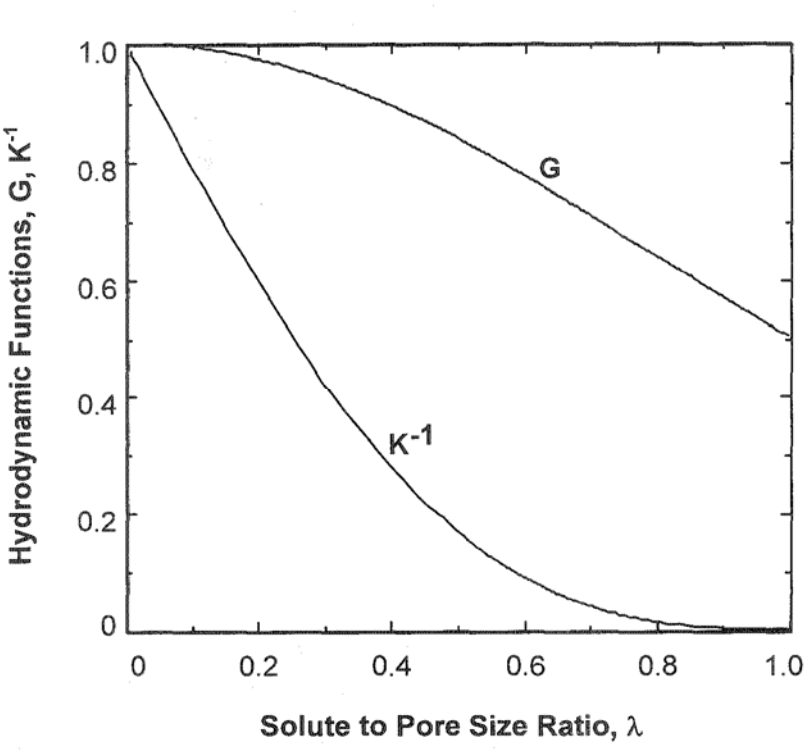

Figure **2.3**: Dependence of hydrodynamic functions G and K^{-1} on λ

2.3.2.2 Transport Parameters: Thermodynamic Contribution

The thermodynamic contribution to solute transport is described by the solute partition coefficient, ϕ, given by Equation (2.31). Smith and Deen (1980, 1983) evaluated the electrostatic contribution to the energy of interaction for a charged sphere in a charged cylindrical pore by solving the linearized Poisson-Boltzmann equation:

$$\nabla^2 \psi = \tau^2 \psi \tag{2.44}$$

where the dimensionless parameter τ is equal to the ratio of the pore radius to the Debye length κ^{-1}:

$$\tau = \kappa r_p \tag{2.45}$$

$$\kappa^{-1} = \left[\frac{F^2}{\varepsilon_o \varepsilon_r RT} \sum_i \left(Z_i^2 C_i \right) \right] \tag{2.46}$$

where F is the Faraday's constant, ε_0 is the permittivity in free space, ε_r is the dielectric constant of the medium, and z_i and C_i are the ion valence and concentration, respectively. Equation (2.44) is valid at low electrical potentials (< 25 mV) due to the linearization of the exponentials in the Boltzmann distribution, a limitation commonly referred to as the Debye-Huckel approximation.

Smith and Deen (1980) solved Equation (2.44) analytically using matching expansions in spherical and cylindrical coordinates. They used an infinite series representation to develop a solution in spherical coordinates and an integral solution in

cylindrical coordinates. The boundary conditions at the particle and pore surfaces were applied to the solutions in spherical and cylindrical coordinates, respectively. The complete solution was then obtained by matching the unknown coefficients in the two coordinate systems using appropriate coordinate transformations (Smith and Deen, 1980). The energy of interaction was subsequently evaluated by calculating the change in energy of the sphere plus cylinder as the particle was brought into the pore following the procedure originally developed by Verwey and Overbeek (1948). For interactions at constant surface charge, the dimensionless energy of interaction for a sphere situated at the center of the cylinder was given by (Smith and Deen, 1980):

$$V_\sigma = \frac{A_s \sigma_s^2 + A_{sp} \sigma_s \sigma_p + A_p \sigma_p^2}{\left[\pi\tau(1+\tau\lambda)\exp(-\tau\lambda) - M_0 h(\tau\lambda)\right]} \qquad (2.47)$$

where

$$A_s = \frac{4\pi\lambda^4 e^{\tau\lambda} M_0}{1+\tau\lambda} \qquad (2.48)$$

$$A_p = \frac{\pi^2 h(\tau\lambda)}{\tau^2 I_1^2(\tau)} \qquad (2.49)$$

$$A_{sp} = \frac{4\pi^2\lambda^2}{I_1(\tau)} \qquad (2.50)$$

I_1 is the modified Bessel function of the first kind of order one and σ_s and σ_p are the dimensionless surface charge densities of the solute (sphere) and pore (cylinder):

$$\sigma_s = \frac{Fr_p q_s}{\varepsilon_o \varepsilon_r RT} \tag{2.51}$$

$$\sigma_p = \frac{Fr_p q_p}{\varepsilon_o \varepsilon_r RT} \tag{2.52}$$

The function $h(\tau\lambda)$ and M_0 are given by:

$$h(\tau\lambda) = (1+\tau\lambda)^{-\tau\lambda} - (1-\tau\lambda)^{\tau\lambda} \tag{2.53}$$

$$M_0 = \int_0^\infty \frac{K_1\left[\left(\tau^2+\alpha^2\right)^{1/2}\right]}{I_1\left[\left(\tau^2+\alpha^2\right)^{1/2}\right]} d\alpha \tag{2.54}$$

where K_1 and I_1 are Bessel functions and α is a dummy variable over which the integration is performed. The integral in Equation (2.54) can be approximated for $\tau \geq 3$ as (Smith and Deen, 1980):

$$M_0 = \frac{\pi}{2}\left(\frac{\pi}{\tau}\right)^{1/2} e^{-2\tau}\left[\tau + \frac{15}{16} - \frac{39}{512\tau} + O\left(1/\tau^2\right)\right] \tag{2.55}$$

The dimensionless interaction energy V_σ is related to $\psi(0)$ by:

$$\psi = r_p \varepsilon_o \varepsilon_r \left[\frac{RT}{F}\right]^2 V_\sigma \qquad (2.56)$$

According to Equation (2.47), the energy of interaction has three distinct contributions: one arising from the deformation of the electrical double layer surrounding the sphere due to the presence of the pore wall (given by the term involving σ_s^2), one arising due to the deformation of the electrical double layer associated with the pore due to the presence of the sphere (the term with σ_p^2), and one associated with direct charge-charge interactions (given by the term involving $\sigma_s \sigma_p$). The relative magnitude of these contributions depends on the charge densities of the sphere and cylinder, the solution ionic strength, and the radii of the sphere and pore. This is discussed in more detail in Chapter 5.

2.3.3 Pore Size Distribution

The analysis presented in the previous sections of this chapter is limited to membranes that are comprised of pores having a single pore radius. Direct measurements using electron (Kim et al., 1990) or atomic force (Dietz et al., 1992) microscopy indicate that the pore size in a single membrane can vary by well over a factor of ten. Mochizuki and Zydney (1993), Saksena (1995), and Saksena and Zydney (1995) have examined the effects of an assumed pore size distribution on both solvent and solute transport in the presence of both electrostatic and steric interactions. This section briefly summarizes the mathematical analysis used to evaluate the effects of a pore size distribution.

2.3.3.1 Log-Normal Pore Size Distribution

Although the real pore size distribution of available membranes is unknown, most previous studies in this area have used a log-normal pore size distribution to characterize and analyze membrane transport (Mochizuki and Zydney, 1993; Causserand et. al., 1996; Saksena, 1995). The log-normal distribution has the distinct advantage of being defined for only positive values of the pore radius in contrast to the standard normal (Gaussian) distribution which includes pore radii from -∞ to +∞. A number of different forms have appeared in the literature for the log-normal distribution; these have been shown to be mathematically equivalent (Zydney et al., 1994). The distribution is most conveniently expressed as:

$$f(r_p) = \frac{n(r_p)}{N_o} = \frac{1}{r_p\sqrt{2\pi b}} \exp\left[-\frac{1}{2b}\left\{ \ln\left(\frac{r_p}{r_{mean}} \right) + \frac{b}{2} \right\}^2 \right] \qquad (2.57)$$

where the parameter b is given by

$$b = \ln\left[1 + \left(\frac{\sigma}{r_{mean}} \right)^2 \right] \qquad (2.58)$$

where r_{mean} is the mean pore radius and σ is the standard deviation of the distribution.

Typical pore size distributions represented by the log-normal density function are shown in Figure 2.4 for several values of the coefficient of variation, or the reduced standard deviation, σ/r_{mean}. The upper panel shows the actual probability density function, $f(r_p)$, and the bottom panel shows the cumulative probability function $F(r_p)$,

which is the integral of $f(r_p)$ and thus represents the fraction of pores in the distribution which have radius $R < r_p$. As shown in the top panel, the most likely pore radius (denoted by the maximum in the probability density function) occurs at a value of r_p/r_{mean} less than one, with the difference between the most likely radius and the mean pore size increasing with an increase in the breadth of the distribution. This behavior arises from the asymmetry in the log-normal pore size distribution, which has a relatively long tail at large r_p corresponding to a significant number of very large pores in the distribution. This can be clearly seen in the bottom panel for the curve with $\sigma/r_{mean} = 1$, in which case more than 10% of all pores have radii $r_p > 2\ r_{mean.}$

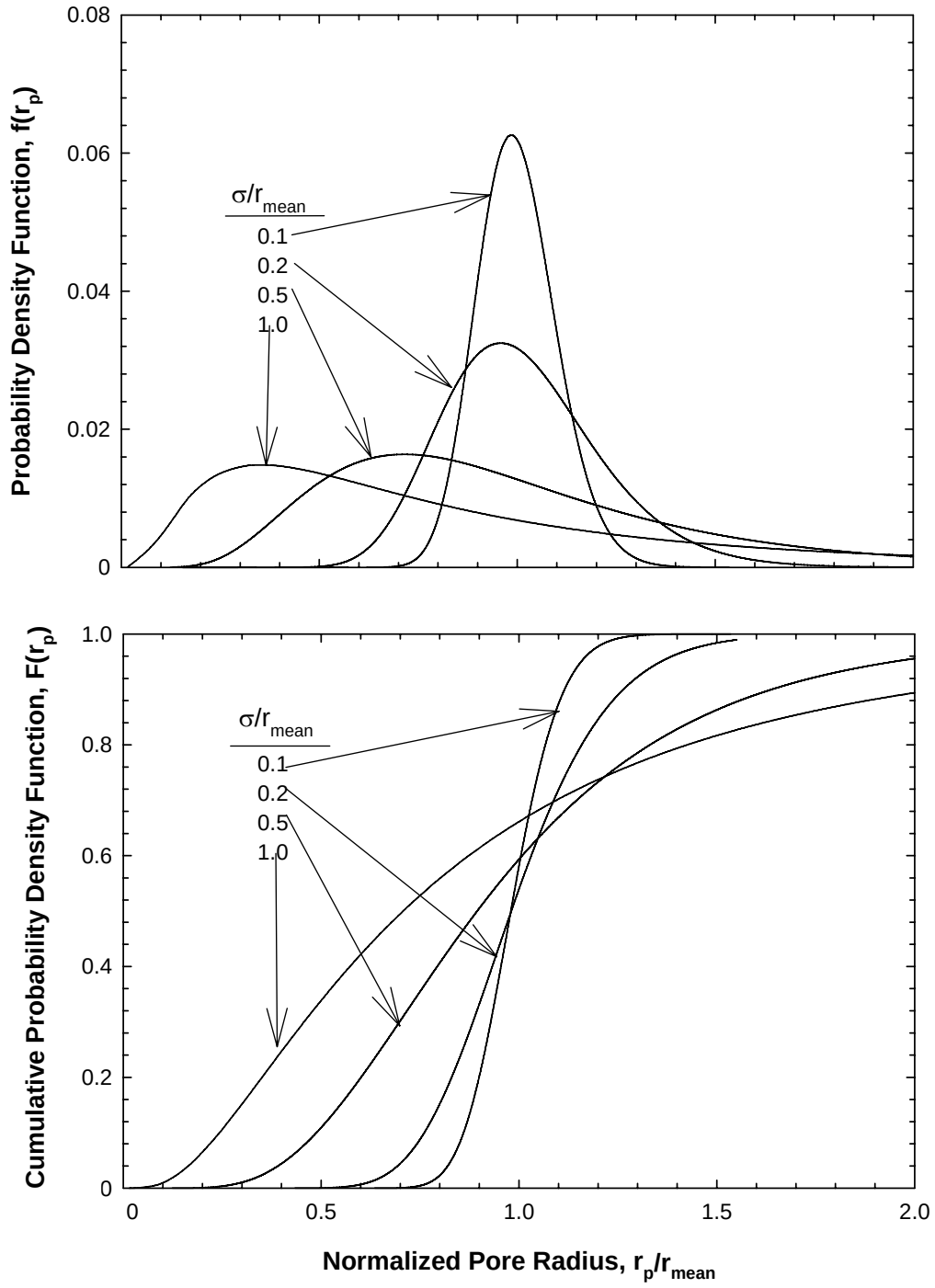

Figure **2.4**: Representative plots of the log-normal probability density function (upper panel) and the cumulative probability function (lower panel) for several values of the reduced standard deviation.

2.3.3.2 Effect of Pore-Size Distribution on Membrane Transport

The average solute flux through a membrane with a pore size distribution can be determined by integrating the solute flux over the distribution:

$$\overline{N_s} = \frac{\int_0^\infty \langle N_s \rangle n(r_p) \pi r_p^2 dr_p}{\int_0^\infty n(r_p) \pi r_p^2 dr_p} \tag{2.59}$$

with $\langle N_s \rangle$ given by Equation (2.33) and $n(r_p)$ given by Equation (2.57).

The average effective asymptotic sieving coefficient is defined experimentally as:

$$\overline{S_{eff}} = \frac{\overline{N_s}}{C_w \overline{V}} \tag{2.60}$$

where $\overline{V}$ is the average filtration velocity through the membrane:

$$\overline{V} = \frac{\int_0^\infty \langle V \rangle n(r_p) \pi r_p^2 dr_p}{\int n(r_p) \pi r_p^2 dr_p} \tag{2.61}$$

with $\langle V \rangle$ given by Equation (2.16). Substituting Equations (2.16), (2.61), and the limiting form of Equation (2.33) (for large Pe_m) into Equation (2.60) yields:

T

$$\overline{S_{eff}} = \frac{\int_0^\infty S_\infty(r_p) n(r_p) r_p^4 dr_p}{\int_0^\infty n(r_p) r_p^4 dr_p} \tag{2.62}$$

The average solute partition coefficient can be evaluated by a similar integration over the pore size distribution:

$$\overline{\phi} = \frac{\int_0^\infty \phi(r_p) n(r_p) r_p^2 dr_p}{\int_0^\infty n(r_p) r_p^2 dr_p} \qquad (2.63)$$

while the average hydraulic permeability is given by:

$$\overline{L_p} = \frac{\varepsilon}{8\eta\delta_m} \frac{\int_0^\infty n(r) r^4 dr}{\int_0^\infty n(r) r^2 dr} \qquad (2.64)$$

The r^4 dependence in the numerator of Equations (2.62) and (2.64) arises from the Hagen-Poiseuille equation, while the r^2 dependence in the denominator reflects the circular cross sectional area of the cylindrical pores.

Figure 2.5 shows the effect of the membrane pore size distribution on the average dimensionless solvent flux, which is given by $\frac{8\eta\overline{V}\delta_m}{\Delta \mathrm{Pr}_{mean}^2}$, for a series of membranes with the same mean pore size. As expected, the dimensionless solvent flux increases sharply as the breath or the variance of the pore size distribution increases, starting with a value close to one for a membrane with σ/r_{mean} of 0 to approximately 32 for a membrane with a σ/r_{mean} of 1.0. This large increase in solvent flux with increasing σ/r_{mean} is due to the r^4 dependence of the flow rate, which leads to a large proportion of the flow occurring through the largest pores in the distribution.

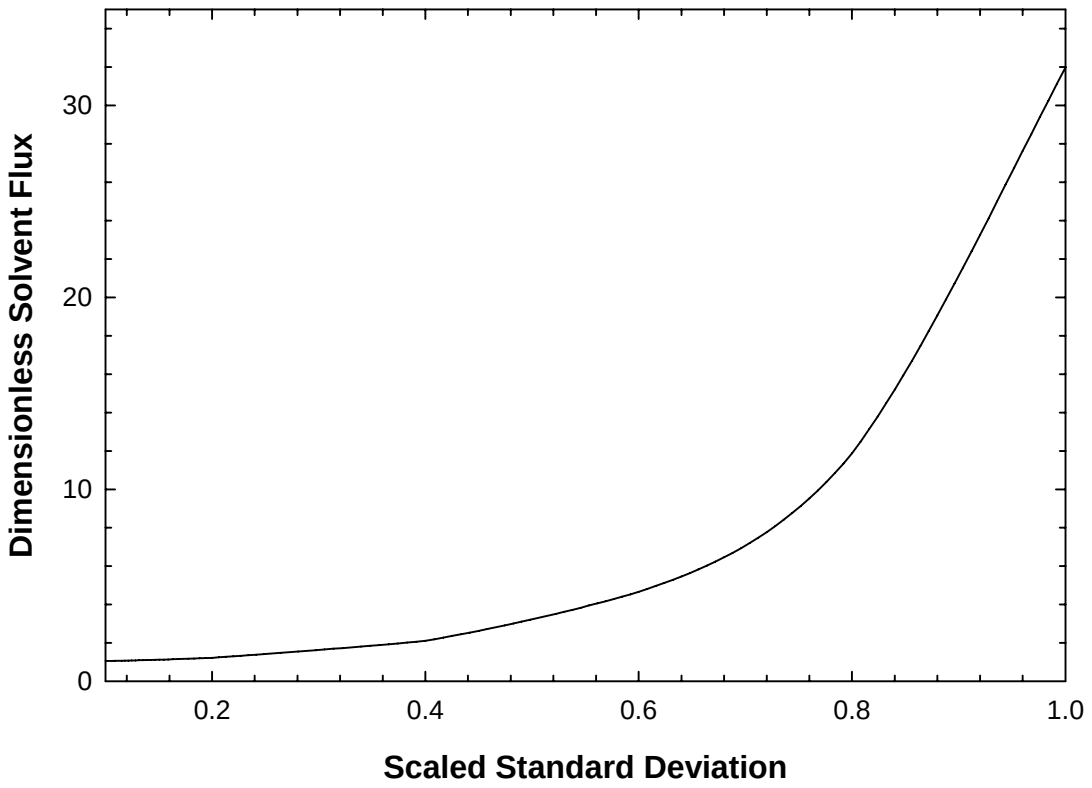

Figure 2.5: Effect of the standard deviation in the log-normal pore size distribution on the pressure driven solvent flow

The corresponding results for the asymptotic sieving coefficient are shown in Figure 2.6. Membranes with a narrow pore size distribution $\sigma/r_{mean} = 0.2$ are able to almost completely reject molecules greater than twice their average pore size, although there is still a small amount of solute transmission due to the presence of a small number of very large pores in the log-normal pore size distribution. The asymptotic sieving coefficient increases significantly with increasing values of σ/r_{mean} due to the minimal solute retention by the largest pores in the pore size distribution.

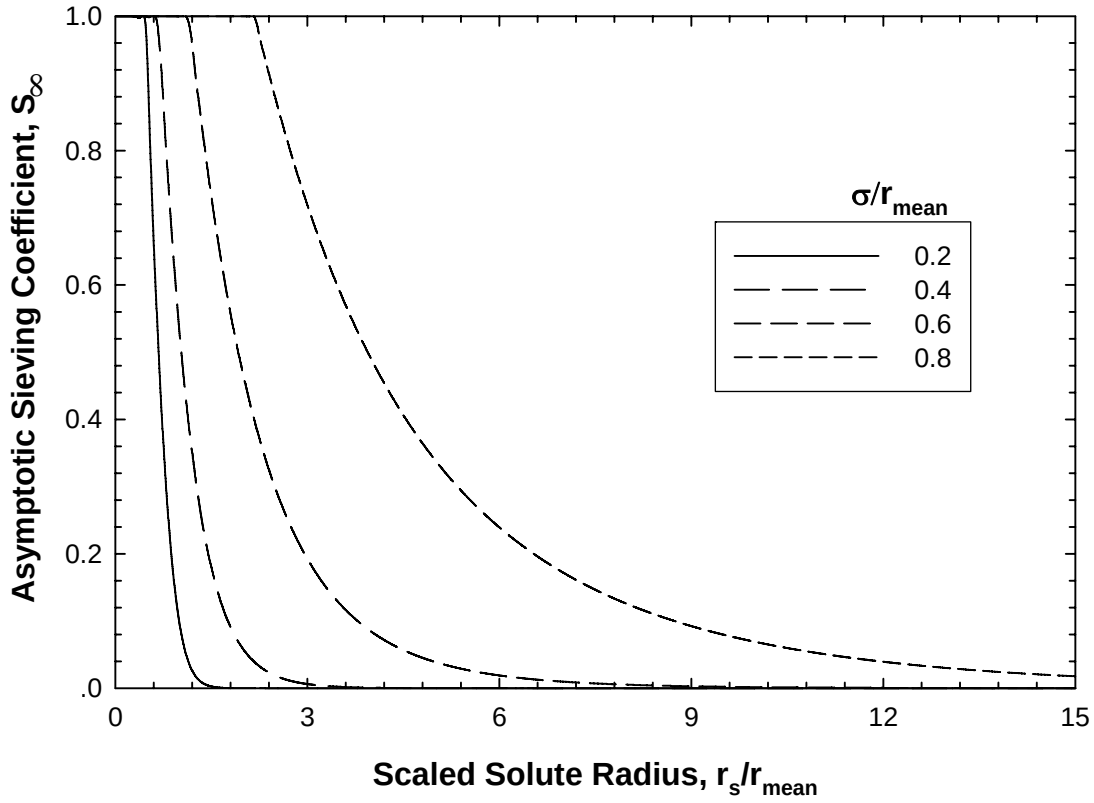

Figure **2.6**: Asymptotic Sieving Coefficient as a function of the scaled solute radius for membranes with different log-normal pore size distributions

Chapter 3

Materials and Methods

3.1 Introduction

This chapter describes the apparatus, materials and methods used for the experimental studies that were common to a lot of studies described in this thesis. Additional details of specific procedures are described in the appropriate chapters.

3.2 Membrane

3.2.1 Membrane Description

All filtration experiments performed in this work were done using asymmetric Composite Regenerated Cellulose (CRC) membranes provided by Millipore Corp. (Bedford, MA). Asymmetric ultrafiltration membranes usually have a thick support layer, which provides the membrane the required structural integrity, and a thin skin layer which is cast on the support layer which gives the membrane its required selectivity. Much larger process fluxes are thus attained with the use of an asymmetric composite membrane with a thin skin layer when compared to a symmetric membrane with comparable selectivity. In the case of CRC membranes the composite membrane consists of a skin layer that is made of cellulose and is cast on a microporous support layer made usually of material such as polyethylene. These cellulosic membranes have a large number of surface hydroxyl groups which make them extremely hydrophilic thus

reducing protein adsorption and thereby fouling. CRC membranes are robust and have high integrity. An SEM image adapted from Christy et. al.,(2004) is shown in Figure 3.1, which clearly shows the membrane skin approximately 0.5 μm which contains the much smaller pores than the substructure and the much thicker microporous support matrix. Regenerated cellulose membranes are not stable to extremely acidic or basic conditions and hence harsh sanitization conditions cannot be used. They can be easily cleaned using 0.1 N -0.5 N sodium hydroxide. CRC membranes are used extensively in the biopharmaceutical industry for the purification of high value protein therapeutics. They are used primarily to condition the protein solution into an appropriate buffer and in protein concentration.

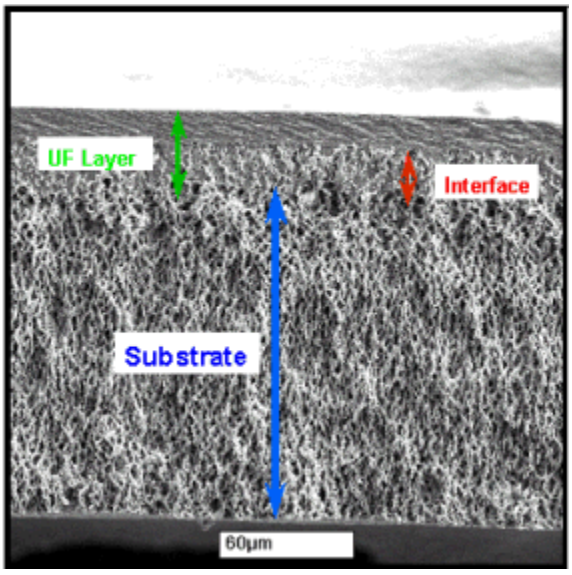

Figure 3.1: SEM image of a composite regenerated cellulose- Ultracel membrane (adapted from Christy et al., 2004)

CRC membranes with a molecular weight cut off of 10, 30 and 100 kD were used in this study. The membranes are rated by a R-90% value which corresponds to a rejection of greater than 90% of a solute with the corresponding molecular weight. Dextrans which are linear polysaccharides are most commonly used by manufactures to define R-90 values. The membranes were provided to us by Millopre Corp. in the form of either flat discs or in Pellicon XL modules, the membranes are commercially available under the trade name Ultracel. The membranes provided in flat sheets were cut to the appropriate size using a specially designed cutting device fabricated in our laboratory. All membranes were flushed with a minimum of 100 L/m^2 of deionized distilled water to remove wetting agents typically glycerol. The membranes were stored in appropriate buffers or in 0.1 N NaOH to prevent collapse of the membrane skin layer by drying. The 10 kD and 30 kD membranes were used for binding experiments and for protein conditioning while the larger molecular weight cut of membrane was used for protein sieving experiments.

Pellicon XL^{TM} tangential flow filtration modules (Millipore Corp. Bedford, MA) having 50 cm^2 of membrane were used to perform the High Performance Tangential Flow experiments. A schematic of the tangential flow filtration module is shown in Figure 3.3. A multi step precondition procedure was employed to remove glycerin and other preservatives form the Pellicon XL module. Tygon tubing (6 mm OD, 3 mm ID) was connected to the feed port, retentate port and one of the permeate ports, the other permeate port was sealed with a barb fitting. The feed line was then connected to a 10-roller peristaltic pump (Rabbit-Plus, Rainin Instrument Co., Woburn, MA) with the one end of the tube in a feed reservoir containing 1 L of deionized distilled water. The ends of

permeate and retentate lines were placed in separate empty beakers. The pump was turned on and the cross flow rate was ramped up to a value of 25 mL/min. Water was flushed through the module till approximately 150 mL of water was collected from the retentate line and 300 mL was collected from the filtrate line to ensure adequate removal of wetting and storage agents. The same procedure was then employed using the appropriate buffer solution to precondition the membrane module before performing filtration experiments

The membrane modules were cleaned with 0.1 N NaOH with a pH of 13. The cleaning step is very similar to the preconditioning step with the exception that the retentate and permeate lines are initially placed in the same reservoir and the pump was turned off after collecting 250 mL of cleaning solution in the waste container and the retentate line was placed back in the feed container. The pump was turned back on and sodium hydroxide solution was recirculated in the module for approximately 30 min. All membrane modules were stored at 4°C

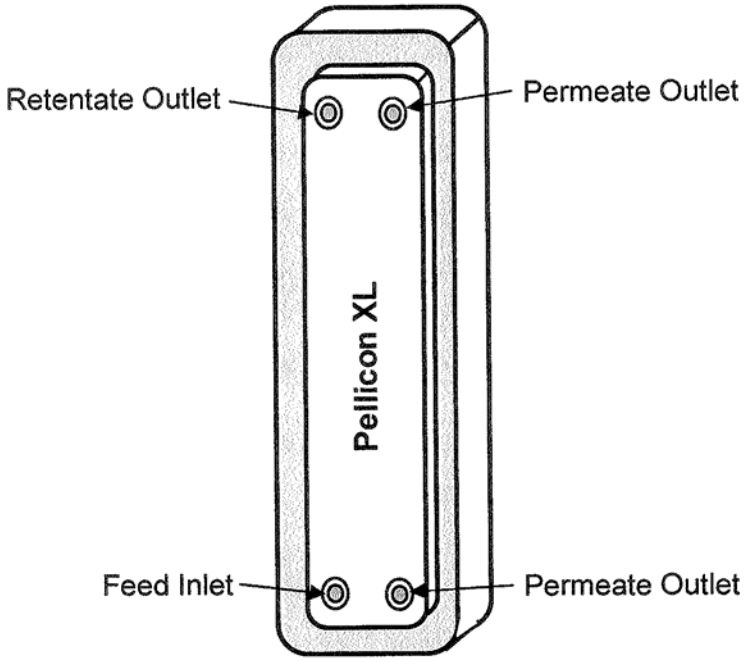

Figure **3.2**: Schematic of the Pellicon XL tangential flow filtration module

3.2.2 Charge Modification

Charge modification reactions with cellulose; usually involve etherification or esterification reactions of the modifying agent with the activated surface hydroxyl groups present in cellulose. The negatively charged version of the 100 kD membrane CRC membrane was used extensively in this study and they were made in our laboratory by the covalent attachment of negatively charged sulfonic acid groups to the surface of the membrane using the base-activated chemistry developed by van Reis (van Reis, R. 2001). Membranes were first flushed with approximately 100 L/m^2. The flat sheet membranes

were then equilibrated with 0.1 N NaOH and immersed in a 2 M solution of 3-Bromopropanesulfonic acid sodium salt (Catalogue #B2912, Sigma Chemical) in 0.1 N NaOH for a known amount of time. The charging reaction was found to be a function of reaction time and membranes with varying surface charge densities were made by varying the extent of charging time. The membranes were then flushed with approximately 100 L/m^2 distilled deionized water to quench the reaction. The reaction is as shown in Figure 3.3.

The 100 kD CRC membrane housed in the Pellicon XL tangential flow filtration module was also charged similarly with the charging solution, a 2 M solution of 3-Bromopropanesulfonic acid sodium salt (Catalogue #B2912, Sigma Chemical) in 0.1 N NaOH, was pumped through the module at a feed flow rate of 240 $L\ m^{-2}\ h^{-1}$ using a Rabbit-Plus peristaltic pump (Rainin Instrument Co., Emeryville, CA). Charging was done for 8 hours with the charging solution flushed through the system in total recycle mode. The membranes were flushed with approximately 100 L/m^2 of distilled water to quench the reaction and were then stored in 0.05 N NaOH until use.

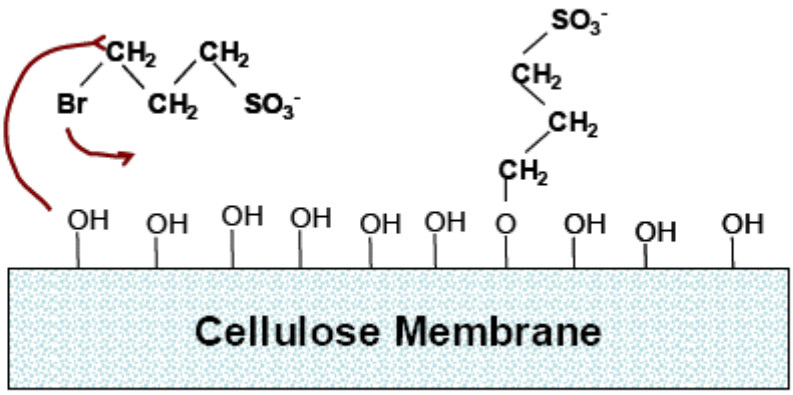

Figure **3.3**: Schematic of the mechanism of the charging reaction

3.2.3 Membrane Charge

The surface charge of the unmodified and the surface modified 100 kD CRC membranes were characterized by streaming potential measurements conducted using the apparatus shown in Figure 3.4. The device consists of two identical Plexiglas chambers which were approximately 2 cm in diameter and 2.4 cm in length. The ends of each chamber were threaded so as to provide a tight seal when they were screwed together. Ag/AgCl electrodes were then screwed tightly into the chambers (with O-rings in place to provide good sealing) to ensure reproducible placement of the electrodes relative to the membrane surface. The electrodes were typically 1- 2 mm away from the membrane surface. The Ag/AgCl electrodes were prepared by placing a 1 mm diameter silver wire (Sigma Chemical Co., St Louis, MO) and a reducing electrode in a 1 M KCl solution. The silver wire and the reducing electrode were connected to a DC source with the

current maintained at 20 mA for approximately 25 minutes to get a uniform deposition of Ag/AgCl layer on the wire surface.

The device was then assembled with the membrane sealed carefully between the two chambers. The chambers were then slowly filled with the appropriate salt solution taking care to remove any entrapped bubbles. A feed reservoir, which contained the same salt solution, was connected to the feed chamber and the exit from the other chamber being directed toward the drain. The system was pressurized by gravity head, i.e. adjusting the height of the feed reservoir and allowed to equilibrate till the system stabilized. After stabilization the transmembrane voltage (E_z) was measured using a high impedance 8060A True RMS Multimeter (Fluke Corp., Everett, WA) connected to two electrodes. Streaming potential measurements were obtained at discrete pressures with the system allowed to equilibrate at each pressure. Wilbert et al. (1999) have demonstrated that this approach gives more reproducible data than the use of a continuous pressure ramp as employed in most commercial zeta-potential devices. The membrane zeta potential was evaluated using the slope of a plot of the streaming potential as a function of applied pressure. The membrane charge was calculated from the zeta potential obtained from the streaming potential measurements.

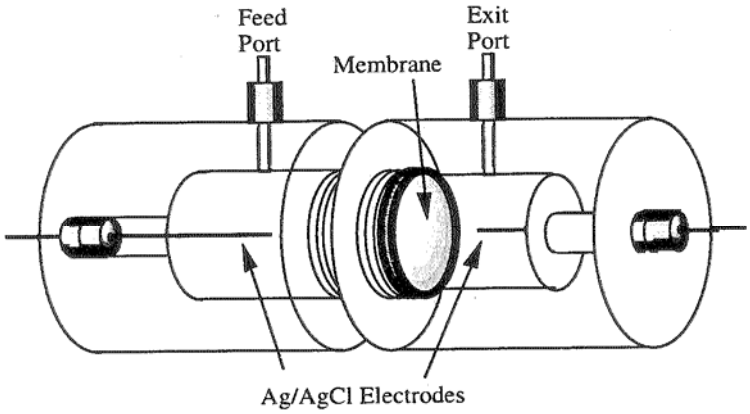

Figure 3.4: Schematic of the streaming potential apparatus

3.3 Model Proteins

Initial experiments were performed using bovine serum albumin (Fraction V heat shock precipitated BSA, catalogue # A 7906 from Sigma Chemical, St. Louis, MO). Due to lot to lot variability in fatty acid content later experiments were conducted using BSA (> 96%, essentially fatty acid free, catalogue # A-6003 from Sigma Chemical, St. Louis, MO). BSA has an isoelectric point (pI) of approximately 4.9 and a molecular weight of 69 kD. BSA was chosen as the model target protein because the protein has significant interactions with Cibacron Blue. Ovalbumin (catalogue # A-5503, Grade V, minimum 98%, agarose gel electrophoresis, from Sigma Chemical, St. Louis, MO) has an isoelectric point (pI) of approximately 4.5 and a molecular weight of 44 kD was picked as the model target impurity because of its limited interactions with Cibacron Blue. Table 3.1 summarizes some of the important physico-chemical properties of both the model

target and impurity. More detailed information on the protein charge characteristics are provided in the appropriate chapters of this thesis.

Table 3.1: Physico-chemical properties of the model protein

Property	BSA	Ovalbumin
Molecular Weight (kD)	67	44
Isoelectric pH	4.9	4.5
Hydrodynamic Radius (nm)	3.45	3.0

3.4 Model Ligand

Cibacron Blue 3GA (Catalogue # C-9534, Sigma Chemical) was used as the small affinity ligand in this work, due to extensive previous work using this dye for numerous affinity chromatographic separations. The molecular structure of Cibacron Blue is shown in Figure 3.5. Cibacron Blue has a molecular weight of 0.774 kD and contains three sulfonic acid groups attached to an aromatic ring structure. Cibacron Blue interacts with proteins through a combination of electrostatic, hydrophobic and hydrogen binding forces. The binding of Cibacron Blue will yield a product-dye complex that is significantly more negatively charged than the native protein.

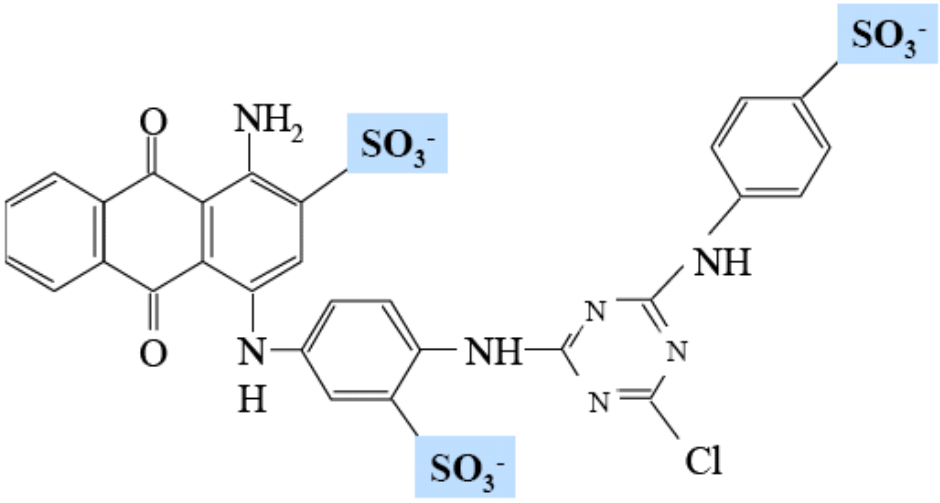

Figure 3.5: Molecular formula of Cibacron Blue

3.5 Preparation of Salt and Protein Solutions

Buffer solutions were prepared by dissolving pre-weighed amounts of the appropriate salts in deionized water obtained from a NANOpure Diamond water purification system (Barnstead Thermolyne Corporation, Dubuque, IA) with a resistivity greater than 18 MΩ–cm. All salts were analytical reagent grade. An acetate buffer composed of CH_3COONa and CH_3COOH (EM Science, Gibbstown, NJ) was used for experiments at pH 5.0, a Bis-Tris buffer (Sigma Chemical, St. Louis, MO) with added HCl (EM Science, Gibbstown, NJ) was used at pH 6.0 and 7.0, and a Tris buffer (Sigma Chemical, St. Louis, MO) with HCl was used at pH 8.0. The solution pH was measured using a 420APlus pH meter (Thermo Orion, Beverly, MA). The ionic strength was

adjusted by adding NaCl (Mallinckrodt Baker, Inc., Phillipsburg, NJ), with the solution conductivity measured using a 105A plus conductivity meter (Thermo Orion, Beverly, MA). All buffer solutions were prefiltered through 0.2 μm pore size Super-200 membranes (Pall Corp., Ann Arbor, MI) to remove particulates and undissolved salts.

Protein solutions were prepared by slowly dissolving the protein powder in the desired buffer. Protein ligand solutions were made by slowly mixing appropriate amounts of protein and ligand solutions to yield a protein-dye solution of known ligand and protein concentration. The resulting solution was filtered through a 0.22 μm syringe filter (Costar Corp., Cambridge, MA) to remove any protein aggregates immediately prior to use. Protein solutions were used within 24 hours to minimize the likelihood of protein aggregation or denaturation during storage.

3.6 Stirred Cell

A schematic of a typical stirred cell is shown in Figure 3.6. All filtration experiments which used flat sheet membranes were done using a 2.5 cm diameter Amicon 8010 ultrafiltration stirred cell (Millipore Corp. Bedford, MA). The membrane is housed in the stirred cell and is placed skin up i.e. the skin surface facing the solution in the stirred cell. A rubber O-ring was placed between the membrane and the sleeve to form a leak free seal. The entire apparatus was then filled with the appropriate solution, taking care to remove any entrapped bubbles. The transmembrane pressure was set by varying the applied pressure by air pressurization. The pressure on the filtrate side was

atmospheric. The stirrer speed was set using a Strobotac Type 1531-AB phototachometer (General Radio Co., Concord, MA).

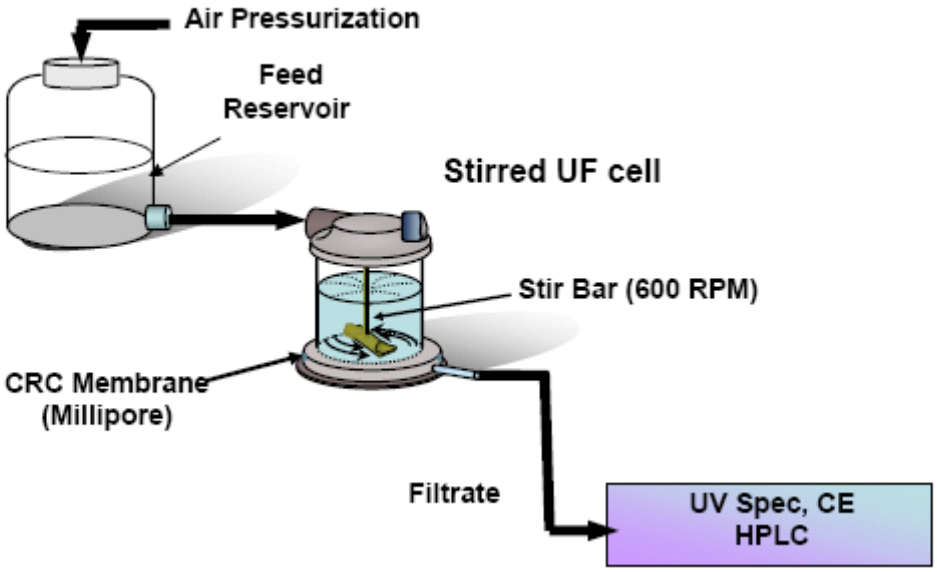

Figure **3.6**: Schematic of the experimental set up using a stirred cell

3.6.1 Hydraulic Permeability

The membrane hydraulic permeability was evaluated by measuring the flow rate of a buffer solution through the membrane as a function of the applied transmembrane pressure drop. Filtrate flow rates were calculated using a timed collection with the filtrate mass determined using a Sartorius digital balance with accuracy of ± 1 mg (Model 1518 Sartorius, Westbury, NY). The transmembrane pressure was varied over a range of 1-5

psi to prevent membrane compression at higher pressures. Hydraulic permeability measurements were typically performed before and after each protein sieving experiment.

3.6.2 Binding Experiments

Binding constants for the BSA-Cibacron Blue system or ovalbumin-Cibacron Blue system was evaluated using an Amicon 8010 stirred cell which housed an appropriate nominal molecular weight cut-off CRC membrane that was fully retentive to the protein. A 10 kD membrane was used for ovalbumin and BSA in high ionic strength buffers and a 30 kD CRC membrane was chosen for all other experiments with BSA. The stirred cell was filled with a mixture of known concentration of BSA and ligand which had been premixed earlier and had been allowed to equilibrate. The cell was then placed on a magnetic stirrer and the stirring speed was set to 600 rpm using a Strobotac 1531-AB phototachometer (General Radio Co., Concord, MA). The stirring minimized the effect of concentration polarization in the vicinity of the membrane surface. The device was then air pressurized to $\Delta P = 21$ kPa (3 psig), and small samples were withdrawn through the membrane for off-line analysis of the free Cibacron Blue concentration. Data were also obtained with pure Cibacron Blue (in the absence of BSA) to evaluate the sieving coefficient of free Cibacron Blue through the 30 kD membrane. These experiments were repeated for a range of Cibacron Blue concentrations for each protein concentration using the same solution conditions to evaluate the binding curves.

3.6.3 Protein Sieving Experiments

Actual sieving experiments were performed in an 8010 Amicon stirred cell which housed the 2.5 cm diameter membrane. The cell was then filled with an appropriate protein solution and the stirring speed was set at 600 RPM using a Strobotac Type 1531-AB strobe light, and the device was air pressurized to the desired value. After the hydraulic permeability of the membrane was evaluated, the stirred cell was then emptied and refilled with a protein - Cibacron Blue solution at the desired ionic strength and pH. The stirrer was reset, the cell was air-pressurized, and the filtrate flux was determined by timed collection using a digital balance (Model AG104, Mettler Toledo, Columbus, OH) with an accuracy of 0.1 mg. A minimum of 500 μL of filtrate was flushed through the membrane to ensure washout of the dead volume beneath the membrane at the bottom of the stirred cell. A 200 μL filtrate sample was then collected for subsequent analysis of the protein and Cibacron Blue concentrations. The filtrate port was immediately clamped and a small (approximately 200 μL) sample of the bulk solution was obtained directly from the stirred cell. Protein concentrations in the filtrate and the bulk samples were evaluated using appropriate diagnostic techniques. The stirred cell was then emptied, rinsed, and refilled with buffer, with the hydraulic permeability of the used membrane evaluated to provide a measure of the extent of fouling. All experiments were performed at room temperature (22 ± 3°C) and conducted in duplicate.

3.6.4 Diafiltration (Stirred Cell)

The actual separation of ovalbumin and BSA was performed using the Amicon stirred cell operated in diafiltration mode. Effective protein separations are accomplished using a diafiltration mode, in which impurities are washed away from the desired product by continuous addition of diafiltrate buffer. The stirred cell was initially filled with 10 ml of the protein mixture. A separate reservoir was filled with a buffer solution (without protein or dye) and attached to the stirred cell with silicone tubing. The filtrate velocity was maintained at nearly a constant value over the course of the diafiltration by a peristaltic pump connected to the filtrate line. The filtrate flux created a vacuum in the stirred cell causing fresh buffer from the reservoir to be drawn into the cell from the solution reservoir at a rate equal to the volumetric filtration rate. Filtrate samples were collected throughout the experiment with periodic samples taken directly from the stirred cell to evaluate the protein concentrations in the retentate.

3.7 Tangential Flow Filtration

Pellicon XL tangential flow filtration modules described in Section 3.2 of this chapter were used in all filtration experiments performed in tangential flow filtration (TFF) mode. All membranes were thoroughly flushed with deionised distilled water and appropriate buffer solution prior to each use. The membrane modules were cleaned with 0.1N NaOH solution by recirculating the solution at a flow rate of 25 ml/min for 30-45 minutes. The membrane modules were then sealed and stored at 4°C.

3.7.1 Protein Sieving Experiments

Initial experiments were performed using total recycle mode to determine optimal conditions for protein separation. Figure 3.7 shows a schematic of the experimental set-up. The feed tank was filled with the appropriate protein solution, and was then pumped through the membrane module using a Rabbit-Plus peristaltic roller pump (Rainin Instrument Co., Emeryville, CA) with both the filtrate and retentate lines recycled back to the feed tank to maintain a constant protein concentration. The filtrate velocity was estimated by a timed collection of the filtrate. Filtrate and bulk samples were collected for subsequent analysis.

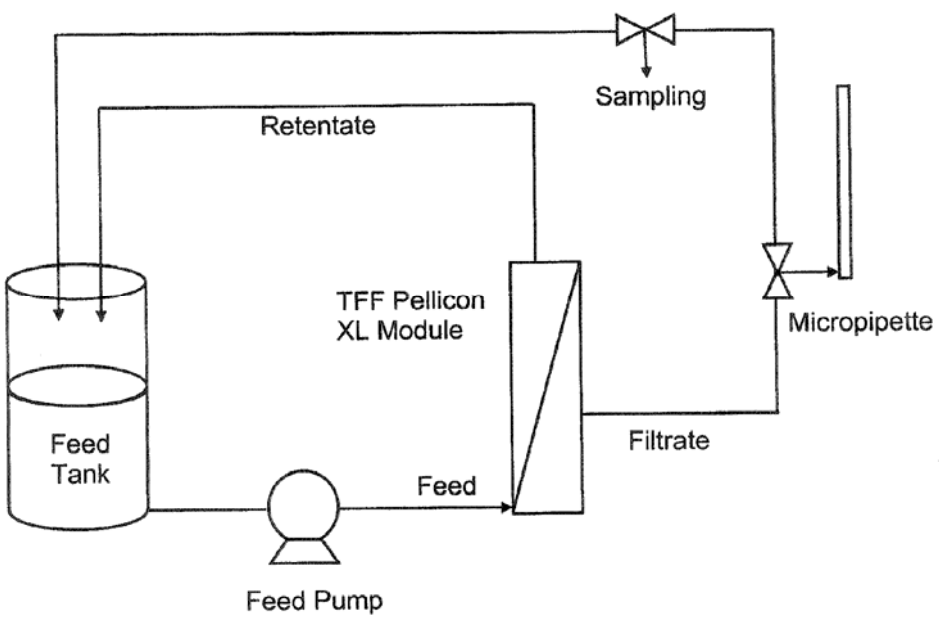

Figure 3.7: Schematic diagram of the tangential flow filtration apparatus in total recycle mode

3.7.2 Diafiltration

A schematic of a typical constant retentate volume diafiltration experimental set up is shown in Figure 3.8. The feed tank is filled with a known volume of a known concentration of protein and ligand. The inlet flow was pumped through the module using a peristaltic pump at a known flow rate flow rate typically set to 300 L m^{-2} h^{-1} (volumetric flow rate normalized by the membrane area). Initially, the filtrate and retentate lines were both returned to the feed tank, providing total recycle until the system had stabilized (typically 10 min). At this point, the diafiltration was begun, with the filtrate directed to a second collecting vessel. The total fluid volume in the feed tank was maintained at a constant level by continuous addition of fresh diafiltration buffer at a rate equal to the ultrafiltration rate. Samples were taken from the feed and filtrate reservoir at appropriate time points throughout the diafiltration for subsequent analysis of the protein concentrations. Additional experimental details are described in subsequent chapters.

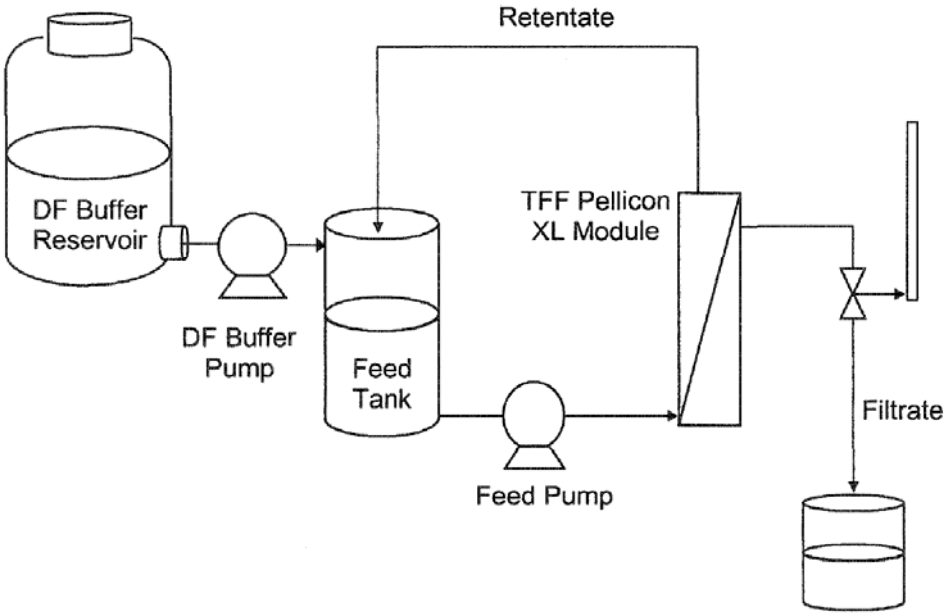

Figure **3.8**: Schematic of the diafiltration set up using the tangential flow filtration mode

3.8 Protein and Ligand Diagnostics

3.8.1 UV/VIS Spectrophotometry

Concentrations of the individual proteins, BSA and ovalbumin in the absence of the dye were determined spectrophotometrically with a UV-VIS spectrophotometer (UV mini 1240, Shimadzu, Kyoto, Japan) using the natural absorbance at 280 nm. Actual concentrations were evaluated by comparison of the measured absorbance with that of

standard solutions of known concentrations. The calibration curves for BSA and ovalbumin are shown in Figure 3.9.

Cibacron Blue concentrations were also determined spectrophotometrically using the natural absorbance at 616 nm. The presence of protein had no effect on the absorbance of the dye at 616 nm over the range of concentrations examined in this study. The calibration curve for Cibacron Blue is shown in Figure 3.10.

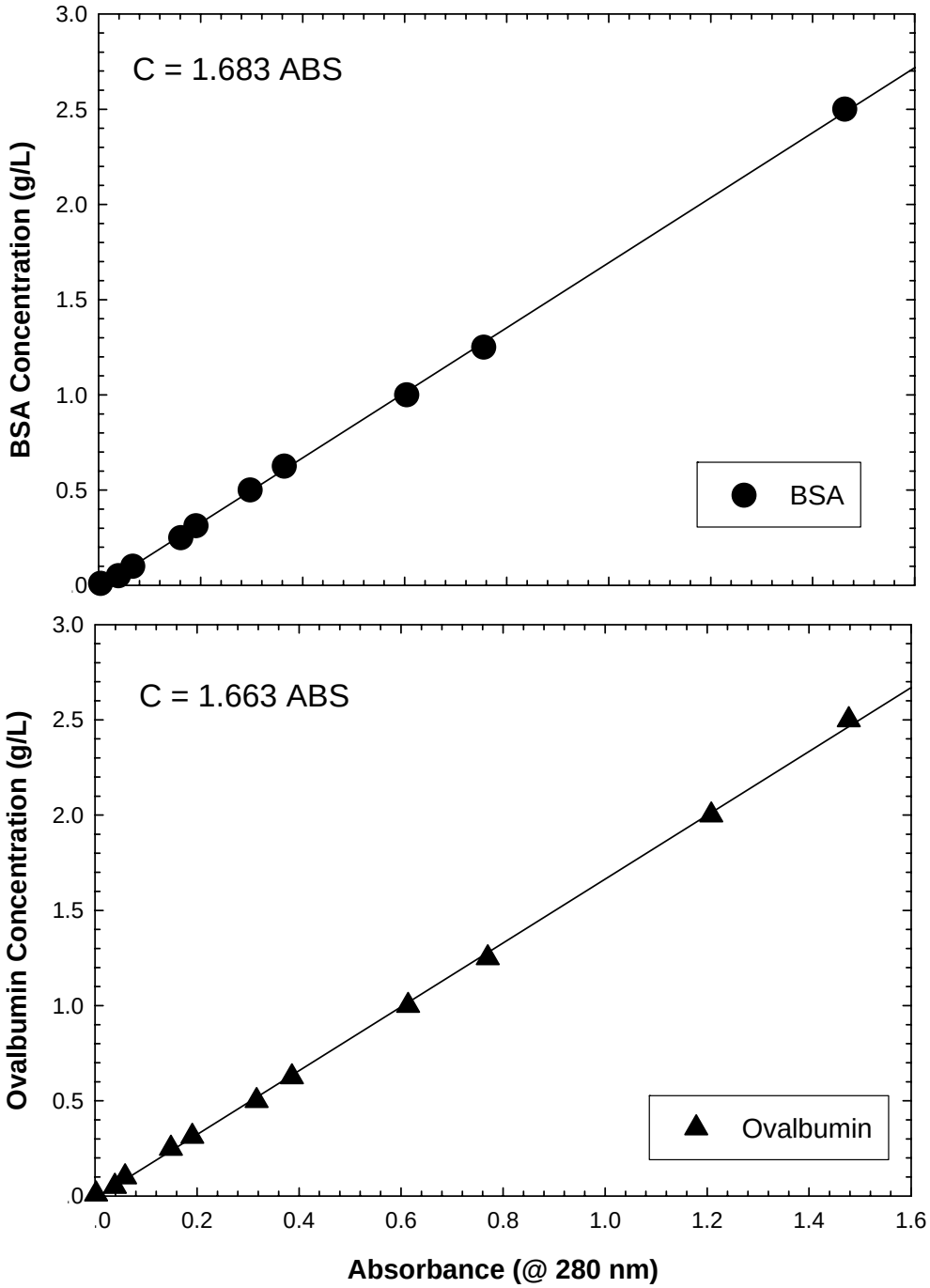

Figure **3.9**: Calibration curve for BSA (top panel) and ovalbumin (lower panel using the UV spectrophotometer.

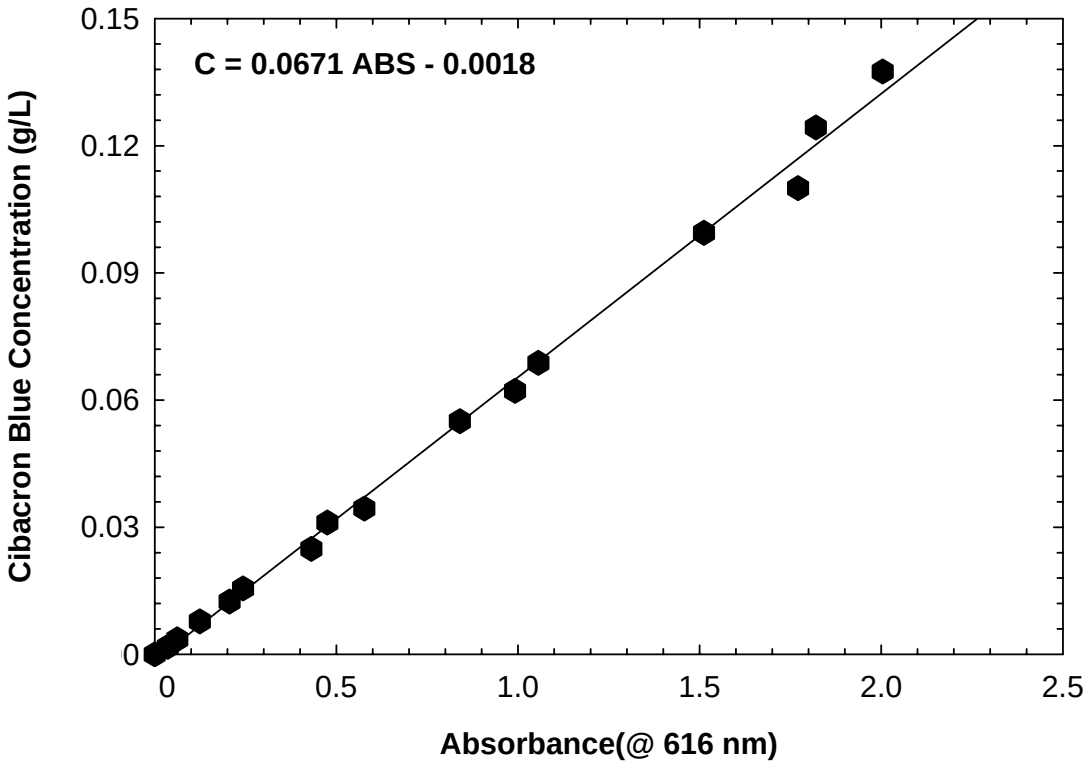

Figure **3.10**: Calibration curve for Cibacron Blue using the UV spectrophotometer.

3.8.2 Capillary Electrophoresis

BSA and ovalbumin concentrations in the presence of Cibacron Blue were evaluated by capillary zone electrophoresis since the strong color of Cibacron Blue interfered with the absorbance measurements. A schematic of the set up is shown in Figure 3.11. A Model G1600A High Performance Capillary Electrophoresis instrument (Agilent Technologies, Palo Alto, CA) equipped with a dual-polarity variable high

voltage DC supply and variable wavelength UV-VIS diode array detector was used. Capillary electrophoresis was performed using fused silica capillaries with an inner diameter of 50 μm and an effective length of 72 cm (Catalogue # G 1600-62211, Agilent Technologies, Palo Alto, CA). The applied voltage was maintained at 25 kV, and a 20 mM borate buffer at pH 9.3 (Catalogue # 8500-6782, Agilent Technologies, Waldbronn, Germany) was used as the running buffer. Protein detection was at a wavelength of 195 nm, with the protein concentration determined by numerical integration of the area under the corresponding peak. The absorbance data was analyzed using Agilent ChemStation software using a Dell Celeron computer. Actual concentrations were evaluated using previously constructed calibration curves determined for the protein in the presence of Cibacron Blue. The calibration curve is shown in Figure 3.12.

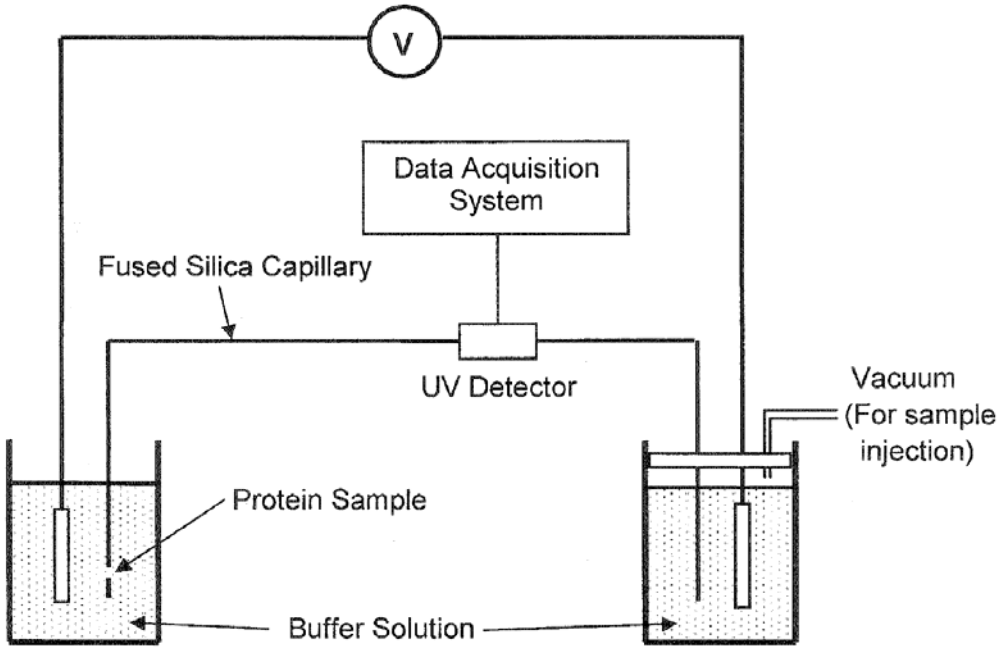

Figure **3.11**: Schematic of capillary electrophoresis apparatus

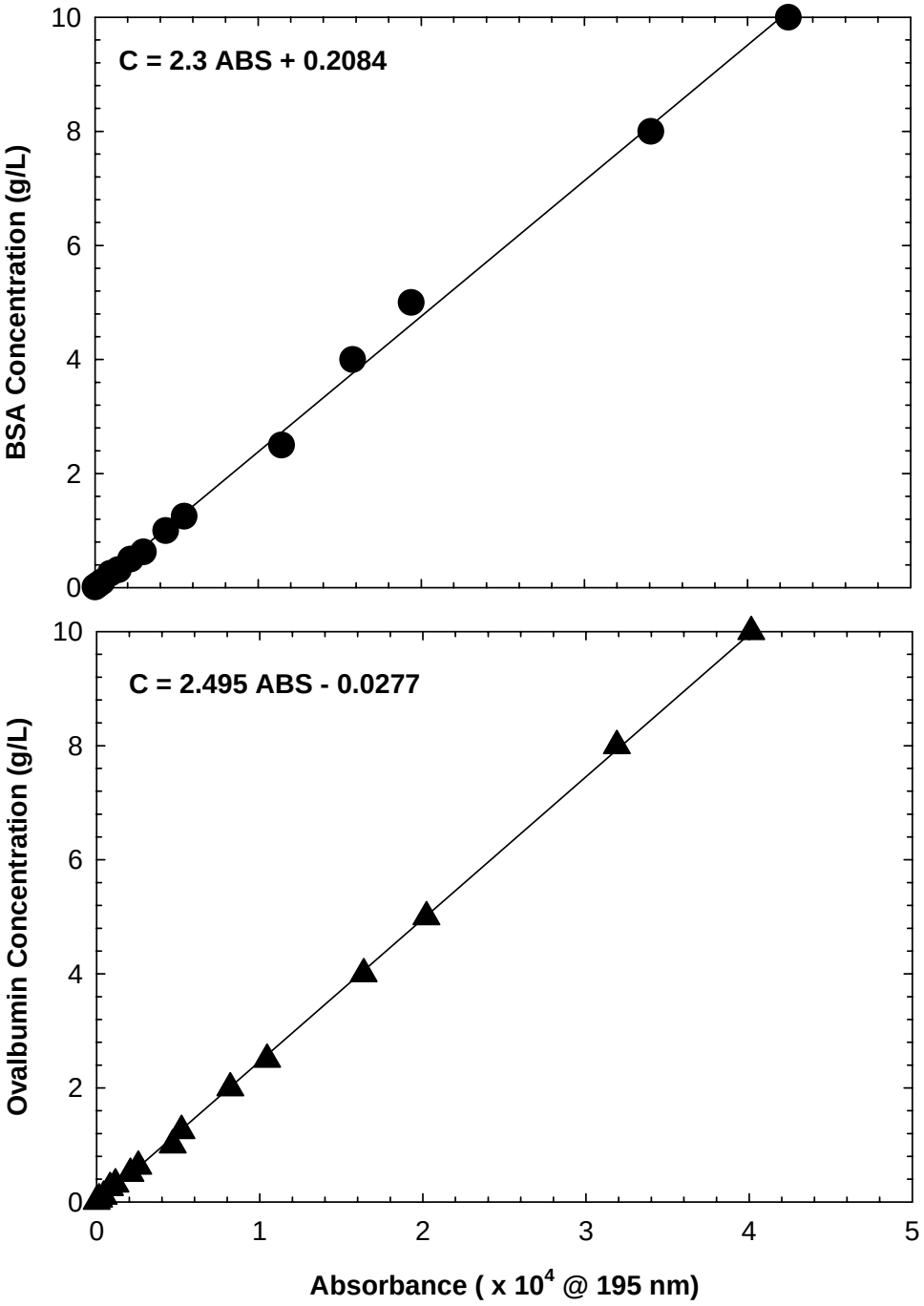

Figure **3.12**: Calibration curve for BSA (top panel) and ovalbumin (lower panel) using capillary electrophoresis

3.8.3 Size Exclusion Chromatography

Protein concentrations in the binary mixture were analyzed by size exclusion (SEC) chromatography (Agilent 1100 series quaternary HPLC system). A schematic of the SEC apparatus is shown in Figure 3.13. Assays were performed using a Superdex 75 column with 13 μm particle size and 10^5 MW exclusion limit (GE Healthcare, Piscataway, NJ). Column calibration was done using binary protein solutions of known concentration. The column was first equilibrated with fresh buffer at a flow rate of approximately 0.3 mL/min for 180 minutes. This also served to flush both the sample and reference cells in the refractive index detector (Agilent 1100 series). Column equilibration was confirmed by tracking the base line refractive index (RI). The mobile phase was a 50 mM phosphate buffer with 0.15 M NaCl at a flow rate of 0.2 mL/min. Protein samples (50 μl) were injected by an autosampler with the data analyzed using Agilent ChemStation software on a Dell Celeron Computer. Figure 3.14 shows a typical SEC chromatogram of a binary mixture of 2 g/L BSA and 1 g/L ovalbumin. Figure 3.15 shows the calibration curves for BSA and ovalbumin.

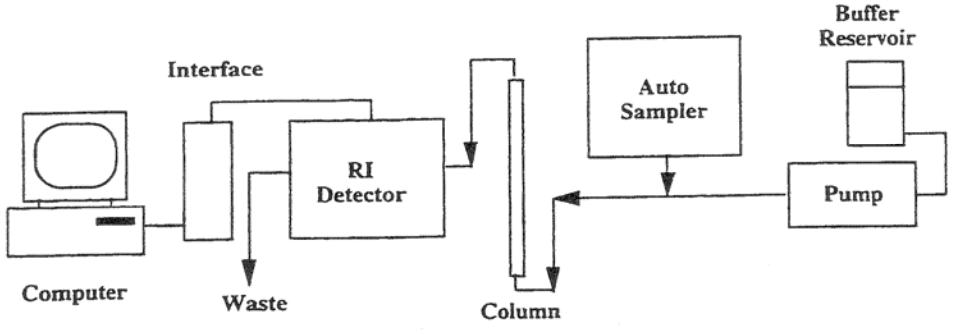

Figure 3.13: SEC apparatus

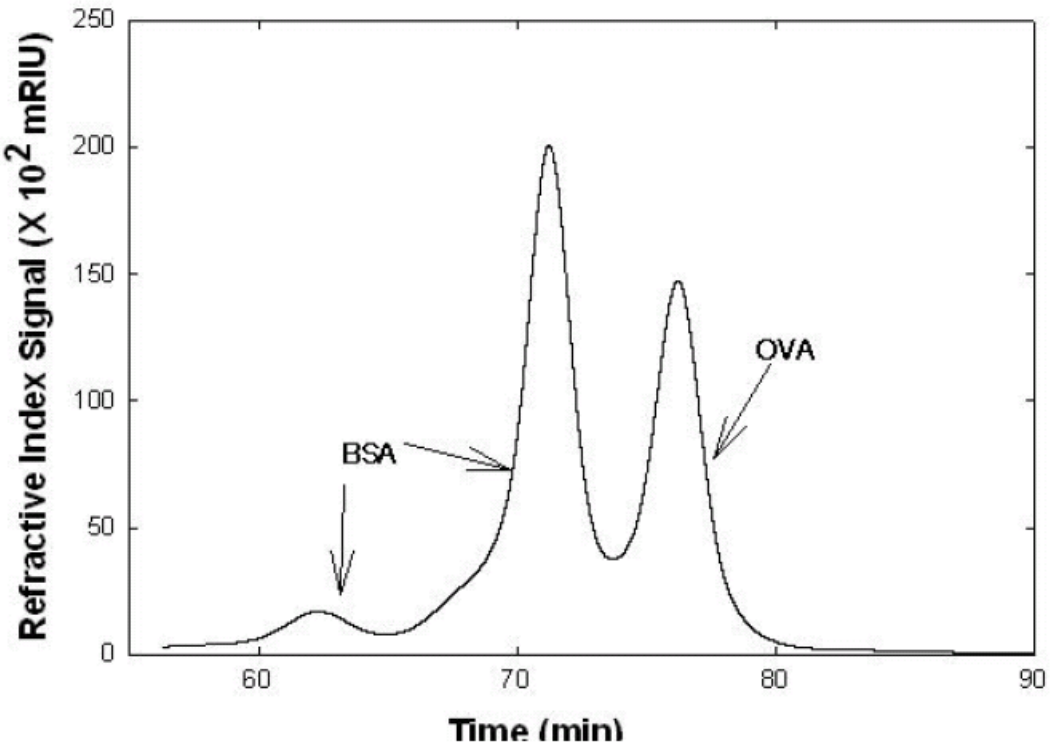

Figure **3.14**: Typical SEC chromatogram for a binary protein mixture of 2 g/L BSA and 1 g/L ovalbumin.

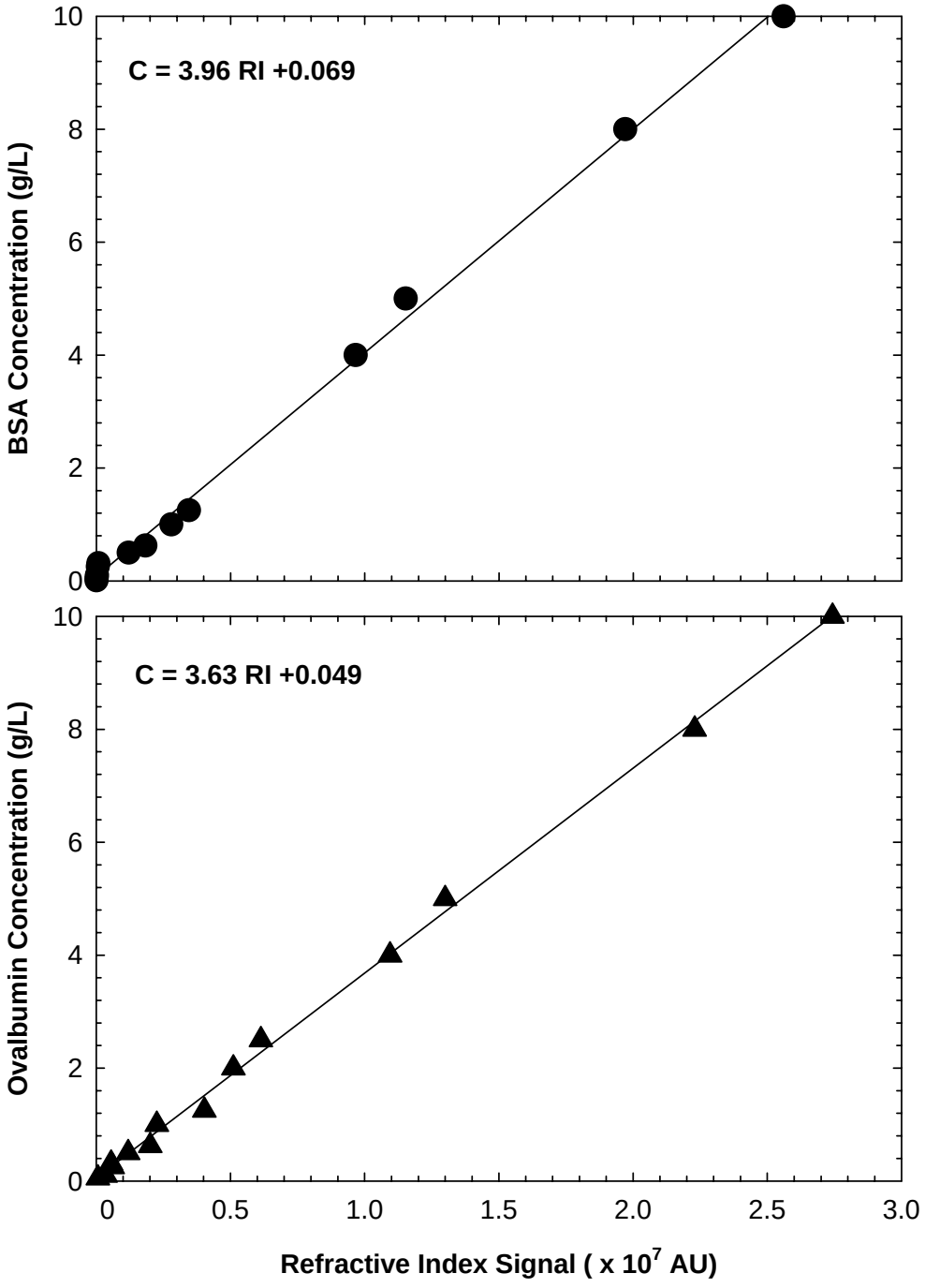

Figure **3.15**: Calibration curve for BSA (top) and ovalbumin (lower panel) using SEC

Chapter 4

BINDING INTERACTIONS BETWEEN CIBACRON BLUE AND ALBUMINS

4.1 Introduction

Cibacron Blue is very well established as an affinity ligand in chromatographic separations; it is probably the most widely used ligand in the field of dye affinity chromatography. The ability of Cibacron Blue to bind different proteins was discovered serendipitously by Haeckel et al. in 1968 based on their observations of anomalous retention of yeast pyruvate kinase in size exclusion chromatography (SEC) experiments performed with a Sephadex G-200 column, where Blue Dextran was used as the large size marker to evaluate the external void volume in the SEC column (Lowe, 1987). Blue Dextran is formed by conjugating a large molecular weight dextran with Cibacron Blue. Subsequent SEC experiments performed in the absence of the Blue Dextran gave the expected enzyme retention times, consistent with the ability of the Blue Dextran to bind the enzyme and hence change its retention characteristics (Haeckel et al., 1968). This accidental discovery spurred numerous studies of the interactions between Blue Dextran and a variety of other proteins including several plasma proteins, interferons, dehydrogenases, and kinases.

The early work on Blue Dextran binding clearly demonstrated that it was the chromophore, Cibacron Blue, and not the dextran that was responsible for protein binding (Kopperschlager et al., 1968; Kopperschlager et al., 1971). Subsequent studies were conducted with gel filtration media made by immobilizing Blue Dextran within the media

such as Sepharose (Easterday and Esterday, 1974), polyacrylamide (Kopperschlager, et al., 1971), and agarose (Easterday and Esterday, 1974; Ryan and Vestling, 1974). The resulting columns could be used to purify glutathione reductases (Staal et al.,, 1969), yeast phosphofructokinase (Kopperschlager et al.,, 1971), human erythrocyte pyruvate kinase (Blume et al., 1971), and blood coagulation Factors II,VII, IX, and X (Swart and Hemker, 1970).

Cibacron Blue interacts with proteins through a combination of electrostatic, hydrophobic, and hydrogen bonding forces. It is thought that the versatility of the molecule to bind various proteins arises from the combination of sulphonic acid (ionic) and aromatic (non polar) groups in the same molecule (Subramanian, 1984). Several investigators have shown that Cibacron Blue binds to a dinucleotide binding domain (the dinucleotide fold) with the anthraquinone, diaminobenzenesulphonate, and triazine groups adopting positions similar to the adenine, adenyl, ribose, and pyrophosphate groups of the co-factor NAD^+ (Biellmann et al., 1979). However Cibacron Blue is also able to interact with many proteins that lack this dinucleotide binding domain.

Serum albumin is the dominant plasma protein (by mass), and it plays a key role in the transport of fatty acids, bilirubin, tryptophan, calcium ions, steroid hormones, and other physiologically important molecules. Serum albumins are able to function as transport proteins because of their ability to bind a wide range of ligands, with these binding interactions having a significant effect on the physiological transport, clearance, modulation, and inactivation of many small molecules. Numerous studies have been conducted to understand small molecule binding to serum albumins from a variety of species. Albumins are able to bind target molecules due to a combination of electrostatic,

van der Waals, hydrogen bonding, and hydrophobic interactions. Goldstein (1949) published an excellent review of the early work done to understand the binding of fatty acids, dyes, drugs, bilirubin, and small ions to albumin.

The exact binding interactions between the various serum albumins and Cibacron Blue are still not completely understood. Leatherbarrow and Dean (1980) demonstrated that immobilized Cibacron Blue interacts strongly and specifically with the three bilirubin sites on human serum albumin (HSA). Dockal et al, (1999) showed that the three recombinant domains in HSA could all be purified using Cibacron Blue affinity chromatography, demonstrating that each domain has specific binding sites for Cibacron Blue. In addition it has been shown that Cibacron Blue can bind to multiple fatty acid binding sites on certain albumins. This is of particular importance for bovine, sheep, and horse albumins since no interaction is seen with the dye and the bilirubin binding sites on these proteins. Compagnini et. al. (1996) found that the binding of Cibacron Blue to HSA increased from 3 moles of ligand bound per mole of protein at a pH 7 to 7.5 molecules of Cibacron Blue at a pH of 4.5 suggesting the importance of ionic interactions. Lascu et al. (1984) found that ovalbumin does not interact with Cibacron Blue immobilized to Blue Sepharose despite the relatively strong homology between ovalbumin and many of the serum albumins.

A number of affinity chromatographic columns with Cibacron Blue as the affinity ligand are available commercially including HiTrap Blue from Amersham Biosciences and Affi-Gel Blue from Biorad. Cibacron Blue is particularly attractive as an affinity ligand since it binds a large number of proteins, it is relatively inexpensive compared to most biological ligands, it is chemically stable over a broad range of solution conditions,

and it is easily immobilized via the reactive chlorine on the triazine ring. In vitro toxicity assays indicate that Cibacron Blue has no effect on the viability of HeLa cells, human fibroblasts, or E. Coli. Most of these advantages will also hold true when using Cibacron Blue as a ligand in free solution. In addition, Cibacron Blue has three negatively charged groups and hence its binding will result in a significant shift in the surface charge of the protein.

The objective of the studies described in this Chapter was to obtain quantitative data on the binding interactions between Cibacron Blue and BSA in free solution, with the goal of identifying conditions that provided strong binding that could be exploited in subsequent affinity ultrafiltration experiments. Binding studies were also performed with ovalbumin to verify that there was minimal binding of the Cibacron Blue to ovalbumin. In addition, data were obtained for the dissociation of the dye from BSA, a critical step if this dye were to be used for actual protein purification.

4.2 Material and Methods

Initial experiments were performed using bovine serum albumin (Fraction V heat shock precipitated BSA, catalogue # A 7906 from Sigma Chemical, St. Louis, MO). Later experiments were performed using essentially fatty acid free BSA (> 96% pure, catalogue # A-6003 from Sigma Chemical, St. Louis, MO) to eliminate variability associated with different levels of fatty acids for the Fraction V product.

Cibacron Blue 3GA (Catalogue # C-9534, Sigma Chemical), which has a molecular weight of 0.774 kD and contains three negatively-charged sulphonic acid groups, was used as the small affinity ligand.

Protein solutions were prepared by slowly dissolving the protein powder in the appropriate buffer, with the resulting solution filtered through a 0.22 μm syringe filter (Costar Corp., Cambridge, MA) to remove any protein aggregates immediately prior to use. Protein and dye concentrations were evaluated using the assays described in Chapter 3.

The binding interactions between each protein and Cibacron Blue were evaluated using the ultrafiltration method which allowed protein-free samples to be collected directly through a semipermeable membrane that was fully retentive to the protein of interest (Chapter 3). Experiments were performed using Ultracel composite regenerated cellulose membranes (Millipore Corp., Bedford, MA) having nominal molecular weight cut offs of 30 kD for BSA or 10 kD for ovalbumin.

4.3 Binding Analysis

The amount of bound Cibacron Blue was determined from a simple mass balance:

$$C_{bound} = C_{total} - C_{free} \qquad \textbf{(4.1)}$$

where the total concentration of Cibacron Blue in the solution was evaluated directly from the mass of dye added to the known volume of buffer. The concentration of free Cibacron Blue was calculated as:

$$C_{free} = \frac{C_{filtrate}}{S_o} \tag{4.2}$$

The observed sieving coefficient for free Cibacron Blue (S_o), which is defined as the concentration of Cibacron Blue in the filtrate to that in the bulk solution, was evaluated immediately prior to performing the binding experiment using the same concentration of pure Cibacron Blue that was added to the protein solution but without any protein present.

Previous studies have shown that Cibacron Blue binds to BSA only at fatty acid binding sites (Leatherbarrow and Dean, 1980), suggesting that the binding data might be effectively fit using a simple multisite Langmuir-type binding isotherm of the form:

$$C_{bound} = \frac{nK_{eq}C_{protein}C_{free}}{1 + K_{eq}C_{free}} \tag{4.3}$$

where n is the number of moles of Cibacron Blue bound per mole of BSA, K_{eq} is the equilibrium binding constant, and $C_{protein}$ is the total concentration of protein in the solution. Values of the binding parameters were obtained by fitting the experimental data using a non-linear least squares (NNLS) Marquardt-Levenberg algorithm, with the individual data points weighted by the inverse of the standard error for each measurement.

Protein binding experiments were performed for both the individual protein solutions and with binary mixtures of BSA and ovalbumin. In the latter experiments, the amount of bound Cibacron Blue was analyzed using a 2-site competitive binding model:

$$C_{bound} = \frac{n_{BSA} K_{BSA} C_{BSA} C_{free}}{1 + K_{BSA} C_{free}} + \frac{n_{OVA} K_{OVA} C_{OVA} C_{free}}{1 + K_{OVA} C_{free}} \quad \textbf{(4.4)}$$

The concentration of free Cibacron Blue was calculated by simultaneously solving Equation (4.4) and the overall mass balance for Cibacron Blue in the system.

4.4 Binding Results

Typical experimental data for Cibacron Blue binding to BSA at pH 5.0, 10 mM ionic strength, over a range of BSA concentrations are shown in Figures 4.1 and 4.2. The x-axis represents the concentration of free Cibacron Blue, which was evaluated directly from the measured filtrate concentrations using Equation (4.2). The observed sieving coefficient for free Cibacron Blue (S_o) was evaluated immediately prior to performing the binding experiment using the same concentration of pure Cibacron Blue that was added to the protein solution assuming that the transmission of free (unbound) Cibacron Blue was unaffected by the presence of the protein. This behavior was confirmed experimentally from limited data obtained with a neutral CRC 100 kD membrane that was non-retentive to the free dye but slightly permeable to both BSA and the protein-dye complex. The sieving coefficient for Cibacron Blue in the presence of BSA was evaluated using only the concentration of free Cibacron Blue and not the total concentration of Cibacron Blue to account for the ligand bound to the protein. The sieving coefficient for free Cibacron Blue in all cases was close to one indicating that the transmission of Cibacron Blue was not affected by the presence of protein.

The sieving coefficient of free Cibacron Blue through the 30 kD membrane varied from 0.53 for a 0.28 g/L solution to 0.80 for a 8.3 g/L solution, all in 10 mM acetate buffer at pH 5.0. The small degree of retention of Cibacron Blue was due to the electrostatic repulsion between the highly charged dye and the small number of negatively-charged groups on the cellulose membrane, which has a surface charge of approximately -0.0006 C/m^2 under the conditions of these experiments as calculated from streaming potential measurements described in more detail in Chapter 5. The extent of electrostatic exclusion decreases as the Cibacron Blue concentration increases due to the corresponding increase in the solution ionic strength. This phenomenon is discussed in more detail by (Shao and Zydney, 2004). There was no evidence of any leakage of the 69 kD BSA through the 30 kD membrane, as determined by capillary electrophoresis of the filtrate samples, for any of the experimental conditions examined in this study.

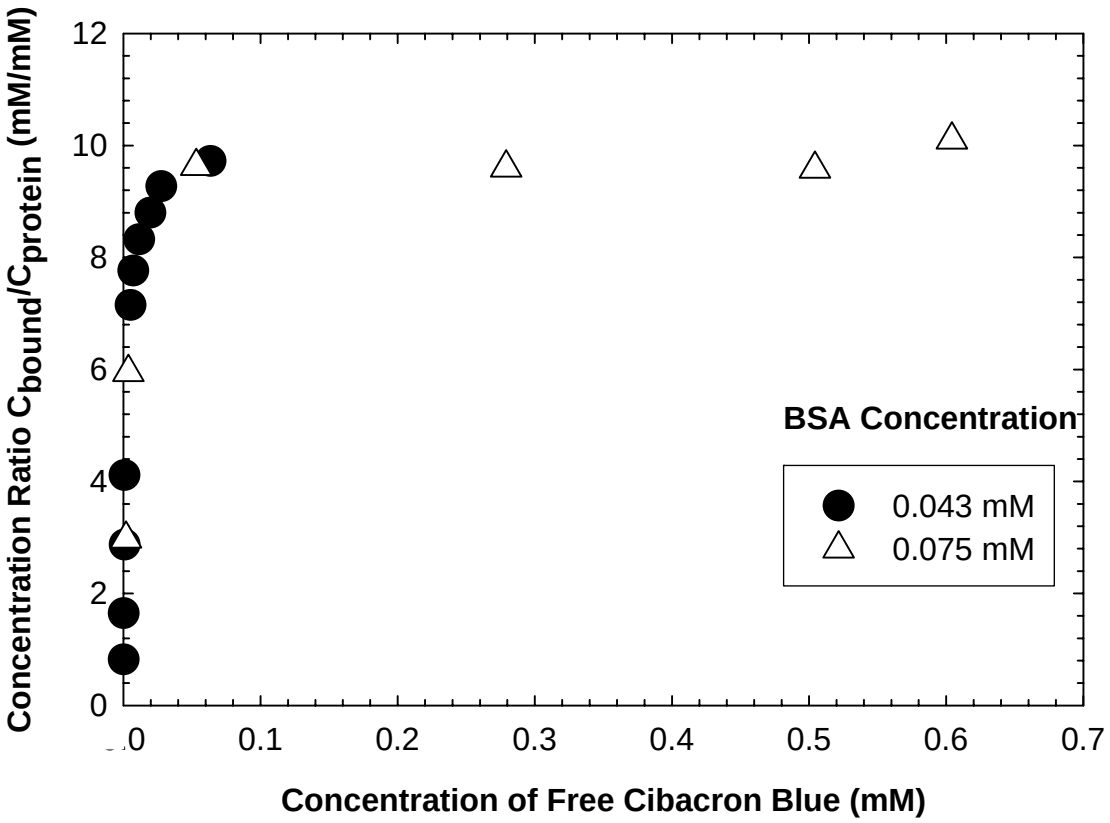

Figure **4.1**: Binding data for Cibacron Blue and BSA at two BSA concentrations of 3 g/L (0.043 mM) and 5 g/L (0.075 mM) at pH 5.0, 10 mM

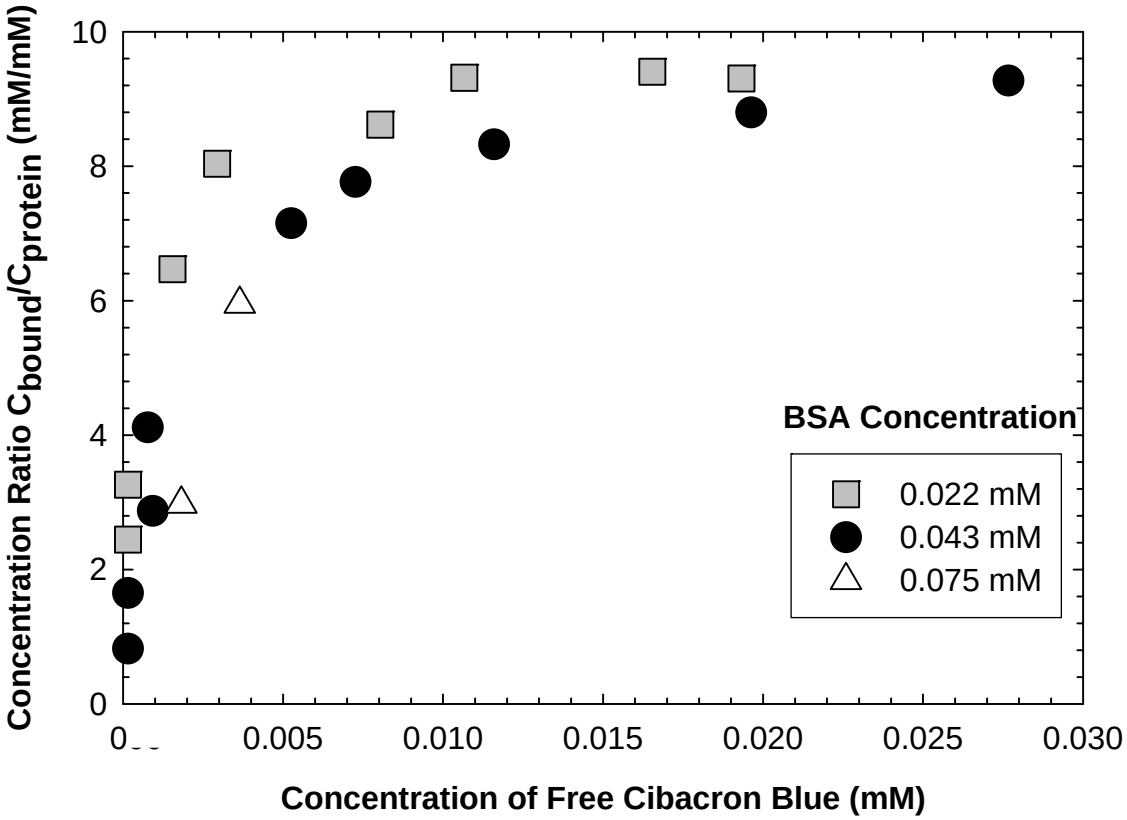

Figure **4.2:** Binding data for Cibacron Blue and BSA for three different protein concentrations. Data are shown over a narrow range of free Cibacron Blue concentrations to capture the low concentration regime in the binding profile. All experiments were performed at a solution pH 5.0 and10 mM ionic strength.

The y- axis in Figures 4.1 and 4.2 shows the concentration of bound Cibacron Blue normalized by the protein concentration used in the particular binding experiment. The amount of bound Cibacron Blue was determined from a simple mass balance as given by Equation (4.1), where the total concentration of Cibacron Blue in the solution was evaluated directly from the mass of dye added to a known volume of buffer. Each

data point in these plots is the average of two replicate experiments performed under identical experimental conditions. The concentration of bound Cibacron Blue rapidly increases with increasing concentration of free Cibacron Blue, but then appears to approach an asymptote of approximately 9.5 moles of Cibacron Blue per mole of BSA at high Cibacron Blue concentrations. This is consistent with the presence of multiple binding sites for Cibacron Blue on each molecule of BSA (Antoni et al., 1982; Johansson and Joelsson, 1991). The low end of the binding profile is shown more clearly in Figure 4.2, with the protein becoming saturated with dye above a Cibacron Blue concentration of about 0.01 mM.

Previous studies have shown that Cibacron Blue binds to BSA only at fatty acid binding sites (Leatherbarrow and Dean, 1980), suggesting that the binding data might be effectively fit using a simple multisite Langmuir-type binding as given by Equation (4.3). The binding data from Figure 4.2 for the 0.043 mM BSA concentration have been replotted in Figure 4.3 in the form of a Hanes plot, in which the ratio C_{free}/C_{bound} is plotted as a function of C_{free}. The data are highly linear when plotted in this manner, with R^2 values greater than 0.99 for all experiments. The Hanes plot was used to obtain initial estimates of the binding parameters based on the slope [$1/nC_{BSA} = 2.46\ mM^{-1}$] and intercept [$1/(nK_{eq}C_{BSA}) = 0.003$] determined from simple linear regression of the Hanes plot.

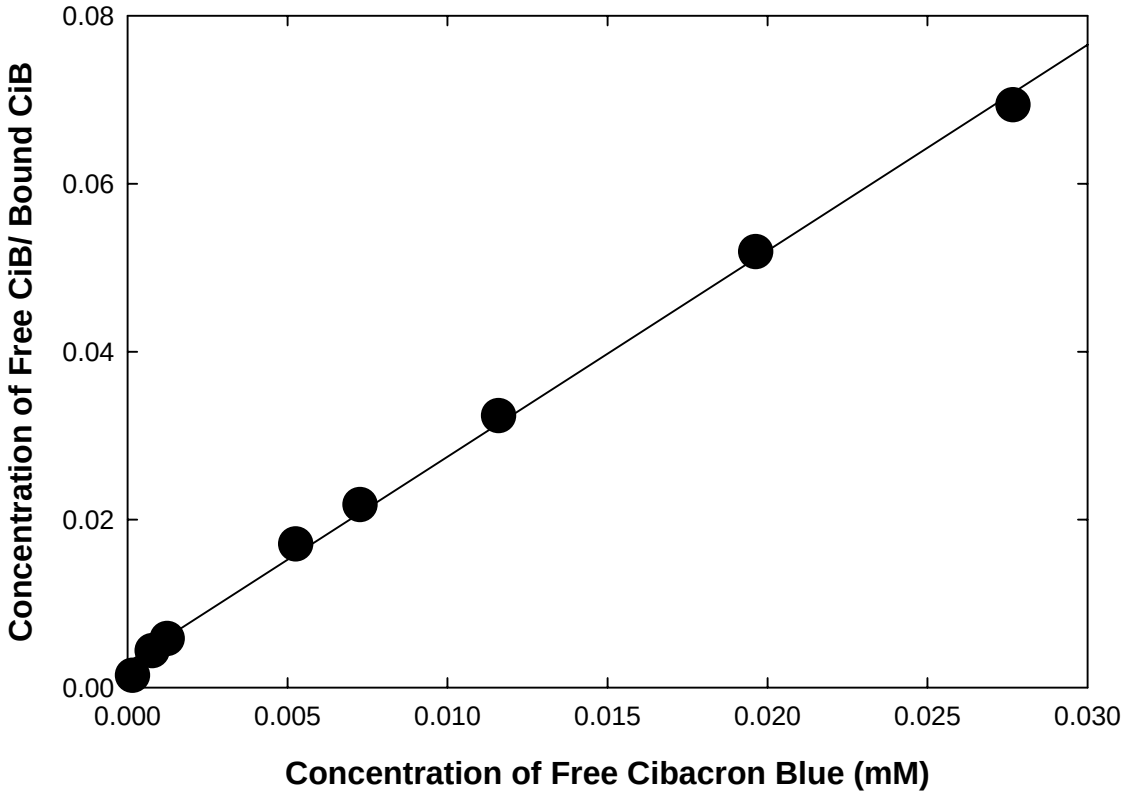

Figure **4.3:** Hanes plot of the data in Figure 4.2 for a BSA concentration of 0.43 mM (3 g/L) in a pH 5.0, 10mM acetate buffer showing linearized form of the binding isotherm.

More accurate values of the binding parameters were obtained by fitting the experimental data over a range of BSA concentrations from 1.5 to 5 g/L using a non-linear least squares (NNLS) Marquardt-Levenberg algorithm, with the individual data points weighted by the inverse of the standard error for each measurement. The best fit values for n and K_{eq} were used to construct the model curve in Figure 4.4, with the binding data plotted in the form of the classical equilibrium isotherm showing the bound ligand concentration as a function of the free ligand concentration. The model is in

excellent agreement with the experimental data, clearly demonstrating that the multisite Langmuir isotherm is able to effectively describe the observed binding interactions between BSA and Cibacron Blue.

Binding experiments were also performed over a range of ionic strengths at a solution pH of 5.0 with the best fit values for n and K_{eq} summarized in Table 4.1. The large error bars on the equilibrium constants are due to the very strong binding between BSA and Cibacron Blue, which made it very difficult to obtain significant data in the linear region of the isotherm. The maximum binding level decreased slightly with increasing ionic strength, varying from 9.8 ± 0.2 in the 10 mM solution to 8.8 ± 0.3 in the 100 mM solution, with n = 6.4 ± 0.3 in the 2.5 mM solution. These values are similar to the 7.5 moles of Cibacron Blue bound per mole of human serum albumin (HSA) reported by (Compagnini et al. 1996) for data obtained in a 25 mM sodium acetate, 100 mM NaCl, pH 4.5 buffer, with these differences probably due to the small differences in experimental conditions and possible differences in the detailed physicochemical characteristics of the BSA and HSA (possibly including differences in the amount of bound fatty acid). In addition, the experiments of Compagnii et al. (1996) were performed using affinity chromatography with immobilized Cibacron Blue, thus it is possible that some of the binding sites were inaccessible to the protein in their experiments.

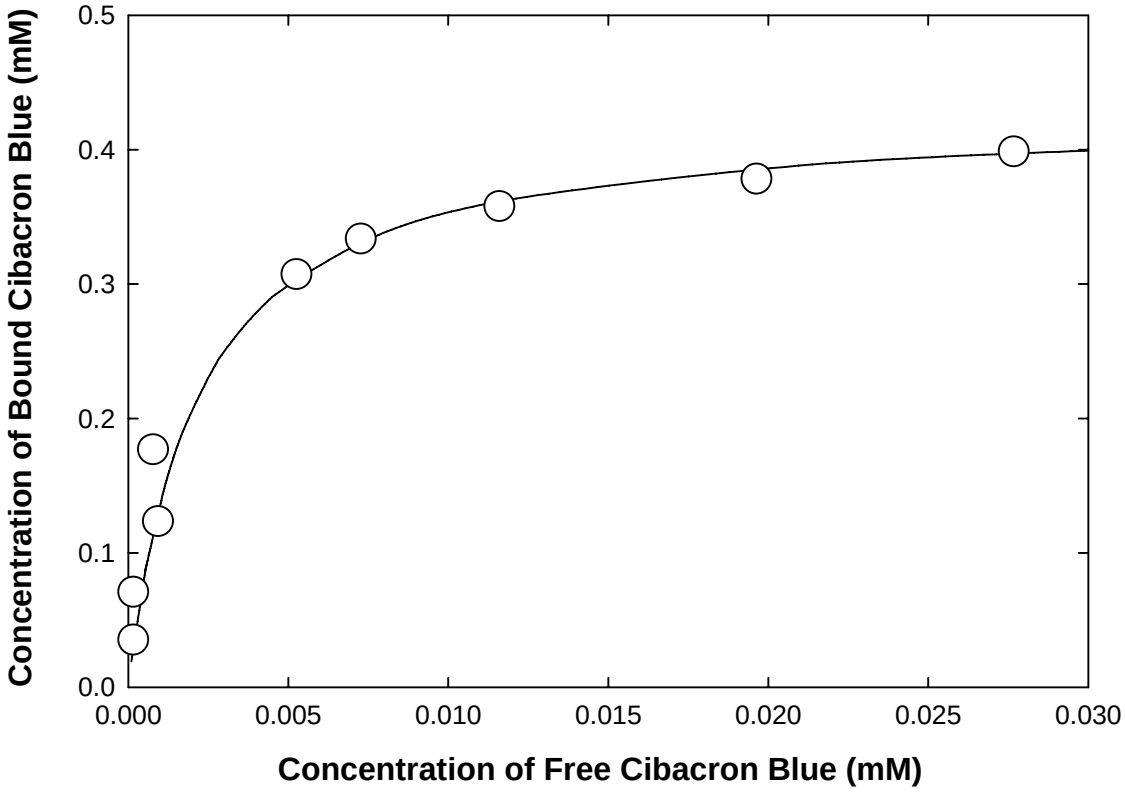

Figure **4.4**: Binding isotherm for Cibacron Blue at pH 5 in a 10 mM acetate buffer at a BSA concentration of 0.043 mM (3 g/L). Solid curve represents model calculation as described in the text.

Table **4.1**:Equilibrium parameters for Cibacron Blue binding to BSA at pH 5.0

Ionic Strength (mM)	Number of Binding Sites, n	Equilibrium Constant, K_{eq} (10^5 M^{-1})
2.5	6.4 ± 0.3	2.1 ± 0.2
10	9.8 ± 0.2	4.7 ± 1.2
50	9.5 ± 0.9	0.2 ± 0.1
100	8.8 ± 0.3	0.3 ± 0.08

The equilibrium binding constant was greatest in the 10 mM ionic strength solution with a value of 4.7 ± 1.2 x 10^5 M^{-1} compared to only 0.2 or 0.3 x 10^5 M^{-1} at the higher salt concentrations. The larger value of K_{eq} in the 10 mM solution may be due to the greater attractive electrostatic interactions between the negatively charged Cibacron Blue and the large number of positively charged lysine amino groups on BSA. Literature values for K_{eq} are highly scattered; Antoni et al. (1982) reported K_{eq} = 10^6 M^{-1} in a 0.05 M tris-HCl, 0.5 M NaCl, pH 8.0 buffer while Metcalf et al. (1981) found K_{eq} = 5.1 x 10^3 M^{-1} in a column equilibrated with 25 mM tris-HCl, pH 8.0 buffer. The values obtained in this study fall within this broad range.

Experiments were also performed over a range of solution pH, with data obtained at relatively low ionic strength (10 mM) to enhance electrostatic interactions between BSA and Cibacron Blue. Sample results are shown in Figures 4.5 to 4.7. The data were all obtained using a 5 g/L BSA solution and each data point represents the average of a minimum of two experiments performed at identical conditions. There was a sharp reduction in the amount of Cibacron Blue bound per mole of BSA at higher pH. In

addition, the concentration of bound ligand reaches saturation at a ligand concentration of approximately 0.4 mM at pH 6.0 compared to only 0.16 mM at pH 8.0. This change in binding affinity is probably due to the increased electrostatic repulsion between the more negatively-charged protein and the negatively-charged dye. There are also small conformational changes in BSA above pH 7 which could potentially alter the accessibility and / or strength of the binding sites.

The best fit values of n and K_{eq} are summarized in Table 4.2 for data obtained with the fatty acid free BSA (in contrast to the Fraction V BSA examined in Figures 4.1 and 4.2 and Table 4.1). The values listed were used to perform the model curves in Figures 4.5 - 4.7. Again, the model results are in good agreement with the data, supporting the use of the multisite Langmuir isotherm to describe Cibacron Blue binding to BSA. The greatest amount of Cibacron Blue binding was obtained at pH 5 with n = 11, with this value decreasing to less than n = 3 at pH 8. The higher value of n obtained in these experiments (compared to that in Figures 4.1 and 4.2) is due to the additional Cibacron Blue binding associated with the greater accessibility of the fatty acid binding domains on the fatty acid-free protein.

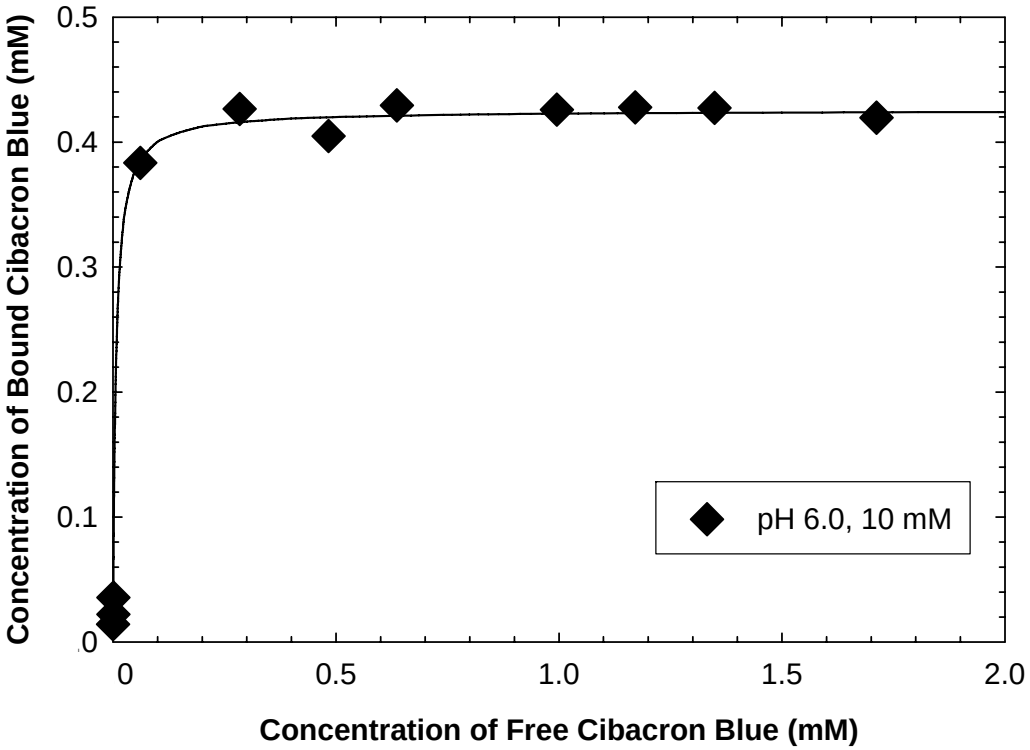

Figure 4.5: Binding isotherm for Cibacron Blue at pH 6 in a 10 mM acetate buffer at a BSA concentration of 0.075 mM (5 g/L). Solid curve represents model calculation as described in the text.

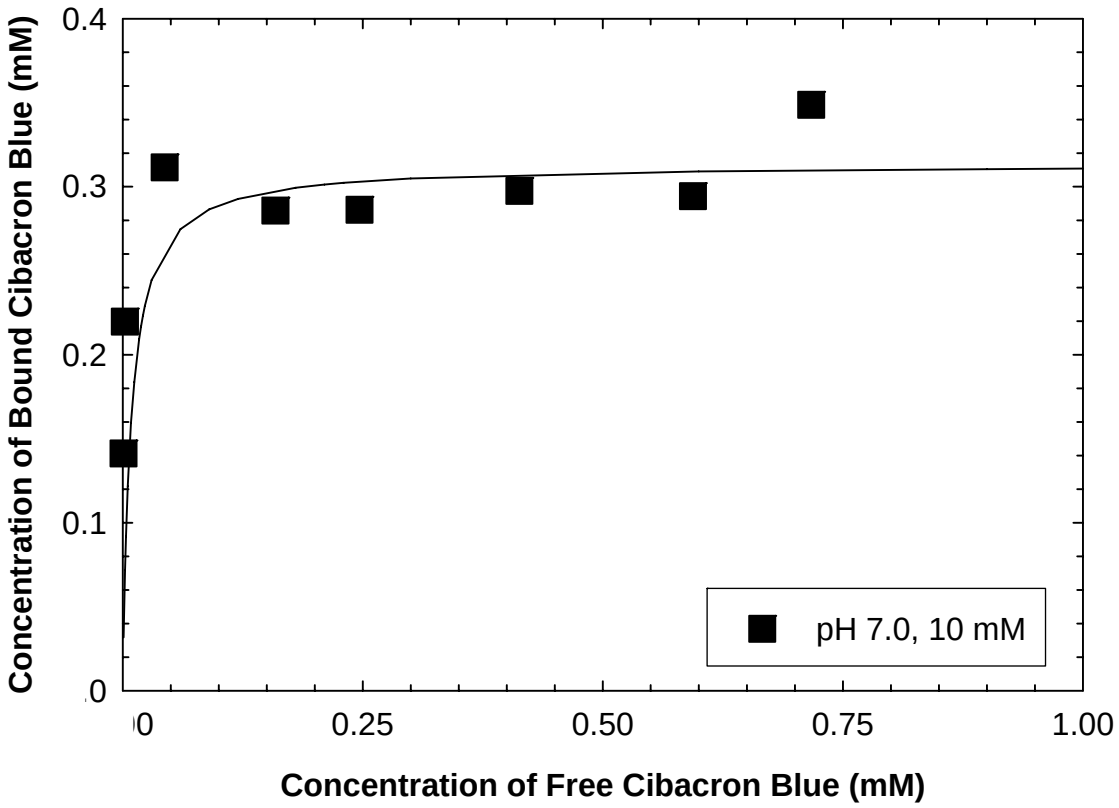

Figure **4.6**: Binding isotherm for Cibacron Blue at pH 7 in a 10 mM acetate buffer at a BSA concentration of 0.075 mM (5 g/L). Solid curve represents model calculation as described in the text.

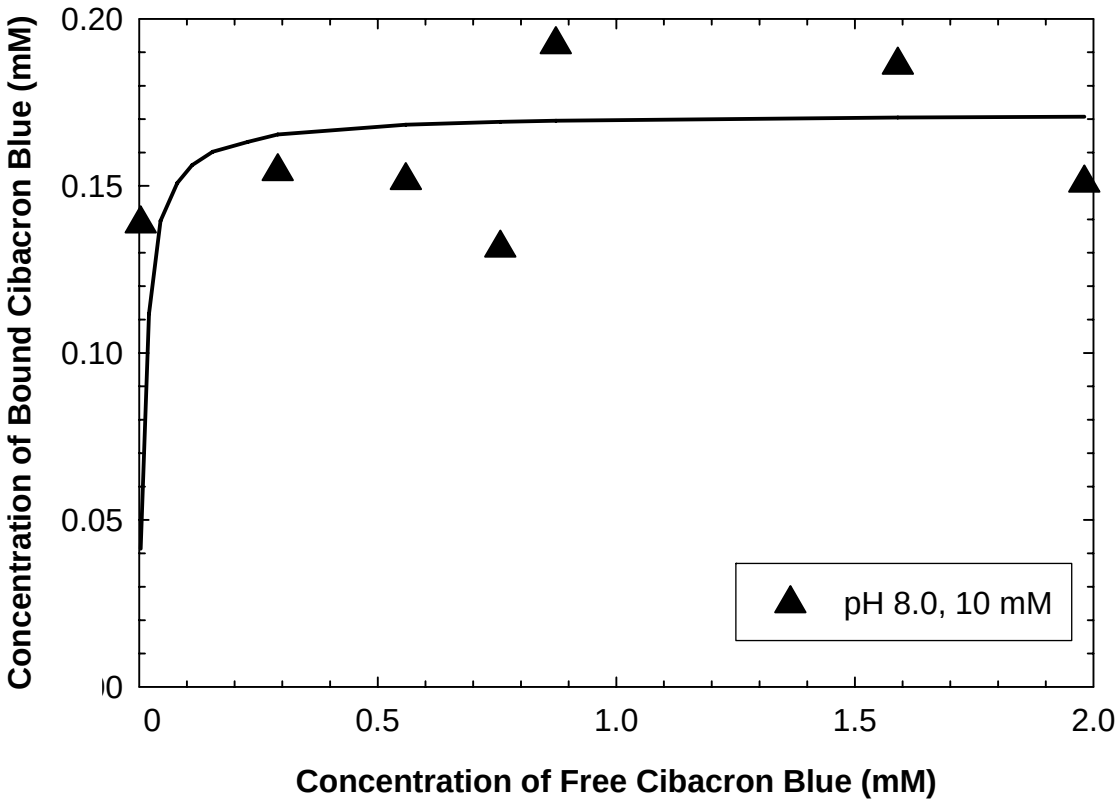

Figure **4.7**: Binding isotherm for Cibacron Blue at pH 8 in a 10 mM acetate buffer at a BSA concentration of 0.075 mM (5 g/L). Solid curve represents model calculation as described in the text.

Table 4.2: Langmuir isotherm parameters for Cibacron Blue to with fatty acid-free BSA at 10 mM ionic strength.

Protein	pH	Moles Cibacron Blue /Mole protein (n)	Equilibrium Constant, K_{eq} x 10^3 (M^{-1})
BSA	5.0	10.9	105
BSA	6.0	5.7	160
BSA	7.0	4.2	118
BSA	8.0	2.3	91

Although the extent of Cibacron Blue binding to BSA decreases significantly with increasing pH, the results in Table 4.2 indicate that there is still significant protein-ligand binding even at pH 8. Previous studies have demonstrated that chaotropic salts like NaSCN can significantly reduce the binding interactions between BSA and Cibacron Blue, which has been exploited for protein elution in previous studies of dye affinity chromatography (Ruckenstein and Zeng, 1998). Binding experiments were thus performed using different amounts of NaSCN in a pH 8.0 Tris-HCl buffer to identify conditions that would facilitate the dissociation of BSA and Cibacron Blue, conditions required for the effective recovery of the dye (and preparation of the purified protein). The addition of 0.5 M NaSCN reduced the number of bound molecules of Cibacron Blue from 2.3 to 1.1. Increasing the NaSCN concentration to 1 M reduced the Cibacron Blue binding to less than one molecule per molecule of BSA. The binding data under these

conditions was scattered, making it difficult to obtain accurate estimates of K_{eq} in the presence of NaSCN. Typical results for the 1 M NaSCN solution are shown in Figure 4.8. The concentration of free Cibacron Blue is approximately equal to the total concentration of the ligand indicating the absence of any significant binding interactions under these conditions.

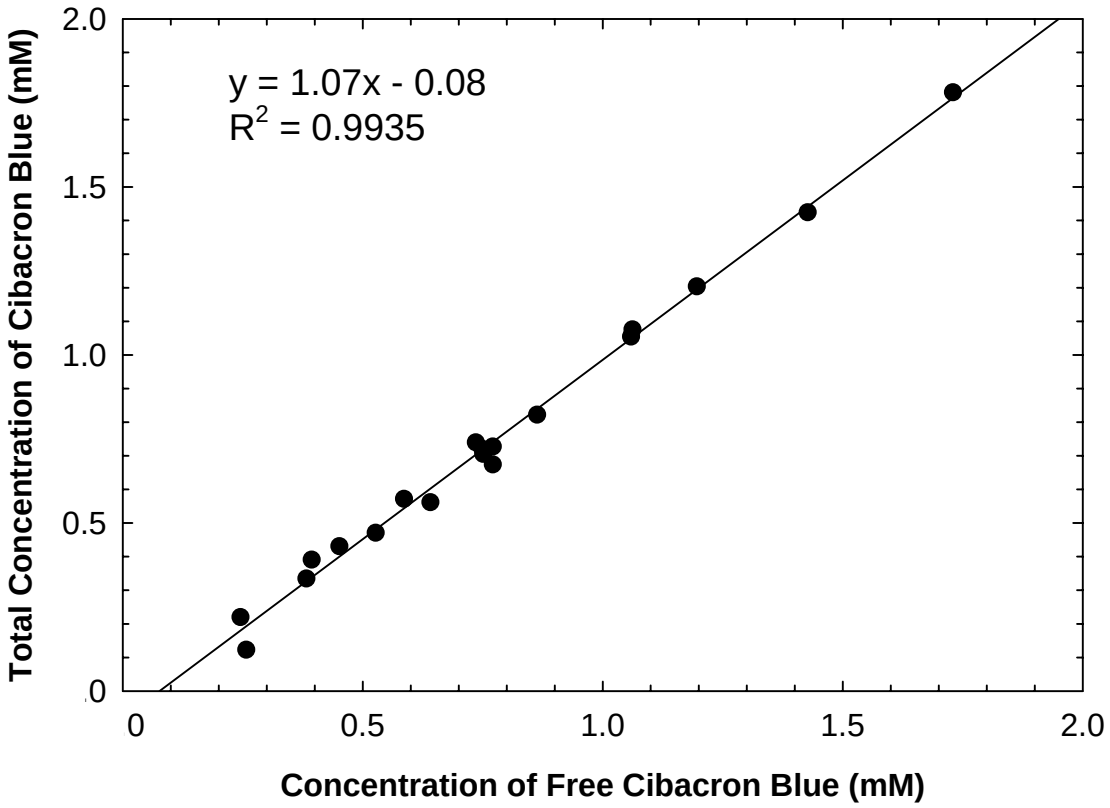

Figure **4.8**: Effect of 1 M NaSCN on Cibacron Blue binding using a 5 g/L BSA solution at pH 8.0.

Figure 4.9 compares the binding characteristics of Cibacron Blue to BSA and ovalbumin at pH 5 and 10 mM ionic strength. These data were obtained from two separate sets of experiments, one using a solution containing 5 g/L BSA (top panel) and one performed with a solution containing 15 g/L ovalbumin (bottom panel). The results are plotted as the molar concentration of bound Cibacron Blue normalized by the molar protein concentration as a function of the concentration of free Cibacron Blue. Note the very different scales on the x-axis in the two plots. The extent of Cibacron Blue binding to BSA rapidly approaches saturation at relatively low Cibacron Blue concentrations. In contrast, Cibacron Blue binding to ovalbumin (15 g/L) doesn't achieve saturation until a Cibacron Blue concentration of about 4 g/L, with K_{eq} values of 1.05×10^5 M^{-1} and 1.7×10^3 M^{-1} for BSA and ovalbumin, respectively. In addition, the saturation value for BSA corresponds to approximately 11 moles of bound Cibacron Blue per mole of BSA compared to only 2.7 moles of bound Cibacron Blue per mole of ovalbumin. The solid curves in the two panels represent the model calculations determined using the multisite Langmuir isotherm using the parameters given above. These results clearly demonstrate that Cibacron Blue has a much stronger binding affinity to BSA compared to ovalbumin in a pH 5, 10 mM ionic strength buffer.

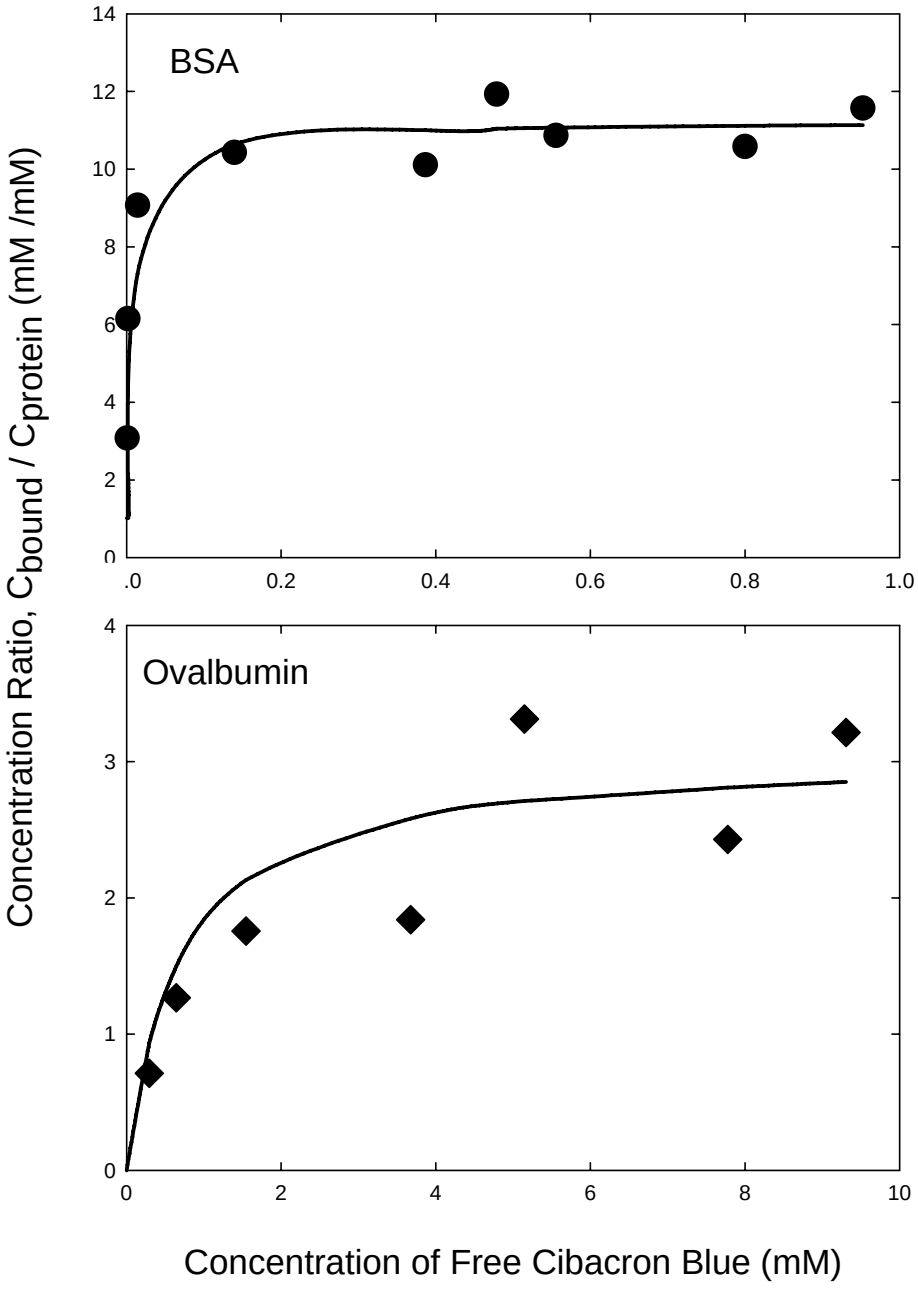

Figure **4.9:** Binding isotherms for Cibacron Blue at pH 5.0 in a 10 mM acetate buffer at a BSA concentration of 5 g/L (top panel) and an ovalbumin concentration of 15 g/L (bottom panel). Solid curves represent model calculations as described in the text.

Figure 4.10 shows the binding characteristics of Cibacron Blue to BSA and ovalbumin in a binary mixture at pH 5 and 10 mM ionic strength. These data were obtained using a solution containing 5 g/L BSA and 5 g/L ovalbumin. The solid curve represents model calculations accounting for competitive binding using Equation (4.4) with the values of n and K_{eq} obtained from experiments performed with the individual proteins from Figure 4.9. The rapid increase in the concentration of bound Cibacron Blue is dominated by binding to BSA with the much slower increase at very high Cibacron Blue concentrations arising from binding to ovalbumin. The model calculations are in good agreement with the experimental results indicating that Cibacron Blue binds independently to the two proteins under the conditions of these experiments as expected.

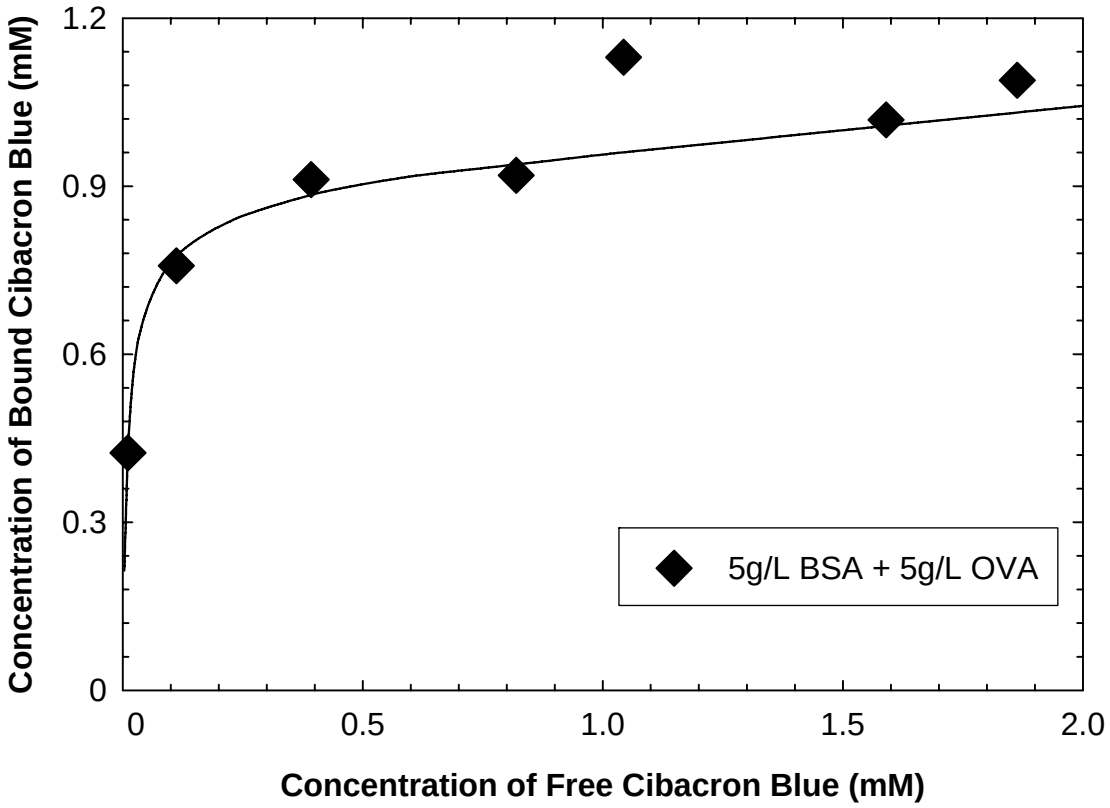

Figure **4.10**: Binding isotherm for Cibacron Blue at pH 5 in a 10 mM acetate buffer using a binary mixture of BSA concentration of 0.075 mM (5 g/L) and ovalbumin 0.11 mM (5g/L). Solid curve represents model calculation as described in the text.

4.5 Charge Calculations

The very different levels of Cibacron Blue binding to BSA and ovalbumin should cause significant differences in the net protein charge even though these two proteins have very similar isoelectric points. Although it might seem like the binding of a single Cibacron Blue molecule would change the surface charge of the protein by -3 electronic charge units due to the 3 sulfonic acid groups on each molecule of Cibacron Blue, the actual situation is considerably more complicated. Cibacron Blue binding will increase the negative charge on the protein surface, but this change in charge will cause an increase in the local hydrogen ion concentration around the protein due to electrostatic interactions between the negative protein and the positive H^+ ions. This increase in local H^+ concentration will cause the protonation of various acidic and basic amino acid residues on the protein, partially compensating for the change in charge due to Cibacron Blue binding, a phenomenon known as charge regulation.

The net protein charge was calculated as a function of solution pH, ionic strength, and Cibacron Blue concentration using a modified form of the charge regulation model developed by Tanford et al. (1955) and Scatchard et al. (1957) that accounts for the binding of the negatively-charged Cibacron Blue and the protonation / deprotonation of the amino acids due to a shift in the local hydrogen ion concentration.

The extent of ionization of a given amino acid is a function of the local H^+ concentration, which can be represented as

$$R - COOH \xleftrightarrow{K_i^{int}} R - COO^- + H^+ \qquad (4.5)$$

for a carboxylic acid. Similar equations can be developed for other ionizable groups. The corresponding equilibrium relation is typically written in the form of the classic Henderson-Hasselbach equation

$$pH = pK_i^{\text{int}} + \log \frac{r_i}{(n_i - r_i)} \tag{4.6}$$

where pH = -log[H^+], pK_i^{int} = -log[K_i^{int}], r_i is the number of ionized or dissociated groups (in this case the concentration of R-COO^-), and n_i is the total number of R-COOH groups in the protein. The local concentration of H^+ ions near the surface of the protein is evaluated assuming an equilibrium Boltzmann distribution:

$$H^+ = H^+_{bulk} \exp\left(\frac{-e\psi_s^*}{kT} \right) \tag{4.7}$$

where ψ_s^* is the electrostatic potential at the protein surface and [H_b^+] is the bulk hydrogen ion concentration.

The net protein charge was evaluated from the difference in the number of protonated amino acids, the number of bound acetate anions, and the number of bound molecules of Cibacron Blue:

$$Z = \upsilon_{H^+} - \upsilon_{acetate} - 3\upsilon_{CiB} \tag{4.8}$$

where each bound Cibacron Blue (CiB) has a charge of –3 due to the three sulphonic acid groups. The number of positively charged amino acid residues was calculated from Equations (4.6) and (4.7) by summing over the different types of ionizable residues (Pujar and Zydney, 1997):

$$\upsilon_{H^+} = \upsilon_{\max} - \sum_i \frac{n_i K_i^{\text{int}}}{K_i^{\text{int}} + [H_b^+]\exp(-e\psi_s^*/kT)} \qquad (4.9)$$

The number (n_i) and intrinsic equilibrium constants (K_i^{int}) for each of the charged amino acid residues are given in Table 4.4 for BSA and Table 4.5 for ovalbumin. The total number of positively charged amino acid residues at very low pH, i.e. where all the available sites are protonated, is $\nu_{max} = 96$ for BSA and $\nu_{max} = 42$ for ovalbumin.

. The electrostatic potential at the protein surface, ψ_s^*, can be related to the net protein charge as:

$$\sigma_s^* = \frac{eZ_{\text{Protein}}}{4\pi r_s^2} = \frac{\varepsilon_0 \varepsilon \psi_s^* (1 + \kappa r_s)}{r_s} \qquad (4.10)$$

where e is the electron charge, r_s is the effective radius of the (spherical) BSA or ovalbumin, ε_0 is the permittivity of free space, ε is the dielectric constant of the medium, and κ is the inverse of the Debye length:

$$\kappa^{-1} = \left(\frac{\varepsilon_0 \varepsilon RT}{F^2 \sum z_i^2 c_i} \right)^{1/2} \qquad (4.11)$$

The summation in Equation (4.11) accounts for the concentration of all ions in solution, including the contribution from free (unbound) Cibacron Blue (with $z_i = -3$ for the Cibacron Blue).

The number of bound acetate ions (CH_3COO^-) was evaluated as (Saifer et al. 1964):

$$\upsilon_{actetate^-} = \sum_j \frac{m_j K_j \gamma [CH_3COO^-] \exp(e\psi_s^*/kT)}{1 + K_j \gamma [CH_3COO^-] \exp(e\psi_s^*/kT)} \quad (4.12)$$

The parameters m_j and K_j for the three distinct acetate binding sites are given in Table 4.3. γ is the activity coefficient of CH_3COO^- and was evaluated as:

$$-\log \gamma = \frac{0.5\sqrt{[CH_3COO^-]/2}}{(1+2\sqrt{[CH_3COO^-]/2})} \quad (4.13)$$

The net protein charge in a given solution was evaluated by simultaneously solving Eqs. 4.5 to 4.11 with the number of bound molecules of Cibacron Blue given by Eq. 4.3 for the individual proteins. The protein radii were estimated as r_s = 3.48 nm for BSA and r_s = 3.0 nm for ovalbumin, both independent of the number of molecules of bound Cibacron Blue.

Table **4.3**: Type and number of titratable groups on BSA (Tanford. et al., 1955)

Type (*i*)	**Number (n_i)**	pK^{i}_{int}
α-Carboxyl	1	3.75
β,γ-Carboxyl	99	4.02
Imidazole	16	6.9
α-Amino	1	7.75
ε-Amino	57	9.8
Phenolic	19	10.35
Guanidine	22	12

Table 4.4: Ionizable residues and pKa values for ovalbumin

Residue	**Number (n_i)**	pK^{i}_{int}
Aspartic Acid	16	3.9
Glutamic Acid	33	4.2
Histidine	7	6.0
Lysine	20	10.5
Arginine	15	12.5

Table 4.5: Values of parameters m_j and K_j in the acetate binding model

Binding Site j	**M_j**	**K_j (L/mol)**
1	1	530
2	6	50
3	14	2

Typical theoretical results for the net charge of BSA as a function of the total concentration of Cibacron Blue are shown in Figure 4.11 for a BSA concentration of 8 g/L at pH 5.0 in the presence of 10 mM acetate buffer. The addition of Cibacron Blue causes a rapid increase in the net negative charge of BSA due to the strong binding interactions. The amount of Cibacron Blue binding achieves its saturation level (in this case corresponding to 11 moles of bound Cibacron Blue per mole of BSA) when the Cibacron Blue concentration exceeds about 1.0 g/L. The reduction in the BSA charge at higher Cibacron Blue concentrations is due to the change in the protonation of the acidic and basic amino acids caused by the reduction in H^+ concentration near the surface of the protein associated with the increased electrostatic shielding as the ionic strength of the solution increases due to the presence of large amounts of free Cibacron Blue. The net charge of BSA in the 10 mM acetate buffer at pH 5.0 was estimated to be +1.2 while the charge in the presence of 1.0 g/L Cibacron Blue is -12.0 even though the BSA is able to bind 11 moles of Cibacron Blue (corresponding to 33 charge groups) under these conditions. This difference is a direct result of the effects of charge regulation, with the increase in negative charge associated with Cibacron Blue binding at least partially compensated for by the increased protonation of some amino acids. The small positive charge on the BSA in the absence of Cibacron Blue is surprising since the isoelectric point of BSA is reported to be 4.9. This discrepancy is likely due to shifts in the pK_a of certain amino acids due to local interactions with other charge groups and / or to the inaccessibility of certain charged amino acids within the protein core.

The y-axis on the right side of Figure 4.11 shows the calculated values of the solution ionic strength

$$I = \frac{1}{2}\sum_i z_i^2 C_i \qquad (4.12)$$

accounting for the concentrations of Na^+, acetate, and free Cibacron Blue. The solution ionic strength is a very weak function of the Cibacron Blue concentration at low concentrations of Cibacron Blue since most of the dye is bound by the protein and thus provides no contribution to the solution ionic strength. The ionic strength begins to increase linearly with the Cibacron Blue concentration for Cibacron Blue concentrations greater than 1.0 g/L since the protein is fully saturated with the dye under these conditions.

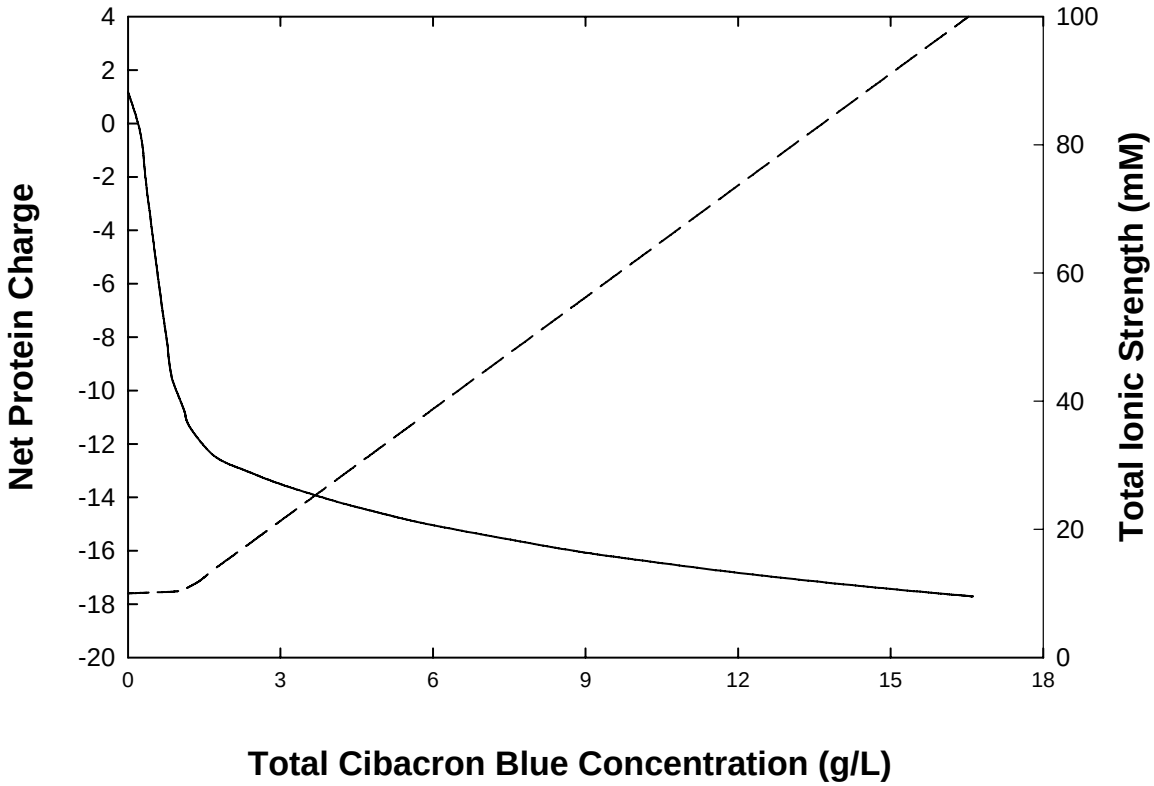

Figure **4.11:** Effect of Cibacron Blue on the net protein charge (solid line) and overall solution ionic strength (dashed line)

Figure 4.12 shows model calculations for the net protein charge as a function of the Cibacron Blue concentration for a binary mixture containing 10 g/L BSA and 6 g/L ovalbumin at pH 5.0 in a 10 mM acetate buffer. Results are shown for independent binding of the individual proteins (top panel) and for competitive binding in a binary mixture (lower panel). The binding parameters were obtained from previously conducted experiments for the BSA-Cibacron Blue system which gave n = 10.9 and K_{eq} = 110 X 10^3 M^{-1} for BSA and n = 2.8 and K_{eq} = 1.7 X 10^3 for ovalbumin. The results for the individual proteins show a rapid and significant reduction in the net charge of BSA with a much more gradual change in the predicted charge of ovalbumin upon the addition of Cibacron Blue. The results for BSA in the binary mixture are similar to those for the individual proteins. However, the predicted charge profile for ovalbumin in the binary mixture is relatively constant at low Cibacron Blue concentrations since almost all of the added Cibacron Blue binds to the much higher affinity binding sites on BSA. The addition of Cibacron Blue causes the predicted charge of BSA to decrease from about +1.1 in the absence of Cibacron Blue to a value of -12 at a Cibacron Blue concentration of 1.4 g/L, while the predicted charge on ovalbumin changes by less than 1 electronic charge under these conditions. Even the addition of 2.9 g/L of Cibacron Blue causes the effective charge of ovalbumin to decrease by only 3.5 charge units. These calculations clearly indicate that the addition of Cibacron Blue can selectively shift the net protein charge, in this case leading to a very large difference in the effective charge on ovalbumin and BSA.

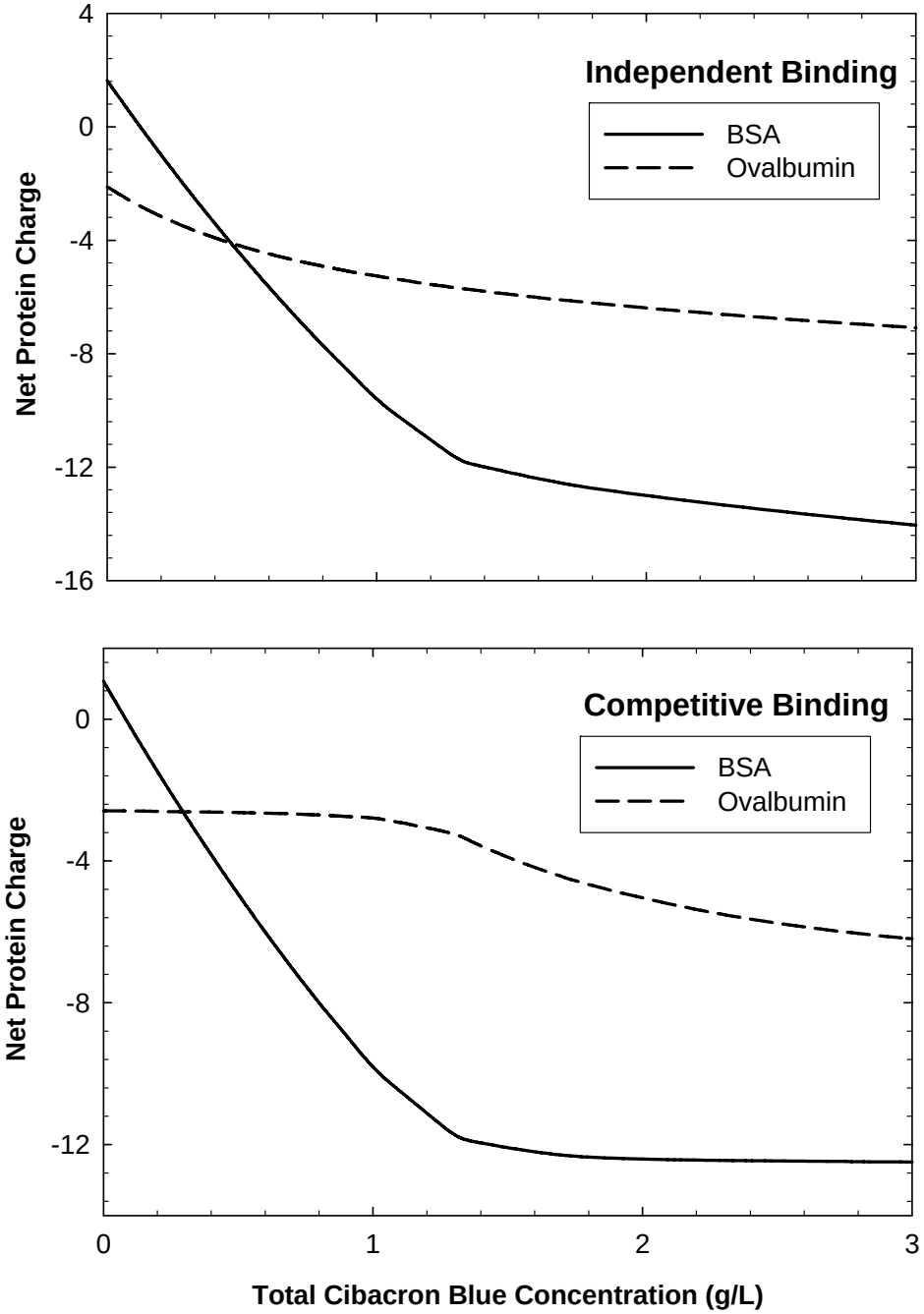

Figure **4.12:** Predicted values of the effective charge for BSA (solid curve) and ovalbumin (dashed curve) in a pH 5.0, 10 mM acetate buffer in the presence of Cibacron Blue accounting for the individual proteins (top panel) and for the binary protein mixture (bottom panel).

4.6 Discussion

The results presented in this Chapter clearly demonstrate the strong binding interactions between BSA and Cibacron Blue, with maximum binding of approximately 11 moles of dye per mole of BSA at pH 5.0, 10 mM ionic strength. The binding parameters were a strong function of both solution pH and ionic strength, probably due to the electrostatic interactions between the negatively-charged dye and the ionized sites on the protein. There was a small reduction in Cibacron Blue binding at high ionic strength (100 mM) and a somewhat larger reduction at very low ionic strength (2.5 mM). The extent of Cibacron Blue binding decreased more significantly at high pH and in the presence of NaSCN.

In contrast to the results with BSA, Cibacron Blue binding to ovalbumin was fairly weak at all pH and ionic strength. For example at pH 5, the addition of 2.6 mM Cibacron Blue to a 15 g/L ovalbumin solution results in the binding of only 1.8 moles of dye per mole of ovalbumin, while these same conditions gave 11 moles of Cibacron Blue bound per mole of BSA.

The effect of Cibacron Blue binding on the net protein charge was evaluated using a charge regulation model that accounts for the change in protonation and deprotonation of the various amino acid residues associated with the change in local pH (H^+ concentration) caused by the electrostatic interactions between the protein and the charged ions. This model is only approximate since it neglects the detailed charge distribution over the surface of the protein, assuming that all carboxylic acid residues are identical and unaffected by the local environment (beyond the average pH at the protein

surface). In addition, the model doesn't account for the detailed pH and ionic strength dependence of Cibacron Blue binding – the extent of dye binding was evaluated using the binding parameters determined at the bulk solution conditions. The model calculations clearly indicate that Cibacron Blue binding causes a large shift in charge of the BSA-Cibacron Blue complex even at relatively low Cibacron Blue concentrations. In contrast, Cibacron Blue binding has relatively little effect on the ovalbumin charge due to the weak binding interactions between ovalbumin and Cibacron Blue. The implications of these results for protein transport, and for the separation of ovalbumin from BSA using affinity high performance tangential flow filtration, are discussed in subsequent chapters.

Chapter 5

CONTROLLING PROTEIN TRANSPORT IN ULTRAFILTRATION USING SMALL CHARGED LIGANDS

5.1 Introduction

A number of recent studies have demonstrated that it is possible to control the rate of protein transport through ultrafiltration membranes by adjusting the solution pH or the ionic strength. For example Pujar and Zydney (1994) showed that the transmission of bovine serum albumin (BSA) through a 100,000 molecular weight cut-off membrane could be reduced by a factor of 100 by simply lowering the solution ionic strength from 150 to 1.5 mM. This dramatic increase in protein retention was a direct result of the electrostatic exclusion of the negatively charged protein from the membrane pores at low salt concentrations. Burns and Zydney (1999) demonstrated that the sieving coefficient of several therapeutic proteins could be reduced by an order of magnitude by shifting the solution pH approximately 2 pH units above or below the protein isoelectric point due to the increase in the effective protein volume associated with the presence of the electrical double layer surrounding the charged protein.

These electrostatic interactions can also be exploited for protein separations using a process known as High Performance Tangential Flow Filtration, also known by the acronym HPTFF. For example, van Reis et al. (1999) were able to achieve 900-fold purification of an antigen-binding fragment of a monoclonal antibody (Fab) from BSA by operating the membrane process near the isoelectric point of the BSA and using a positively-charged membrane to obtain very high rejection of the positively-charged Fab.

Although the use of solution pH and ionic strength to control protein transmission is very attractive, there are many systems where this is not practical due to issues of protein stability or when the product and impurity have very similar surface charge characteristics. Menon and Zydney (1999) demonstrated that it is also possible to control protein transmission through the choice of buffer due to the change in protein charge caused by ion binding. For example, the BSA sieving coefficient at pH 4.4 was 50% larger in a 10 mM solution of NaSCN than in a corresponding solution of NaCl due to the differences in anion binding, although this effect was relatively small under most conditions and ion binding interactions typically have low specificity. Kanani et al. (2004) showed that the addition of BSA increased the retention of lysozyme, which was attributed to the attractive interactions between lysozyme and the large molecules of BSA. In contrast, the presence of BSA reduced the transmission of myoglobin, which Kanani et al. attributed to Donnan effects. The combination of these phenomena actually reversed the selectivity for the separation of lysozyme and myoglobin. However, it is unlikely that this general approach would be practical for commercial separations given the high cost of the added protein and the need to subsequently remove that protein to parts per million levels for the final product.

A much more attractive approach would be to use a small charged ligand that binds specifically to the protein of interest, thereby altering the protein charge and in turn its transmission during ultrafiltration. Charged dyes have been used extensively in dye – ligand affinity chromatography; thus, there is a considerable database already available for dye – protein interactions that can be used to identify appropriate candidate structures. For example, Cibacron Blue 3GA is known to bind to a variety of proteins including

many dehydogensases and kinases, nucleotide dependent enzymes, reductases, interferons, and serum protein such as albumin (Lowe, 1987). As discussed in Chapter 4, the versatility of Cibacron Blue binding is apparently due to the combination of aromatic and multiple sulphonate groups within the dye molecule (Subramanian, 1984). Cibacron Blue has been shown to bind to BSA at multiple hydrophobic fatty acid-anion binding sites on the protein surface (Leatherbarrow and Dean, 1980).

The overall objective of the work described in this Chapter was to determine the effects of Cibacron Blue on the ultrafiltration of BSA, with the ultimate goal of being able to use this small dye to control BSA transmission through semipermeable ultrafiltration membranes. Experiments were performed with essentially neutral and negatively-charged versions of a composite regenerated cellulose membrane to explore the effects of electrostatic interactions on protein transmission. The data were analyzed using available theoretical models for the transport of charged proteins through charged membranes, with the protein charge calculated by accounting for the extent of dye binding.

5.2 Material and Methods

Experiments were performed using Bovine Serum Albumin and ovalbumin as model proteins. Cibacron Blue 3GA (Catalogue number C-9534, Sigma Chemical), which has a molecular weight of 0.774 kD and contains three negatively-charged sulphonic acid groups, was used as the small affinity ligand due to its extensive binding interactions with BSA.

Protein solutions were prepared using appropriate buffers: acetate at pH 5, Bis-Tris at pH 6.0 and 7.0, and Tris with HCl at pH 8.0. The ionic strength of the buffer was adjusted by adding appropriate amounts of NaCl. Protein solutions were prepared by slowly dissolving BSA powder in the buffer, with the resulting solution filtered through a 0.22 μm syringe filter (Costar Corp., Cambridge, MA) to remove any protein aggregates immediately prior to use. Additional details on the protein and buffer preparation are provided in Chapter 3.

Protein concentrations in the absence of the dye were determined spectrophotometrically with a UV-VIS spectrophotometer (UV mini 1240, Shimadzu, Kyoto, Japan) using the natural absorbance at 280 nm. Protein concentrations in the presence of Cibacron Blue were evaluated by capillary zone electrophoresis (Model G1600A, Agilent Technologies, Palo Alto, CA) since the strong blue color of Cibacron Blue interfered with the absorbance measurements.

All filtration experiments were performed with Ultracel composite regenerated cellulose membranes (Millipore Corp., Bedford, MA) having nominal molecular weight cut offs of 100 kD. These cellulosic membranes are nearly uncharged and have very low protein adsorption due to their high degree of hydrophilicity. Individual membrane discs (25 mm diameter) were cut from large flat sheets using a specially designed cutting device.

Negatively-charged versions of the 100 kD membrane were made in our laboratory by the covalent attachment of negatively charged sulphonic acid groups to the surface of the membrane using the base-activated chemistry developed by van Reis (2001) and described in Chapter 3.

5.2.1 Protein Filtration

Protein filtration experiments were also conducted in the 25 mm diameter stirred ultrafiltration cell. The membrane hydraulic permeability was measured before and after each experiment as described in Chapter 3. Ultrafiltration experiments were performed over a range of ionic strength and pH, with the stirred cell filled with a fresh protein solution for each measurement. All experiments were performed at room temperature (22 ± 3°C) using the same lot of protein for a given set of experiments.

5.2.2 Determination of Membrane Charge

The membrane charge was evaluated from streaming potential measurements following the procedure described in Chapter 3 which is based directly on the work by Burns and Zydney (2000). Data were obtained using a 10 mM pH 5.0 acetate buffer solution with the streaming potential evaluated at several transmembrane pressures.

5.2.3 X-Ray Photoelectron Spectroscopy

X-ray photoelectron spectroscopy (XPS) was used to determine the elemental compositions of charge-modified membranes. After reaction, the membranes were flushed with at least 250 L/m^2 of deionized distilled water to completely remove any residual charging ligand. The membranes were then dried in a clean chamber, cut using a razor blade, and mounted on conducting carbon tape using tweezers.

XPS analysis was performed using a Kratos Analytical Axis Ultra instrument (Kratos Analytical Inc., Chestnut Ridge, NY) available at the Materials Research Institute at The Pennsylvania State University. Data were obtained using monochromatic Al as the x-ray source (1486.6 eV photons). The photoelectron take-off angle was 90^{o} with respect to the sample plane. The analysis spot size was 110 μm with a sampling depth of approximately 25 Å. All binding energies were referenced to the C-1s hydrocarbon peak at 285 eV. The XPS data were analyzed by integrating the peak areas and applying the appropriate relative sensitivity factors to account for the x-ray cross section and the transmission function of the spectrometer.

5.3 Results

Figure 5.1 shows experimental data obtained for the streaming potential (E_z) as function of the applied transmembrane pressure for both the neutral and the negatively-charged version of the Ultracel membrane. The apparent zeta potential of the membrane (ζ) was evaluated from the slope of the voltage as a function of applied pressure from the Helmoltz-Smoluchowski equation:

$$\frac{\mathbf{d}E_z}{\mathbf{d}\Delta P} = \frac{\varepsilon_o \varepsilon_r \zeta}{\mu \Lambda} \qquad (5.1)$$

where Λ is the solution conductivity, ε_o is the electrical permittivity of a vacuum, and ε_r is the dielectric constant of the fluid. The zeta potential of the un-modified membrane was -0.0008 V with this small value reflecting the absence of any fixed charge groups on

the base cellulose membrane. The small negative zeta potential is likely due to the preferential adsorption of negative anions from the electrolyte solution. The zeta potential of the surface modified membrane was -0.04 V, consistent with the addition of the sulphonic acid groups to the membrane surface.

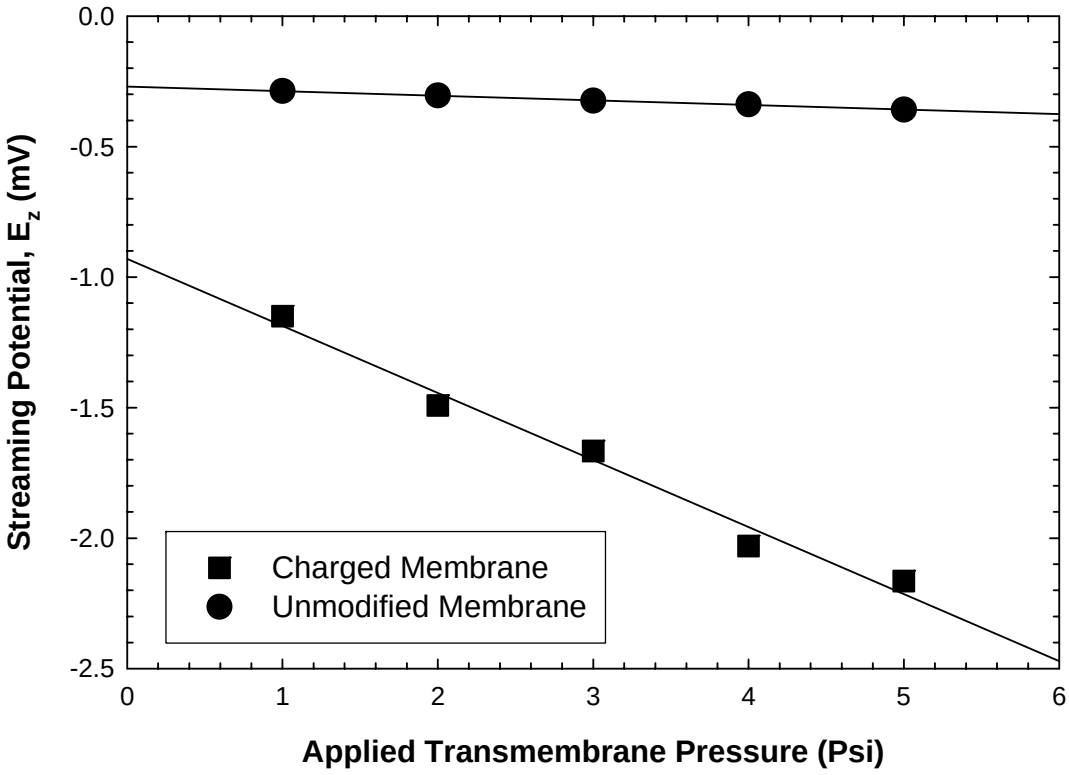

Figure **5.1**: Streaming potential data for the neutral and charged modified Ultracel 100 kD membrane using a pH 5.0, 10 mM buffer

The presence of the sulphonate functionality was also confirmed by X-ray Photoelectron Spectroscopy (XPS) through the detection of the sulfur atoms that are present in the sulphonate group but completely absent in the base cellulose. XPS scans were obtained for the unmodified Ultracel membrane and for the membranes exposed to

the charging solution for 2, 8, and 24 hours with the results shown in Figure 5.2. The sulfur peak appears at a binding energy of approximately 166 eV. This peak is completely absent in the unmodified cellulose membrane and increases as the reaction time increases. Quantitative analysis of the XPS data gave a sulfur concentration of approximately 0.4% for the membrane that was charged for 24 hours.

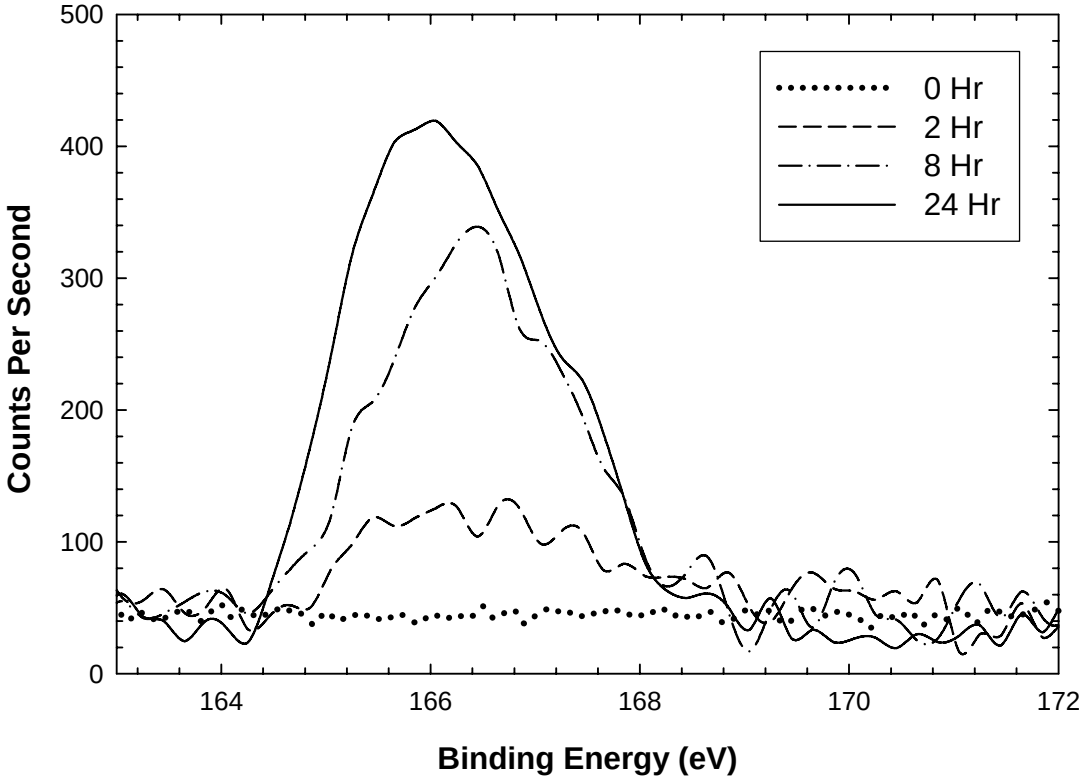

Figure 5.2: XPS results for the unmodified Ultracel membrane and for a series of charge modified membranes. The peak at approximately 166 eV corresponds to sulfur.

Figure 5.3 shows typical experimental data for the observed sieving coefficient of BSA through a negatively-charged version of the 100 kD Ultracel membrane as a function of the total concentration of Cibacron Blue added to the solution. The data were all obtained using a BSA concentration of 8 g/L in a 10 mM acetate buffer at pH 5.0. Each data point is an average of at least three replicate experiments, performed under identical experimental conditions and using the same membrane, the standard deviation was within the size of the data symbol. In each case, the observed sieving coefficient (S_o) was evaluated as the ratio of the BSA concentration in the filtrate solution to that in the bulk solution in the stirred cell, with the BSA concentrations determined by capillary electrophoresis. The BSA sieving coefficient initially decreases with increasing concentration of Cibacron Blue, with S_o decreasing from a value of 0.02 in the absence of Cibacron Blue to a value of 0.0001 at a Cibacron Blue concentration of approximately 1.1 g/L. This small value of the observed sieving coefficient was confirmed using a separate experiment with a 32 g/L BSA solution with Cibacron Blue again added in a 12:1 molar ratio. This experiment gave a filtrate concentration of 0.003 g/L, which is the lower limit of detection for the protein assay, confirming the very high degree of BSA retention in this experiment. Further increases in the Cibacron Blue concentration cause an increase in BSA transmission, with the sieving coefficient attaining a value of more than 0.08 at Cibacron Blue concentrations above 15 g/L. Thus, the addition of Cibacron Blue causes the BSA sieving coefficient to vary by more than a factor of 800 fold.

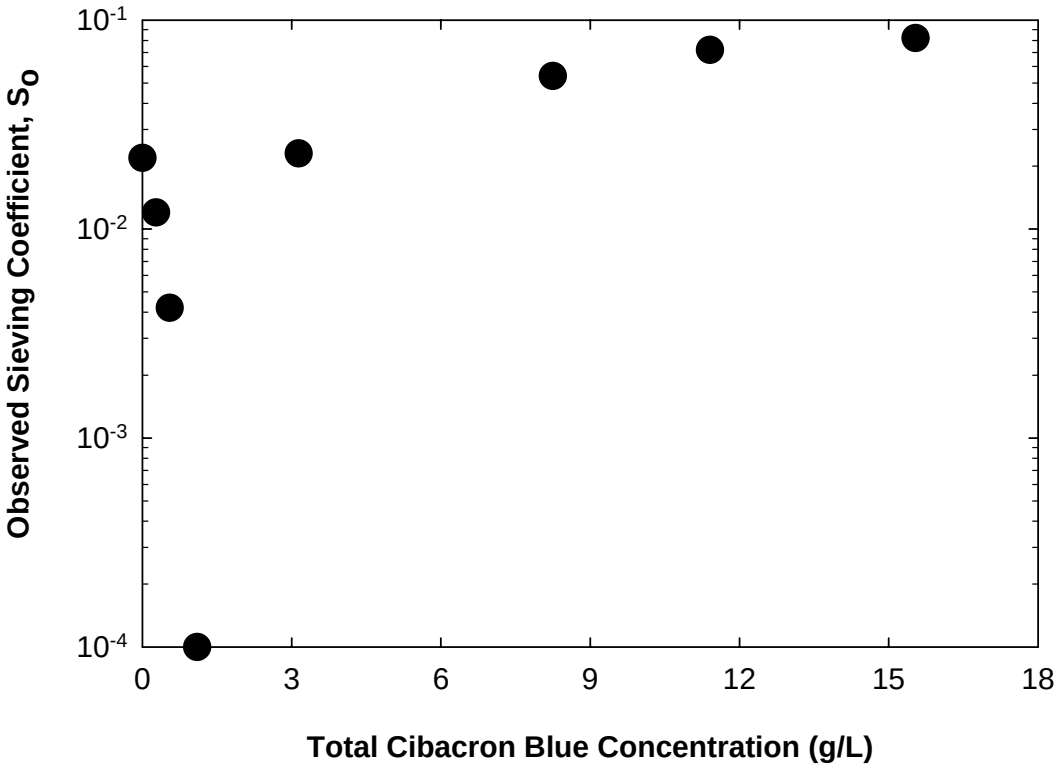

Figure 5.3: Observed sieving coefficients for BSA as a function of the total Cibacron Blue concentration. Data were obtained using a negatively charged 100 kD Ultracel membrane in a 10 mM acetate buffer at pH 5.0 with 8 g/L BSA.

The location of the minimum in the BSA sieving coefficient seen in Figure 5.3 occurs at a molar ratio of Cibacron Blue to BSA of approximately 12:1, which is only slightly larger than the maximum number of molecules of Cibacron Blue that can be bound to a molecule of BSA under these experimental conditions (n = 9.8 in the 10 mM acetate buffer). Thus, the reduction in the BSA sieving coefficient at low Cibacron Blue concentrations is likely due to the increased binding of Cibacron Blue, which causes a significant increase in the net negative charge on the protein as discussed in Chapter 4.

The increase in the BSA sieving coefficient at high Cibacron Blue concentrations is instead due to the increase in the concentration of free Cibacron Blue, and the corresponding increase in the solution ionic strength and electrostatic shielding, that occurs after the protein is essentially saturated with bound Cibacron Blue.

In order to understand the complex behavior seen in Figure 5.3, experiments were performed at fixed ratios of Cibacron Blue to BSA for several values of the solution ionic strength, which was adjusted by the addition of sodium chloride. Results are shown in Figure 5.4 for both an unmodified composite regenerated cellulose membrane (top panel) and a negatively charged version of the Ultracel membrane (bottom panel), with the data plotted as the mean plus/minus the standard deviation as determined from a minimum of three replicate experiments. The data were highly reproducible, with the BSA sieving coefficients typically varying by less than 7 percent among the replicates. The sieving coefficients obtained in the 100 mM solution are nearly independent of the Cibacron Blue concentration, with values of approximately 0.6 for the neutral membrane and 0.12 for the negatively-charged membrane. The smaller sieving coefficients for the negatively-charged membrane at high salt concentrations are primarily due to the reduction in pore size associated with the chemical attachment of the ligand within the membrane pores. The measured value of the hydraulic permeability of the charge-modified membrane was approximately 25% smaller than that for the native membrane, consistent with a reduction in effective pore size of about 0.8 nm as determined using the Hagen-Poiseuille equation (Equation 2.64). In contrast, the BSA sieving coefficient through the negatively-charged membrane in the 25 mM ionic strength solution decreased by more than 2 orders of magnitude upon addition of Cibacron Blue, going from 0.044 in the

absence of Cibacron Blue to 0.0001 at a ratio of 12 molecules of Cibacron Blue to each molecule of BSA. A much smaller effect was seen with the unmodified CRC membrane, with the sieving coefficient decreasing by less than a factor of two over this same range of Cibacron Blue concentrations.

The large reduction in protein transmission in the low ionic strength solution is due to the strong electrostatic exclusion of the negatively-charged complex formed when BSA binds a large number of negatively-charged Cibacron Blue molecules. Model calculations for the net protein charge, accounting for the effects of charge regulation (see Chapter 4), indicate that the BSA charge decreases by approximately 13 electronic charges upon the addition of 12 moles of Cibacron Blue per mole of BSA. This large increase in the net negative charge causes a very large electrostatic exclusion of the BSA from the pores of the negatively-charged membrane due to the direct charge-charge repulsion under these conditions. This effect is much less pronounced with the unmodified membrane, and it is almost completely eliminated at high ionic strength due to the strong electrostatic shielding provided by the bulk electrolyte under these conditions.

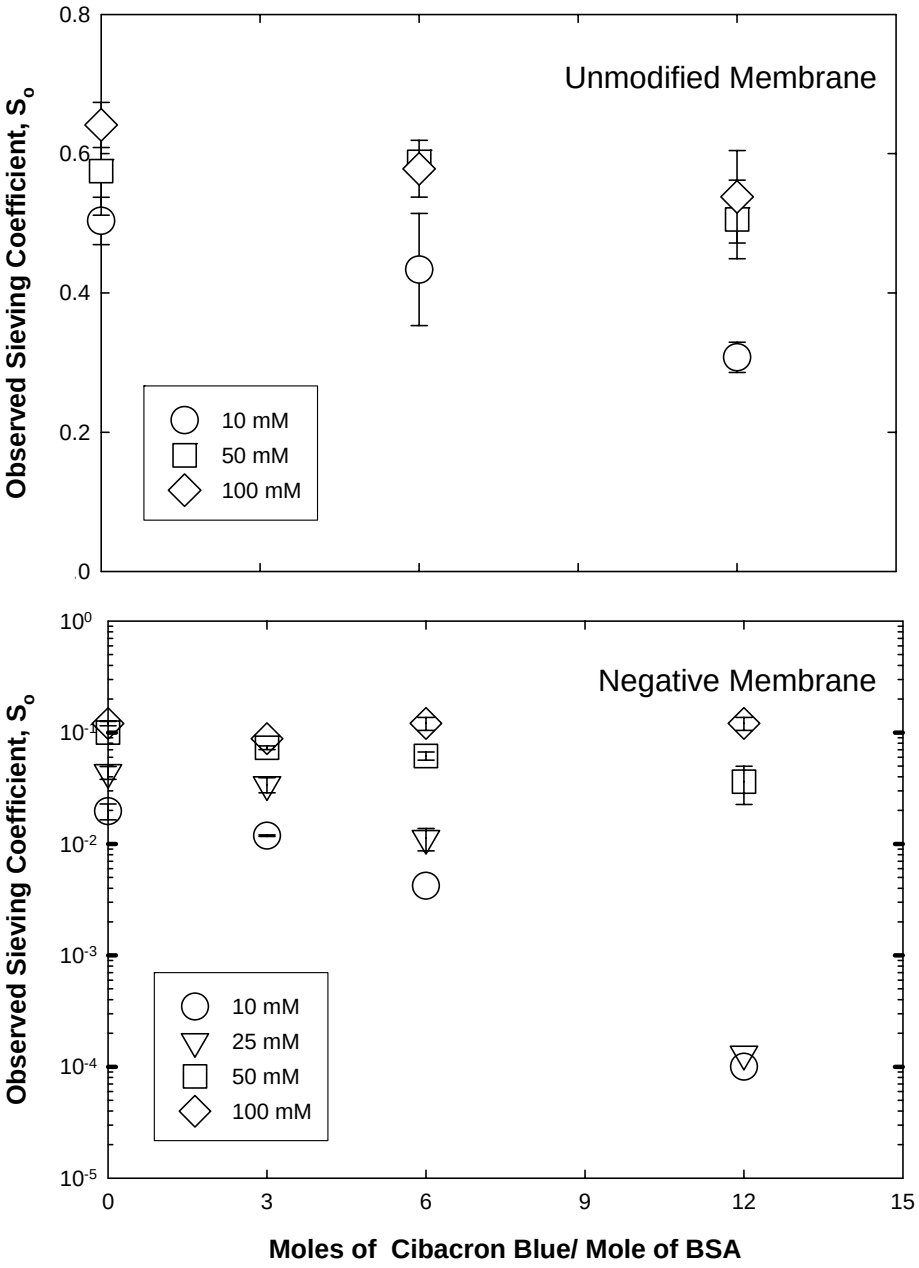

Figure 5.4: Observed sieving coefficients as a function of the molar ratio of Cibacron Blue to BSA at several ionic strength for an unmodified (top panel) and negatively charged (bottom panel) Ultracel membrane. All data were obtained at pH 5.0 using 8 g/L BSA.

The effect of Cibacron Blue on protein sieving at different pH is shown in Figure 5.5. All of the data were obtained using 10 g/L BSA in a 10 mM solution using a 100 kD Ultracel membrane with a surface charge density of -2.3 mC/m^2 over a range of pH. In each case, the BSA sieving coefficient initially decreases with increasing Cibacron Blue concentration due to the increase in negative charge associated with Cibacron Blue binding. The sieving coefficient then passes through a minimum at a Cibacron Blue concentration around 0.5 g/L before increasing at high Cibacron Blue concentrations due to the increased degree of electrostatic shielding. In the absence of any Cibacron Blue, the sieving coefficient decreases with an increase in solution pH due to the increase in net repulsive electrostatic interactions associated with the greater negative charge on the protein at higher pH. In contrast, the sieving coefficient in the presence of 5 g/L of Cibacron Blue is smallest at pH 6 and increases as the pH increases. This behavior is a direct result of the pH dependence of the binding interactions between Cibacron Blue and BSA. BSA binds Cibacron Blue much more strongly at low pH, with the corresponding increase in the net negative charge on the protein leading to the low value of the sieving coefficient obtained in the pH 6 solution at high Cibacron Blue concentrations.

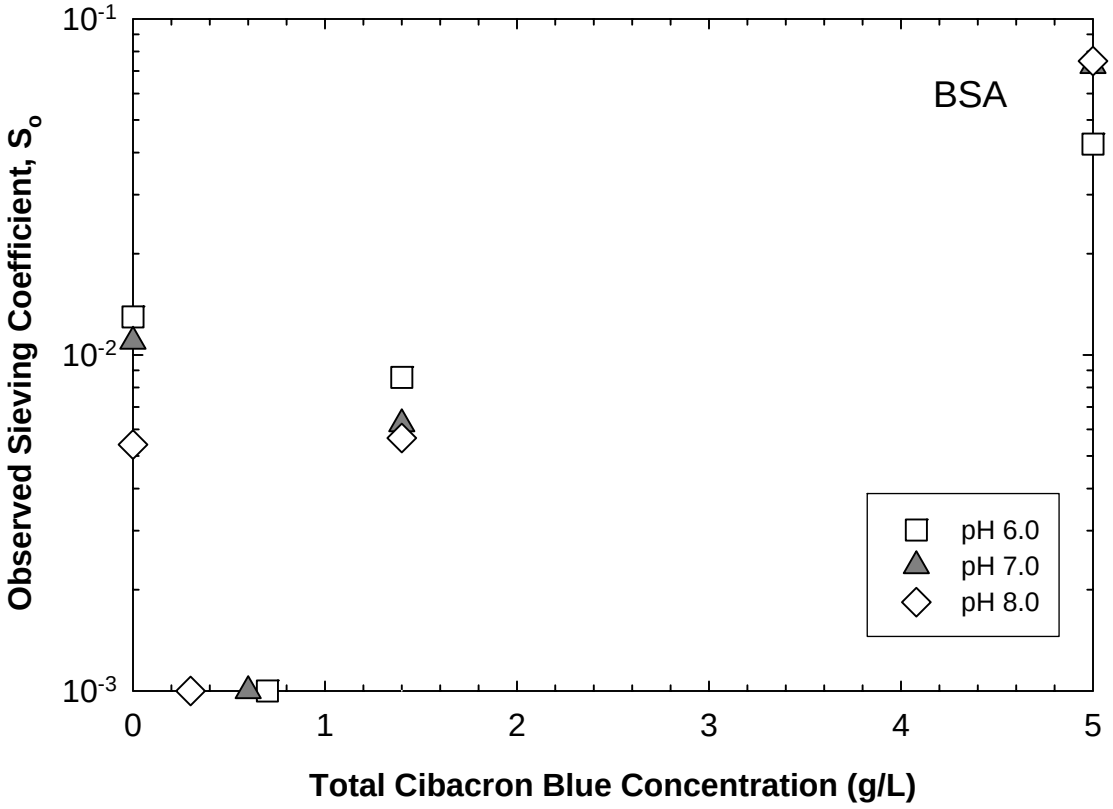

Figure 5.5: Observed sieving coefficients for BSA as a function of the total Cibacron Blue concentration. Data were obtained using a negatively charged 100 kD Ultracel membrane in a 10 mM acetate buffer at various pH with 10 g/L BSA

Additional experimental studies were performed using a 15 g/L ovalbumin solution in 10 mM ionic strength buffers over a range of pH again using a 100 kD charged Ultracel membrane with a surface charge density of -2.3 mC/m^2. The decrease in ovalbumin transmission with increasing pH is directly related to the increase in repulsive electrostatic interactions between the membrane and the protein due to the greater negative protein charge at high pH. The addition of Cibacron Blue causes an increase in the ovalbumin sieving coefficient at all three pH values, consistent with the absence of any significant binding interactions between Cibacron Blue and ovalbumin. Thus, the addition of Cibacron Blue simply shields the electrostatic interactions between the protein and the negatively-charged membrane, an effect that is more pronounced at high pH where the protein has a larger negative charge.

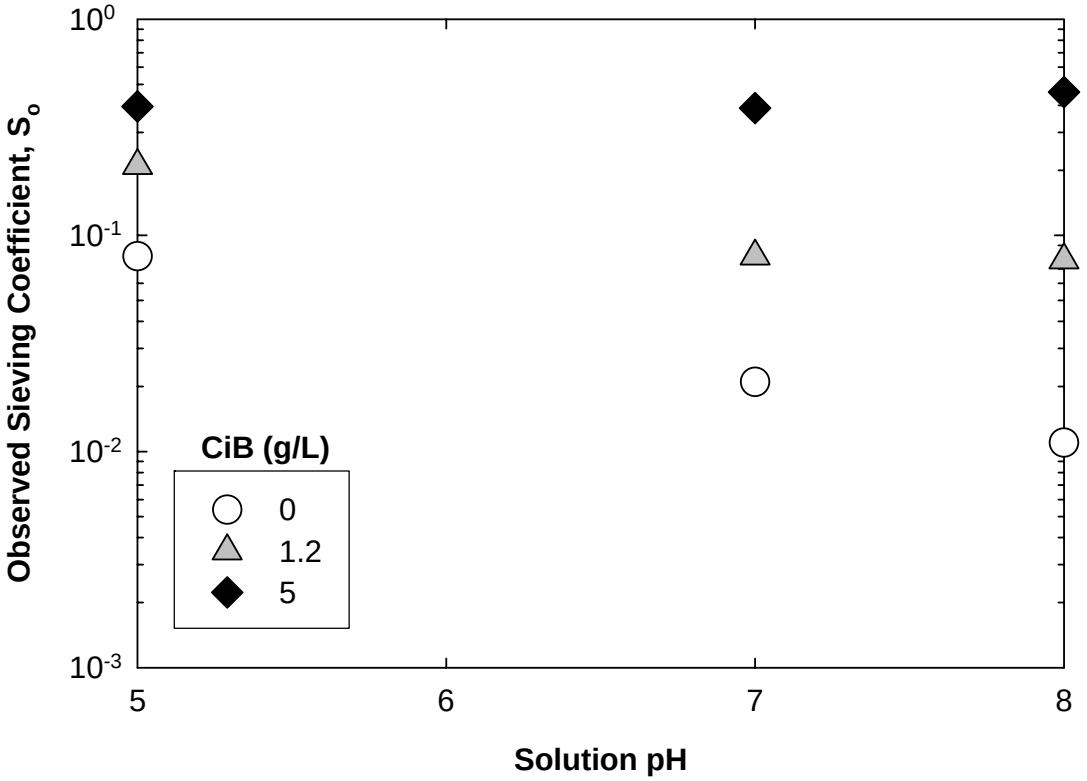

Figure **5.6**: Observed sieving coefficients for ovalbumin as a function of solution pH. Data were obtained using a negatively charged 100 kD Ultracel membrane in a 10 mM buffer and a 15 g/L ovalbumin with varying amounts of Cibacron Blue.

5.4 Data Analysis

The protein sieving coefficient data were analyzed using available hydrodynamic models accounting for the presence of a pore size distribution (Zeman and Zydney, 1996):

$$S_a = \frac{\int_0^\infty \phi K_c n(r) r^4 dr}{\int_0^\infty n(r) r^4 dr} \qquad (5.2)$$

where S_a is the actual sieving coefficient, which is equal to the ratio of the protein concentration in the filtrate solution to that in the solution immediately upstream of the membrane. ϕ is the equilibrium partition coefficient for the protein entering the pore and K_c is the hindrance factor for convection, which accounts for the additional hydrodynamic drag on the solute molecule in the presence of a pore wall. The r^4 weighting in the numerator and denominator of Equation (5.2) accounts for the dependence of the volumetric filtrate flow rate on the pore radius assuming Poiseuille flow through the pores. All calculations were performed using a log-normal pore density function, *n(r),* where *r* is the pore radius (Zydney et al. 1994):

$$n(r) = \frac{n_o}{r\sqrt{2\pi}\left[\ln\left(1+\frac{\sigma}{r_{mean}}\right)^2\right]^{1/2}} \exp\left[-\frac{\left(\ln\frac{r}{r_{mean}}\left[1+\left(\frac{\sigma}{r_{mean}}\right)^2\right]^{1/2}\right)}{2\ln\left[1+\left(\frac{\sigma}{r_{mean}}\right)^2\right]}\right] \qquad (5.3)$$

The equilibrium partition coefficient for the protein was evaluated using the model developed by Smith and Deen (1980) for the partitioning of a charged sphere in a charged cylindrical pore:

$$\phi = (1-\lambda)^2 \exp(-\frac{\psi}{kT}) \qquad (5.4)$$

where ψ/kT is the dimensionless electrostatic potential energy of interaction and λ is the ratio of the solute to pore radii. The pre-exponential term accounts for the steric exclusion of the solute from the region within one solute radius of the pore wall.

The electrostatic potential energy of interaction was determined for a sphere located at the pore axis based on the centerline approximation. ψ/kT was evaluated by Smith and Deen (1980) by solving the linearized Poisson-Boltzmann equation using matched expressions in spherical and cylindrical coordinates yielding:

$$\frac{\psi}{kT} = A_{ss}\sigma_s^2 + A_{sp}\sigma_s\sigma_p + A_{pp}\sigma_p^2 \qquad (5.5)$$

where σ_s and σ_p are the surface charge density of the solute and pore wall, respectively, and A_{ss}, A_{sp} and A_{pp} are all positive coefficients which depend on the solution ionic strength, pore radius, and solute radius. Expressions for these parameters have been summarized by (Burns and Zydney, 2001) and are reproduced in Table 2.2. As described by Equation (5.5), the electrostatic energy of interaction has three distinct contributions: one from the distortion of the electrical double layer surrounding the sphere (given by the term involving σ_s^2), one from direct charge-charge interactions between the charged sphere and the membrane pores, and one that accounts for the deformation of the

electrical double layer within the pore. These phenomena have been discussed in more detail by Burns and Zydney (2001) and in Chapter 2 of this thesis.

The membrane surface charge density was evaluated from streaming potential measurements. The effective surface charge density of the membrane can be calculated directly from the zeta potential as:

$$\sigma_p = 4c_o F\kappa^{-1} \sinh(F\zeta / 2RT) \qquad (5.6)$$

where c_0 is the bulk salt concentration, F is Faradays constant, R is the gas constant, T is the absolute temperature, and κ^{-1} is the thickness of the electrical double layer

$$\kappa^{-1} = \left[\frac{F^2}{\varepsilon_o \varepsilon_r RT} \sum z_i^2 C_i \right]^{1/2} \qquad (5.7)$$

where z_i and C_i are the valence and concentration of each ion. Equations (5.5) and (5.6) neglect the effects of surface conductance and a thick double layer, thus the calculated values of σ_p represent an effective (and approximate) surface charge density of the membrane pores.

Model calculations were performed as follows. First, the extent of Cibacron Blue binding to the protein was evaluated using the previously determined binding isotherm (Equation 4.3). The net charge on the protein-Cibacron Blue complex was then evaluated using the charge regulation model described in Chapter 4 which accounts for the dissociation of the acidic and basic amino acids on the protein as well as the binding of acetate anions (Eqs. 4.5 to 4.13). The solution ionic strength was then determined as:

$$I = \frac{1}{2}\sum_i z_i^2 C_i \qquad (5.8)$$

where the summation is over all (free) ionic species with z_i the ion valence and C_i the concentration of the free ion. Equation (5.8) thus accounts for the presence of acetate, Na^+, Cl^-, and the negatively-charged Cibacron Blue, with the concentration of the latter determined from the free Cibacron Blue concentration (evaluated from the binding isotherm) with $z_i = -3$. The surface charge density of the unmodified cellulose membrane at pH 5 and 10 mM ionic strength was σ_p = -0.0002 C/m^2 while that for the negatively-charged membrane was σ_p = -0.01C/m^2, with both of these values determined from the streaming potential measurements.

The electrostatic energy of interaction was then calculated from Equation (5.5) using the experimentally determined values of membrane surface charge density, with the actual sieving coefficient determined by integration over the log-normal distribution using a mean pore radius of 62 Å for the unmodified membrane and 54 Å for the negatively-charged membrane with $\sigma/r_{mean} = 0.2$ in both cases. The choice of σ/r_{mean} = 0.2 was based on previous studies of similar ultrafiltration membranes (Zeman and Zydney, 1996). The mean pore radius was evaluated by fitting the Hagen-Poiseuille equation, Equation (2.64), to the experimentally measured values of the hydraulic permeability ($L_p = 3.0 \times 10^{-12}$ m for the unmodified membrane and $L_p = 2.3 \times 10^{-12}$ m for the charge modified version) using a membrane porosity of 50% and skin thickness of 1 μm.

Figure 5.7 shows a comparison between the model calculations and the experimental data for the actual protein sieving coefficient, S_a, as a function of the

Cibacron Blue concentration for the 10 mM ionic strength solution using both the unmodified and negatively-charged membranes. The actual sieving coefficients were calculated from the measured values of the observed sieving coefficients using a simple stagnant film model to account for the effects of concentration polarization in the stirred cell (Zeman and Zydney, 1996):

$$S_a = \frac{S_o}{(1 - S_0)\exp\left(\frac{J_v}{k}\right) + S_0} \qquad (5.9)$$

where J_v is the filtrate flux and k is the bulk mass transfer coefficient, which was estimated as 9.6 μm/s under the conditions of these experiments (Pujar and Zydney, 1994). The model calculations are in good agreement with the data for both the unmodified and negatively-charged versions of the Ultracel membrane over the entire range of Cibacron Blue concentrations. The model does tend to over-predict the actual sieving coefficient for the negatively-charged membrane in the absence of Cibacron Blue, which is due to the small positive charge that is calculated for BSA under these conditions using the charge regulation model presented in Chapter 4. If the BSA charge were reduced by only a single electronic charge, the calculated value for S_a would be in excellent agreement with the data at zero Cibacron Blue concentration. Such small deviations in the BSA charge can arise from the presence of different isoforms of BSA (e.g., different intermolecular disulfide linkages) and / or different amounts of fatty acid. Alternatively, this discrepancy may simply reflect the approximations in the charge regulation model, in particular the assumptions of a perfectly uniform surface charge and

equal pK_a values for each type of amino acid, irrespective of the detailed location of the various charged residues over the surface of the protein.

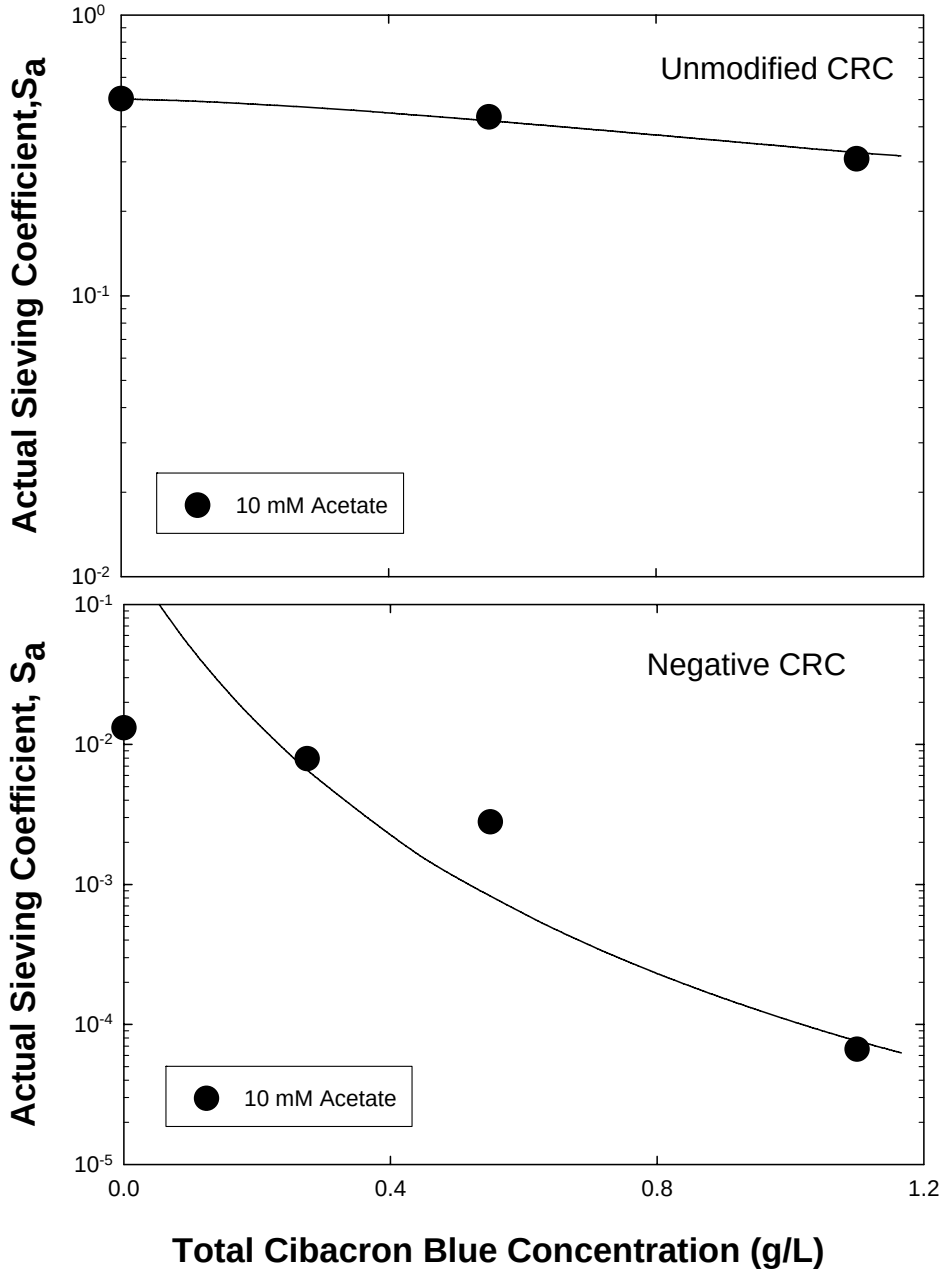

Figure 5.7: Actual sieving coefficients for BSA through the unmodified (top panel) and negatively charged (bottom panel) 100 kD CRC membrane as a function of the total Cibacron Blue concentration in a 10 mM acetate buffer at pH 5.0. Solid curves represent model calculations as described in the text.

The different contributions to the energy of interaction associated with the three terms in Equation (5.5) are shown in Figure 5.8 along with the experimental data for the actual sieving coefficient, S_a, for the neutral (top panel) and the charged version (bottom panel) of the 100 kD Ultracel membrane. Also shown for comparison is the purely steric contribution $(1-\lambda)^2$. The contribution of the term $A_{pp}\sigma_p^2$ is quite small for both membranes. The predominant contribution to the electrostatic energy arises from the charge-charge interaction as described by the term $A_{sp}\sigma_s\sigma_p$. This term is attractive when there is no dye bound to the protein but becomes repulsive after the binding of only a single mole of Cibacron Blue due to the corresponding shift in the net protein charge. The effect of charge - charge interactions is much more pronounced with the negative membrane as expected. The term $A_s\sigma_s^2$ accounts for the distortion of the electrical double layer around the complex and is always repulsive.

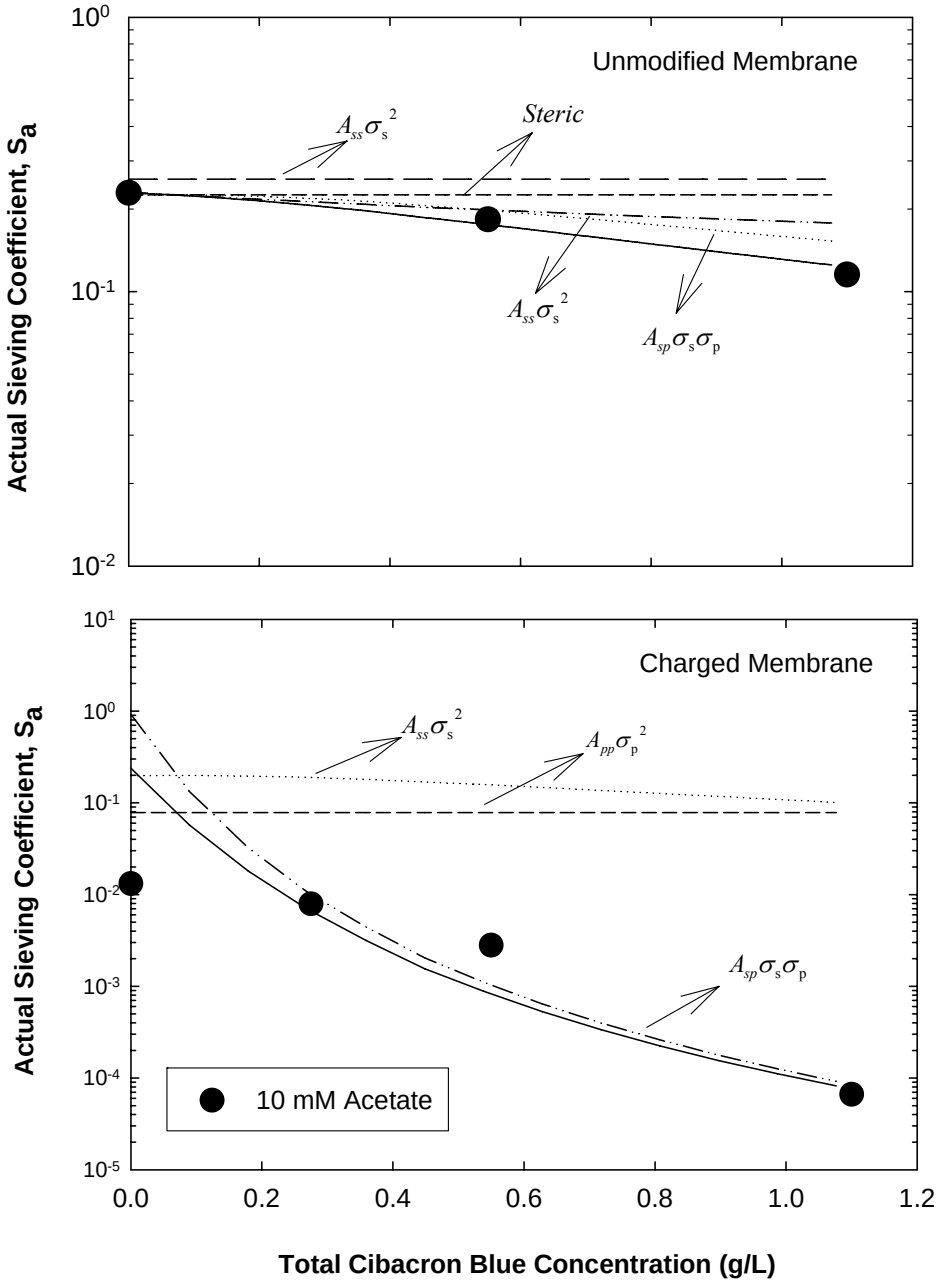

Figure **5.8**: Contributions of the individual terms to the dimensionless electrostatic energy of interaction using a neutral (top panel) and negatively charged (bottom panel) membrane.

The effect of the Cibacron Blue concentration on the sieving behavior of BSA is examined in more detail in Figure 5.9 with the calculated values of the actual sieving coefficient being plotted as a function of the total concentration of Cibacron Blue. The solid symbols are the experimental results, with the S_a values calculated from the observed sieving coefficient data in Figure 5.3 using the stagnant film model (Equation 5.9). The solid curve is the full model calculation, which properly captures both the reduction in BSA sieving coefficient at low Cibacron Blue concentrations and the minimum at a Cibacron Blue concentration of 1.0 g/L. The dashed curve shows the model calculations accounting for the change in BSA charge upon the addition of Cibacron Blue but neglecting any change in the solution ionic strength (which was kept constant at 10 mM). The dashed curve accurately describes the data at low Cibacron Blue concentrations, confirming that the reduction in the sieving coefficient under these conditions is a direct result of the change in net protein charge associated with the binding of the negatively-charged Cibacron Blue molecules. The dashed curve dramatically underpredicts the sieving coefficient at higher Cibacron Blue concentrations since it neglects the increase in ionic strength, and thus the reduction in electrostatic repulsion, that occurs under these conditions. The full model, which accounts for both the change in protein charge and the change in solution ionic strength, is in excellent agreement with the experimental data over the full range of Cibacron Blue concentrations.

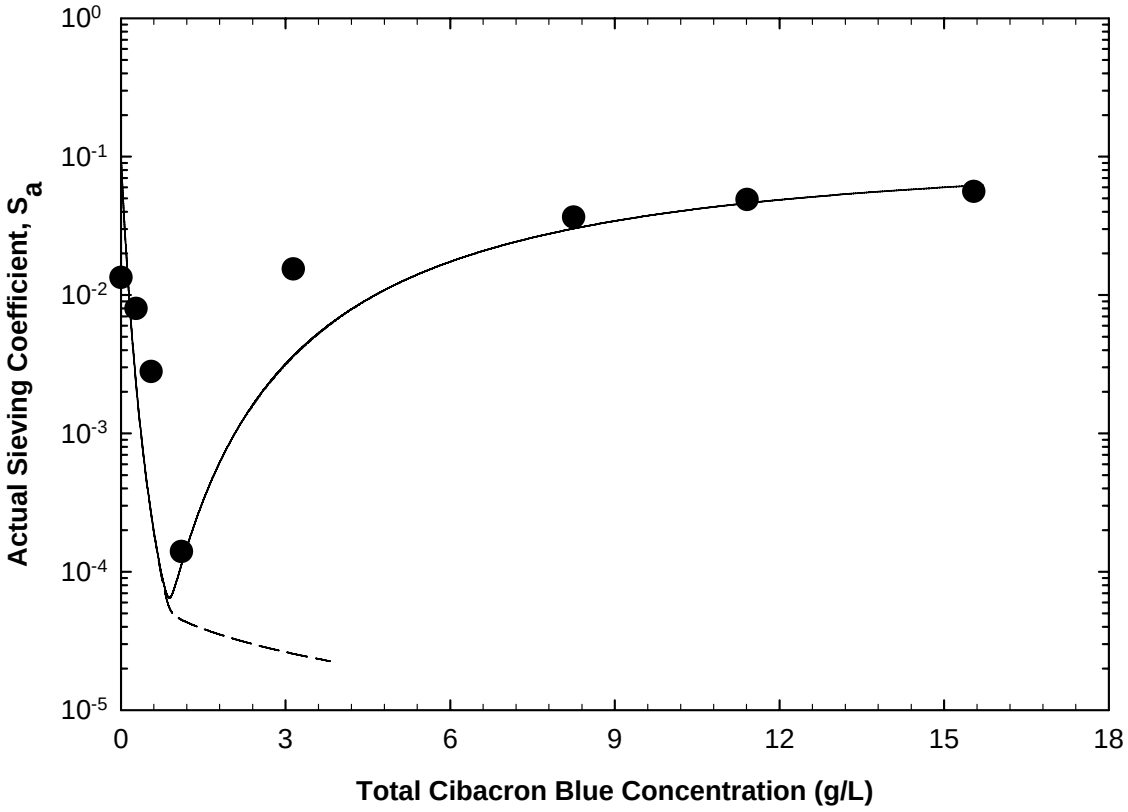

Figure **5.9**: Effect of Cibacron Blue on the actual sieving coefficient for BSA in a 10 mM acetate buffer at pH 5 using an 8 g/L BSA solution. The solid curve is evaluated using the full model while the dashed curve assumes a constant ionic strength of 10 mM irrespective of the concentration of free Cibacron Blue.

The effect of Cibacron Blue on the transmission of ovalbumin is examined in Figure 5.10. The upper panel shows the calculated values of the net protein charge on the left axis and the calculated values of the solution ionic strength on the right axis, both as a function of the total Cibacron Blue concentration added to the protein solution. Model calculations for the net protein charge were performed using an ovalbumin concentration of 15 g/L in a pH 5.0 buffer. The addition of Cibacron Blue causes a significant increase in the net negative charge of ovalbumin due to the weak (but significant) binding interactions between ovalbumin and the Cibacron Blue in combination with the shift in the solution ionic strength associated with the free Cibacron Blue.

The lower panel shows the calculated values of the actual sieving coefficient as a function of the total concentration of Cibacron Blue. The solid symbols are the experimental data, with the S_a values calculated from the observed sieving coefficient data in Figure 5.6 using the stagnant film model (Equation 5.9). The solid curve is the full model calculation, which predicts a slight decrease in ovalbumin sieving coefficient from a value of 0.1 to 0.068 at low Cibacron Blue concentrations followed by a slight increase in the sieving coefficient at high Cibacron Blue concentrations. This behavior is in sharp contrast to the dramatic decrease in predicted sieving coefficient (over two orders of magnitude) for BSA. The model calculations significantly over-predict the ovalbumin sieving coefficient in the absence of Cibacron Blue, which may again be due to small discrepancies in the protein charge under these conditions.

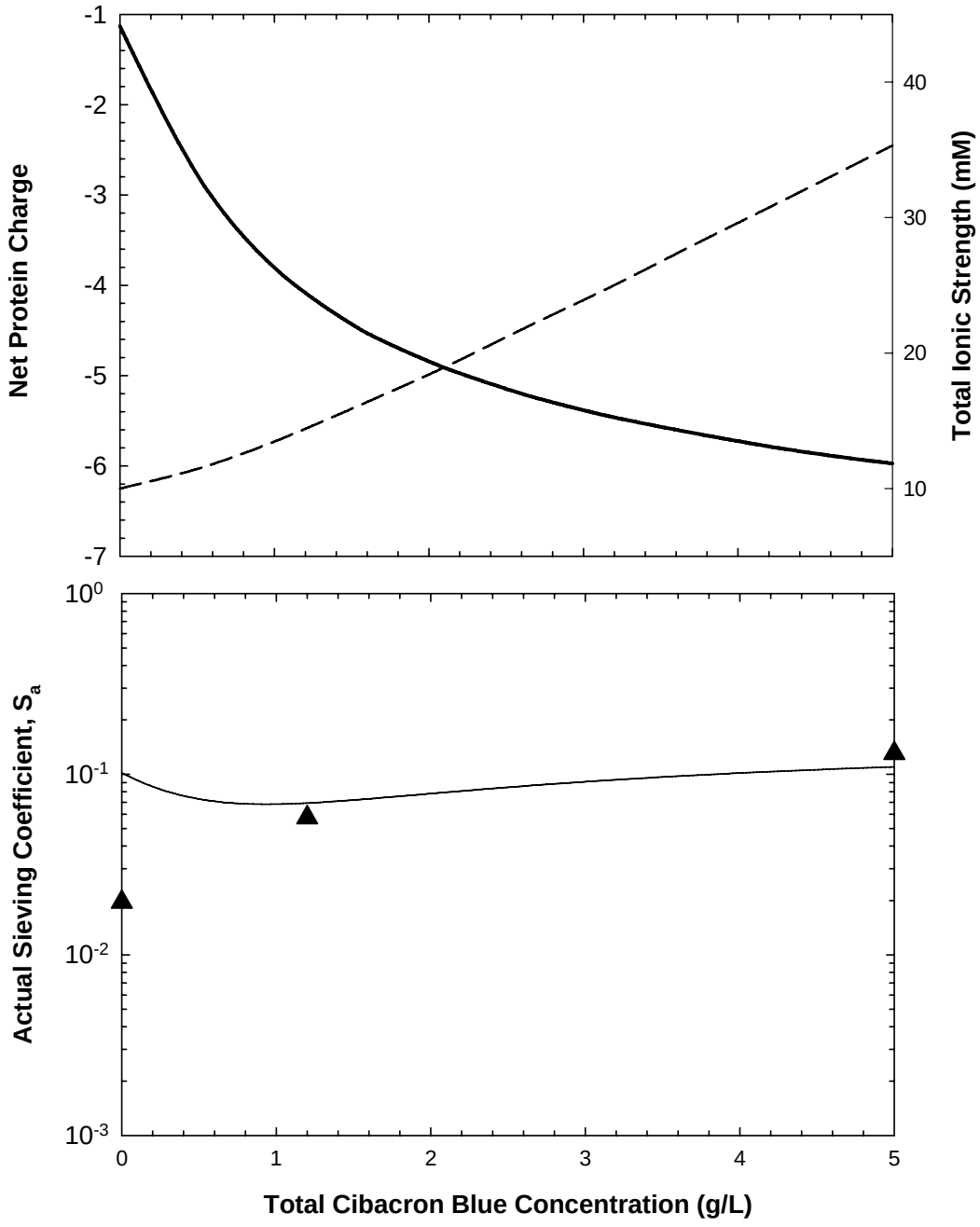

Figure **5.10**: Effect of Cibacron Blue on the actual sieving coefficient for ovalbumin in a 10 mM acetate buffer at pH 5 using a 15 g/L ovalbumin solution. The top panel shows the net protein charge (solid line) and overall solution ionic strength (dashed line). The bottom panel shows the actual sieving coefficient, with the solid curve evaluated using the full model.

5.5 Model Simulations

5.5.1 Effect of Equilibrium Binding Parameters

A series of model simulations were performed to understand the effects of the equilibrium binding parameters n and K_{eq} on protein transport. All of the model simulations were performed for a 10 g/L (1.45 mM) BSA solution in a 10 mM pH 5.0 buffer. Acetate binding was assumed to be negligible. Calculations were performed using a 100 kD membrane with a pore size of 5.4 nm and a surface charge density of - 0.01 C/m^2.

The simulations were performed as described previously using specified values of n and K_{eq}. In each case, the protein surface charge density was calculated as a function of the solution pH and the amount of Cibacron Blue using the charge regulation model, with the electrostatic interactions evaluated accounting for the contribution of free Cibacron Blue. The actual sieving coefficient was the determined using Equations 5.2 to 5.9 using a log-normal pore size distribution with a $\sigma/r_{mean} = 0.2$.

Figure 5.11 examines the effect of the number of moles of Cibacron Blue bound per mole of BSA (n) on the BSA sieving coefficient with the equilibrium binding constant kept constant at $K_{eq} = 10^5\ M^{-1}$. The sieving coefficient in the absence of Cibacron Blue is unaffected by the value of n as expected. The location of the minimum in the BSA sieving shifts to larger Cibacron Blue concentrations with increasing n since the protein becomes saturated with the dye at a higher Cibacron Blue concentration. In addition, the depth of the minimum in the sieving coefficient becomes much more

pronounced at higher values of n; the predicted sieving at n =10 is more than two orders of magnitude smaller than that at n = 2. The protein sieving coefficients at very high concentrations of Cibacron Blue approach a constant asymptotic value that is independent of n since the excess dye shields the electrostatic interactions under these conditions. However, the Cibacron Blue concentration needed to achieve this asymptote increases with increasing values of n since the greater amount of bound dye increases the net negative charge on the protein while simultaneously reducing the concentration of the free Cibacron Blue.

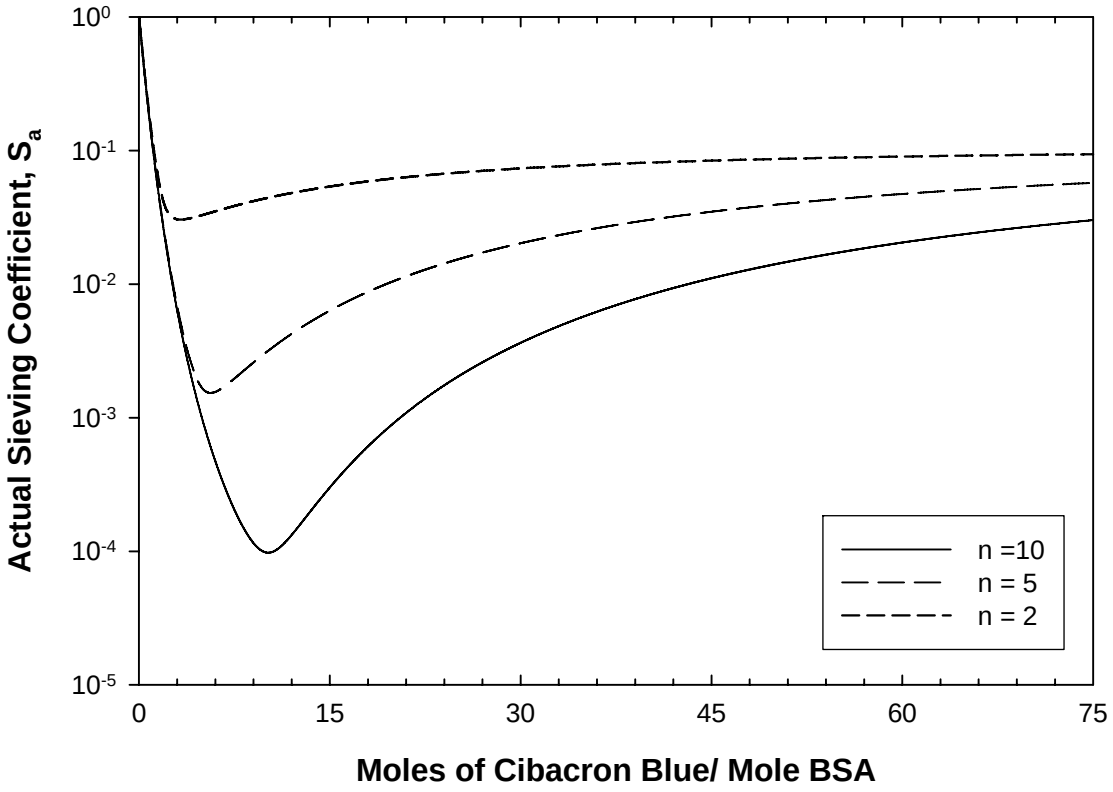

Figure **5.11**: Model simulations to predict values of S_a for different values of n with the K_{eq} kept constant at a value of 10^5 M^{-1}.

These phenomena can be understood more clearly by plotting the calculated values of the net protein charge (top panel) and solution ionic strength (bottom panel) as a function of the amount of added Cibacron Blue for several values of n. The protein charge was again evaluated using the charge regulation model accounting for the change in charge due to binding of Cibacron Blue. The predicted protein charge is nearly independent of n at very low concentrations of Cibacron Blue but becomes much more negative as n increases due to the greater number of molecules of Cibacron Blue bound by the protein. The solution ionic strength remains constant at low Cibacron Blue concentrations since nearly all of the dye is bound to the protein (resulting in a very low concentration of free dye). The ionic strength increases linearly with increasing Cibacron Blue concentration at high dye concentrations, i.e. after the BSA becomes fully saturated. The ionic strength decreases with increasing values of n since more of the dye is bound to the protein under these conditions.

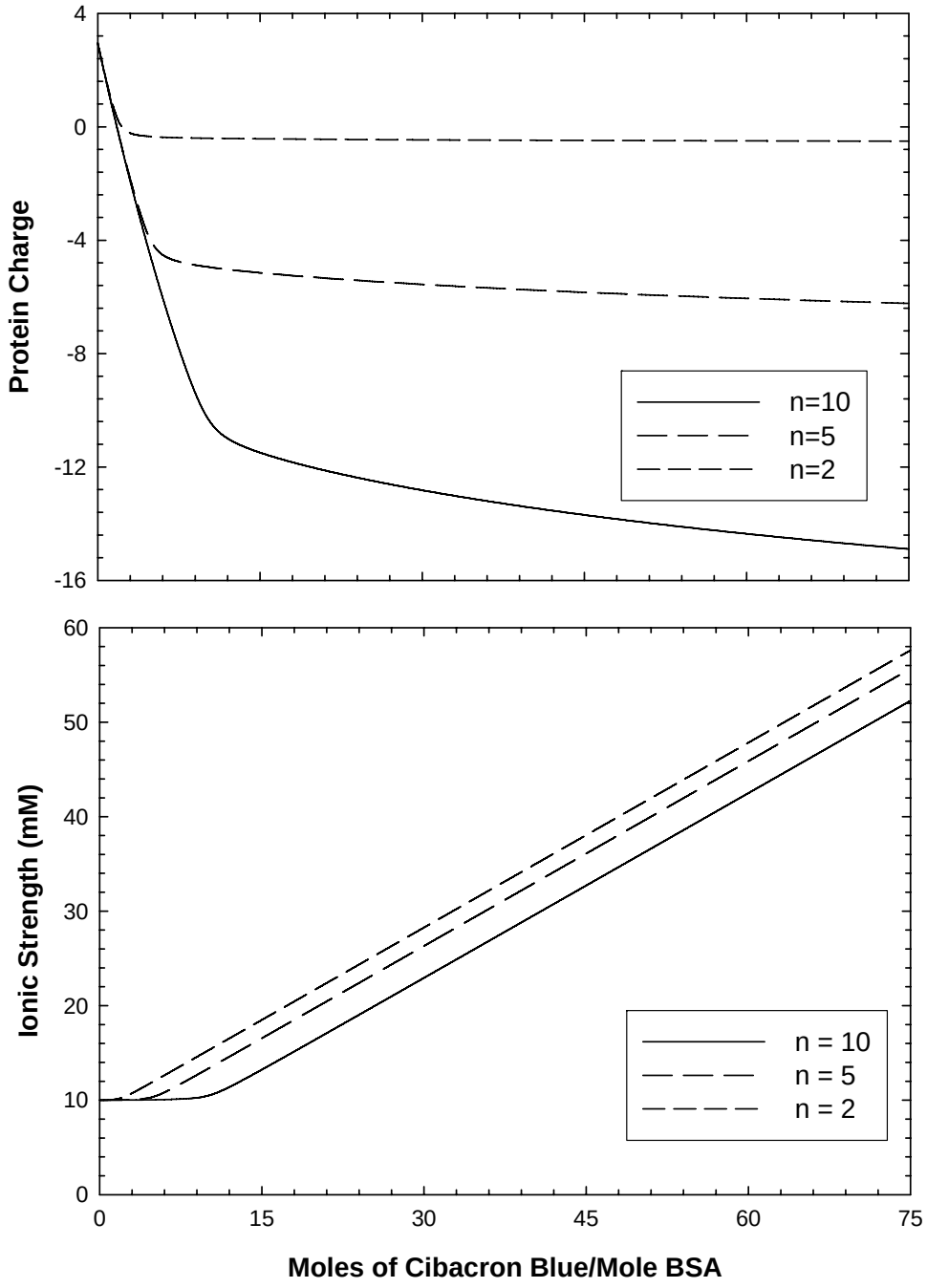

Figure **5.12**: Predicted variation in protein charge (top panel) and solution ionic strength (bottom panel) as a function of n, upon addition of ligand with the K_{eq} kept constant at a value of 10^5 M^{-1}.

Figure 5.13 shows the corresponding set of simulations using a range of values for the equilibrium binding constant K_{eq} with the number of moles of Cibacron Blue bound per mole of BSA kept constant at n = 10. The BSA sieving coefficient decreases with increasing Cibacron Blue concentration, with the slope of the initial decline increasing with increasing values of K_{eq} due to the increase in the amount of ligand bound to the protein. The simulations with $K_{eq} \geq 10^3$ M^{-1} show a distinct minima in the sieving coefficient due to the trade-off between the increase in the net negative charge of the protein and the increase in solution ionic strength with increasing Cibacron Blue concentration. This minimum is absent at smaller values of K_{eq} due to the very weak ligand binding under these conditions. Instead, the sieving coefficient decreases monotonically with increasing Cibacron Blue concentration due to the increase in ionic strength associated with the free dye. Note that the model predicts a small attractive interaction in the absence of Cibacron Blue since the BSA has a small positive charge. Simulations at slightly higher pH show a monotonic increase in the BSA sieving coefficient with increasing Cibacron Blue concentrations at small K_{eq} due to the shielding of the repulsive interactions. The results clearly indicate that equilibrium binding constants greater than 10^3 M^{-1} are needed to achieve the desired control of the protein sieving coefficient using small charged affinity ligands for this system.

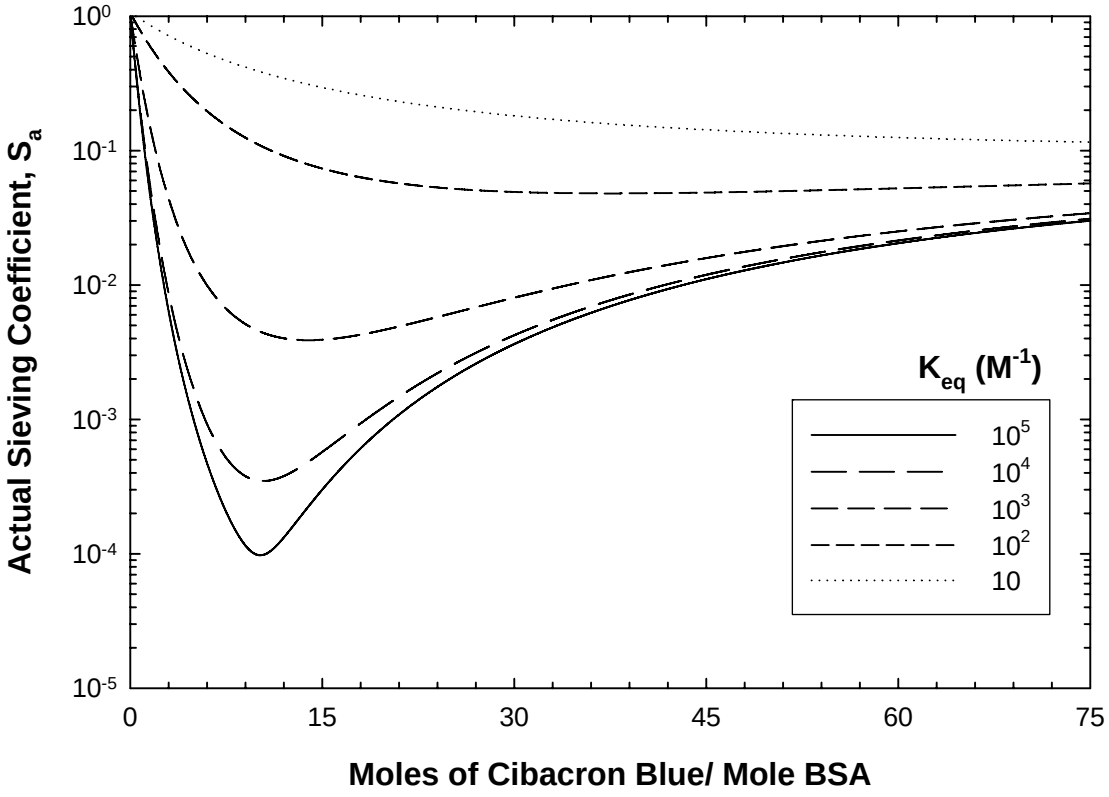

Figure **5.13**: Model simulations for the effects of the equilibrium binding constant (K_{eq}) on the BSA sieving coefficient with n = 10.

5.5.2 Effect of Membrane Pore Size and Standard Deviation

Figure 5.14 shows model simulations for the actual protein sieving coefficient of BSA as a function of Cibacron Blue concentration with n being kept constant at a value of 10 and K_{eq} being kept constant at a value of 10^5 M^{-1}. In all the simulations the membrane surface charge was kept constant at -0.01 C/m^2. The top panel shows model calculations with the standard deviation of the membrane kept constant at a value of 0.2 over a range of average membrane pore radius and the lower panel shows calculations performed for a range of standard deviations with the average pore size being kept constant at 6.0 nm. The effect of average pore size is clearly demonstrated by the simulations shown in the top panel, in each case the actual sieving coefficient follows the same trend with increasing Cibacron Blue concentration with a mimima being obtained at values where there is just enough Cibacron Blue in the system to saturate the binding sites on the protein. As expected there is a dramatic increase in the sieving of the protein as a the membrane pore size is increased with the predicted sieving coefficient of the protein being over four orders of magnitude greater using a membrane with a pore size of 10 nm compared with a pore size of 4.5 nm at conditions that correspond to the addition of approximately 12 moles of Cibacron Blue per mole of BSA. The larger the pore size the greater the probability that the protein follows a flow path in the system where it does not feel the effect of the electrostatic repulsive interactions prevalent in areas adjacent to the membrane pore surface. However at conditions of higher ionic salt, i.e. corresponding to the addition of a higher concentration of dye in the system, the differences in the sieving coefficient decreases to less than two orders of magnitude

clearly demonstrating the effect of pore size and the effect of electrostatic interactions in the system.

A similar trend is observed with simulations for the actual sieving coefficient over a range of standard deviations as shown in the lower panel. For a membrane with a tight pore size distribution (0.1) the transmission profile of the protein is well defined with the presence of a distinct minima at low dye concentrations with a corresponding increase at high ligand concentrations. In this case the membrane primarily consist of pores with are similar is size to the average pore size. However with an increase in the breath of the distribution the membrane looses selectivity because of the enhanced protein transmission through the larger pores.

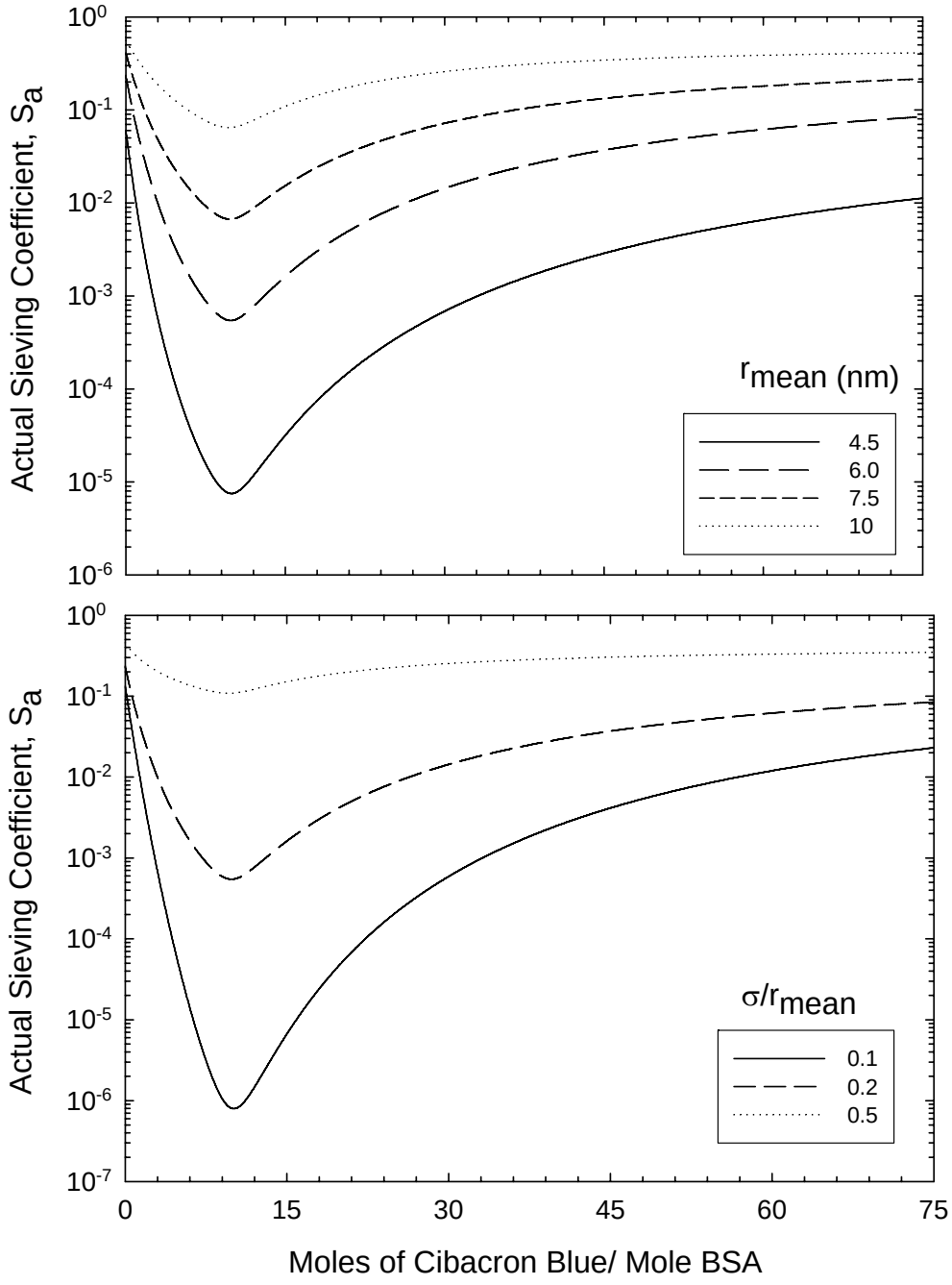

Figure **5.14**: Model simulations showing the effect of pore size with the standard deviation kept constant at 0.2 (top panel) and the effect of standard deviation with the pore size kept constant at 6.0 nm (bottom panel) on the actual sieving coefficient

5.6 Discussion

The experimental data obtained in this Chapter clearly demonstrate the feasibility of using a small charged ligand to control protein transport during ultrafiltration. In this case, the addition of approximately 1 g/L of Cibacron Blue to an 8 g/L solution of BSA caused a reduction in the BSA sieving coefficient by more than two orders of magnitude, from 0.02 to approximately 10^{-4}, due to the strong electrostatic exclusion of the negatively-charged BSA complex from the negatively-charged membrane. This effect is completely eliminated at high ionic strengths and is reduced when using a neutral version of the Ultracel membrane due to the reduction in the electrostatic repulsion.

The effect of Cibacron Blue on the BSA sieving coefficient arises from two distinct phenomena: the change in net protein charge due to binding of the negatively-charged dye and the change in solution ionic strength due to the presence of free ligand in solution. The first effect dominates at low Cibacron Blue concentrations since most of the added dye binds to the protein. The second effect dominates at high Cibacron Blue concentrations where the binding sites on the protein are fully saturated with dye. Model calculations accounting for both of these phenomena are in excellent agreement with the experimental data for BSA transmission. Simulations performed over a range of binding parameters were used to further explore the effects of dye binding and changes in solution ionic strength on the behavior of this type of affinity ultrafiltration system.

The presence of these two contributions leads to a distinct optimum in the ligand concentration for maximizing the electrostatic interactions and in turn maximizing the extent of protein retention. For the BSA – Cibacron Blue system, this optimal ligand

concentration corresponds to conditions in which there are just sufficient ligand to fully saturate all of the binding sites on the protein. Since BSA can bind up to 10 molecules of Cibacron Blue, the increase in electrostatic interactions is quite dramatic, leading to a two order of magnitude reduction in protein transmission through the negatively-charged membrane.

In contrast to the sieving behavior of BSA the transmission of ovalbumin is largely unaffected by the presence of the ligand since there are minimal binding interactions between Cibacron Blue and ovalbumin. The binding selectivity of Cibacron Blue binding can thus be used to modulate the surface charge, and in turn the protein transmission, providing an opportunity to significantly enhance the resolution of membrane processes for protein separations. This is discussed in more detail in Chapter 6 of this thesis.

Chapter 6

HIGH RESOLUTION PROTEIN SEPARATIONS USING AFFINITY ULTRAFILTRATION WITH SMALL CHARGED LIGANDS

6.1 Introduction

Affinity ultrafiltration can provide high resolution separations by exploiting the selectivity of biomolecular binding interactions while maintaining the high throughput characteristics of conventional ultrafiltration processes. Mattiasson and Ramstrop (1984) demonstrated the feasibility of using affinity ultrafiltration for the purification of Concanavalin A using heat killed Saccharomyces cerevisae as the affinity ligand. The separation was performed using a standard hollow fiber membrane with a molecular weight cut-off of 1,000 kD which was fully retentive to the very large binding complex formed between Concanavalin A and the S. cerevisiae while allowing the unbound protein to pass relatively freely through the membrane.

Subsequent studies of affinity ultrafiltration have examined the isolation of urokinase using N-acryloyl-m-aminobenzamide copolymerized with acrylamide as an affinity macroligand (Male et. al., 1990), the purification of avidin using biotinylated liposomes (Power et al., 1990), the isolation of human serum albumin and lysozyme using Cibacron Blue bound to agarose (Herrak. and Merrill, 1989), and the recovery of BSA using highly substituted blue sepharose (He et al., 1998). Affinity ultrafiltration has also been used to separate chiral molecules using stereoselective macroligands. For example, BSA has been used for the optical resolution of racemic mixtures of tryptophan

(Poncet et al., 1997; Romero and Zydney, 2001) and human serum albumin has been used for the separation of ibuprofen (Itoh et al., 1997).

These applications of affinity ultrafiltration all used very large macroligands, relative to the size of the desired product, to obtain the desired retention of the ligand-product complex using conventional ultrafiltration membranes. However, these macroligands tend to be very expensive, which has severely limited the viability of affinity ultrafiltration for commercially relevant separation processes. In addition, the use of small ligands bound to large carriers, e.g., Cibacron Blue bound to agarose (Herrak and Merrill, 1989), can result in a loss of ligand accessibility, mass transfer limitations, and/or problems with leaching of the ligand from the large carrier over time. The net result is that there are currently no large-scale commercial applications of affinity ultrafiltration for the purification of high value products.

Affinity ultrafiltration would be much more attractive commercially if one could employ a relatively small inexpensive affinity ligand to effect the separation. Recent work by Rao and Zydney (2005), as discussed in Chapter 5, has demonstrated that small charged dyes can dramatically alter the rate of protein transport through electrically charged ultrafiltration membranes due to the strong electrostatic interactions between the dye-protein complex and the charged membrane. For example, the addition of 1 g/L of Cibacron Blue to an 8 g/L solution of bovine serum albumin reduced the BSA sieving coefficient by more than two orders of magnitude.

The objective of this study was to demonstrate the feasibility of using affinity ultrafiltration with the small charged ligand Cibacron Blue for separation of the model protein mixture of BSA and ovalbumin. Ovalbumin and BSA have similar size and

surface charge, but the data obtained in Chapter 4 clearly indicate that ovalbumin has limited binding interactions with Cibacron Blue. Experiments were performed in this Chapter to identify the optimal conditions for the separation of ovalbumin and BSA using this affinity ultrafiltration process. The results clearly demonstrate that high resolution protein separations can be achieved using a small charged affinity ligand with high binding specificity in combination with an electrically-charged ultrafiltration membrane to retain the like-charged affinity complex.

6.2 Material and Methods

Experiments were performed using bovine serum albumin and ovalbumin. BSA has an isoelectric point (pI) of approximately 4.9 and a molecular weight of 67 kD while ovalbumin has an isoelectric point (pI) of approximately 4.5 and a molecular weight of 44 kD. Cibacron Blue 3GA was used as the small affinity ligand. Cibacron Blue has a molecular weight of 0.774 kD and contains three sulfonic acid groups attached to an aromatic ring structure.

Buffer solutions were prepared by dissolving pre-weighed amounts of the appropriate salts in deionized water obtained from a NANOpure Diamond water purification system (Barnstead Thermolyne Corporation, Dubuque, IA) with a resistivity greater than 18 MΩ–cm. An acetate buffer was used for experiments at pH 5.0, a Bis-Tris buffer with added HCl was used at pH 6.0 and 7.0, and a Tris buffer with HCl was used at pH 8.0. The solution pH was measured using a 420APlus pH meter (Thermo Orion, Beverly, MA). The ionic strength was adjusted by adding NaCl (Mallinckrodt

Baker, Inc., Phillipsburg, NJ), with the solution conductivity measured using a 105A plus conductivity meter (Thermo Orion, Beverly, MA). All buffer solutions were prefiltered through 0.2 μm pore size Super-200 membranes (Pall Corp., Ann Arbor, MI) to remove particulates and undissolved salts.

Protein solutions were prepared by slowly dissolving the protein powder in the desired buffer, with the resulting solution filtered through a 0.22 μm syringe filter (Costar Corp., Cambridge, MA) to remove any protein aggregates immediately prior to use. Concentrations of the individual proteins in the absence of the dye were determined spectrophotometrically with a UV-VIS spectrophotometer (UV mini 1240, Shimadzu, Kyoto, Japan) using the natural absorbance at 280 nm. BSA concentrations in the presence of Cibacron Blue were evaluated by capillary zone electrophoresis (Model G1600A, Agilent Technologies, Palo Alto, CA) since the strong color of Cibacron Blue interfered with the absorbance measurements. Protein concentrations in the binary mixture were analyzed by size exclusion chromatography (Agilent 1100 series quaternary HPLC system) using a Superdex 75 column with 13 μm particle size and 10^5 MW exclusion limit (GE Healthcare, Piscataway, NJ). Additional details on the solution preparation and assays are provided in Chapter 3.

All filtration experiments were performed using Ultracel Composite Regenerated Cellulose (CRC) membranes obtained from Millipore Corp. (Bedford, MA) with nominal molecular weight cut offs of 30 kD or 100 kD. A negatively-charged version of the 100 kD membrane was made in our laboratory by the covalent attachment of negatively charged sulfonic acid groups to the surface of the membrane using the base-activated chemistry developed by van Reis (2001) and described in Chapter 3.

6.2.1 Membrane Charge

The membrane charge was evaluated from streaming potential measurements following the procedure developed by Burns and Zydney (2000) and described in Chapter 3. The membrane was sealed between two Plexiglas chambers which were then filled with a 10 mM NaCl solution. The transmembrane voltage (E_z) was measured over a range of pressures using a high impedance 8060A True RMS Multimeter (Fluke Corporation, Everett, WA) connected to the two electrodes. The membrane zeta potential was evaluated from the streaming potential data using Equation (5.1) with the effective surface charge evaluated from Equation (5.6).

6.2.2 Protein Sieving

Protein filtration experiments were conducted in a 25 mm diameter stirred ultrafiltration cell. The membrane hydraulic permeability (L_p) was evaluated both before and after the filtration experiment from data for the filtration velocity (J_v) as a function of the transmembrane pressure drop (ΔP). Protein sieving coefficients were evaluated from samples taken from the filtrate and bulk solutions using the procedures described in Chapter 3.

6.2.3 Diafiltration

The actual separation of ovalbumin and BSA was performed using the Amicon stirred cell operated in diafiltration mode. The stirred cell was initially filled with 10 ml

of the protein mixture. A separate reservoir was filled with a buffer solution (without protein or dye) and attached to the stirred cell with silicone tubing. The filtrate velocity was maintained at nearly a constant value over the course of the diafiltration by a peristaltic pump connected to the filtrate line. The filtrate flux created a vacuum in the stirred cell causing fresh buffer from the reservoir to be drawn into the cell from the solution reservoir at a rate equal to the volumetric filtration rate. Filtrate samples were collected throughout the experiment with periodic samples taken directly from the stirred cell to evaluate the protein concentrations in the retentate.

6.3 Data Analysis

The design of any protein separation process involves a trade off between purification and yield. Thus, higher purification is often obtained by sacrificing product yield and vice versa. van Reis and Saksena (1997) have developed a set of process optimization diagrams that quantitatively describe the trade-off between purification factor and yield for a membrane process operated in a diafiltration mode (shown schematically in Figure 6.1). Fresh diafiltration buffer is added to the feed tank at the same rate at which filtrate is removed maintaining a constant retentate (feed) volume throughout the process. The more permeable species, solute (1), is continuously washed through the membrane and collected in the filtrate while the more strongly retained species remains in the feed / recycle loop.

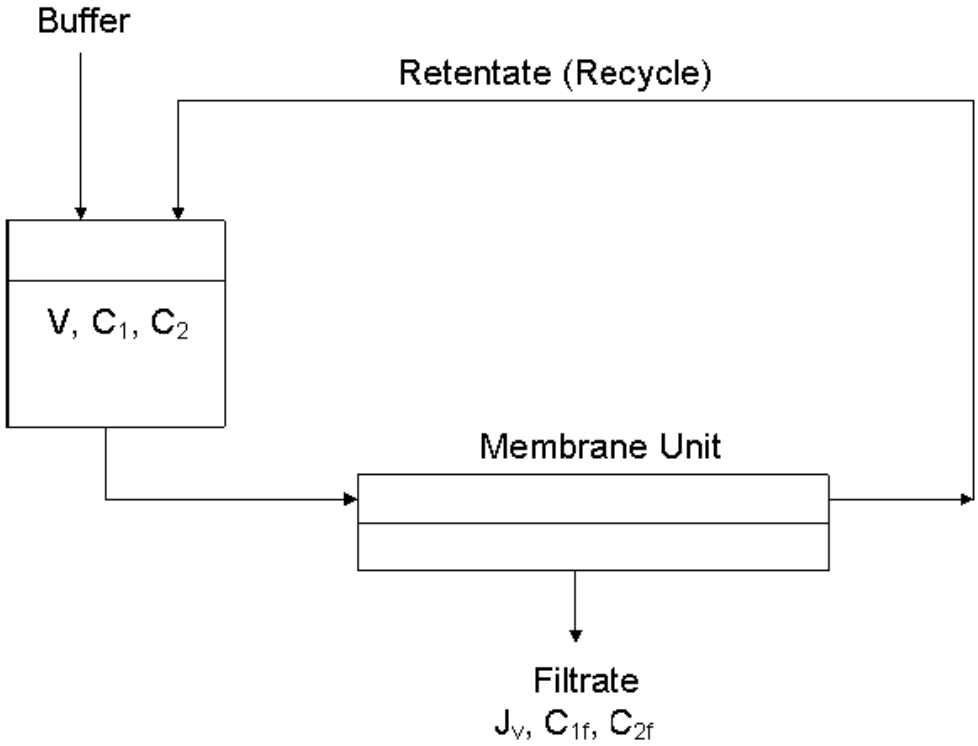

Figure **6.1**: Schematic representation of a membrane diafiltration process

van Reis and Saksena (1997) developed a set of equations to describe the trade off between the purification factor and yield, with the results expressed in terms of two key dimensionless parameters: the selectivity, ψ,

$$\psi = \frac{S_{o,1}}{S_{o,2}} \qquad (6.1)$$

and a throughput parameter, NΔS,

$$N\Delta S = N(S_{o,1} - S_{o.2}) \qquad (6.2)$$

where $S_{o,1} = \frac{C_{1f}}{C_1}$ and $S_{o,2} = \frac{C_{2f}}{C_2}$ are the observed sieving coefficients of solute 1 and 2 respectively. N is the number of diavolumes, which is equal to the total collected filtrate volume divided by the constant retentate volume:

$$N = \frac{J_v A t}{V} \tag{6.3}$$

where J_v is the (constant) filtrate flux, A is the membrane area, t is the process time, and V is the retentate volume

For a product collected in the retentate (solute 2) the process yield is given by:

$$Y_2 = \frac{VC_2}{VC_{2,i}} \tag{6.4}$$

where $C_{2,i}$ and C_2 are the initial and final concentrations of solute 2 in the retentate. The purification factor is defined as the ratio of the yield of the target solute divided by the yield of the impurity:

$$P = \left(\frac{VC_2}{\mathrm{VC}_{2,\mathrm{i}}}\right)\left(\frac{VC_{1,i}}{VC_1}\right) \tag{6.5}$$

Simple mass balances on solute 1 and 2 during a diafiltration process can be used to evaluate the yield and purification factors as discussed by van Reis and Saksena (1997). The final results for the product in the retentate are:

$$Y_2 = P_2^{1/(1-\psi)} \tag{6.6}$$

$$P_2 = \exp(N\Delta S) \tag{6.7}$$

The corresponding expressions for the product collected in the filtrate solution are:

$$P_1 = \frac{Y_1}{1-(1-Y_1)^{1/\psi}} \tag{6.8}$$

$$P_1 = \frac{Y_1}{1+(Y_1-1)\exp(N\Delta S)} \tag{6.9}$$

Figure 6.2 shows an optimization diagram for the desired product in the retentate constructed using Equations (6.6) and (6.7). The diagram consists of two families of curves, both plotted on yield - purification factor coordinates, with each family described by a single parameter (either the selectivity or mass throughput). The solid curves represent the path for a given diafiltration process for fixed values of the selectivity. The process begins with a yield of 100% and a purification factor of 1 because the product is completely contained in the retentate solution at the start of the process. The product yield decreases as the process proceeds due to the leakage of solute 2 through the membrane. However, this is accompanied by a large increase in the purification factor as the more permeable species, solute 1, is continually washed out of the retentate and through the membrane at a rate that is much greater than that of the product.

The vertical lines in Figure 6.2 represent the purification factor attained after different values of the mass throughput, NΔS. Hence, if the selectivity for a given separation process is 40, a purification factor of 100 can be attained with a corresponding yield of 88.8% using NΔS = 4.6. Thus, the larger the difference in the observed sieving coefficients of the two solutes (ΔS), the smaller the number of diavolumes required for a given purification. This reduction in the number of diavolumes not only reduces the

required buffer consumption it also means that the separation can be achieved with less membrane area and / or a shorter filtration time.

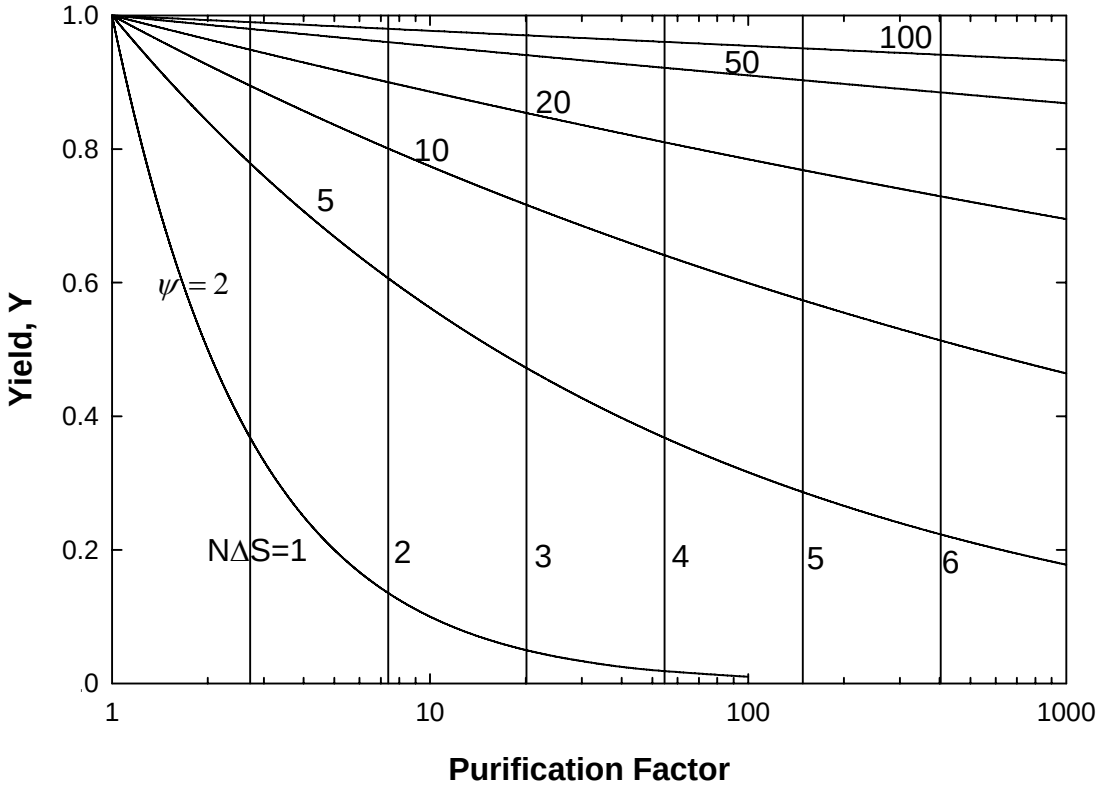

Figure **6.2**: Optimization diagram for a product in the retentate showing yield as a function of the purification factor for different values of the selectivity (ψ) and NΔS (adapted from van Reis and Saksena, 1997)

van Reis and Saksena (1997) also constructed optimization diagrams for the product in the filtrate using Equations (6.8) and (6.9), with typical results shown in Figure 6.3. In this case, the process begins in the lower right hand corner with zero product yield and the maximum purification, with the purification factor decreasing while the product yield increases as the diafiltration proceeds. As expected, the best performance is attained at large values of the selectivity and NΔS, with the selectivity determining the trade-off between the yield and purification factor while NΔS determines how quickly the separation traverses this path.

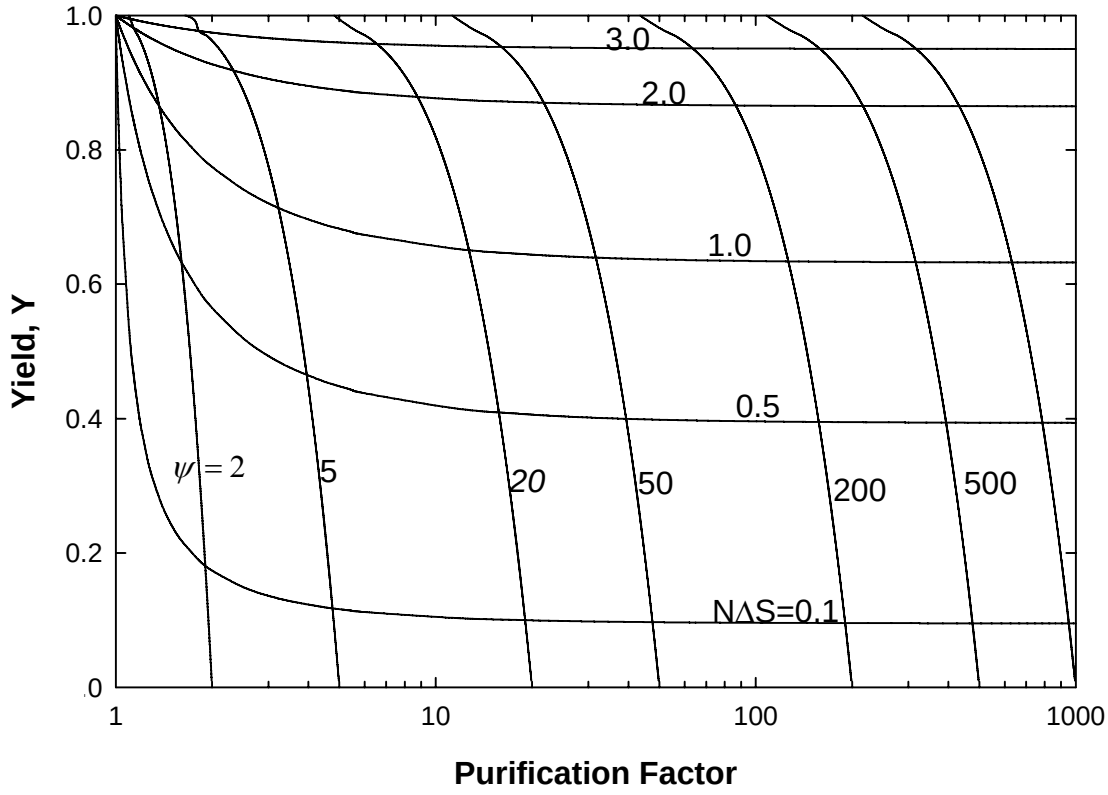

Figure **6.3**: Optimization diagram for a product in the filtrate showing the yield as a function of the purification factor for different values of the selectivity (ψ) and NΔS (adapted from van Reis and Saksena, 1997)

6.4 Results

6.4.1 Membrane Characterization

Typical experimental data for the measured streaming potential as a function of applied transmembrane pressure are shown in Figure 6.4 for a series of Ultracel membranes that were modified by the covalent attachment of a negatively charged sulphonic acid functionality to the hydroxyl groups on the cellulose surface. The individual membranes were produced by exposing the cellulose to the charging ligand for different periods of time varying from 2 to 72 hours. The streaming potential data were highly reproducible with the r^2 values being greater than 0.98 in each case. The slope of the streaming potential versus pressure, which provides a direct measure of the membrane surface charge density, increases with an increase in reaction time as expected. The non-zero intercepts in the data in Figure 6.4 arise from small asymmetries in the Ag/AgCl electrodes and have no affect on the results. This is discussed in more detail by Burns and Zydney (2000).

The membrane zeta potential was calculated directly from the streaming potential data using the Helmholtz –Smoluchowski equation (Equation 5.1) with the results summarized in Table 6.1. The zeta potential for the unmodified Ultracel membrane was -2.7 ± 0.2 mV, with this small negative charge arising from the preferential adsorption (or binding) of negatively-charged anions (Cl^-) from the bulk electrolyte solution. Chemical modification caused a significant increase in the magnitude of the zeta potential, with a

value of -12.4 mV for the membrane modified for 24 hours. Further increases in the reaction time caused only small changes in the zeta potential.

The third column in Table 6.1 shows the calculated values of the membrane surface charge density determined from Equation (5.6). The surface charge becomes more negative after longer reaction times, varying from -0.6 mC/m^2 to -3.3 mC/m^2 for the membranes charged between 0 and 72 hrs. This charge density corresponds to a spacing of approximately 4.3 nm between the charge groups, assuming a uniform hexagonal distribution of charges over the membrane surface. The more highly charged membranes did have a lower hydraulic permeability (last column in Table 6.1), due to the constriction of the pores associated with the finite size of the charging ligand. The 30% reduction in permeability for the most heavily charged membrane corresponds to a reduction in pore radius of approximately 1.1 nm (from 6.2 to 5.1 nm) as calculated using the Hagen-Poiseuille equation for flow through a membrane comprised of a parallel array of uniform cylindrical pores.

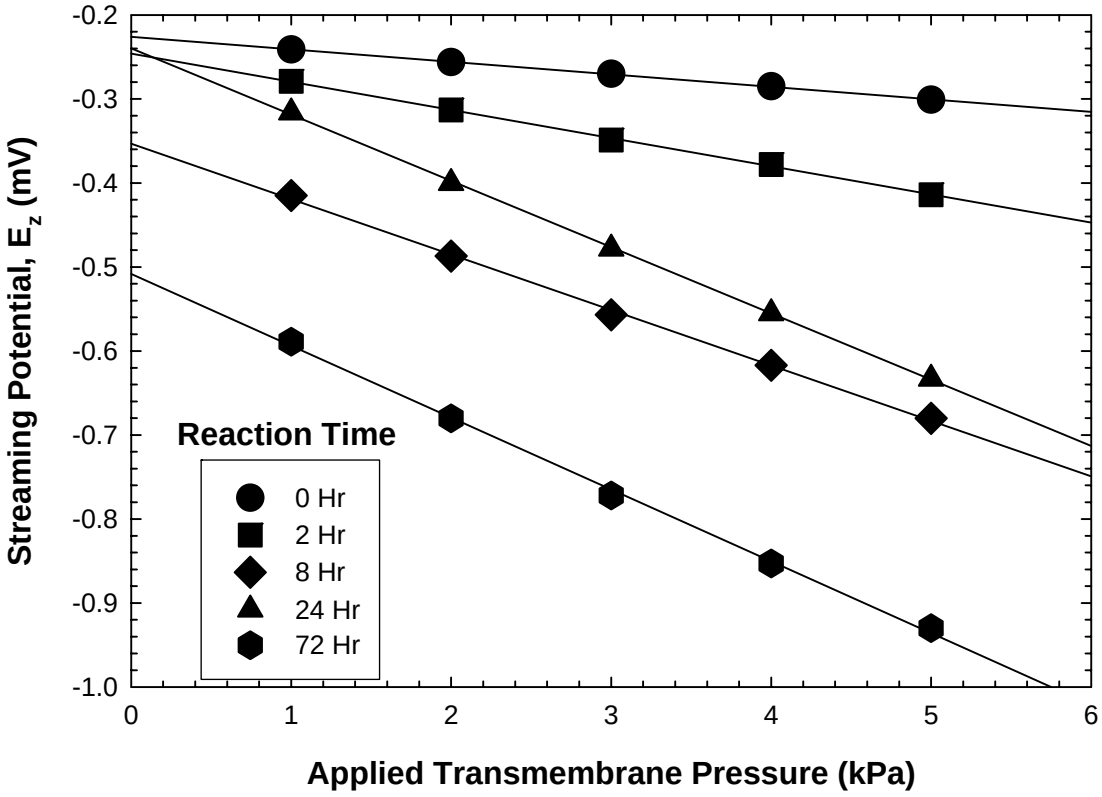

Figure **6.4**: Streaming potential data for a series of charge modified Ultracel 100 kD membranes obtained using a 10 mM NaCl solution

Table 6.1: Zeta potential and membrane charge for a series of charge modified cellulose membranes

Charging Time (Hr)	Zeta Potential (mV)	Charge Density (mC/m^2)	Reduction in Permeability (%)
0	-2.7 ± 0.2	-0.6 ± 0.05	NA
2	-4.6 ± 0	-1.1 ± 0	13
8	-10.9 ± 0.8	-2.3 ± 0.2	14
24	-12.4 ± 0	-2.9 ± 0	28
72	-13.9 ± 0.9	-3.3 ± 0.22	30

6.4.2 Process Optimization

Figure 6.5 shows experimental data for the BSA and ovalbumin sieving coefficients, evaluated separately using solutions of the individual proteins, over a range of solution pH at an ionic strength of 10 mM. Experiments were performed using a series of 100 kD Ultracel membranes, each produced by chemical modification of a separate membrane disk for different reaction times. The surface charge densities of the resulting membranes are provided in Table 6.1. Note that these are only rough estimates of the

surface charge density since no attempt was made to account for the effects of double layer overlap or surface conduction in the analysis of the streaming potential data.

The top panel shows results for a 10 g/L BSA solution and the bottom panel shows results for a 15 g/L ovalbumin solution, both without any added Cibacron Blue. The transmission of both proteins decreases as the membrane surface charge density increases. The BSA sieving coefficient in a pH 5.0, 10 mM acetate buffer varies from a value of 0.6 for the unmodified CRC membrane to a value of 0.042 for the membrane with a surface charge density of -0.0023 C/m^2. The corresponding values for the ovalbumin sieving coefficient are somewhat higher, with the sieving coefficient varying from 0.73 for the unmodified Ultracel membrane to 0.13 for the 8 hour charged membrane. This difference is likely due primarily to the smaller size of the 44 kD ovalbumin relative to the 67 kD BSA. The protein transmission is greatest at pH 5, which is near the isoelectric point of both proteins, and decreases at higher pH due to the increase in repulsive electrostatic interactions between the negatively-charged membrane and the negatively-charged proteins. The sieving coefficient for BSA decreases to 0.003 at pH 7 using the most negatively-charged membrane, although this value is still only a factor of 2.5 smaller than the ovalbumin sieving coefficient under these conditions due to the similar surface charge characteristics for the two proteins.

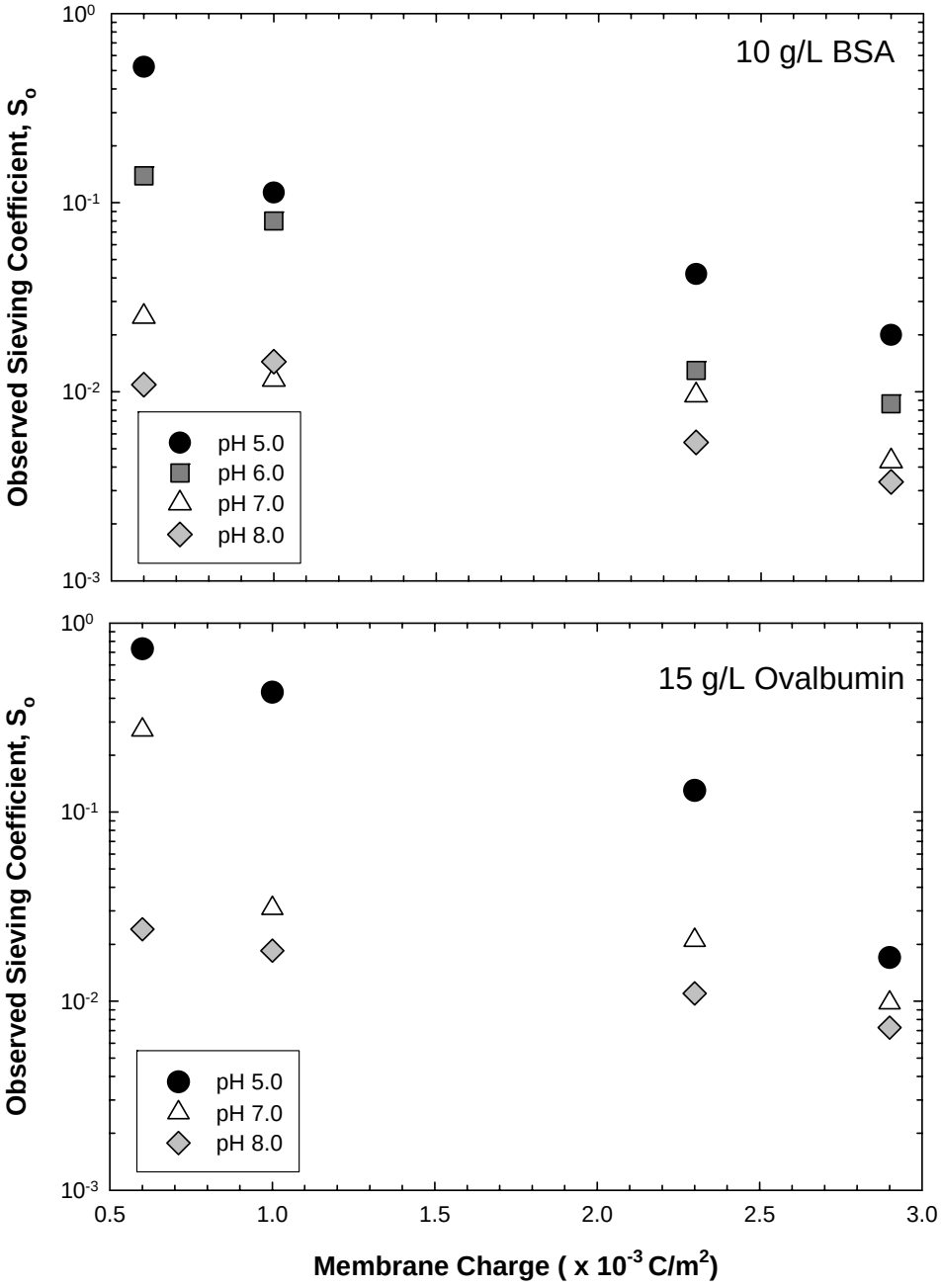

Figure **6.5**: Observed protein sieving coefficients for BSA (top panel) and ovalbumin (bottom panel) in 10 mM buffer as a function of membrane surface charge over a range of pH..

Figure 6.6 shows experimental data for the affect of Cibacron Blue on the protein sieving coefficients, again evaluated separately for solutions of either BSA or ovalbumin. The top panel shows results for a 10 g/L solution of BSA in a pH 5, 10 mM acetate buffer both alone and in the presence of Cibacron Blue using a 12:1 molar ratio of Cibacron Blue to BSA (corresponding to a Cibacron Blue concentration of 1.4 g/L). The BSA sieving coefficient in the absence of Cibacron Blue decreases from a value of 0.60 for the unmodified CRC membrane to a value of 0.02 for the membrane with a surface charge density of –0.0029 C/m^2 due to the electrostatic interactions between the weakly charged BSA and the sulfonic acid groups on the highly charged membrane. The reduction in the BSA sieving coefficient is even more pronounced in the presence of Cibacron Blue, with the protein sieving coefficient decreasing by more than two orders of magnitude over this same range of membrane charge. This behavior is a direct result of the strong degree of Cibacron Blue binding to BSA, which significantly increases the net negative charge of the protein thereby increasing the electrostatic exclusion from the negatively-charged membrane.

Corresponding results for ovalbumin are shown in the bottom panel of Figure 6.6. In the absence of Cibacron Blue, the ovalbumin sieving coefficient decreases from 0.73 for the unmodified membrane to 0.018 for the membrane with a surface charge density of –0.0029 C/m^2. In contrast to the data for BSA, the addition of 1.2 g/L of Cibacron Blue has relatively little effect on ovalbumin sieving, with the data showing a small increase in the sieving coefficients in the presence of Cibacron Blue, particularly for the more highly charged membranes. This small increase in the sieving coefficient is due to the increase in ionic strength due to the presence of a high concentration of free (unbound) dye.

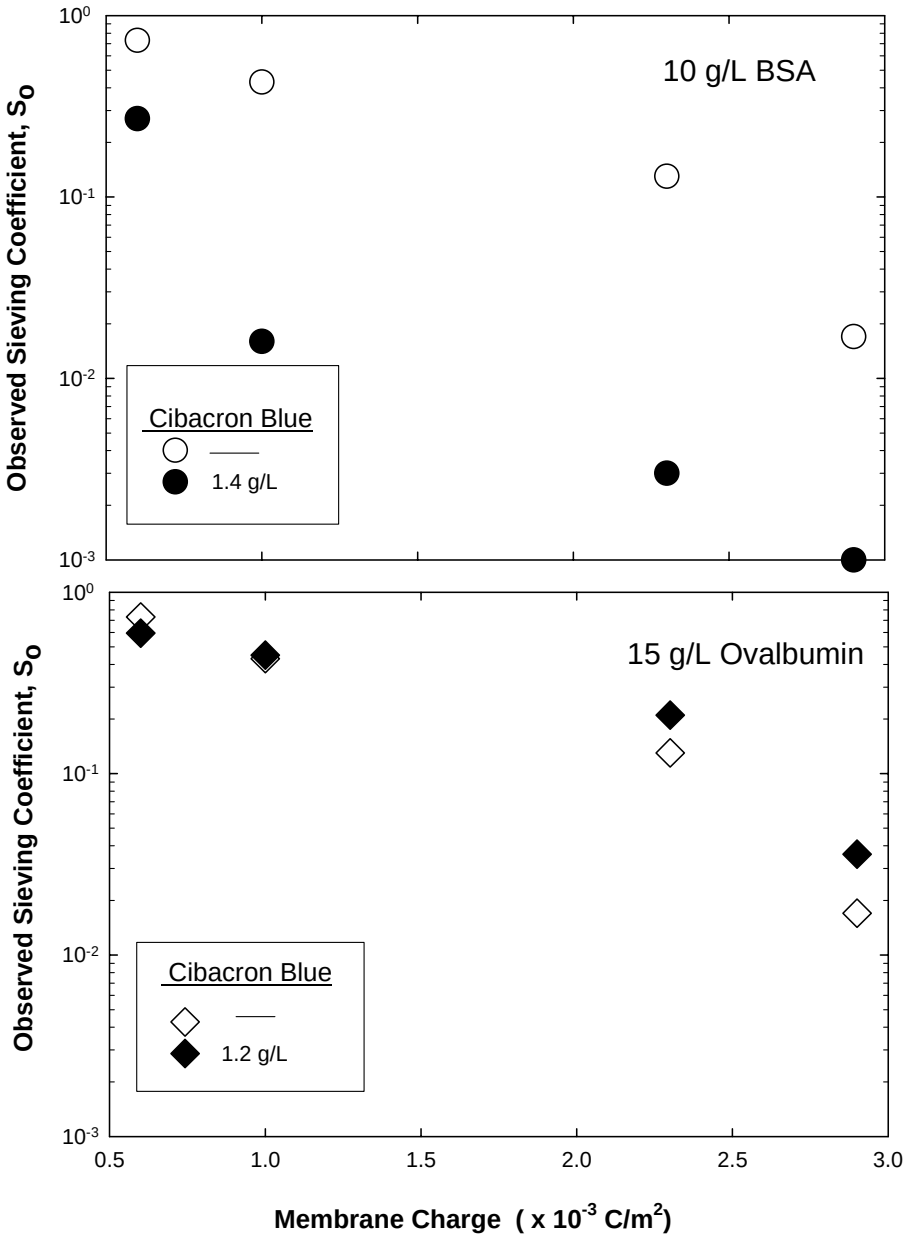

Figure **6.6**: Observed protein sieving coefficients for BSA (top panel) and ovalbumin (bottom panel) in a pH 5, 10 mM acetate buffer as a function of membrane surface charge. Data are shown in the absence (open symbols) and presence (filled symbols) of Cibacron Blue.

The effect of different operating conditions on the separation of ovalbumin and BSA can be determined using the process optimization diagrams developed by van Reis and Saksena (1997) and discussed in some detail in Section 6.3. The separation performance is determined by two key parameters: the selectivity $\psi = S_{ovalbumin}/S_{BSA}$ and the throughput $J_v\Delta S = J_v(S_{ovalbumin} - S_{BSA})$, with the calculated values for the experiments in Figure 6.7 provided in Table 6.2. It is important to note that these calculations provide estimated values of the selectivity and mass throughput since the experiments were done with solutions of the individual proteins, neglecting any protein – protein interactions and the competitive binding of Cibacron Blue to BSA and ovalbumin. The predicted values for the number of diavolumes (N) and the yield (Y) were evaluated using Equations (6.7) and (6.6) with the purification factor arbitrarily set to a target value of 100. Results are shown only for experiments performed in the presence of Cibacron Blue since the selectivity in the absence of the affinity dye was always less than 3.0, which is insufficient for effective separation of BSA and ovalbumin. The small selectivity obtained in the absence of Cibacron Blue is due primarily to small differences in the size and / or surface charge characteristics of the two proteins.

The selectivity for the membrane with the highest surface charge density of -0.0029 C/m^2 was ψ =36, with this large value arising from the strong retention of the BSA-dye complex. However, this membrane had a relatively low throughput ($J_v\Delta S$ = 0.35 μm/s), with the net result that the separation of BSA and ovalbumin would require more than 130 diavolumes under these conditions. In contrast, the membrane with a surface charge density of -0.0011 C/m^2 has a much high throughput ($J_v\Delta S$ = 4.3 μm/s)

allowing one to achieve the target 100-fold purification after only 11 diavolumes. However, the somewhat smaller selectivity ($\psi = 28$) for this membrane gives a final product yield of below 85%. The best separation characteristics, as determined from the optimization diagrams presented by van Reis and Saksena (1997), were predicted for the membrane having a surface charge density of -0.0023 C/m^2. This membrane could achieve the target purification factor using 22 diavolumes with a product yield of 94 %, conditions that are well within the range of the separation objectives for most downstream purification processes. Based on these calculations, all subsequent experiments were performed using charge-modified membranes that had a surface charge density of -0.0023 C/m^2.

Table **6.2**: Predicted yield and number of diavolumes required to achieve a purification factor of 100.

Charge Density C/m^2	Selectivity ψ	Mass Throughput $J_v\Delta S$ (μm/s)	Number of Diavolumes, N	Yield BSA (%)
-0.0006	2.2	3.3	14	2
-0.0011	28	4.4	11	84
-0.0023	70	2.0	22	94
-0.0029	36	0.35	132	88

Figure 6.7 examines the effect of the Cibacron Blue concentration on the protein sieving coefficients for the negatively-charged 100 kD CRC membrane with a surface

charge density of 0.0023 C/m^2. These experiments were performed with a binary mixture containing 10 g/L BSA and 6 g/L ovalbumin in a pH 5.0, 10 mM acetate buffer. The BSA sieving coefficient initially decreases upon addition of Cibacron Blue, attaining a minimum value (S_o=0.0064) at a Cibacron Blue concentration of approximately 1.4 g/L, corresponding to the addition of approximately 12 moles of dye per mole of BSA. Higher concentrations of Cibacron Blue cause an increase in BSA transmission, with the observed sieving coefficient at high ligand concentrations approaching a value of 0.04. This increase in BSA transmission is due to the shielding of the electrostatic interactions associated with the presence of significant amounts of free (unbound) Cibacron Blue in the solution, an effect that was discussed previously in Chapter 5. In contrast to the data for BSA, the observed sieving coefficient of ovalbumin increases with increasing Cibacron Blue concentration even at very low ligand concentrations, but then passes through a weak maximum at a Cibacron Blue concentration of about 2.1 g/L. The reduction in ovalbumin transmission at high Cibacron Blue concentrations could be due to some ligand binding under these conditions, consistent with the high concentrations required for saturation of the ovalbumin binding sites as seen in Chapter 4. It is also possible that there is some Cibacron Blue binding to the membrane at very high ligand concentrations, which would lead to an increase in the net negative charge of the membrane and a corresponding reduction in protein transmission. Note that there were small discrepancies in the sieving results obtained with the single solute and binary mixture experiments, although these differences may simply reflect the inherent variability between membranes and the small differences in operating conditions.

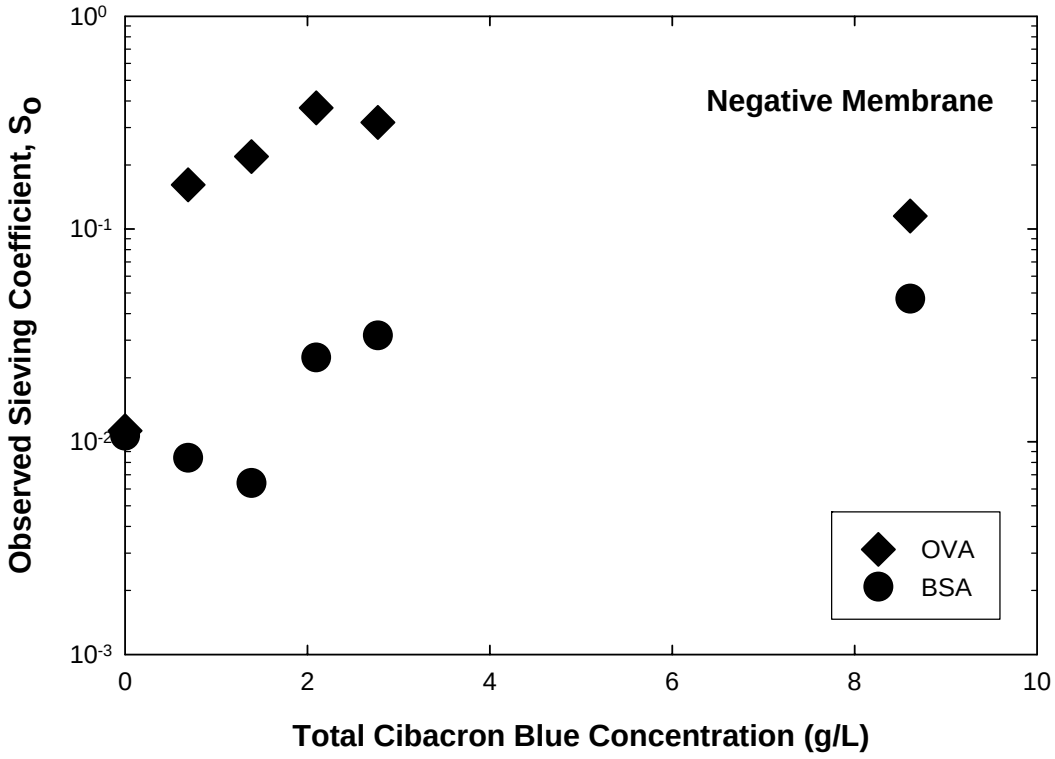

Figure **6.7**: Observed sieving coefficients for BSA and ovalbumin in a binary mixture for the negatively charged 100 kD CRC membrane. Data were obtained using a 10 mM acetate buffer at pH 5.0 over a range of Cibacron Blue concentrations

The experimental data in Figure 6.7 have been replotted in Figure 6.8 in terms of the selectivity, which is defined as the ratio of the transmission of ovalbumin to that of BSA (S_{OVA}/S_{BSA}). Also shown for comparison are results obtained with a neutral (un-modified) CRC membrane. The selectivity in the absence of Cibacron Blue is negligible for both membranes, with a value less than 1.1. The selectivity for the negatively-charged membrane increases dramatically upon addition of Cibacron Blue, attaining a maximum value of more than 30-fold at a Cibacron Blue concentration of 1.4 g/L, which

corresponds to the minimum in the BSA sieving coefficient seen in Figure 6.7. Further increases in the Cibacron Blue concentration cause a reduction in the selectivity, with the selectivity decreasing to below three in the presence of 8.6 g/L of Cibacron Blue. This decrease in selectivity is due primarily to the increase in BSA transmission seen at high concentrations of Cibacron Blue, which is directly associated with the shielding of the electrostatic interactions by the excess (unbound) Cibacron Blue. It is important to note that the maximum selectivity with the unmodified CRC membrane is less than 5.0 due to the much weaker electrostatic interactions with the unmodified membrane.

The solid and dashed curves in Figure 6.8 are model calculations for the uncharged and charged membranes, respectively. The surface charge density of the charged membrane was taken as -0.0023 C/m^2, while that for the uncharged membrane was -0.0006 C/m^2 based on the zeta potential results presented in Figure 6.4. The sieving coefficients were evaluated using the model equations presented previously, with the selectivity evaluated directly from the ratio of the sieving coefficients, ignoring any possible protein – protein interactions (although the model does account for the competitive binding of Cibacron Blue to both proteins). The model calculations are in good agreement with the experimental data, properly capturing the maximum in the selectivity at an intermediate value of the Cibacron Blue concentration along with the much higher selectivities for the negatively-charged membrane due to the much stronger electrostatic interactions.

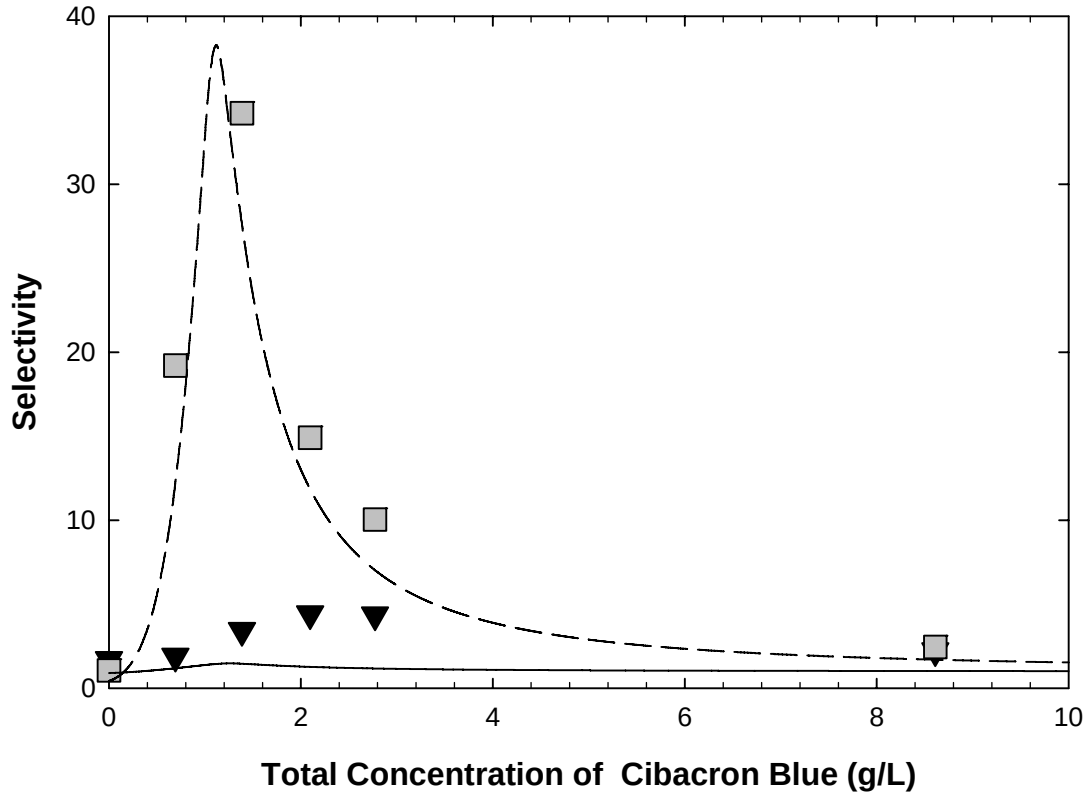

Figure **6.8**: Selectivity for the separation of BSA and ovalbumin as a function of the total Cibacron Blue concentration for an unmodified and negatively-charged membrane. Solid and dashed curves are model calculations for the uncharged and charged membranes, respectively.

Figure 6.9 shows the corresponding values for the mass throughput parameter $J_v\Delta S$ which is simply the product of the filtrate flux and the difference of the sieving coefficients where $\Delta S = S_{OVA} - S_{BSA}$. Since these experiments were all performed at a filtrate flux of 10 μm/s, the variation in the mass throughput is simply due to changes in the sieving coefficients for the two proteins. The value of $J_v\Delta S$ is nearly zero in the

absence of Cibacron Blue since BSA and ovalbumin have similar size and electrical charge under these conditions. The throughput increases with increasing Cibacron Blue concentration due to the reduction in BSA transmission caused by the binding of Cibacron Blue in combination with the small increase in ovalbumin transmission, with the latter due primarily to the increase in solution ionic strength associated with the presence of the unbound dye. The maximum throughput is attained at a Cibacron Blue concentration of approximately 2.1 g/L. Further increases in the concentration of Cibacron Blue cause a reduction in the value of $J_v\Delta S$ due to the increase in BSA transmission associated with the high ionic strength caused by the high concentration of free Cibacron Blue. The mass throughput for the neutral membrane is greater than that for the negatively charged membrane due to the much weaker electrostatic interactions, but this improvement in $J_v\Delta S$ is insufficient to overcome the very low selectivity obtained with the neutral membrane.

The solid and dashed curves in Figure 6.9 are again the model calculations. The model captures some of the qualitative trends in the data but there are significant quantitative discrepancies, with the model under-predicting the mass throughput over most of the experimental conditions. The model tends to under-predict the sieving coefficients for both proteins, leading to the discrepancy in $J_v\Delta S$ even though the model accurately predicts the selectivity data. This could be due to small errors in the value of the membrane pore size used for the calculations and / or to some discrepancy in the extent of concentration polarization in the experimental device.

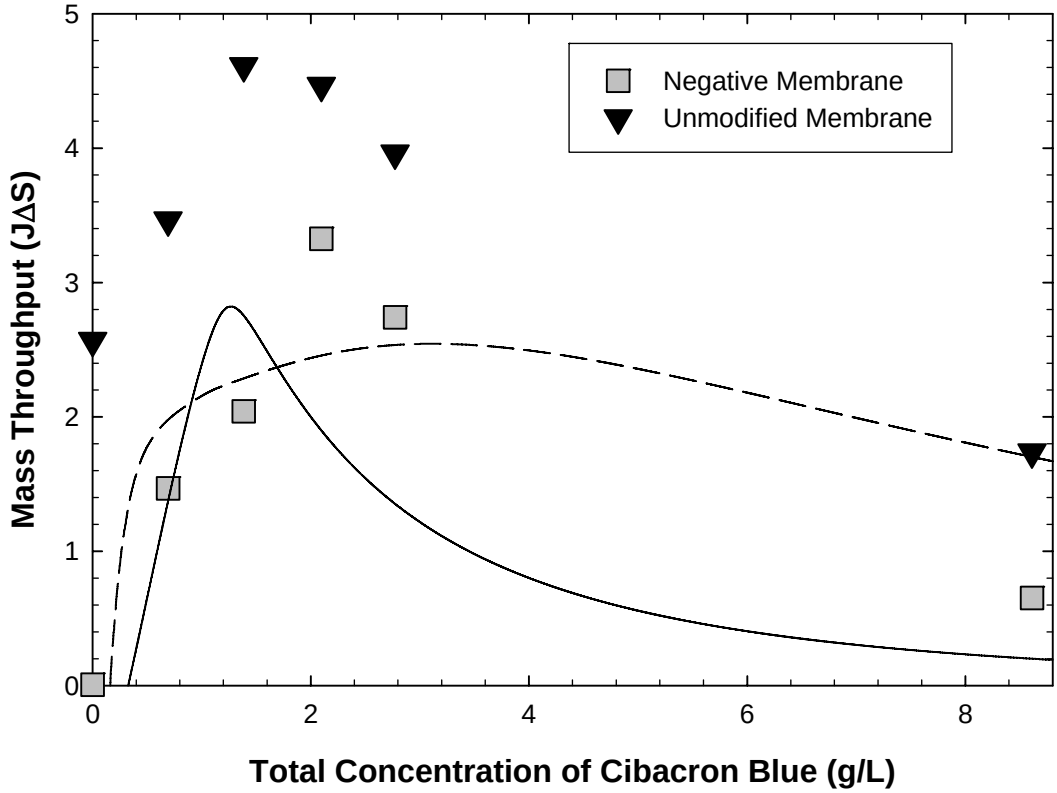

Figure **6.9**: Mass Throughput for the separation of BSA and ovalbumin as a function of the total Cibacron Blue concentration for an unmodified and negatively-charged membrane. Solid and dashed curves are model calculations for the uncharged and charged membranes, respectively.

The experimentally determined values of the selectivity and mass throughput were then used to predict the number of diavolumes (N) and the yield for a process designed to separate ovalbumin and BSA with a purification factor of 50, with the results shown in Figure 6.10. The number of diavolumes was calculated using Equation (6.7) and the yield of BSA in the retentate was estimated using Equation (6.6). The predicted number of diavolumes, N, in the absence of Cibacron Blue is more 6000, which is clearly

impractical for any real application. This very high value of N is a direct result of the very small value of the mass throughput parameter under these conditions. Increasing the Cibacron Blue concentration initially causes a reduction in N, with a minimum value of N =11 obtained at a Cibacron Blue concentration of 2.1 g/l (corresponding to a molar ratio of Cibacron Blue to BSA of 18:1). Further increases in the Cibacron Blue cause an increase in the required number of diavolumes because of the reduction in $J_v\Delta S$ associated with the increased electrostatic shielding under these conditions. The same general trends are seen with the unmodified Ultracel membrane, although the required numbers of diavolumes are uniformly smaller due to the reduction in electrostatic interactions and the corresponding increase in the protein sieving coefficients.

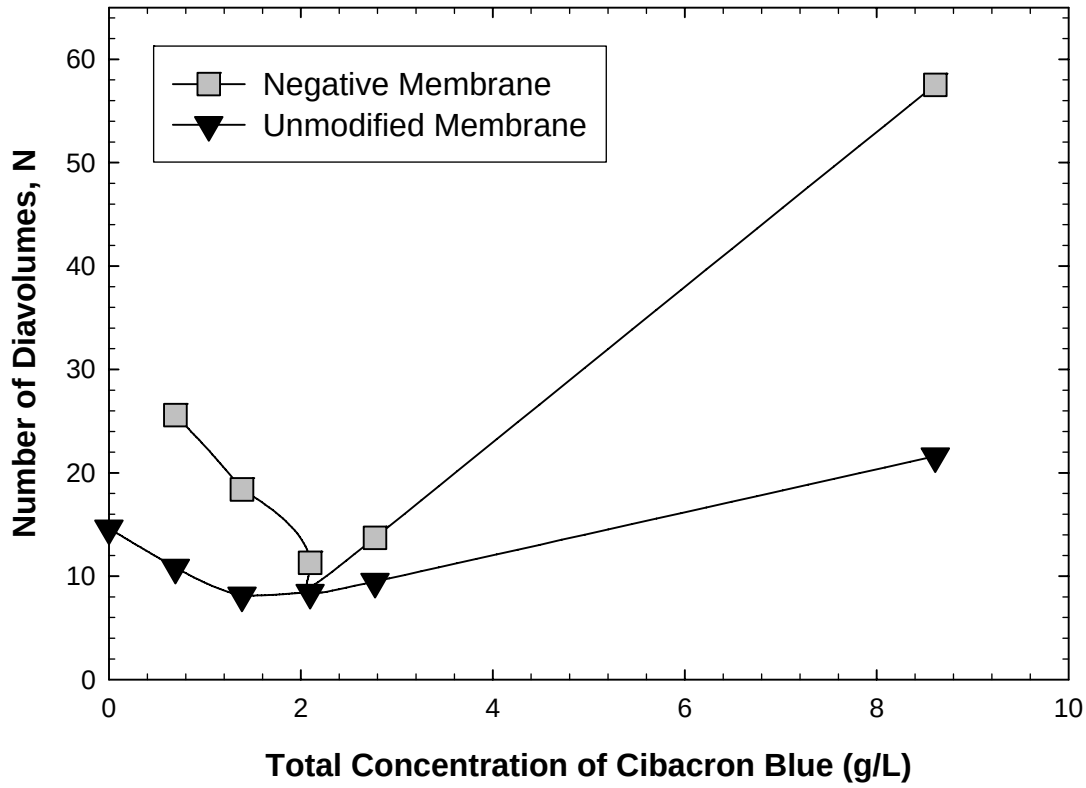

Figure **6.10**: Predicted number of diavolumes required to obtain a 50-fold purification of BSA

The corresponding results for the predicted yield of BSA in the retentate are shown in Figure 6.11, again for a purification factor of 50. The solid curves are spline fits and are provided to aid the visual interpretation of the data. As expected the yield is close to zero for both membranes in the absence of Cibacron Blue because of the very low selectivity under these conditions. Addition of Cibacron Blue causes a significant increase in the predicted yield due to the enhanced retention of BSA. This effect is most pronounced with the negatively charged membrane, with a maximum predicted yield of 94 % at a Cibacron Blue concentration of 1.1 g/L (corresponding to a Cibacron Blue to

BSA mole ratio of 12:1). The predicted yield decreases at high Cibacron Blue concentrations due to the strong electrostatic shielding under these conditions. Similar trends are seen with the unmodified Ultracel membrane, although the predicted BSA yields are considerably lower due to the much smaller selectivity.

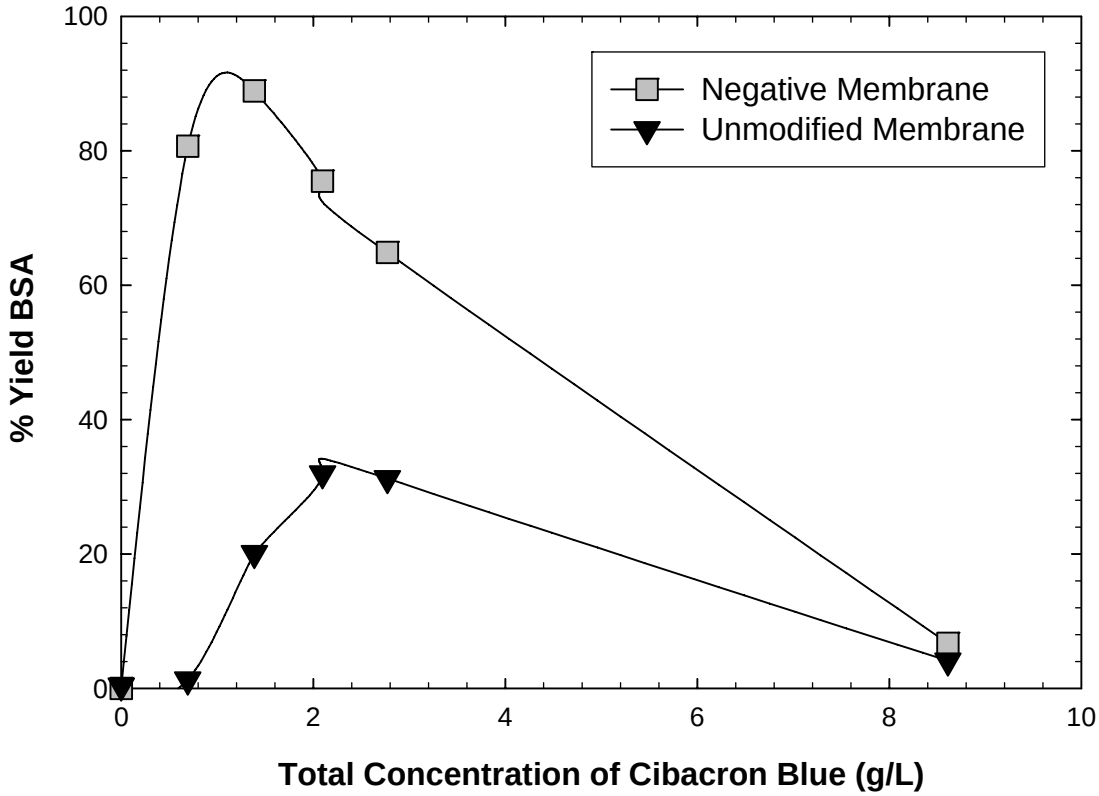

Figure **6.11**: Predicted yield of BSA for a diafiltration process designed to obtain a purification factor of 50 for the separation of BSA and ovalbumin.

6.4.3 Protein Separation

Based on the results presented in the previous section, a diafiltration process was designed for the actual separation of BSA and ovalbumin using a pH 5.0, 10 mM ionic strength acetate buffer and a negatively charged 100 kD CRC membrane having a nominal surface charge density of –0.0023 C/m^2. The diafiltration was performed at a constant retentate volume in which the diafiltration buffer is added to the feed reservoir at the same rate at which the filtrate is removed. The feed solution contained 2 g/L BSA and 1 g/L ovalbumin, with Cibacron Blue added to the feed at a concentration of 0.28 g/L (corresponding to 12 moles of Cibacron Blue per mole of BSA). A control experiment was performed without Cibacron Blue to obtain a direct measure of the effects of the protein – ligand interaction on the diafiltration process. A small amount of NaCl was added to the buffer used in the control experiment so that the solution ionic strength was identical to that measured experimentally for the buffer that included the Cibacron Blue.

Figure 6.12 shows data for the normalized protein concentration in the stirred cell as a function of the number of diavolumes (N), which is equal to the total collected filtrate volume divided by the constant volume in the stirred cell. The solid curves represent the model calculations evaluated by integration of the differential mass balance assuming a constant observed sieving coefficient (van Reis, and Saksena, 1997):

$$C/C_o = \exp(-NS_o) \qquad (6.10)$$

The observed sieving coefficients for both proteins were evaluated from the data in Figure 6.7 as $S_o = 0.0064$ for BSA and $S_o = 0.219$ for ovalbumin. The concentration of ovalbumin decreased rapidly with increasing number of diavolumes, dropping to nearly

undetectable levels after 16 diavolumes. There was a small loss of BSA over the course of the diafiltration, with the BSA concentration decreasing from 2.0 to 1.75 g/L after 14 diavolumes. The diafiltration thus yielded a BSA product with a purification factor greater than 90-fold at a yield of more than 90%. Ovalbumin was collected in the permeate solution with a purification factor greater than 10-fold and essentially 100% yield.

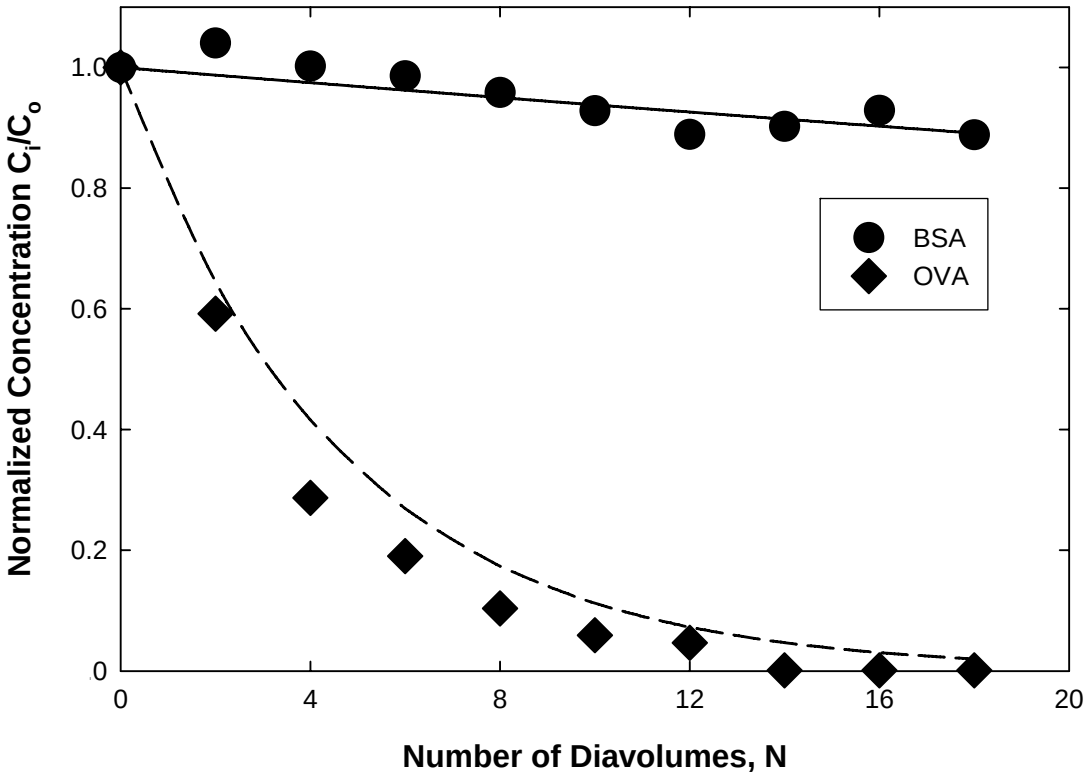

Figure **6.12**: Normalized protein concentrations during diafiltration experiments performed in the presence of Cibacron Blue in a molar ratio of 12:1 per mole BSA using a negatively charged 100 kD CRC membrane. Solid and dashed curves are model calculations as described in the text.

Figure 6.13 shows the corresponding results for the separation of a binary mixture BSA and ovalbumin but in the absence of any Cibacron Blue. In contrast to the results in Figure 6.12, the BSA concentration decreased by approximately 75% over the course of the diafiltration due to the relatively low BSA retention in the absence of the affinity ligand. The net result is a purification factor less than 2-fold for both BSA and ovalbumin, compared to the more than 90-fold purification for BSA seen in the presence of the Cibacron Blue. The solid and dashed curves in Figure 6.13 are the model calculations, in this case performed by fitting the data to Equation (6.10) yielding S_o = 0.085 for BSA and S_o = 0.1 for ovalbumin. The differences between these best fit values of S_o and the data in Figure 6.7 are due to: (1) the difference in ionic strength caused by the addition of NaCl, (2) the possible effects of protein-protein interactions, and (3) the inherent variability between experiments performed with different membrane samples.

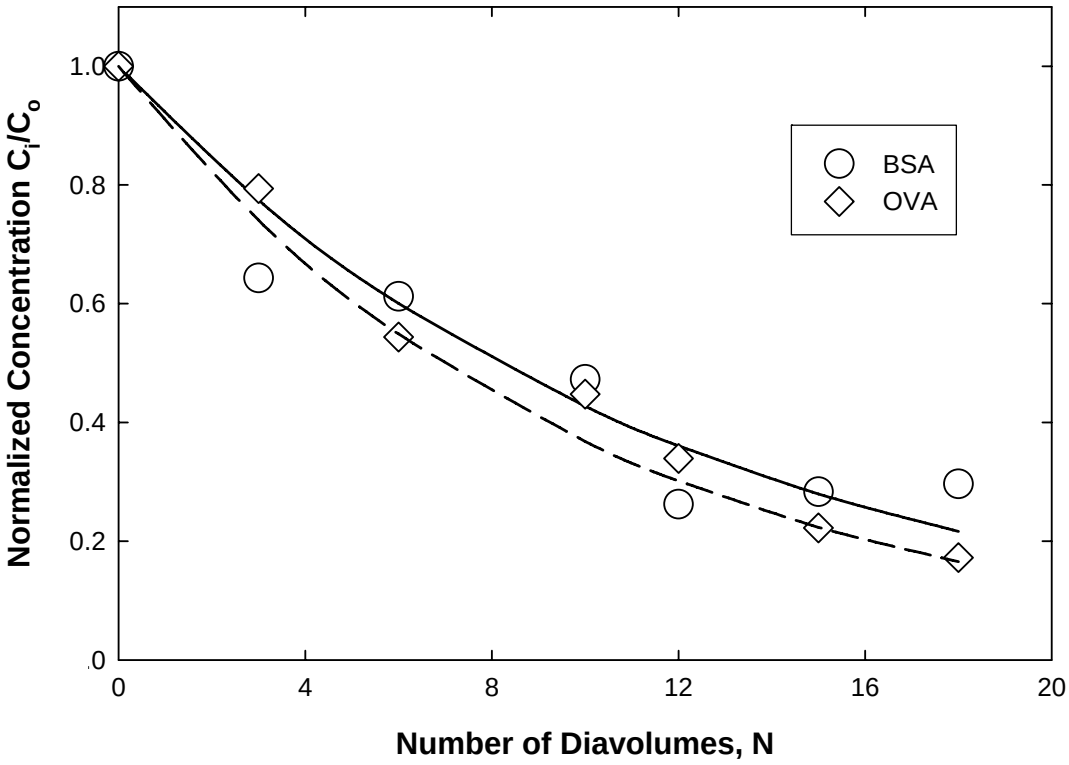

Figure **6.13**:Normalized protein concentrations during diafiltration experiments performed in the absence of Cibacron Blue using a negatively charged 100 kD CRC membrane. Solid and dashed curves are model calculations as described in the text.

An additional diafiltration experiment was performed using a higher concentration of Cibacron Blue (0.42 g/L), with the results shown in Figure 6.14. The solid and dashed curves are the model calculations, with the sieving coefficients evaluated from the experimental data in Figure 6.7. The ovalbumin concentration decreases rapidly during the diafiltration, again reaching essentially undetectable values after 14 diavolumes. However, there is a noticeable loss of BSA in this experiment, with

the final yield of BSA being less than 75%. This reduction in BSA yield is a direct result of the increase in protein transmission arising from the shielding of the electrostatic interactions in the presence of excess Cibacron Blue. These results clearly demonstrate the importance of optimizing the concentration of the charged affinity ligand for effective protein separations.

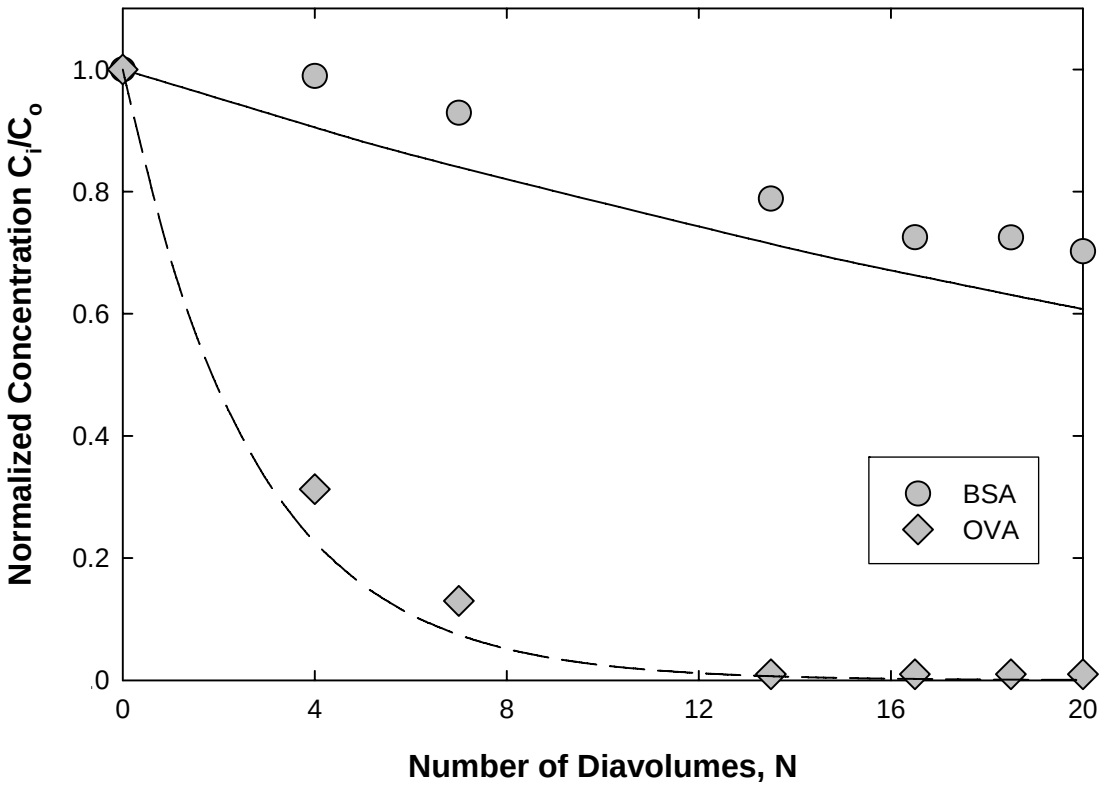

Figure **6.14**: Normalized protein concentrations during diafiltration experiments performed in the presence of Cibacron Blue in a molar ratio of 18:1 per mole BSA using a negatively charged 100 kD CRC membrane. Solid and dashed curves are model calculations as described in the text.

In order to examine the behavior of the diafiltration process in more detail the experimental data in Figure 6.12 were replotted in the form of a process optimization diagram, with the product yield shown as a function of the purification factor. Results for BSA in the retentate solution are plotted in the top panel of Figure 6.15 while data for ovalbumin in the permeate solution are shown in the bottom panel. The solid curves are the model calculation developed using Equations (6.7) and (6.9) using a selectivity of ψ = 34 based on the data in Figure 6.8. The diafiltration process for BSA starts at the upper left corner with a yield of 100% and a purification factor of 1 because both proteins are fully contained in the feed (retentate) vessel at the start of the process. The purification factor for BSA increases during the diafiltration due to the removal of ovalbumin from the stirred cell, with a purification factor greater than 90 after 14 diavolumes. The model calculations are in excellent agreement with the experimental data, allowing one to determine the most appropriate combination of yield and purification factor for a given separation process.

The bottom panel shows the corresponding results for ovalbumin collected in the filtrate solution. In this case, the diafiltration process begins in the lower right hand corner with a yield of zero but with the maximum purification factor achieved for the very first drop of collected filtrate. The ovalbumin yield increases throughout the process as the protein is washed through the membrane and into the filtrate, although the rate at which the yield increases becomes slower with the time due to the dilution of the ovalbumin remaining in the stirred cell by the continuous addition of diafiltration buffer. The purification factor for ovalbumin decreases throughout the process due to the leakage of some BSA through the membrane. The ovalbumin yield at the end of 14 diavolumes

was approximately 100% with the purification factor being close to 10. The model underpredicts the ovalbumin purification factor at the start of the diafiltration, suggesting that the initial selectivity for the BSA – ovalbumin system is greater than 34. This discrepancy may simply reflect the lot-to-lot variability in the membranes, although it could also be associated with an initial transient that was not seen in the total recycle experiments due to the long equilibration time before obtaining any filtrate or feed samples. Additional experiments will be required to fully understand this behavior.

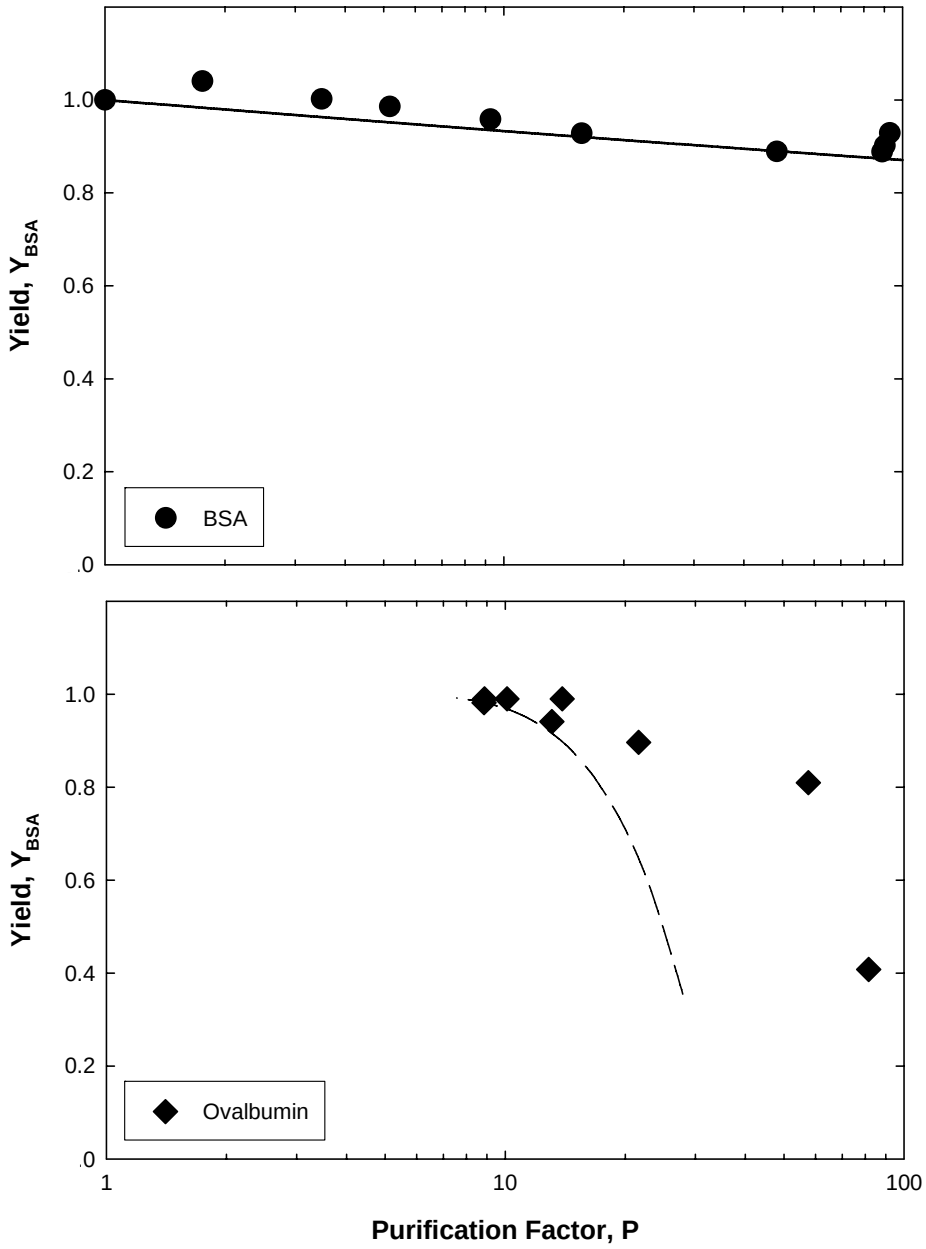

Figure **6.15**: Yield as a function of purification factor for BSA collected in the retentate (top panel) and ovalbumin collected in the filtrate (bottom panel) for the separation performed with the addition of Cibacron Blue in a molar ratio of 12:1 per mole BSA. Solid and dashed curves are model calculations as described in the text

Figure 6.16 shows size exclusion chromatograms for the feed (top panel) and the final retentate solution (bottom panel) based on samples obtained at the end of the 16-diavolume diafiltration performed in the presence of Cibacron Blue. The small peak at a retention time of 62.5 min is due to the presence of a small amount of BSA dimer in the feed, corresponding to approximately 13 % of the main BSA peak which appears at a retention time of 71 min. The ovalbumin appears as the large peak at 76 min; this peak is almost completely absent for the chromatogram at the end of the diafiltration, consistent with the very high degree of BSA purification obtained in this experiment. There is no significant change in the BSA peak over the course of the diafiltration, indicating that there was a negligible amount of BSA aggregation or dimerization during this experiment.

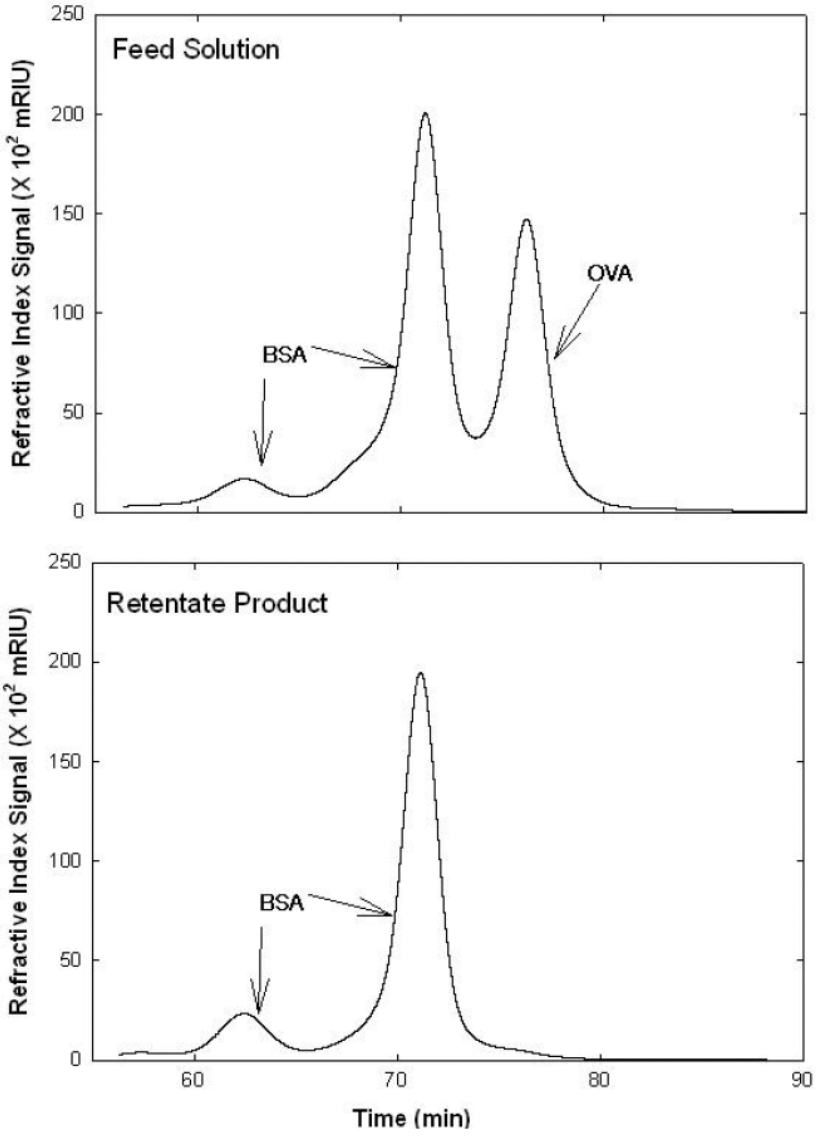

Figure **6.16**: Size exclusion chromatograms for the initial feed (top panel) and final retentate (bottom panel) for the diafiltration process performed in the presence of 0.28 g/L Cibacron Blue.

6.5 Discussion

Although a number of previous studies have shown the feasibility of using affinity ultrafiltration with large macroligands, the results presented in this Chapter provide the first demonstration that it is possible to use small charged ligands for highly selective affinity ultrafiltration, with the product of interest retained by electrostatic interactions using an electrically-charged membrane. A selectivity of more than 30-fold was obtained for the separation of ovalbumin and BSA upon the addition of Cibacron Blue, compared to less than a 2-fold selectivity in the absence of the affinity ligand. This dramatic increase in selectivity was a direct result of the strong electrostatic exclusion of the highly charged complex formed between BSA and Cibacron Blue.

The design of an effective affinity ultrafiltration process using a charged microligand is a complex function of the membrane charge, the solution pH and ionic strength, and the concentration of the affinity ligand. Low concentrations of the affinity ligand lead to inadequate selectivity due to the absence of significant binding while very high concentrations of the ligand reduce the electrostatic interactions due to the increase in ionic strength associated with the presence of a significant amount of free ligand in solution. The net result is the presence of an optimal ligand concentration, properly balancing the selectivity of the binding interactions with the strong electrostatic repulsion that occurs at low ionic strength. The membrane charge also has a large effect on the separation efficiency, with weakly charged membranes providing inadequate electrostatic repulsion.

An affinity diafiltration process was performed to obtain both BSA and ovalbumin as highly purified products in the retentate and filtrate, respectively. Appropriate conditions for the diafiltration were determined from the measured protein selectivity determined from protein sieving experiments. The resulting process gave a purification factor for BSA of greater than 90-fold at more than 90 % yield after 14 diavolumes. The ovalbumin product was collected in the filtrate solution with a purification factor of more than 10-fold at nearly 100 % yield. It should also be possible to recover the Cibacron Blue at the end of this process by performing a second diafiltration at high pH and in the presence of a chaotrope like NaSCN, conditions that were shown in Chapter 4 to reverse the binding of Cibacron Blue to BSA. This is discussed in more detail in the next Chapter of this thesis.

Chapter 7

HIGH PERFORMANCE TANGENTIAL FLOW FILTRATION USING CHARGED AFFINITY LIGANDS

7.1 Introduction

Microfiltration and ultrafiltration have been traditionally limited to separating solutes that differ by at least an order of magnitude in size. High Performance Tangential Flow Filtration (HPTFF) is an emerging technology that is able to separate solutes irrespective of the relative size of the product and impurity (van Reis and Zydney, 2001). HPTFF obtains high selectivities for protein separations by: (1) operation in the pressure-dependent regime to minimize fouling and exploit concentration polarization effects, (2) proper selection of pH and ionic strength to maximize differences in effective volume of the product and impurity, (3) using an electrically charged membrane to enhance repulsion of like-charged species, and (4) using a diafiltration mode to obtain high purification factors and yields.

Several recent studies have demonstrated the potential of HPTFF for protein purification. For example, van Reis et al., (1999) were able to achieve 900-fold purification at more than 90% yield for the separation of an antigen-binding fragment (Fab) of a monoclonal antibody from bovine serum albumin (BSA) using high performance tangential flow filtration. High selectivities were obtained by operating close to the isoelectric point of the Fab (pH 8.4) and using low salt concentrations and a negatively charged membrane, conditions that gave high retention of the negatively

charged BSA. It was also possible to purify the Fab in the retentate by operating near the isoelectric point of BSA using a positively-charged membrane. van Einhoven et al., (1995) reported purification factors of close to 100 and yields of nearly 70 % for the separation of BSA and hemoglobin, with the separation driven by the large difference in isoelectric point for the hemoglobin (pI = 7.0) and BSA (pI = 4.8). Lu et al., (2005) were able to separate lysozyme from ovalbumin using high performance ultrafiltration at pH 10-11, again exploiting the large difference in surface charge for the two proteins.

Applications of HPTFF for the separation of proteins with similar electrical charge are much more limited. Ebersold and Zydney (2003) obtained moderate purification of protein variants differing at only a single amino acid residue, in this case exploiting the difference in protein charge arising from the substitution of a negatively-charged carboxylic acid moiety for the positively-charged amine group on the amino acid lysine. A two-stage system was required to obtain reasonable yield and purification factor due to the relatively low selectivity between the product and variant associated with the small charge difference in this system. Wan et al., (2005) used ultrafiltration to remove dimers and higher order oligomers from a monoclonal antibody product based primarily on the difference in physical size, although the purification factor for the single stage system was less than four.

Recent studies by Rao and Zydney (2005, 2006) have demonstrated that the effective protein charge can be "controlled" through the use of small charged ligands that selectively bind to the protein of interest. Experimental studies performed with BSA and the dye Cibacron Blue showed that each molecule of BSA could bind up to 11 molecules of the dye, causing the net protein charge at pH 5 to shift from approximately +1 to -12.

This shift in charge caused a dramatic change in the rate of protein transport. For example, the addition of 1.1 g/L of Cibacron Blue to an 8 g/L BSA solution caused the transmission of BSA to drop by more than a factor of 100 due to the strong electrostatic repulsion between the negatively-charged complex of BSA and Cibacron Blue and the negatively-charged membrane. Rao and Zydney (2006)demonstrated that the bio-specific binding characteristics of Cibacron Blue could be used to dramatically increase the selectivity between BSA and ovalbumin during ultrafiltration.

Although the studies by Rao and Zydney (2005, 2006) clearly demonstrate that small charged affinity ligands can be used to alter the rate of protein transport, all of the experimental data were obtained in a small stirred ultrafiltration cell which is not representative of the tangential flow filtration (TFF) systems used for large-scale protein purification (van Reis et al., 1997). In addition, these studies never examined the recovery of the dye or the preparation of the dye-free protein product. The objective of this work was to extend these previous studies to TFF, providing an appropriate framework for the analysis of HPTFF systems using small charged affinity ligands to enhance the selectivity. Experiments were performed using the model system of ovalbumin and BSA with Cibacron Blue used as the affinity ligand. Data were obtained in a Pellicon XL tangential flow filtration module, which is linearly scalable to commercial bioprocesses (van Reis et al., 1997). The results clearly demonstrate that high resolution protein separations can be achieved using HPTFF by exploiting a small charged affinity ligand to control the net protein charge.

7.2 Material and Methods

Experiments were performed using bovine serum albumin (> 96% pure, essentially fatty acid free, catalogue # A-6003 from Sigma Chemical, St. Louis, MO) and ovalbumin (>98% pure, A-5503, Sigma Chemical). Cibacron Blue 3GA (Catalogue # C-9534, Sigma Chemical) was used as the small affinity ligand. Cibacron Blue has a molecular weight of 0.774 kD and contains three negatively-charged sulfonic acid groups attached to an aromatic ring structure. Previous work as shown in Chapter 4 has indicated that as many as 11 molecules of Cibacron Blue can bind to a single molecule of BSA, probably through the fatty acid and anion binding sites on the protein. Ovalbumin displays minimal binding of Cibacron Blue up to fairly high ligand concentrations (Lascau, 1984).

Buffer solutions were prepared by dissolving pre-weighed amounts of the appropriate salts in deionized water. An acetate buffer composed of CH_3COONa and CH_3COOH (EM Science, Gibbstown, NJ) was used for experiments at pH 5.0. The dye was separated from the BSA by ultrafiltration at pH 8.0 using Tris–HCl buffer with sodium thiocyanate (Sigma Chemical, St Louis, MO) at a total ionic strength of 1 M. The solution pH was measured using a 420APlus pH meter (Thermo Orion, Beverly, MA), and the solution conductivity was measured using a 105A plus conductivity meter (Thermo Orion, Beverly, MA). All buffer solutions were prefiltered through 0.2 μm pore size Supor-200 membranes (Pall Corp., Ann Arbor, MI) to remove particulates and undissolved salts.

Protein solutions were prepared by slowly dissolving the protein powder in the desired buffer, with the resulting solution filtered through a 0.22 μm syringe filter (Costar Corp., Cambridge, MA) to remove any protein aggregates immediately prior to use. Protein solutions were used within 24 hours of preparation to minimize the likelihood of protein aggregation or denaturation during storage. Additional details on the preparation of buffer and protein-dye solutions are available in Chapter 3.

Protein concentrations in the binary mixture were analyzed by size exclusion chromatography (Agilent 1100 series quaternary HPLC system). Assays were performed using a Superdex 75 column with 13 μm particle size and 10^5 MW exclusion limit (GE Healthcare, Piscataway, NJ). The column was first equilibrated with fresh buffer at a flow rate of approximately 0.3 mL/min for 180 min. This also served to flush both the sample and reference cells in the refractive index detector (Agilent 1100 series). Column equilibration was confirmed by tracking the baseline refractive index (RI). The mobile phase was a 50 mM phosphate buffer with 0.15 M NaCl at a flow rate of 0.2 mL/min. Protein samples (50 μl) were injected by an autosampler with the data analyzed using Agilent ChemStation software on a Dell Celeron Computer.

Cibacron Blue concentrations were determined spectrophotometrically using the natural absorbance at 616 nm. The presence of protein had no effect on the absorbance of the dye at 616 nm over the range of concentrations examined in this study.

All filtration experiments were performed using Ultracel composite regenerated cellulose membranes in Pellicon XL tangential flow filtration modules provided by Millipore Corp. (Bedford, MA). These cellulosic membranes are nearly uncharged and have very low protein binding due to their high degree of hydrophilicity. Protein

separations were performed using a charge-modified version of the 100 kD nominal molecular weight cut-off membranes with the Cibacron Blue recovered using a conventional 10 kD membrane. All membranes / modules were thoroughly flushed with deionized distilled water prior to use to remove any residual storage agents.

The negatively-charged version of the 100 kD membrane was made in our laboratory by the covalent attachment of negatively charged sulfonic acid groups to the surface of the membrane using the base-activated chemistry developed by van Reis (2001). Membranes were first flushed with deionized distilled water followed by 0.1 N NaOH. The charging solution, a 2 M solution of 3-Bromopropanesulfonic acid sodium salt (Catalogue #B2912, Sigma Chemical) in 0.1 N NaOH, was pumped through the module at a feed flow rate of 20 mL/min using a Rabbit-Plus peristaltic pump (Rainin Instrument Co., Emeryville, CA). Charging was done for 8 hours with the charging solution flushed through the system in total recycle mode. The membranes were flushed with approximately 100 L/m^2 of distilled water to quench the reaction and were then stored in 0.05 N NaOH until use.

7.2.1 Protein Sieving

Initial protein filtration experiments were conducted using the Pellicon XL module with the charge-modified 100 kD Ultracel membrane in total recirculation mode to determine the appropriate conditions for the protein separation. The feed tank was filled with the binary protein mixture containing a specified concentration of Cibacron Blue. The feed was pumped through the module using a Rabbit-Plus peristaltic pump

(Rainin Instrument Co., Emeryville, CA) at flow rates from 18 ml/min to 25 ml/min. The transmembrane pressure was monitored using pressure gauges (Millipore Corp, Bedford, MA) in both the feed and filtrate lines. The filtrate and retentate solutions were recycled back to the feed tank to maintain a constant concentration of the proteins and affinity ligand. The filtration velocity was measured by timed collection, with periodic samples taken from both the filtrate and bulk samples. Data were obtained over a range of filtrate flux, set by varying the transmembrane pressure drop. All experiments were performed at room temperature (22 ± 3°C) using the same lots of protein.

7.2.2 Diafiltration

A two stage separation process was performed using a diafiltration mode as shown schematically in Figure 7.1. Stage 1 employed a Pellicon XL module with a negatively charged version of the 100 kD Ultracel membrane. A binary mixture of BSA and ovalbumin, with an appropriate concentration of Cibacron Blue, was added to the feed tank. The inlet flow was pumped through the module using a peristaltic pump at a flow rate of 300 L m^{-2} h^{-1} (volumetric flow rate normalized by the membrane area). Initially, the filtrate and retentate lines were both returned to the feed tank, providing total recycle until the system had stabilized (typically 10 min). At this point, the diafiltration was begun, with the filtrate directed to a second collecting vessel. The total fluid volume in the feed tank was maintained at a constant level by continuous addition of fresh diafiltration buffer (10 mM acetate, pH 5.0) at a rate equal to the ultrafiltration rate.

Samples were taken from the feed and filtrate reservoir at appropriate time points throughout the diafiltration for subsequent analysis of the protein concentrations.

The final retentate from Stage 1 was further purified in Stage 2 to recover the Cibacron Blue and yield a dye-free BSA product. Experiments were performed using a Pellicon XL module with an unmodified (essentially neutral) 10 kD Ultracel membrane. The diafiltration buffer was 1 M NaSCN at pH 8, conditions which are known to cause the dissociation of Cibacron Blue from BSA. The filtrate flux in the second stage was maintained at approximately 50 L m^{-2} h^{-1} throughout the diafiltration process.

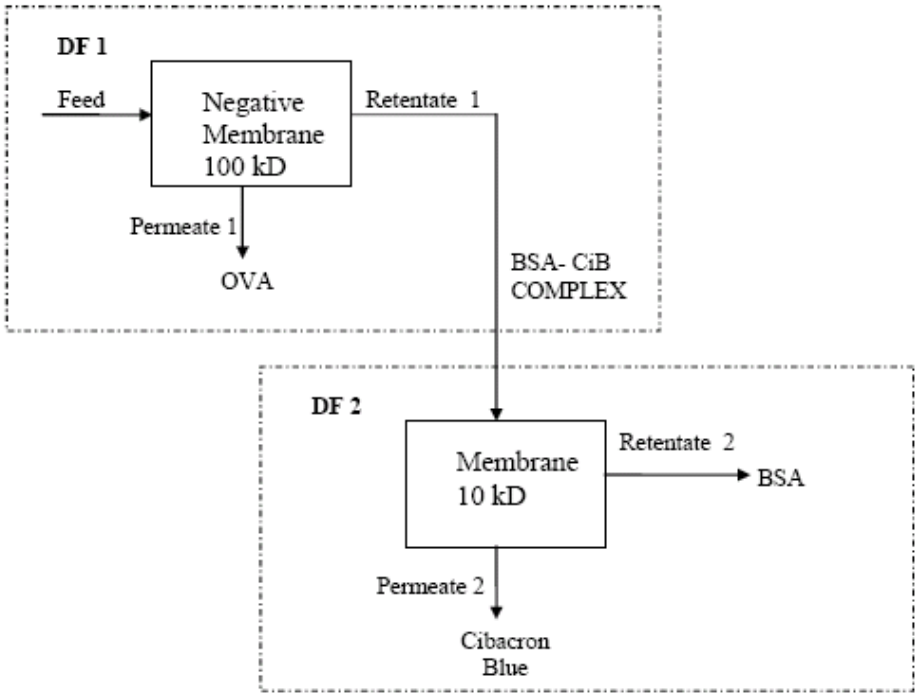

Figure 7.1: Schematic of the 2-stage separation process

7.3 Results

Initial protein sieving experiments were performed in a total recycle mode using the Pellicon XL module with a negatively charged version of the 100 kD Ultracel membrane. The negative membrane was produced by recirculating a 2 M solution of 3-Bromopropanesulfonic acid at pH 11 for 8 hrs. Previous data obtained with small membrane discs charged in a stirred ultrafiltration cell under these conditions yielded a membrane with a zeta potential of -12.4 mV. The sieving data were obtained with a solution containing a binary mixture of 10 g/L BSA and 6 g/L of ovalbumin both in the absence of any ligand and with a Cibacron Blue concentration of 1.4 g/L (corresponding to a molar ratio of 12 molecules of dye per molecule of BSA). The solution pH was adjusted to 5.0 using a 10 mM acetate buffer based on data obtained previously (Chapter 4,5 and 6) in a stirred ultrafiltration cell. Results are shown in Table 7.1 at a feed flow rate of 25 mL/min, equal to an area normalized feed flow rate of 300 L m^{-2} h^{-1} or 83 μm/s, and a filtrate flow rate of 35 L m^{-2} h^{-1} (6.9 μm/s) . The observed sieving coefficients for BSA and ovalbumin, defined as the ratio of the protein concentration in the filtrate solution to that in the bulk (feed) solution, differ by less than a factor of five in the absence of Cibacron Blue with values of S_o = 0.020 for BSA and S_o = 0.098 for ovalbumin. The greater sieving coefficient for ovalbumin under these conditions is likely due to the smaller size (MW of 44 kD versus 69 kD for BSA) and possibly the different surface charge. The addition of Cibacron Blue caused a 10-fold reduction in the observed sieving coefficient for BSA, with the sieving coefficient for ovalbumin

decreasing by less than 35%. The net result is that the addition of Cibacron Blue causes the selectivity for the BSA-ovalbumin system:

$$\psi = \frac{S_{o,OVA}}{S_{o,BSA}} \qquad (7.1)$$

to increase from less than 5 to more than 30. This large increase in selectivity is a direct result of the strong electrostatic exclusion of the negatively-charged complex formed between BSA and Cibacron Blue from the negatively-charged Ultracel membrane. Data obtained with a neutral membrane in a stirred cell ultrafiltration cell shown in Figure 5.4 showed only a small increase in selectivity upon the addition of Cibacron Blue due to the much weaker electrostatic repulsion.

Table 7.1:Observed sieving coefficients at a normalized feed flux of 300 L m^{-2} h^{-1} and a filtrate flux of 35 L m^{-2} h^{-1}

	Negative 100 kD CRC	
CiB Concentration (g/L)	$S_{o\ BSA}$	$S_{o\ OVA}$
0	0.020	0.098
1.4	0.002	0.064

Figure 7.2 shows typical sieving data obtained using a negatively charged version of the Pellicon XL membrane. The data were again obtained using a binary mixture of 10 g/L BSA and 6 g/L of ovalbumin and 1.4 g/L of Cibacron Blue in a 10 mM acetate buffer at a pH of 5.0. Cibacron Blue has been added in a molar ratio of 12 moles of dye per mole of BSA to ensure complete saturation, previous studies by Rao and Zydney (2005) have found approximately 11 moles of Cibacron Blue bind per mole of BSA in a 10 mM,

pH 5.0 buffer with ovalbumin having limited interaction with the dye molecules at these concentrations. The sieving data represented by the observed sieving coefficient S_o (defined as the ratio of the concentration of a particular solute in the feed to that in the bulk solution) was obtained as a function of the filtrate flux at two different feed fluxes. These experiments were performed to evaluate the effect of flux on protein transmission with the experiments performed in total recycle mode to maintain the total protein concentration levels relatively constant. The feed and filtrate flux were run at constant rates using a peristaltic pump. The observed sieving coefficient of ovalbumin is greater than BSA over the entire set of conditions studied. Ovalbumin is only slightly smaller with a radius of 3.0 nm compared to BSA which has a radius of 3.48 nm and both proteins have highly comparable isoelectric points with the pI of ovalbumin being 4.5 and BSA having a pI of 4.8. The large difference in the observed sieving coefficient is due to the significant repulsive electrostatic interactions present between the negatively charged BSA-Cibacron Blue complex at the conditions used in the experiment and the negatively charged pores of the semipermeable 100 kD charge modified CRC membrane. Previous studies done with the results shown in the previous chapters have clearly demonstrated that a large shift in charge of BSA is caused by the binding of 11 moles of Cibacron Blue per mole of BSA in a pH of 5.0, 10 mM acetate buffer, i.e. at a pH close to the isoelectric point of the protein, conditions that minimize the repulsive electrostatic interactions between Cibacron Blue and BSA. This increase in negative charge of BSA results in a large increase in repulsive electrostatic interactions between the complex and pores of the charged membrane and causes a dramatic increase in the retention of BSA. The sieving coefficient of ovalbumin is 0.064 compared to 0.002 for BSA - Cibacron Blue complex at

a feed flow flux at 300 LMH and a corresponding filtrate flux of 36 LMH. The effect of filtration velocity on the transmission of both proteins is reflected in the increase in transmission with the increase in filtration flux at both feed fluxes of 216 and 300 LMH. This increase in the observed sieving coefficients is probably due to the effect of concentration polarization in the system with the effect being more pronounced for the BSA-Cibacron Blue complex. This phenomenon has been reported by van Reis et al (1999) in the separation of BSA monomer from the oligomer.

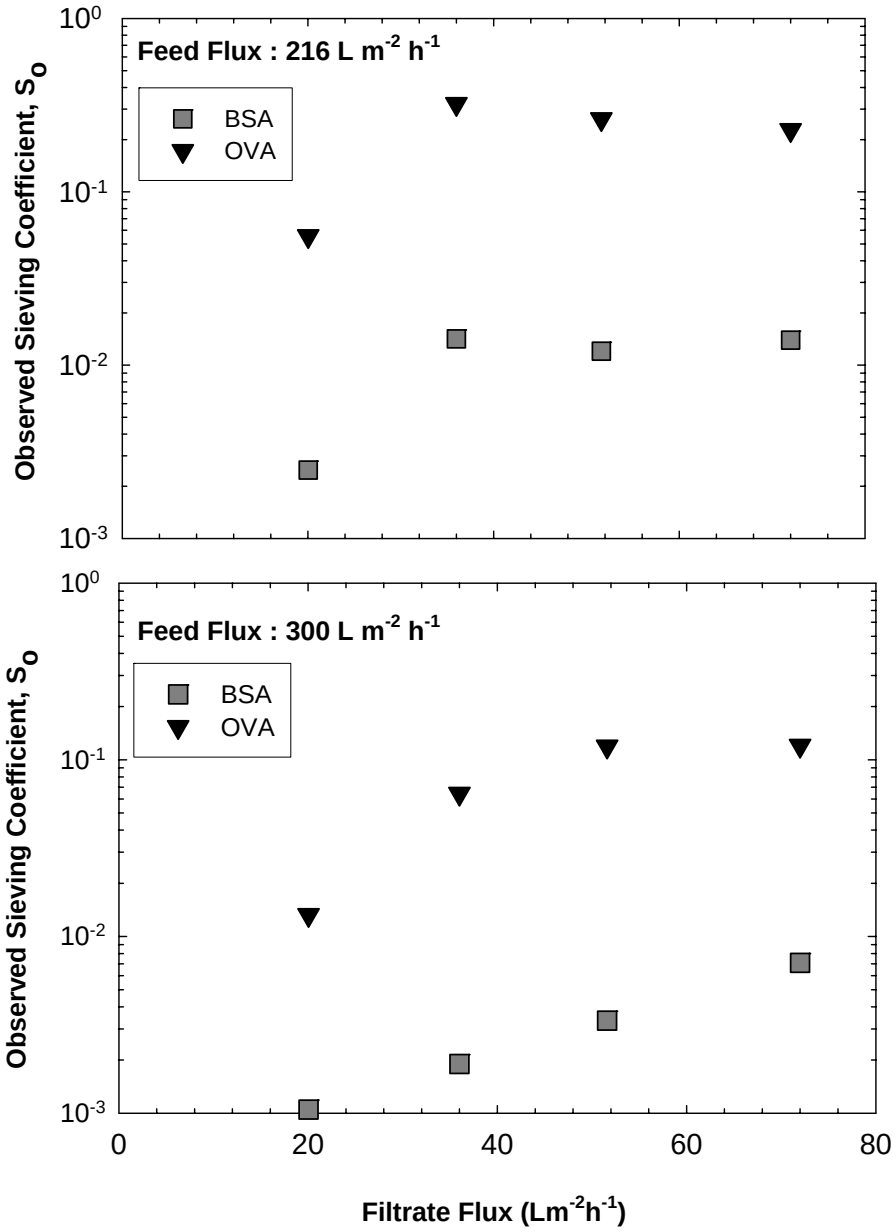

Figure 7.2: Observed sieving coefficients of BSA and ovalbumin over a range of filtrate fluxes obtained with a binary protein mixture of 10 g/L and 6 g/L ovalbumin with Cibacron Blue added in a molar ratio of 12:1 per mole of BSA using a negatively charged 100 kD Ultracel membrane at two different feed fluxes

The effects of the feed and filtrate flow rates on the separation characteristics are examined in Figures 7.3 and 7.4. The experimental data shown in Figure 7.2 were replotted in terms of selectivity given by Equation 7.1 over a range of filtrate fluxes for both values of feed flux. The selectivity initially increases with increasing filtrate flux, attaining its largest value of $\psi = 36$ at a filtrate flux of 50 L m^{-2} h^{-1} and a feed flow rate of 300 L m^{-2} h^{-1}. The selectivity decreases at very high filtrate flux, which is likely due to the greater increase in the observed sieving coefficient of BSA associated with the greater degree of concentration polarization for the more highly retained species. The selectivity at a feed flow of 216 L m^{-2} h^{-1} was significantly smaller than that obtained at 300 L m^{-2} h^{-1} at intermediate values of the filtrate flux, but the reverse behavior was seen at the lowest flux (20 L m^{-2} h^{-1}) where the selectivity at 216 L m^{-2} h^{-1} was more than twice that at a feed flux of 300 L m^{-2} h^{-1}. These differences are likely due to the different degrees of concentration polarization arising from the flow rate dependence of the mass transfer coefficient along with the different variations in the protein concentration with axial position associated with the different conversions (ratio of filtrate to feed flow rate) at the two feed flow rates.

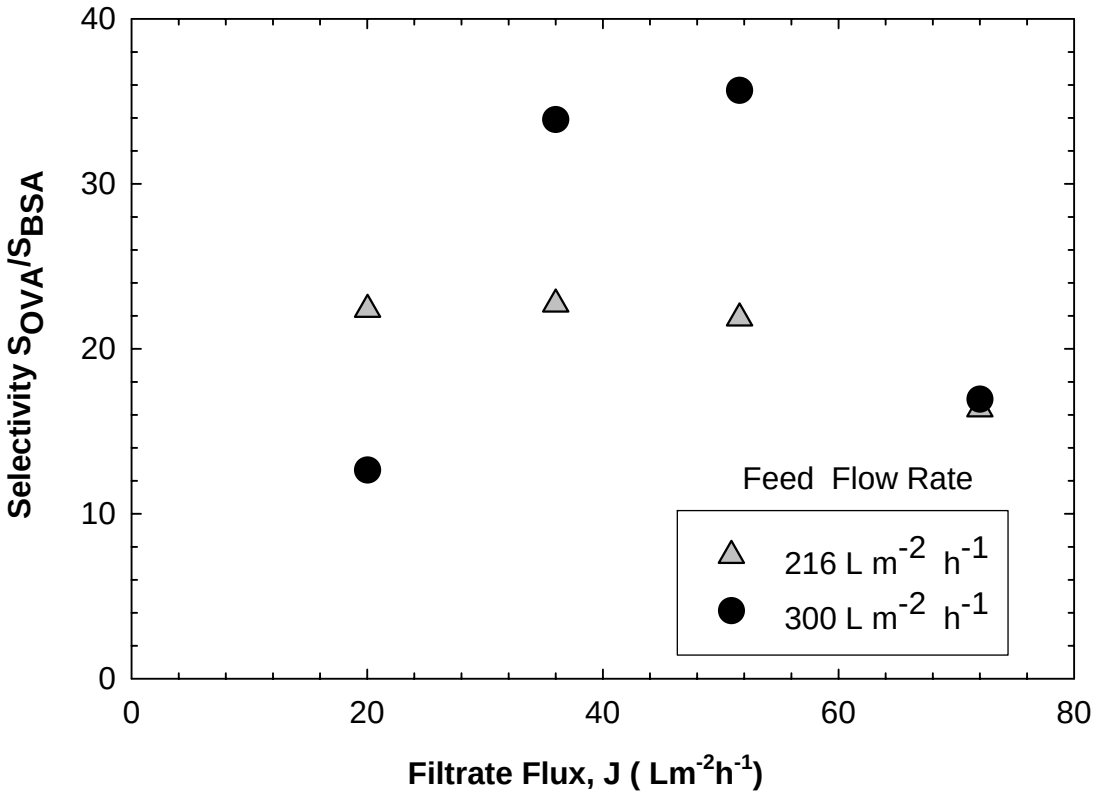

Figure **7.3**: Selectivity for separation of a binary mixture of 10 g/L BSA and 6 g/L ovalbumin with 1.4 g/L Cibacron Blue for a negatively charged 100 kD Ultracel membrane

The results of Figure 7.4 shows the calculated values of the mass throughput parameter, JΔS, which determines the economics and practicality of the separation (van Reis and Saksena, 1997). High values of JΔS allow effective separations to be achieved using less membrane area, shorter diafiltration times, and/or with less diafiltration buffer. In contrast to the results for the selectivity, the JΔS values are uniformly higher at the lower feed flux due to the higher values of the ovalbumin sieving coefficient obtained under these conditions. This increase in S_o arises from the greater

degree of concentration polarization at the lower feed flow rate due to the lower value of the mass transfer coefficient. JΔS increases monotonically with increasing filtrate flux, although the rate of increase becomes much less pronounced at high values of the filtrate flux due to the reduction in ΔS at high flux, particularly at the lower feed flow rate.

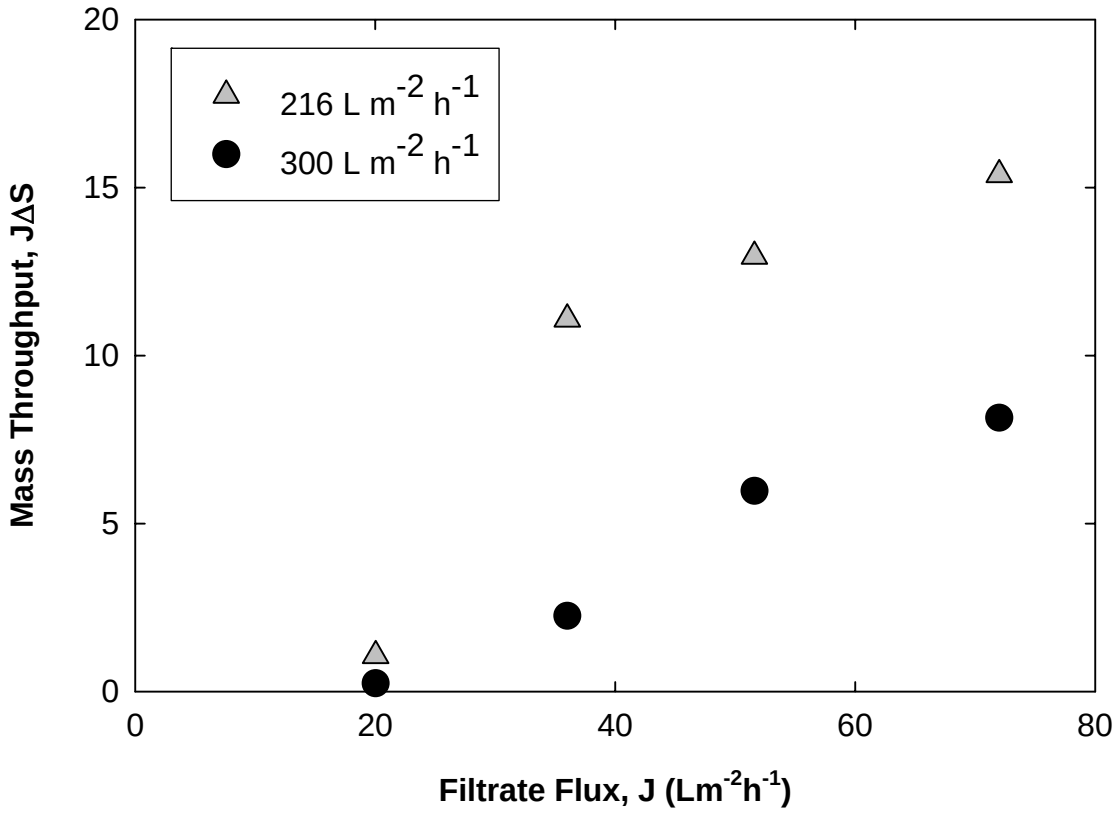

Figure 7.4: Mass throughput values for separation of a binary mixture of 10 g/L BSA and 6 g/L ovalbumin with 1.4 g/L Cibacron Blue for a negatively charged 100 kD Ultracel membrane

Figure 7.5 shows selectivity data plotted as a function of the mass throughput parameter at both the feed fluxes of 216 L m^{-2} h^{-1} and 300 L m^{-2} h^{-1}. The largest value of selectivity of 36 is obtained at a intermediate value of mass throughput with a feed flux of 300 L m^{-2} h^{-1}. Hence, the data obtained with the feed flux of 300 L m^{-2} h^{-1} were used in the subsequent theoretical calculations described.

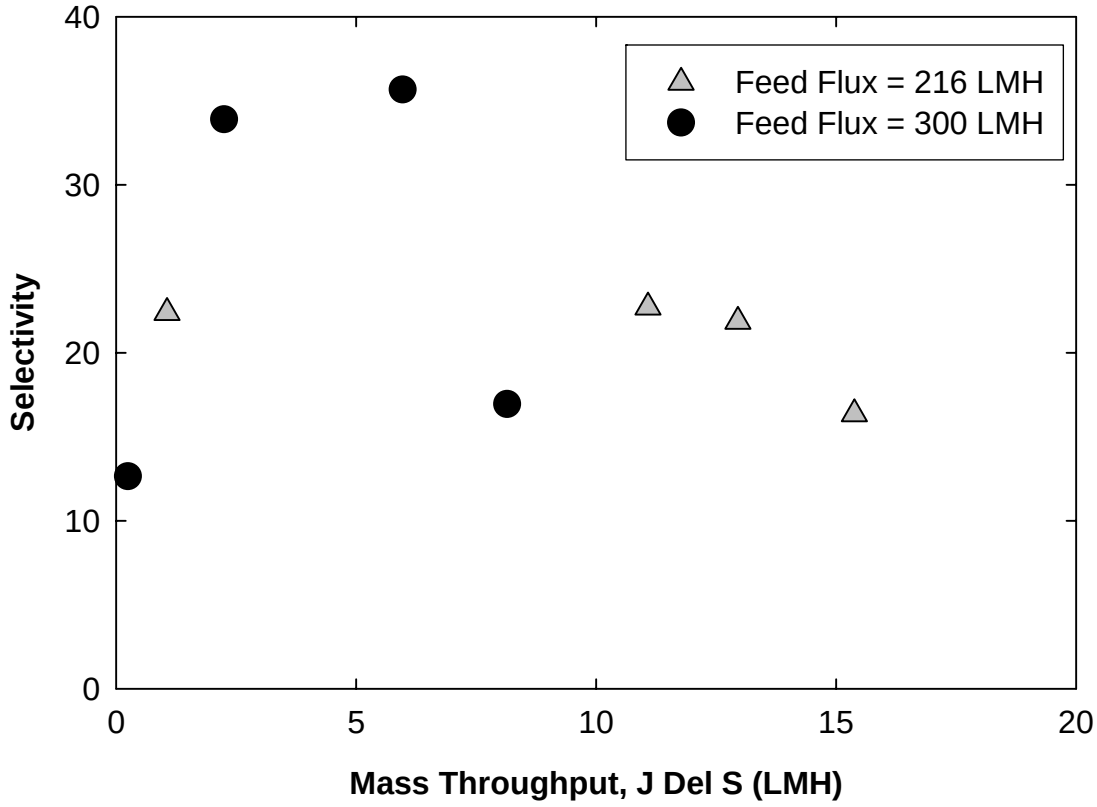

Figure 7.5: Selectivity as a function of mass throughput

The most appropriate conditions for separating ovalbumin and BSA using the affinity HPTFF process were identified using process optimization diagrams following the approach developed by van Reis and Saksena (1997). The process optimization involves a trade-off between the purification factor, yield, membrane area, process time, and buffer requirements, all of which are functions of the selectivity and the mass throughput parameters. This phenomenon has been described in greater detail in Chapter 6. The product yield is defined as the percent recovery of the desired product in either the final retentate or filtrate stream, while the purification factor is equal to the yield of the desired product divided by the yield of the impurity. In this case, ovalbumin is the impurity for the BSA product collected in the retentate while BSA is the impurity for the ovalbumin product collected in the filtrate solution. Theoretical calculations were performed by fixing the BSA yield in the retentate at a value of 95 %, with the purification factor for BSA and the required number of diavolumes (N) for the separation evaluated as:

$$P_{BSA} = Y_{BSA}^{1-\psi} \tag{7.2}$$

$$N = \frac{\ln(P_{BSA})}{\Delta S} \tag{7.3}$$

where N is the ratio of the cumulative filtrate volume to the constant volume of the feed reservoir (tank) during a constant volume diafiltration. The corresponding values for the yield and purification factor for ovalbumin collected in the filtrate solution were calculated as:

$$P_{OVA} = \frac{Y_{OVA}}{1-(1-Y_{OVA})^{1/\psi}} \tag{7.4}$$

$$N = \frac{\ln\left[\left(Y_{OVA}/P_{OVA}-1\right)/\left(Y_{OVA}-1\right)\right]}{\Delta S} \tag{7.5}$$

The results are summarized in Table 7.2 for calculations performed at the feed flow rate of 300 L m^{-2} h^{-1}over the full range of filtrate flux. Similar trends were seen using other values for the BSA yield. The purification factor for BSA is fairly small at low values of the filtrate flux due to the small selectivity under these conditions. In addition, the required number of diavolumes is very large (N = 49 at a feed flow rate of 300 L m^{-2} h^{-1}), indicating that this separation would be very difficult to effect in a large scale commercial process. The use of very large filtrate flux significantly reduces the required number of diavolumes, but the purification factor for BSA becomes very small and the yield and purification factor for ovalbumin are also reduced. The optimal conditions for the separation would depend on the detailed economics and separation constraints for the commercial process, including the value for the two protein products, the required degree of purification and the overall process design. However the use of a feed flow rate of 300 L m^{-2} h^{-1} and a filtrate flow rate of 50 L m^{-2} h^{-1} should provide a reasonable combination of purification factor and yield for both BSA and ovalbumin with moderate requirements for the number of diavolumes. These conditions were thus used in all subsequent experiments.

Table 7.2: Calculated values of the Yield, Purification Factor, and Number of Diavolumes for a diafiltration process providing 95% yield of BSA for a feed flux of 300 L m^{-2} h^{-1}

Filtrate Flux (L m^{-2} h^{-1})	Selectivity (ψ)	Mass Throughput (L m^{-2} h^{-1})	N	P_{BSA}	Y_{OVA}	P_{OVA}
20	13	0.24	49	2	47	10
36	34	2.26	27	5	82	16
50	36	5.83	15	6	83	17
72	17	8.15	7	2	56	12

The separation of BSA and ovalbumin was performed using a constant volume diafiltration to effectively wash the more permeable ovalbumin through the membrane and into the filtrate while the highly charged BSA – Cibacron Blue complex was retained in the feed reservoir. Figure 7.6 shows experimental data obtained during a diafiltration experiment using the negatively-charged version of the 100 kD Ultracel membrane in the Pellicon XL tangential flow filtration module at a feed flow rate of 300 L m^{-2} h^{-1} and a filtrate flow rate of 50 L m^{-2} h^{-1}. The initial (feed) was 2 g/L BSA and 1 g/L ovalbumin, with 0.28 g/L of Cibacron Blue added as the affinity ligand. Experiments were performed using 10 mM acetate at pH 5 as the diafiltration buffer; the retention of Cibacron Blue (bound to BSA) was sufficiently high that the Cibacron Blue

concentration in the feed reservoir remained nearly constant throughout the diafiltration even without the presence of additional Cibacron Blue in the diafiltration buffer.

The data in Figure 7.6 have been plotted as the normalized protein concentration in the feed reservoir (with C normalized by the initial feed concentration) as a function of the total number of diavolumes. The normalized protein concentration decreases with increasing number of diavolumes, with the rate of decrease being much more dramatic for ovalbumin due to the much greater degree of ovalbumin transmission through the negatively-charged membrane. The ovalbumin concentration at the end of the 20-diavolume process was less than 0.05 g/L, corresponding to removal of more than 95 % of the ovalbumin present in the original feed solution. In contrast, the BSA concentration at the end of the diafiltration was greater than 1.6 g/L providing a BSA yield of more than 80 % in the retentate solution. Greater values of the BSA yield could be obtained by stopping the diafiltration after a smaller number of diavolumes, with the yield of BSA being greater that 90% for $N < 7$.

The solid and dashed curves in Figure 7.6 represent the calculated values of the normalized protein concentration evaluated by integration of a differential mass balance assuming a constant observed sieving coefficient:

$$C/C_o = \exp(-NS_o) \qquad (7.6)$$

The solid curves were generated using the protein sieving coefficients evaluated from data obtained in the total recycle experiments, with the model over-predicting the protein concentrations throughout the diafiltration. The dashed curves in Figure 7.6 represent the model calculations using the best fit values of the sieving coefficients

determined by fitting the experimental data in Figure 7.6 to Equation (7.6) yielding $S_{o,BSA}$ = 0.01 and $S_{o,OVA}$ = 0.16. These values for the sieving coefficients were both somewhat larger than those determined from the total recycle experiments causing the model to give a more rapid reduction in the concentrations of both BSA and ovalbumin during the diafiltration. This discrepancy is likely due to the inherent variability between membranes / modules used in these experiments.

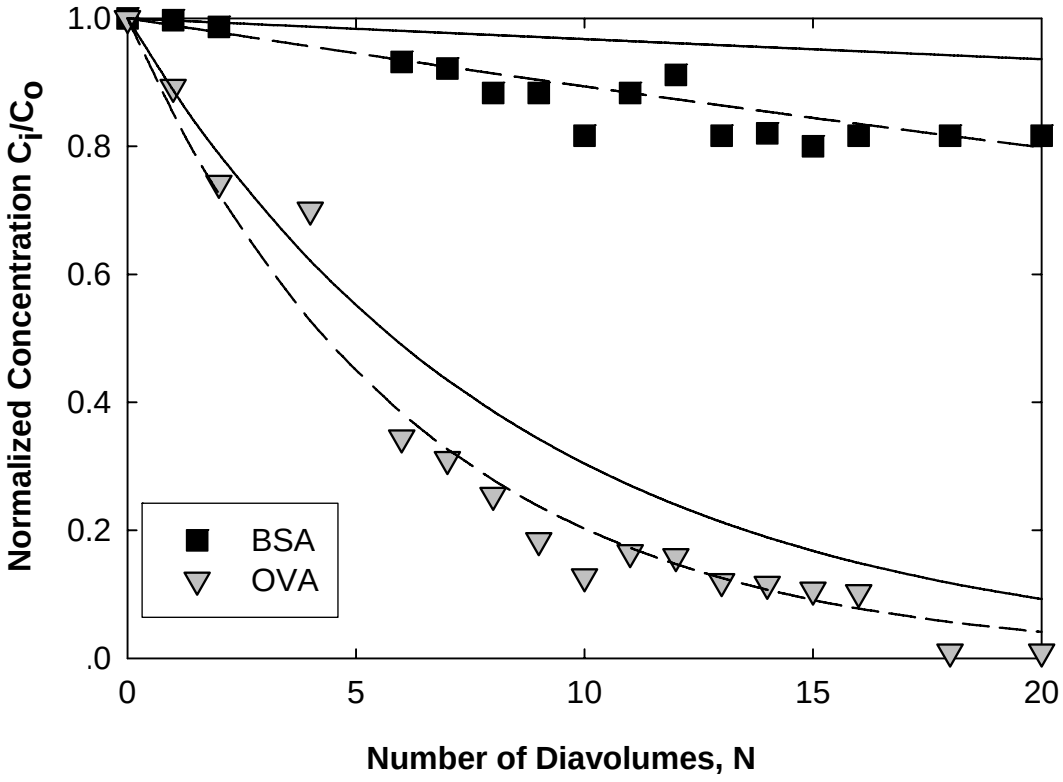

Figure 7.6: Normalized protein concentrations during diafiltration of a feed containing 2 g/L BSA and 1 g/L ovalbumin in the presence of 0.28 g/L Cibacron Blue using a negatively charged 100 kD Ultracel membrane. Solid curves are model calculations as described in the text.

The behavior of the BSA – ovalbumin separation was examined in more detail by replotting the data from Figure 7.6 as the protein yield as a function of the purification factor. Results for BSA (in the retentate solution) are shown in the top panel of Figure 7.7 while those for ovalbumin (in the filtrate solution) are shown in the bottom panel. The dashed curves are model calculations given by Equations (7.2) and (7.4) with the selectivity calculated from the best fit values of the observed sieving coefficients as determined from the data in Figure 7.6. The diafiltration process for BSA starts in the upper left corner with a yield of 100% and a purification factor of 1 because both proteins are fully contained in feed reservoir at the start of the process. The purification factor for BSA increases throughout the diafiltration due to the rapid removal of ovalbumin, with the BSA yield decreasing slightly due to the slow leakage of BSA into the filtrate. The final purification factor for BSA is nearly 15-fold, with the BSA yield remaining greater than 80% throughout the diafiltration due to the strong retention of the charged complex formed between BSA and Cibacron Blue. Note that a separate diafiltration experiment performed in the absence of Cibacron Blue gave a maximum purification factor for BSA of less than 1.7 with a final yield less than 30 % due to the significant reduction in BSA retention in the absence of Cibacron Blue.

The diafiltration process for ovalbumin begins in the lower right corner with a yield of zero and a maximum purification factor of about 35 for the data and closer to 16 for the model. The origin of this discrepancy is unclear, although the data suggest that there may have been a rapid reduction in the selectivity during the initial phase of the diafiltration. The ovalbumin yield increases throughout the diafiltration process as the ovalbumin passes into the filtrate solution, but there is a corresponding reduction in the

purification factor due to the continual leakage of BSA through the membrane. This effect is relatively small near the start of the diafiltration, but it becomes very pronounced as the ovalbumin yield approaches 100%. The final ovalbumin product had a yield of more than 95 % although the purification factor for this process was less than 5.

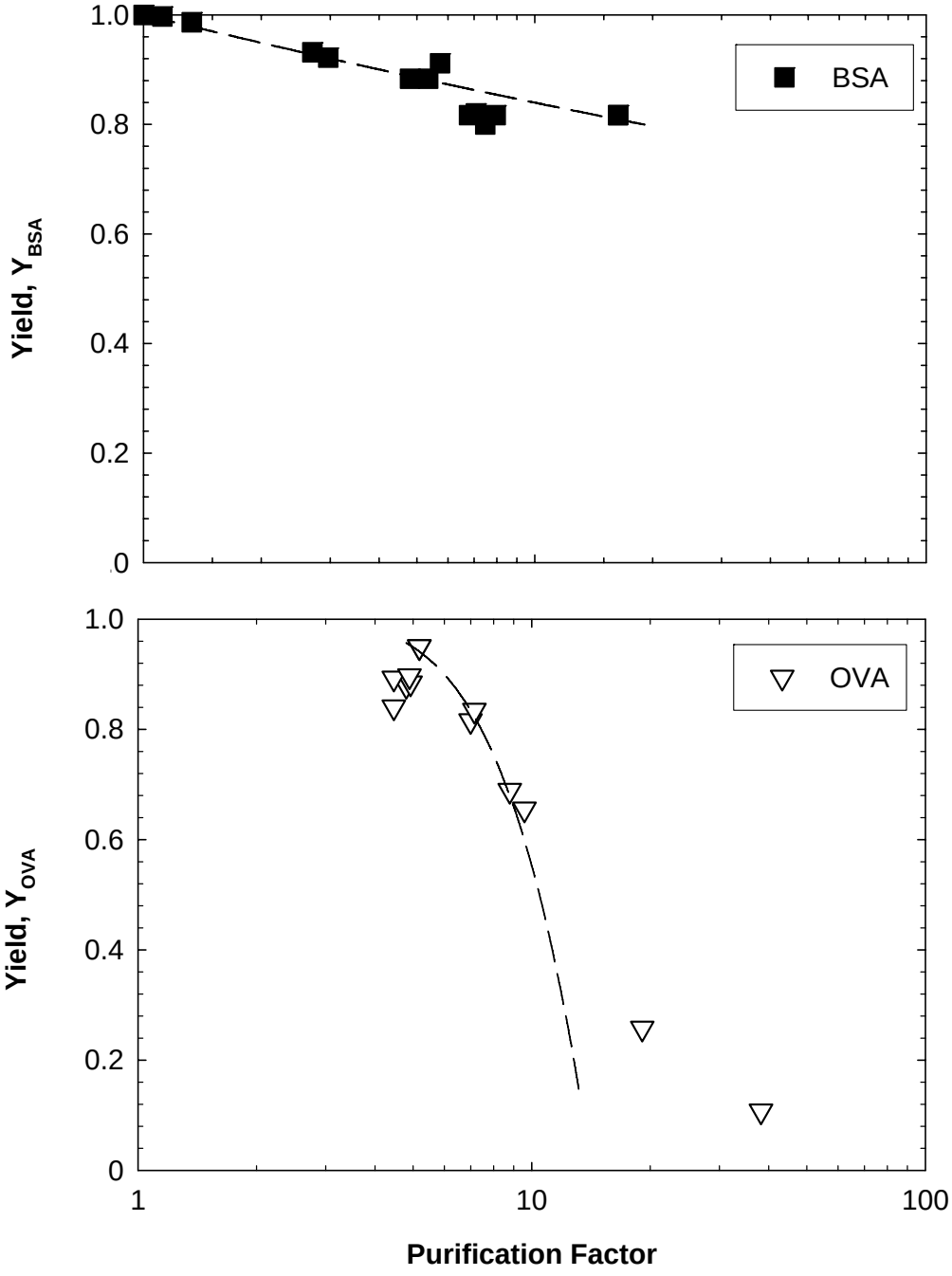

Figure 7.7: Yield as a function of purification factor for BSA collected in the retentate (top panel) and ovalbumin collected in the filtrate (bottom panel). Dashed curves are model calculations as described in the text

Figure 7.8 shows size exclusion chromatograms for the feed (top panel) and final retentate (bottom panel) for the separation process presented in Figure 7.6. The small peak seen in the feed solution at a retention time of 62.5 min is due to the presence of a small amount of BSA dimer in the feed, corresponding to approximately 13 % of the main BSA peak (which appears at a retention time of 71 min). The final retentate product has a BSA purity of greater than 96%, with the ovalbumin peak at 77 min just barely visible in the chromatogram.

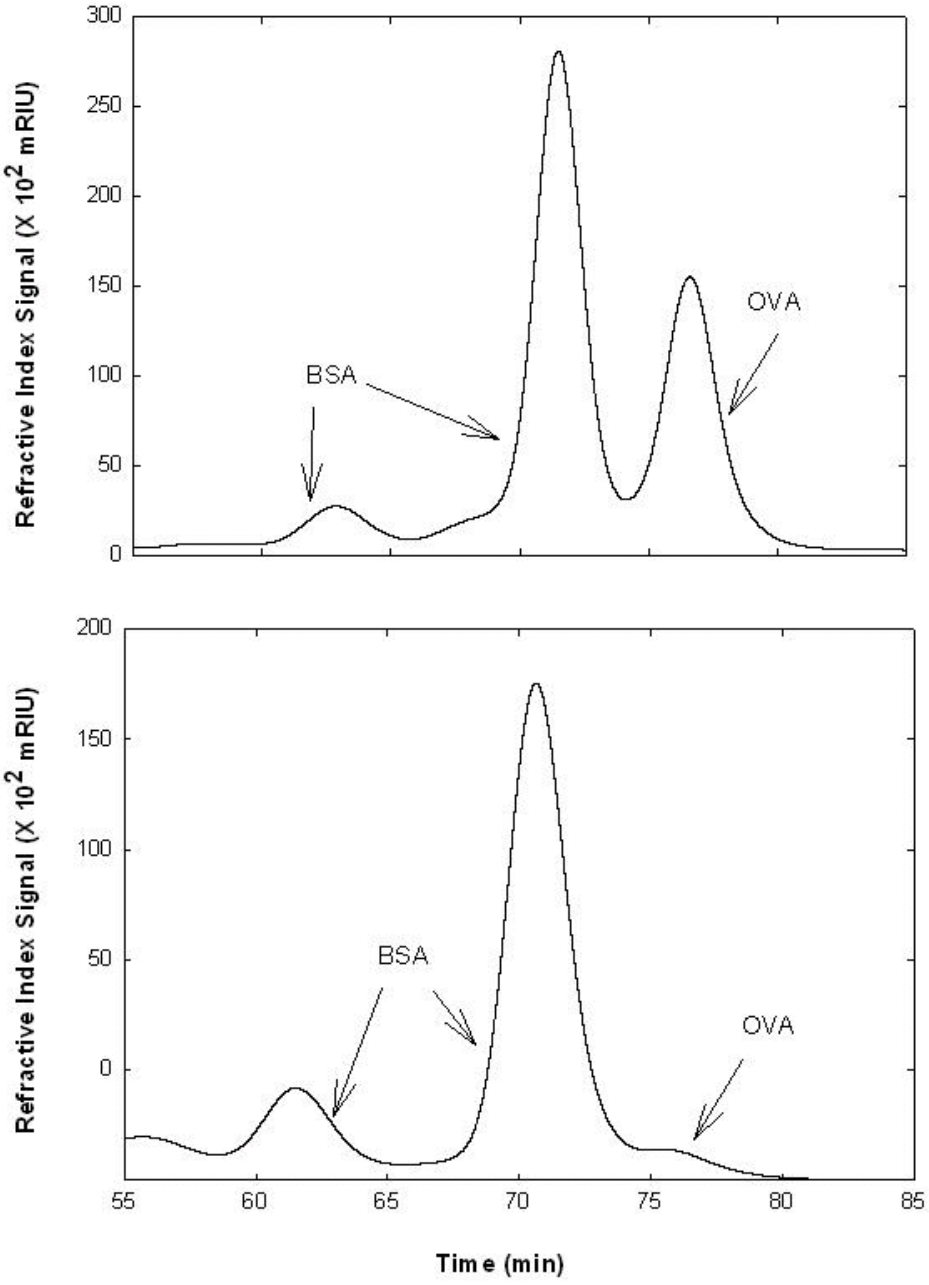

Figure **7.8**: Size exclusion chromatograms for the initial feed (top panel) and final retentate (bottom panel) for the diafiltration process examined in Figure 7.6.

In order to develop an effective commercial process for protein purification using HPTFF employing an affinity ligand, it would be necessary to recover the ligand while at the same time generating a ligand-free protein product. Experiments were thus performed to examine the separation of BSA and Cibacron Blue using a second diafiltration employing a 10 kD unmodified (neutral) Ultracel membrane in a Pellicon XL module. It was impractical to perform this diafiltration at pH 5 because of the strong binding between BSA and Cibacron Blue; model calculations indicated that more than 1000 diavolumes would be needed to recover 99% of the Cibacron Blue under these conditions. Previous studies of Cibacron Blue binding shown in Chapter 4 have clearly demonstrated that the binding strength is significantly reduced at higher pH due to repulsive electrostatic interactions between the negatively-charged dye and the negatively-charged protein. In addition, NaSCN is known to displace Cibacron Blue from BSA (Ruckenstein and Zeng, 1998). Diafiltration experiments were thus performed at pH 8.0 using a 10 mM Tris buffer with 1 M NaSCN. The feed solution was the final retentate obtained from the first stage protein separation without any pre-conditioning.

Figure 7.9 shows results for the normalized concentration of Cibacron Blue as a function of the number of diavolumes for this second diafiltration. The rate of Cibacron Blue removal increased during the initial stages of the diafiltration due to the increase in solution pH and NaSCN concentration associated with the displacement of the original acetate buffer from the feed reservoir. The Cibacron Blue concentration then decreases exponentially with increasing number of diavolumes, consistent with the expected washout of the unbound dye from the protein solution. The final concentration of Cibacron Blue after 10 diavolumes was only 0.23 mg/L, corresponding to 99.9 %

removal of the Cibacron Blue. The BSA yield for this process was greater than 98%; there was no detectable BSA (detection limit of approximately 0.05 g/L) in the filtrate solution collected through the 10 kD membrane.

The solid curve in Figure 7.9 is the model calculation using a Cibacron Blue sieving coefficient through the 10 kD membrane of 0.59. The model is in good agreement with the experimental data; there is a small discrepancy at large numbers of diavolumes which is likely due to the inherent difficulties in accurately measuring the very small concentrations of the dye under these conditions. Model calculations indicate that it should be possible to reduce the concentration of Cibacron Blue in the product solution to less than 1 ppm (based on BSA) using a 20-diavolume process. The change in solution pH with an increase in diavolumes has also been shown.

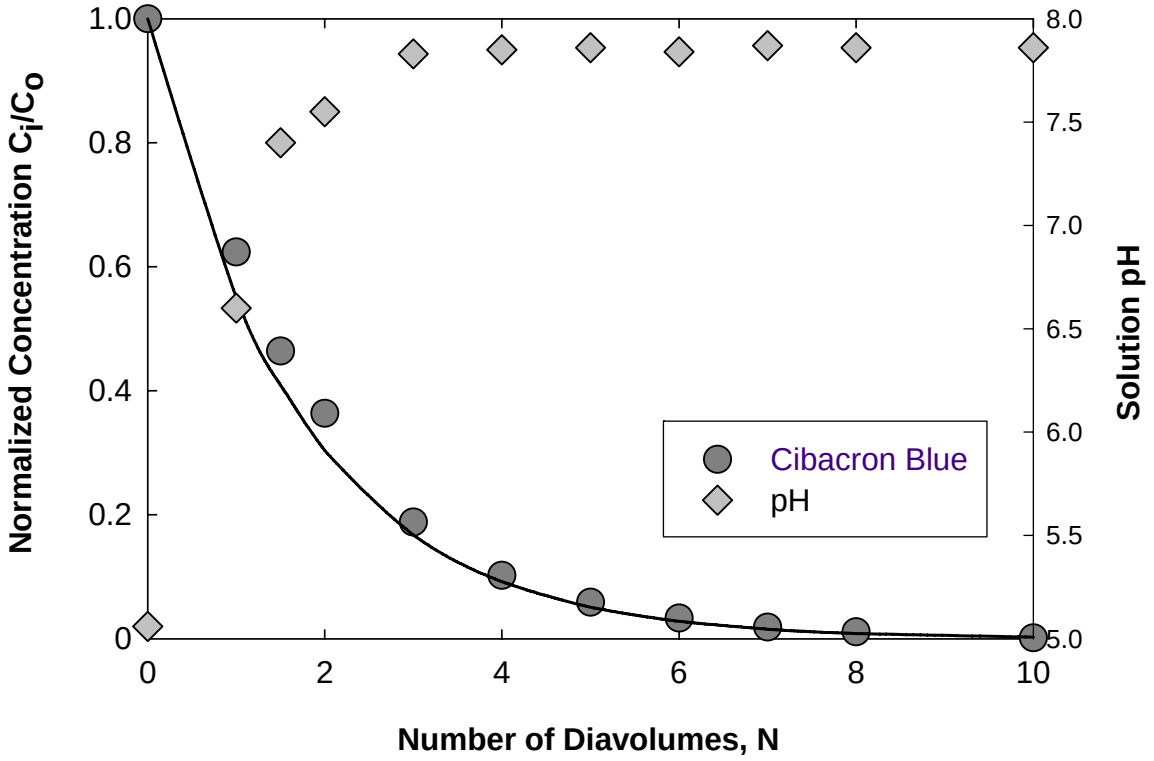

Figure **7.9**: Normalized ligand concentration in the second stage diafiltration using a 10 kD unmodified Ultracel membrane with a pH 8.0, 10 mM tris, 1 M NaSCN diafiltration buffer. Solid curves are model calculations as described in the text. Change in solution pH has also been shown

7.4 Conclusions

Although a number of studies have demonstrated the potential of high performance tangential flow filtration for protein separations, most of the results have been obtained with proteins having significantly different electrical charge allowing high selectivities to be generated by exploiting differences in electrostatic interactions. The data presented in this manuscript clearly demonstrate that it is possible to use small charged affinity ligands to selectively shift the charge of the product (or impurity), greatly enhancing the performance of the HPTFF process. Experiments performed with a binary mixture of BSA and ovalbumin, using Cibacron Blue as the affinity ligand, gave a retentate product with greater than 80% yield and 15-fold purification factor of BSA. The ovalbumin was collected in the filtrate with 95% yield and several-fold purification. The performance characteristics could be easily adjusted by altering the numbers of diavolumes to achieve the desired yield and purification factor.

A second stage diafiltration process was used to produce a dye-free protein while at the same time recovering the affinity ligand, which could potentially be recycled for use in subsequent protein purification. The small affinity ligand was easily separated from the BSA using a conventional ultrafiltration process operated with a diafiltration buffer in which the dye-protein binding was minimal. In this case, we used a high pH to enhance the repulsive interactions between the negatively-charged protein and dye with NaSCN added to facilitate the displacement of the dye from the protein surface. 99.9% recovery of the Cibacron Blue was obtained after only 10 diavolumes, with even greater removal possible by simply increasing the number of diavolumes.

The affinity HPTFF process was performed using Pellicon XL tangential flow filtration modules that have been specifically designed to be linearly scalable to commercial processes with more than 80 m^2 of membrane area. The protein separation was accomplished at a flux of 50 L m^{-2} h^{-1}, which is similar to the flux currently used in large-scale ultrafiltration systems. These results indicate that there should be no significant technical barrier to the implementation of this type of affinity HPTFF system in commercial protein purification. However, future studies will be needed to demonstrate the actual practicality and overall economics of these system.

Chapter 8

CONCLUSIONS AND RECOMMENDATIONS

8.1 Conclusions

The growing interest in the production of high-value protein therapeutics has created a critical need to develop separation techniques capable of providing high resolution and high throughput protein separations with reasonable cost. Membrane systems have significant potential for meeting the needs of the biotechnology industry since these processes can provide high throughput protein purification and they are readily scalable to commercial production of high value proteins. However, membrane systems typically have much lower selectivity than chromatographic processes.

The objective of this thesis was to examine the potential of using affinity ultrafiltration with small charged ligands to obtain high-resolution protein separations by exploiting biospecific binding interactions to alter the electrical charge and thus the transmission characteristics of the target protein. The next few subsections summarize some of the key experimental and theoretical findings of this work along with recommendations for appropriate future work in this area.

8.1.1 Effects of Ligand Binding

Experimental studies were performed over a wide range of solution conditions to determine the equilibrium binding interactions between Cibacron Blue and the proteins BSA and ovalbumin. These studies clearly demonstrated that the binding interactions between BSA and Cibacron Blue are a strong function of the solution conditions. Very high degrees of binding were obtained at pH 5.0 and 10 mM ionic strength, with as many as 11 molecules of Cibacron Blue bound by each molecule of BSA, probably involving the multiple fatty acid binding sites on the protein. It was possible to significantly reduce the binding between BSA and Cibacron Blue using high pH, and the binding interactions were minimal in the presence of a displacement agent, in this case sodium thiocyanate. In contrast to the results with BSA, Cibacron Blue to ovalbumin was relatively weak under all experimental conditions even though there is a high degree of homology between ovalbumin and BSA. These results clearly demonstrate the strong selectivity of the dye binding interactions.

The effect of ligand binding on the effective protein charge was estimated using a charge regulation model that accounts for both the binding of the negatively-charged dye and the change in the degree of protonation / deprotonation of the various amino acids associated with the shift in local hydrogen ion concentration near the surface of the protein. The model calculations indicate that the binding of Cibacron Blue causes a dramatic shift in electrical charge for BSA of approximately 13 electronic charges due to the strong affinity between the protein and dye. In contrast, Cibacron Blue has relatively little effect on the ovalbumin charge, providing a means to selectively control the surface

charge characteristics of the proteins by exploiting the high selectivity of biospecific binding interactions.

8.1.2 Effect of Ligand Binding on Protein Transport

The experimental studies in Chapter 5 provide the first demonstration that the addition of a small charged affinity ligand can significantly alter the rate of protein transport through a semipermeable membrane by changing the extent of electrostatic interactions between the charged protein-ligand complex and the membrane pores. For example, the addition of 1.1 g/L of Cibacron Blue to a 8 g/L solution of BSA caused the BSA sieving coefficient through a negatively-charged ultrafiltration membrane to decrease by more than two orders of magnitude. This effect was much weaker when using an unmodified (neutral) version of the cellulose membrane, and it could be almost completely eliminated upon the addition of NaCl since the salt shields the electrostatic interactions.

The effect of the charged ligand on protein transport is quite complex, with a distinct minimum in protein transmission occurring at an intermediate value of the Cibacron Blue concentration. At low Cibacron Blue concentrations, the dominant effect is the increase in the net negative charge on the protein-ligand complex caused by the increased binding of the negatively-charged ligand. This increase in negative charge causes a significant increase in the electrostatic repulsion between the protein-ligand complex and the negatively-charged membrane thereby increasing the protein rejection from the membrane pores. At high dye concentrations, the dominant effect is the

increase in solution ionic strength caused by the increase in concentration of the free ligand that occurs after all of the binding sites on the protein are saturated with the dye. This increase in ionic strength shields the electrostatic interactions between the charged protein-ligand complex and the charged membrane, leading to a significant increase in protein transmission.

In contrast to the data for BSA, the sieving coefficient for ovalbumin increases monotonically with an increase in Cibacron Blue concentration. In this case, the change in the protein charge due to binding of the dye is quite small, with most of the dye present as free ligand in solution. Thus, the dominant effect on protein sieving is the increase in solution ionic strength, which shields the electrostatic repulsion between the charged protein and the charged membrane.

Model calculations for protein sieving were in good agreement with the experimental data for both BSA and ovalbumin. The model explicitly accounts for the change in protein charge due to ligand binding, which is evaluated using the charge regulation model and the experimentally determined binding constants in the equilibrium (Langmuir) binding isotherm, as well as the charge in the solution ionic strength associated with the presence of the free dye. The electrostatic interactions between the protein and the membrane were evaluated using a partitioning model that includes the affects of both steric exclusion and the increase in free energy for the protein in the pore due to long-range electrostatic forces. The membrane charge was estimated from streaming potential measurements for the charge-modified membrane. The model calculations properly capture the minimum in the protein sieving coefficient at a dye

concentration that is just sufficient to almost completely saturate the ligand binding sites on the protein.

8.1.3 Effect of Membrane Charge

Previous studies by Mehta and Zydney (2006) have clearly shown the importance of the membrane surface charge density in determining the performance of ultrafiltration systems. The data obtained in Chapters 5 and 6 demonstrate that the membrane charge is a critical parameter in the design of affinity ultrafiltration systems using small charged affinity ligands. Experiments were performed with a series of membranes having different surface charge densities, made by chemical modification of the base cellulose membrane for different reaction times to control the extent of surface modification. The transmission of the negatively-charged protein-ligand complex decreased significantly through the more negatively charged membranes due to the strong electrostatic repulsive interactions. This affect was exploited in the affinity ultrafiltration process to provide high selectivity between BSA and ovalbumin using Cibacron Blue to obtain a large difference in electrical charge, and thus transmission, between the two proteins.

Although the selectivity of the affinity ultrafiltration process increased significantly with increasing membrane charge, the mass throughput parameter decreased significantly for the heavily charged membranes due to the reduction in ovalbumin transmission associated with the greater electrostatic interactions. The net result is that the membrane charge alters the trade-off between protein yield and purification factor, with the optimal performance for the affinity ultrafiltration process obtained at an

intermediate surface charge density (approximately -0.0023 C/m^2 for the separation of BSA and ovalbumin using Cibacron Blue as the small affinity ligand).

8.1.4 Protein Separations

The results presented in Chapters 6 and 7 provide the first demonstration that it is possible to use small charged affinity ligands to achieve high-resolution protein separations for proteins with nearly identical size and electrical charge by exploiting the selectivity of the affinity binding interactions. Simple stirred cell ultrafiltration experiments were performed using a diafiltration process. Purified BSA was obtained in the retentate solution at a yield of more than 90% and a purification factor greater than 90-fold. Ovalbumin was collected in the filtrate solution at a yield of nearly 100 % and a purification factor of more than 10.

Similar results were obtained using Pellicon XL tangential flow filtration modules which are linearly scalable to commercial manufacturing systems. In addition, it was possible to recover the charged ligand using a two-stage diafiltration process, thereby generating a ligand-free protein product. In the case of BSA and Cibacron Blue, this was accomplished by increasing the solution pH to approximately 8 and adding NaSCN as a displacement agent. A diafiltration process was used to reduce the ligand concentration by 1000-fold, with even lower ligand concentrations attainable by increasing the number of diavolumes.

These results clearly demonstrate to the feasibility of using small charged affinity ligands to dramatically enhance the potential applicability of high performance tangential

flow filtration systems for protein purification. This technology effectively exploits the biospecificity of ligand binding to selectively alter the electrical charge of the desired protein product (or impurity), with this charge difference used to achieve high resolution separations through electrically-charged ultrafiltration membranes. In contrast to prior work on affinity ultrafiltration, all of which employed very large affinity ligands to achieve size-based separations, the small affinity ligands used in this work are much less expensive and have minimal mass transfer limitations, significantly improving the overall practicality of the separation.

8.2 Recommendations

The results presented in this thesis provide important insights into the use of small charged affinity ligands to separate proteins with very similar surface size and charge characteristics. However, there are numerous important areas which require additional experimental and theoretical investigation.

All of the data presented in this thesis were obtained using Cibacron Blue as the charged affinity ligand. There are several advantages to using Cibacron Blue as the affinity ligand: it is well known to bind selectively to certain classes of proteins, it has three negative charges per dye molecule leading to large shifts in protein charge, and multiple dye molecules can bind to a single protein (BSA was shown to bind as many as 11 molecules of Cibacron Blue). Future studies are clearly needed to demonstrate that this approach also works with other affinity ligands. Initial studies in this direction might target the behavior of other dye ligands such as Evans Blue, which has 4 negative

charges, and Porcion Red, which has 6 negative charges per dye molecules. Both of these dyes have strong affinities to certain proteins (Clonis, 1987), and the large charge per dye molecule should enable high resolution separations to be achieved using electrically-charged membranes.

It would also be very interesting to examine the use of small peptides, nucleotides, and enzymatic co-factors or substrate-mimics as small affinity ligands. These ligands would potentially have much higher selectivity than dye-based ligands, although they will typically have only a single binding site on the protein of interest. High resolution separations under these conditions might be feasible only if the ligand has a particularly high surface charge density, providing the necessary shift in protein charge even upon binding only a single ligand molecule. This might well require the design of custom ligands for this type of affinity ultrafiltration process. For example, one could start with a known substrate that has high binding affinity (but low charge) and then chemically modify that ligand to increase its charge, e.g., by adding sulphonic acid groups to the "back" end of the ligand.

An alternative approach to ligand design would be to use combinatorial chemistry and high throughput screening methods to synthesize specially designed binding ligands. This would require screening for binding strength, binding selectivity, and electrical charge, although several of these could be pre-selected for by the choice of the starting materials and the type of chemistry. Model calculations could be used to identify the combination of binding characteristics that would be most suitable for affinity ultrafiltration processes.

Another experimental system that would be very interesting to study is the use of divalent metal cations as affinity ligands to purify histidine-tagged proteins. His-tags are very commonly used to simplify protein purification, with the desired protein product captured on an immobilized metal affinity column by exploiting the strong binding interactions between the amino acid histidine and divalent metal cations like nickel and cobalt. The his-tag is generated by altering the DNA sequence of the target protein so that multiple histidine groups (typically 6) are added to either the amino or carboxy terminus of the protein. It should also be possible to exploit these same binding interactions in free solution using an affinity ultrafiltration process, in this case employing a positively-charged membrane to achieve high retention of the positively-charged complex formed between the his-tagged protein and the divalent metals. There are several attractive features to this approach. First, each histidine can associate with the divalent metals, leading to a large change in the net protein charge. Second, this approach may be highly generic, with the same basic strategy used for all his-tagged proteins. Third, the use of affinity ultrafiltration eliminates issues of non-specific adsorption, diffusional mass transfer limitations, and sterically hindered binding that can occur when the divalent ions are immobilized on a solid support.

Although the high resolution separations achieved in this thesis exploited relatively large differences in electrical charge, obtained by binding of multiple molecules of Cibacron Blue to BSA, previous work by Ebersold and Zydney (2000) showed that it was possible to use membrane systems to separate protein variants that differ at only a single amino acid residue through the substitution of a carboxylic acid for a lysine amino group. These results indicate that it should be possible to use affinity

ultrafiltration for selective separations even if the ligand binding causes only a small shift in the net protein charge. This type of separation would likely require more extensive optimization of the membrane surface charge density and solution conditions to enhance the difference in electrical interactions between the proteins and membrane. Theoretical simulations, using the model framework developed in this thesis, could be performed to aid in this multivariable optimization and to identify appropriate conditions for subsequent experimental studies.

All of the separation experiments performed in this thesis used simple binary mixtures of BSA and ovalbumin (with added Cibacron Blue). Future work should be done to extend these studies to examine the behavior of multi-component mixtures, including the type of complex multi-component systems characteristic of harvested cell culture fluids. These studies might well employ his-tagged proteins that selectively bind divalent metals, with the shift in electrical charge of the protein-metal complex exploited using positively-charged ultrafiltration membranes. Another interesting system would be the purification of monoclonal antibodies produced by Chinese Hamster Ovary cells. Monoclonal antibodies tend to be one of the largest and most basic species present in the harvested cell culture fluid, factors that have already been exploited in applications of high performance tangential flow filtration. The use of a properly designed positively charged affinity ligand could further increase the net positive charge on the antibody, leading to significant improvements in the performance of the membrane separation.

Based on the results from these experimental studies, it would also be important to examine the overall economics of the affinity ultrafiltration process in much greater detail. The use of small charged ligands provides a very attractive platform for this type

of separation. For example, the cost of Cibacron Blue is only $ 0.75/g, thus the total cost of ligand needed to purify 1 kg of BSA is only about $100. However, custom affinity ligands will clearly be significantly more expensive, with the overall economics determined by both the performance of the membrane system and the effectiveness of the ligand recovery and recycle. The application of affinity ultrafiltration for the purification of his-tagged proteins could be compared directly with the use of immobilized metal affinity chromatography (IMAC) to determine which of these processes had the best yield, purification factor, and economic characteristics. The economics of the affinity ultrafiltration process would also need to be compared with other separation technologies employed in downstream processing, including both affinity and ion exchange chromatography, to determine the most attractive separation process for a given set of purification requirements and economic constraints.

Bibliography

Adamski-Medda, D., Q. T. Nguyen and E. Dellacherie 1981. "Biospecific ultrafiltration: A promising purification technique for proteins?" *Journal of Membrane Science* 9(3): 337.

Afeyan, N. B., S. P. Fulton, N. F. Gordon, I. Mazsaroff, L. Varady and F. E. Regnier 1990. "Perfusion chromatography-An approach to purifying biomolecules." *Bio-Technology* 8: 203.

Anderson, J. L., Quinn,J.A. 1974. "Restricted transport in small pores. A model for steric exclusion and hindered particle motion." *Biophysical Journal* 14(2): 130.

Antoni, G., M. C. Casagli, M. Bigio, G. Borri and P. Neri 1982. "Different interactions of human and bovine serum albumin with Cibacron Blue and Blue Dextran." *Ital J Biochem* 31(2): 100.

Baker, R. W. and H. Strathmann 1970. "Ultrafiltration of macromolecular solutions with high-flux membranes." *Journal of Applied Polymer Science* 14(5): 1197.

Biellmann, J. F., J. P. Samama, C. I. Branden and H. Eklund 1979. "X-ray studies of the binding of Cibacron blue F3GA to liver alcohol dehydrogenase." *Eur J Biochem* 102(1): 107.

Birkenmeier, G. and G. Kopperschlager 1982. "Application of dye-ligant chromatography to the isolation of alpha-1-proteinase inhibitor and alpha-1-acid glycoprotein." *J Chromatogr* 235(1): 237.

Birkenmeier, G., E. Usbeck, L. Saro and G. Kopperschlager 1983. "Triazine dye binding of human alpha-fetoprotein and albumin." *J Chromatogr* 265(1): 27.

Blanch, H. W. and D. S. Clark (1997). *Biochemical Engineering*. New York, Marckel Dekker.

Blume, K. G., R. W. Hoffbauer, D. Busch, H. Arnold and G. W. Lohr 1971. "Purification and properties of pyruvate kinase in normal and in pyruvate kinase deficient human red blood cells." *Biochim Biophys Acta* 227(2): 364.

Branovic, K., A. Buchacher, M. Barut, A. Strancar and D. Josic 2003. "Application of semi-industrial monolithic columns for downstream processing of clotting factor IX." *Journal of Chromatography B Preparative Chromatography of Proteins* 790(1-2): 175.

Brenner, H. and L. J. Gaydos 1977. "The constrained brownian movement of spherical particles in cylindrical pores of comparable radius : Models of the diffusive and convective transport of solute molecules in membranes and porous media." *Journal of Colloid and Interface Science* 58(2): 312.

Bungay, P. M. and H. Brenner 1973. "The motion of a closely-fitting sphere in a fluid-filled tube." *International Journal of Multiphase Flow* 1(1): 25.

Burns, D. B. (2000). Electrostatic interactions in protein transport using ultrafiltration membranes: Effects of solution conditions and membrane charge. Ph.D. University of Delaware, Newark, DE.

Burns, D. B. and A. L. Zydney 1999. "Effect of solution pH on protein transport through ultrafiltration membranes." *Biotechnology and Bioengineering* 64(1): 27.

Burns, D. B. and A. L. Zydney 2000. "Buffer effects on the zeta potential of ultrafiltration membranes." *Journal of Membrane Science* 172(1-2): 39.

Burns, D. B. and A. L. Zydney 2001. "Contributions to electrostatic interactions on protein transport in membrane systems." *Aiche Journal* 47(5): 1101.

Butler, M. 2005. "Animal cell cultures: recent achievements and perspectives in the production of biopharmaceuticals." *Applied Microbiology and Biotechnology* V68(3): 283.

Butterfield, D. A., D. Bhattacharyya, S. Daunert and L. Bachas 2001. "Catalytic biofunctional membranes containing site-specifically immobilized enzyme arrays: a review." *Journal of Membrane Science* 181(1): 29.

Causserand, C., M. Meireles and P. Aimar 1996. "Protein transport through charged porous membranes." *Trans. IChem E.* 74A: 113.

Causserand, C., M. Nystrom and P. Aimar 1994. "Study of streaming potentials of clean and fouled ultrafiltration membranes." *Journal of Membrane Science* 88(2-3): 211.

Chapman Wilbert, M., S. Delagah and J. Pellegrino 1999. "Variance of streaming potential measurements." *Journal of Membrane Science* 161(1-2): 247.

Cheang, B. and A. L. Zydney 2003. "Separation of alpha-lactalbumin and beta-lactoglobulin using membrane ultrafiltration." *Biotechnology and Bioengineering* 83(2): 201.

Christy, C., G. Adams and T. Allegrezza 2004. "Milliipore Corporation, Next generation ultrafiltration membranes."

Clonis, Y. D. (1990). Process affinity chromatography. Separation Processes in Biotechnology. Asenjo, J. A. New York, Marcel Dekker.

Compagnini, A., S. Fisichella, S. Foti, G. Maccarrone and R. Saletti 1996. "Isolation by gel-permeation chromatography of a non-covalent complex of Cibacron Blue F3G-A with human serum albumin." *J Chromatogr A* 736(1-2): 115.

Deen, W. M. 1987. "Hindered transport of large molecules in liquid-filled pores." *AIChE Journal* 33(9): 1409.

Denizli, A., B. Salih, A. Kozluca and E. Piskin 1997. "Comparison of albumin binding capacities of three different reactive dye-derivatized poly(ethylene glycol dimethacrylate-hydroxyethyl methacrylate) microbeads." *J Biomater Sci Polym Ed* 8(6): 411.

Dermot M. Malone, J. L. A. 1977. "Diffusional boundary-layer resistance for membranes with low porosity." *AIChE Journal* 23(2): 177.

Dietz, P., P. K. Hansma, O. Inacker, H.-D. Lehmann and K.-H. Herrmann 1992. "Surface pore structures of micro- and ultrafiltration membranes imaged with the atomic force microscope." *Journal of Membrane Science* 65(1-2): 101.

Dockal, M., D. C. Carter and F. Ruker 1999. "The three recombinant domains of human serum albumin. Structural characterization and ligand binding properties." *J Biol Chem* 274(41): 29303.

Doherty, P. and G. B. Benedek 1974. "The effect of electric charge on the diffusion of macromolecules." *The Journal of Chemical Physics* 61(12): 5426.

Dordick, J. S. 1991. "Affinity-based separations and purifications. Patents and literature." *Appl Biochem Biotechnol* 27(1): 93.

Douglas, N. G., A. A. Humffray, H. R. C. Pratt and G. W. Stevens 1995. "Electrophoretic mobilities of proteins and protein mixtures." *Chem. Eng.Sci* 50: 743.

Easterday, R. L. and I. M. Esterday (1974). *Immobilised Biochemicals and Affinity Chromatography*. New York, Plenum.

Ebersold, M. F. and A. L. Zydney 2004. "Separation of protein charge variants by ultrafiltration." *Biotechnol Prog* 20(2): 543.

Ebersold, M. F. and A. L. Zydney 2004. "Use of protein charge ladders to study electrostatic interactions during protein ultrafiltration." *Biotechnology and Bioengineering* 85(2): 166.

Fuglistaller, P. 1989. "Comparison of immunoglobulin binding capacities and ligand leakage using eight different protein A affinity chromatography matrices." *J Immunol Methods* 124(2): 171.

Galaev, I. Y. and B. Mattiasson (2001). Protein Purification by Affinity Ultrafiltration. Membrane Separations in Biotechnology. Wang, W. K. New York, Marcel Dekker Inc.**:** 243.

Garg, N., I. Galaev and B. Mattiasson 1996. "Dye-affinity techniques for bioprocessing: recent developments." *J Mol Recognit* 9(4): 259.

Ghosh, R. 2002. "Protein separation using membrane chromatography: opportunities and challenges." *Journal of Chromatography A* 952(1-2): 13.

Gianazza, E. and P. Arnaud 1982. "Chromatography of plasma proteins on immobilized Cibacron Blue F3-GA. Mechanism of the molecular interaction." *Biochem J* 203(3): 637.

Gianazza, E. and P. Arnaud 1982. "A general method for fractionation of plasma proteins. Dye-ligand affinity chromatography on immobilized Cibacron blue F3-GA." *Biochem J* 201(1): 129.

Goldstein, A. 1949. "The Interaction of Drugs in Plasma Proteins." *Pharmacological Reviews* 1: 102.

Haber 1992. "Engineered antibodies as pharmacological tools." *Immunological reviews* 130: 189.

Haeckel, R., B. Hess, W. Lauterborn and K. H. Wuster 1968. "Purification and allosteric properties of yeast pyruvate kinase." *Hoppe Seylers Z Physiol Chem* 349(5): 699.

Hage, D. S. 1998. "Survey of recent advances in analytical applications of immunoaffinity chromatography." *J Chromatogr B Biomed Sci Appl* 715(1): 3.

Hage, D. S. 1999. "Affinity Chromatography: A review of Clinical Applications." *Clinical Chemistry* 45(5): 593.

Hanggi, D. and P. Carr 1985. "Analytical evaluation of the purity of commercial preparations of Cibacron Blue F3GA and related dyes." *Anal Biochem* 149(1): 91.

He, L.-Z., X.-Y. Dong and Y. Sun 1998. "Modeling and Analysis of the Affinity Filtration Process, Including Broth Feeding, Washing, and Elution Steps." *Biotechnol. Prog.* 14(4): 594.

Herrak, D. C. and E. W. Merrill 1989. "Affinity Cross-Flow Filtration:Experimental and Modelling Work Using the System of HSA and Cibacron Blue Agarose." *Biotechnol. Prog.* 5: 9.

Higuchi, A., M. Hara, T. Horiuchi and T. Nakagawa 1994. "Optical resolution of amino acids by ultrafiltration membranes containing serum albumin." *Journal of Membrane Science* 93(2): 157.

Higuchi, A., T. Hashimoto, M. Yonehara, N. Kubota, K. Watanabe, S. Uemiya, T. Kojima and M. Hara 1997. "Effect of surfactant agents and lipids on optical resolution of amino acid by ultrafiltration membranes containing bovine serum albumin." *Journal of Membrane Science* 130(1-2): 31.

Higuchi, A., Y. Ishida and T. Nakagawa 1993. "Surface modified polysulfone membranes: Separation of mixed proteins and optical resolution of tryptophan." *Desalination* 90(1-3): 127.

Hunter, R. J. (1981). *Zeta Potential in Colloid Science. Academic Press: London, 1981; pp 188-190.* London, Academic Press.

Itoh, Y., Y. Saura, Y. Tsuda and H. Yamada 1997. "Stereoselectivity and Enantiomer-Enantiomer Interactions in the Binding of Ibuprofen to Human Serum Albumin." *Chirality* 9: 643.

Ivarie, R. 2006. "Competitive bioreactor hens on the horizon." *Trends in Biotechnology* 24(3): 99.

Jankowski, W. J., W. von Muenchhausen, E. Sulkowski and W. A. Carter 1976. "Binding of human interferons to immobolized Cibacron Blue F3GA: The nature of molecular interaction." *Biochemistry* 15(23): 5182.

Jayme, D. W. and S. R. Smith 2000. "Media formulation options and manufacturing process controls to safeguard against introduction of animal origin contaminants in animal cell culture." *Cytotechnology* V33(1): 27.

Johansson, G. and M. Joelsson 1991. "Protein-ligand intercations studied on bovine serum albumin with free and polymer-bound Cibacron Blue F3GA with reference to affinity partitioning." *Journal of Chromatography* 537: 219.

Kanani, D. A., R. Ghosh and C. D. M. Filipe 2004. "A novel approach for high-resolution protein-protein separation by ultrafiltration using a dual-facilitating agent." *Journal of Membrane Science* 243(1-2): 223.

Kim, K. J., A. G. Fane, C. J. D. Fell, T. Suzuki and M. R. Dickson 1990. "Quantitative microscopic study of surface characteristics of ultrafiltration membranes." *Journal of Membrane Science* 54(1-2): 89.

Kirchberger, J. and G. Kopperschlager 1982. "Preparation of homogeneous alkaline phosphatase from calf intestine by dye-ligand chromatography." *Prep Biochem* 12(1): 29.

Klein, E. (1991). *Affinity Membranes: Their chemistry and performance in adsorptive separation processes*. New York, Wiley.

Knudsen, H. L., R. L. Fahrner, Y. Xu, L. A. Norling and G. S. Blank 2001. "Membrane ion-exchange chromatography for process-scale antibody purification." *Journal of Chromatography A* 907(1-2): 145.

Kopperschlager, G., W. Diezel, R. Freyer, S. Liebe and E. Hofmann 1971. "[Reciprocity of yeast-phosphofructokinase with dextran blue 2000]." *Eur J Biochem* 22(1): 40.

Kopperschlager, G., R. Freyer, W. Diezel and E. Hofmann 1968. "Some kinetic and molecular properties of yeast phosphofructokinase." *FEBS Lett* 1(3): 137.

Kopperschlager, G. and G. Johansson 1982. "Affinity partitioning with polymer-bound Cibacron blue F3G-A for rapid, large-scale purification of phosphofructokinase from Baker's yeast." *Anal Biochem* 124(1): 117.

Labrou, N. and Y. D. Clonis 1994. "The affinity technology in downstream processing." *J Biotechnol* 36(2): 95.

Ladisch, M. R. (2001). *Bioseparations Engineering: Principles,Practice and Economics*. New York, Wiley Interscience.

Lagercrantz, C. and T. Larsson 1983. "Comparative studies of the binding of some ligands to human serum albumin non-covalently attached to immobilized Cibacron Blue, or covalently immobilized on Sepharose, by column affinity chromatography." *Biochem J* 213(2): 387.

Lascu, I., H. Porumb, T. Porumb, I. Abrudan, C. Tarmure, I. Petrescu, E. Presecan, I. Proinov and M. Telia 1984. "Ion-exchange properties of Cibacron Blue 3G-A Sepharose (Blue Sepharose) and the interaction of proteins with Cibacron Blue 3G-A." *J Chromatogr* 283: 199.

Lawrence, S. 2005. "Biotech drug market steadily expands." 23(12): 1466.

Leatherbarrow, R. J. and P. D. Dean 1980. "Studies on the mechanism of binding of serum albumins to immobilized cibacron blue F3G A." *Biochem J* 189(1): 27.

Leinweber, F. C. and U. Tallarek 2003. "Chromatographic performance of monolithic and particulate stationary phases: Hydrodynamics and adsorption capacity." *Journal of Chromatography AInternational Symposium on Preparative and Industrial Chromatography and Allied Techniques* 1006(1-2): 207.

Ling, T. G. and B. Mattiasson 1982. "Comparison between binding analyses performed by equilibrium dialysis and partitioning in aqueous two-phase systems exemplified by the binding of Cibacron Blue to serum albumin." *J Chromatogr* 252: 159.

Lowe, C. R. (1987). Introduction to the use of reactive dyes in biotechnology. Reactive Dyes in Protein and Enzyme Technology. Y.D.Clonis, A. A., C.J.Burton and C.R.Lowe. London, Stockton Press.

Lu, J., Y. Wan and Z. Cui 2005. "Fractionation of lysozyme and chicken egg albumin using ultrafiltration with 30-kDa commercial membranes." *Ind. Eng. Chem. Res* 44(20): 7610.

Luong, J. H. T., K. B. Male and A. L. Nguyen 1988. "A continuous affinity ultrafiltration process for trypsin purification." *Biotechnology and Bioengineering* 31(6): 516.

Male, K. B., A. L. Nguyen and J. H. T. Luong 1990. "Isolation of Urokinase by Affinity Ultrafiltration." *Biotechnology and Bioengineering* 35: 87.

Marc W. T. Werten, T. J. v. d. B., Richèle D. Wind, Hans Mooibroek, Frits A. de Wolf, 1999. "High-yield secretion of recombinant gelatins by <I>Pichia pastoris</I>." *Yeast* 15(11): 1087.

Martin del Valle, E., M. A. Galan Serrano and R. L. Cerro 2003. "Use of Ceramic Monoliths as StationaryPhase in Affinity Chromatography." *Biotechnol. Prog.* 19(3): 921.

Mattiasson, B. and M. Ramstrop 1984. "Ultrafiltration affinity purification :Isolation of concanavalin a from seeds of Canavalia Ensiformis." *Journal of Chromatography A* 283: 323.

Mavrovouniotis, G. M. and H. Brenner 1988. "Hindered sedimentation, diffusion, and dispersion coefficients for brownian spheres in circular cylindrical pores." *Journal of Colloid and Interface Science* 124(1): 269.

Mehta, A. and A. L. Zydney 2006. "Effect of membrane charge on flow and protein transport during ultrafiltration." *Biotechnol Prog* 22(2): 484.

Menon, M. K. (1999). Effects of protein charge and electrostatic interactions in ultrafiltration and size exclusion chromatrography. Ph.D. University of Delaware, Newark,DE.

Menon, M. K. and A. L. Zydney 1998. "Measurement of protein charge and ion binding using capillary electrophoresis." *Anal Chem* 70(8): 1581.

Menon, M. K. and A. L. Zydney 1999. "Effect of ion binding on protein transport through ultrafiltration membranes." *Biotechnology and Bioengineering* 63(3): 298.

Menon, M. K. and A. L. Zydney 2000. "Determination of effective protein charge by capillary electrophoresis: effects of charge regulation in the analysis of charge ladders." *Anal Chem* 72(22): 5714.

Metcalf, E. C., B. Crow and P. D. Dean 1981. "The effect of ligand presaturation on the interaction of serum albumins with an immobilized Cibacron Blue 3G-A studied by affinity gel electrophoresis." *Biochem J* 199(3): 465.

Mislovicova, D., M. Chudinova, P. Gemeiner and P. Docolomansky 1995. "Affinity chromatography of invertase on concanavalin A-bead cellulose matrix: the case of an extraordinary strong binding glycoenzyme." *J Chromatogr B Biomed Appl* 664(1): 145.

Mochizuki, S. and A. L. Zydney 1992. "Dextran transport through asymmetric ultrafiltration membranes: Comparison with hydrodynamic models." *Journal of Membrane Science* 68(1-2): 21.

Mochizuki, S. and A. L. Zydney 1993. "Theoretical analysis of pore size distribution effects on membrane transport." *Journal of Membrane Science* 82(3): 211.

Mohan, S. B. and A. Lyddiatt (1997). Recent developments in affinity separation technologies. Affinity Separations: A practical Approach. Matejtschuk, J. Oxford, Oxford University Press.

Naumann, M., R. Reuter, P. Metz and G. Kopperschlager 1989. "Affinity chromatography of bovine heart lactate dehydrogenase using dye ligands linked directly or spacer-mediated to bead cellulose." *J Chromatogr* 466: 319.

Naval, J., M. Calvo, F. Lampreave and A. Pineiro 1982. "Interactions of different albumins and animal sera with insolubilized Cibacron Blue, Evaluation of apparent affinity constants." *Comp Biochem Physiol B* 71(3): 403.

Newman, J. S. (1973). Electrokinetic Phenomena. Electrochemical Systems. Englewood Cliffs, Prentice-Hall**:** 190.

Newman, J. S. (1991). *Electrochemical Systems*. Englewood Cliffs, Prentice-Hall.

Nystrom, M., M. Lindstrom and E. Matthiasson 1989. "Streaming potential as a tool in the characterization of ultrafiltration membranes." *Colloids and Surfaces* 36(3): 297.

Ohshima, H., T. W. Healy and L. R. White 1982. "Accurate analytic expressions for the surface charge density/surface potential relationship and double-layer potential distribution for a spherical colloidal particle." *Journal of Colloid and Interface Science* 90(1): 17.

Podgornik, A., M. Barut, I. Mihelic and A. Strancar 2003. "[Monolithic] tubes." *J Chromatogr Lib* 67: 77.

Poncet, S., J. Randon and J. Rocca 1997. "Enantiomeric Separation of Tryptophan by Ultrafiltration Using the BSA Solution System." *Separation Sci. Tech.* 32: 2029.

Porath, J. 1988. "High-performance immobilized-metal-ion affinity chromatography of peptides and proteins." *J Chromatogr* 443: 3.

Porath, J. 1992. "Immobilized metal ion affinity chromatography." *Protein Expr Purif* 3(4): 263.

Powers, J. D., P. K. Kilpartik and R. G. Carbonell 1990. "Trypsin Purification by Affinity Binding to Small Unilammelar Liposomes." *Biotechnogy and Bioengineering* 36: 506.

Przybycien, T. M., N. S. Pujar and L. M. Steele 2004. "Alternative bioseparation operations: life beyond packed-bed chromatography." *Current Opinion in Biotechnology* 15(5): 469.

Pujar, N. S. (1996). Electrostatic and electrokinetic interactions during protein filtration using semi-permeable membranes. Ph.D. University of Delaware, Newark, DE.

Pujar, N. S. and A. L. Zydney 1994. "Electrostatic and electrokinetic interactions during protein transport through narrow pore membranes." *Industrial & Engineering Chemistry Research* 33(10): 2473.

Pujar, N. S. and A. L. Zydney 1996. "Boundary effects on the sedimentation and hindered diffusion of charged particles." *Aiche Journal* 42(8): 2101.

Pujar, N. S. and A. L. Zydney 1997. "Charge Regulation and Electrostatic Interactions for a Spherical Particle in a Cylindrical Pore." *Journal of Colloid and Interface Science* 192(2): 338.

Pujar, N. S. and A. L. Zydney 1998. "Electrostatic effects on protein partitioning in size-exclusion chromatography and membrane ultrafiltration." *J Chromatogr A* 796(2): 229.

Rao, S. and A. L. Zydney 2005. "Controlling protein transport in ultrafiltration using small charged ligands." *Biotechnology and Bioengineering* 91(6): 733.

Rao, S. and A. L. Zydney 2006. "High resolution protein separations using affinity ultrafiltration with small charged ligands." *Journal of Membrane Science* 280: 781.

Robertson, B. C. and A. L. Zydney 1990. "Hindered protein diffusion in asymmetric ultrafiltration membranes with highly constricted pores." *Journal of Membrane Science* 49(3): 287.

Romero, J. and A. L. Zydney 2001. "Chiral separations using ultrafiltration with a stereoselective binding agent." *Separation Science and Technology* 36(7): 1575.

Romero, J. and A. L. Zydney 2002. "Affinity ultrafiltration: effects of ligand binding on selectivity and process optimization." *Biotechnoogy andl Bioengineering* 77(3): 256.

Ruckenstein, E. and X. F. Zeng 1998. "Albumin separation with Cibacron Blue carrying macroporous chitosan and chitin affinity membranes." *Journal of Membrane Science* 142(1): 13.

Ryan, L. D. and C. S. Vestling 1974. "Rapid purification of lactate dehydrogenase from rat liver and hepatoma: a new approach." *Arch Biochem Biophys* 160(1): 279.

Saifer, A., F. Westley and J. Steigman 1964. "Binding of actetate ions to bovine serum albumin." *Biochemistry* 3(11): 1624.

Saksena, S. (1995). Protein transport in selective membrane filtration. Ph.D. University of Delaware, Newark, DE.

Saksena, S. and A. L. Zydney 1994. "Effect of solution pH and ionic strength on the separation of albumin from immunoglobulins (IgG) by selective filtration." *Biotechnology and Bioengineering* 43(10): 960.

Saksena, S. and A. L. Zydney 1995. "Pore size distribution effects on electrokinetic phenomena in semipermeable membranes." *Journal of Membrane Science* 105(3): 203.

Scatchard, G., J. S. Coleman and A. L. Shen 1957. "Physical chemistry of protein solutions, VII. The binding of small anions to serum albumin." *J Am Chem Soc* 79: 12.

Scopes, R. K. 1987. "Dye-ligands and multifunctional adsorbents: an empirical approach to affinity chromatography." *Anal Biochem* 165(2): 235.

Shao, J. H. and A. L. Zydney 2004. "Optimization of ultrafiltration/diafiltration processes for partially bound impurities." *Biotechnology and Bioengineering* 87(3): 286.

Shao, J. H. and A. L. Zydney 2004. "Retention of small charged impurities during ultrafiltration." *Biotechnology and Bioengineering* 87(1): 7.

Smith, I., Frank G. and W. M. Deen 1983. "Electrostatic effects on the partitioning of spherical colloids between dilute bulk solution and cylindrical pores." *Journal of Colloid and Interface Science* 91(2): 571.

Smith III, F. G. and W. M. Deen 1980. "Electrostatic double-layer interactions for spherical colloids in cylindrical pores." *Journal of Colloid and Interface Science* 78(2): 444.

Smith, K. A., C. K. Colton, E. W. Merrill and L. B. Evans 1968. "Convective transport in a batch dialyzer: Determination of the true membrane permeability from a single measurement." *AIChE Symp. Ser.* 64: 45.

Staal, G. E. 1970. "Some properties of pyruvate kinase of human erythrocytes." *Bull Soc Chim Biol (Paris)* 52(11): 1297.

Staal, G. E., P. W. Helleman, J. de Wael and C. Veeger 1969. "Purification and properties of an abnormal glutathione reductase from human erythrocytes." *Biochim Biophys Acta* 185(1): 63.

Staal, G. E., J. Visser and C. Veeger 1969. "Purification and properties of glutathione reductase of human erythrocytes." *Biochim Biophys Acta* 185(1): 39.

Subramanian, S. 1984. "Dye-ligand affinity chromatography: the interaction of Cibacron Blue F3GA with proteins and enzymes." *CRC Crit Rev Biochem* 16(2): 169.

Sun, Y., L. Gu, X. D. Tong, S. Bai, S. Ichikawa and S. Furusaki 1999. "Protein separation using affinity-based reversed micelles." *Biotechnol Prog* 15(3): 506.

Sun, Y., S. Ichikawa, S. Sugiura and S. Furusaki 1998. "Affinity extraction of proteins with a reversed micellar system composed of Cibacron Blue-modified lecithin." *Biotechnology and Bioengineering* 58(1): 58.

Swart, A. C. and H. C. Hemker 1970. "Separation of blood coagulation factors II, VII, IX and X by gel filtration in the presence of dextran blue." *Biochim Biophys Acta* 222(3): 692.

Taira, Z. and H. Terada 1985. "Specific and non-specific ligand binding to serum albumin." *Biochem Pharmacol* 34(11): 1999.

Tanford, C., S. A. Swanson and W. S. Shore 1955. "Hydrogen ion equilibria of bovine serum albumin." *J Am Chem Soc* 77: 6414.

van Eijndhoven, R. H. C. M., S. Saksena and A. L. Zydney 1995. "Protein fractionation using electrostatic interactions in membrane filtration." *Biotechnology and Bioengineering* 48(4): 406.

van Reis, R. (2001). Charged filtration membranes and uses therefor. USA.

van Reis, R., J. M. Brake, J. Charkoudian, D. B. Burns and A. L. Zydney 1999. "High-performance tangential flow filtration using charged membranes." *Journal of Membrane Science* 159(1-2): 133.

van Reis, R., S. Gadam, L. N. Frautschy, S. Orlando, E. M. Goodrich, S. Saksena, R. Kuriyel, C. M. Simpson, S. Pearl and a. Zydney et 1997. "High performance tangential flow filtration." *Biotechnology and Bioengineering* 56(1): 71.

van Reis, R., E. M. Goodrich, C. L. Yson and L. N. Frautschy 1997. "Linear scale ultrafiltration." *Biotechnology and Bioengineering* 55: 737.

van Reis, R. and S. Saksena 1997. "Optimization diagram for membrane separations." *Journal of Membrane Science* 129(1): 19.

van Reis, R. and A. Zydney 2001. "Membrane separations in biotechnology." *Curr Opin Biotechnol* 12(2): 208.

Verwey, E. J. W. and J. T. G. Overbeek (1948). *Theory of stability of lyophobic colloids*. Amsterdam, Elsevier.

Vilker, V. L., C. K. Colton and K. A. Smith 1981. "The osmotic pressure of concentrated protein solutions: Effect of concentration and ph in saline solutions of bovine serum albumin." *Journal of Colloid and Interface Science* 79(2): 548.

W. Senyo Opong, A. L. Z. 1991. "Diffusive and convective protein transport through asymmetric membranes." *AIChE Journal* 37(10): 1497.

Walsh, G., Gary 2006. "Biopharmaceutical benchmarks 2006." *Nature biotechnology* 24(7): 769.

Walsh, G. and D. Headon (1994). *Protein Biotechnology*. West Sussex, England, John Wiley & Sons.

Wan, Y., S. Vasan, R. Ghosh and G. Hale 2005. "Separation of monoclonal antibody alemtuzumab monomer and dimers using ultrafiltration." *Biotechnol Bioeng.* 90(4): 422.

Young, M. E., P. A. Carroad and R. L. Bell 1980. "Estimation of diffusion coefficients of proteins." *Biotechnology and Bioengineering* 22(5): 947.

Zeman, L. J. and A. L. Zydney (1996). *Microfiltration and Ultrafiltration: Principles and Applications*. New York, Marcel Dekker, Inc.

Zhang, S. and Y. Sun 2001. "Further studies on the contribution of electrostatic and hydrophobic interactions to protein adsorption on dye-ligand adsorbents." *Biotechnology and Bioengineering* 75(6): 710.

Zhang, X., T., H. Liu Hz and J. Chen Jy 2000. "Effect of Cibacron Blue and Bovine Serum Albumin on Electrical Conductivity of Reversed Micelles." *J Colloid Interface Sci* 226(1): 71.

Zhu, L., M.-C. van de Lavoir, J. Albanese, D. O. Beenhouwer, P. M. Cardarelli, S. Cuison, D. F. Deng, S. Deshpande, J. H. Diamond, L. Green, E. L. Halk, B. S. Heyer, R. M. Kay, A. Kerchner, P. A. Leighton, C. M. Mather, S. L. Morrison, Z. L. Nikolov, D. B. Passmore, A. Pradas-Monne, B. T. Preston, V. S. Rangan, M. Shi, M. Srinivasan, S. G. White, P. Winters-Digiacinto, S. Wong, W. Zhou and R. J. Etches 2005. "Production of human monoclonal antibody in eggs of chimeric chickens." *Nat Biotech* 23(9): 1159.

Zydney, A. L., P. Aimar, M. Meireles, J. M. Pimbley and G. Belfort 1994. "Use of the log-normal probability density function to analyze membrane pore size distributions: functional forms and discrepancies." *Journal of Membrane Science* 91(3): 293.

Zydney, A. L. and N. S. Pujar 1998. "Protein transport through porous membranes: effects of colloidal interactions." *Colloids and Surfaces a-Physicochemical and Engineering Aspects* 138(2-3): 133.

Appendix A

COMPUTER PROGRAMS

A.1 Introduction

This section lists some of the computer programs used to perform model calculations described in this thesis.

A.2 Evaluation of Protein Charge using the Competitive Binding Model

This mathematica notebook was written to determine the BSA charge taking into account competitive binding of Cibacron Blue with both BSA and ovalbumin. The net protein charge was calculated from data for the intrinsic disassociation constants of all ionizable groups of the protein and taking into account Cibacron Blue binding. Experimentally determined values for the equilibrium binding parameters n and K_{eq} were used in this analysis. Similar analysis was performed for ovalbumin.

```
CibTotal = (10 / 67000) * 75(*in Moles*)
keq = 105000 ; (*in Mole inverse*)
n = 10.92;
w = 2.8;
k2 = 1700;

BSA = 10 / 67000; (*in Moles*)
OVA = 6 / 44000;
poly = CibTotal - (x + (u*k1*BSA*x)/(1 + k1*x) + (w*k2*OVA*x)/(1 + k2*x));
NSolve[poly == 0, x]
FreeCiB = 0.00920697458433606`
(*FreeCiB=( -(1+n*keq*ProteinConc-CibTotal*keq) +
      √((1+n*keq*ProteinConc-CibTotal*keq)^2 +
         4*keq*CibTotal))/(2*keq);(*in Moles*)*)
BoundCib = (u*k1*BSA*FreeCiB)/(1 + k1*FreeCiB) ; (*in Moles*)
e = 1.6*10^-19;
k = 1.38*10^-13;
T = 298;
pH = 5;
R = 8.314*10^10;
F = 96500;
ϵ0 = 8.314*10^-32;
ϵr = 80;
```

$$C_1 = 10 * 10^{-30};$$

$$C_2 = 10 * 10^{-30};$$

$$C_3 = \text{FreeCiB} * 10^{-27};$$

$$z_1 = 1;$$

$$z_2 = -1;$$

$$z_3 = -3;$$

$$\kappa = \left(\frac{F^2 * (\sum_{i=1}^{3} z_i^{\,2} * C_i)}{e_0 * e_r * R * T} \right)^{0.5};$$

$$\text{Ion} = 0.5 * 10^{27} * \sum_{i=1}^{3} z_i^{\,2} * C_i$$

(*Ionic Strength in Molar strength*);

$$r_s = 34.8;$$

$$n_1 = 1;$$

$$n_2 = 99;$$

$$n_3 = 16;$$

$$n_4 = 1;$$

$$n_5 = 57;$$

$$n_6 = 19;$$

$$n_7 = 22;$$

$$n_8 = 3 * \text{BoundCib} / \text{BSA};$$

$$pk_1 = 3.75;$$

$$pk_2 = 4.02;$$

$$pk_3 = 6.9;$$

$$pk_4 = 7.75;$$

$$pk_5 = 9.8;$$

$$pk_6 = 10.35;$$

$$pk_7 = 12;$$

$$pk_8 = 1;$$

$$m_1 = 1;$$

$$m_2 = 6;$$
$$m_3 = 14;$$
$$K_1 = 530;$$
$$K_2 = 50;$$
$$K_3 = 2;$$

$$g = 10^{-\frac{0.5\sqrt[2]{c_i/2}}{1+2\sqrt[2]{c_i/2}}};$$

$$Y = \sum_{i=1}^{8} \frac{n_i}{1 + 10^{pk_i - pH - 0.43 * \frac{e*\psi}{k*T}}};$$

$$AC = \sum_{j=1}^{3} \frac{m_j * K_j * 10 * 10\text{^}-3 * g * \text{Exp}[\frac{e*\psi}{k*T}]}{1 + K_j * 10 * 10\text{^}-3 * g * \text{Exp}[\frac{e*\psi}{k*T}]};$$

$$\text{ans} = \text{FindRoot}\left[\psi == \frac{e * (96 - Y - AC)}{4 * \pi * \epsilon_0 * \epsilon_r * r_s * (1 + \kappa * r_s)}, \{\psi, 10000000\}\right];$$

$$\text{Charge} = \frac{4 * 3.14 * \epsilon_0 * \epsilon_r * r_s * (1 + \kappa * r_s) * \psi}{e} /. \text{ans};$$

```
Print["charge=", Charge]
Print["pH=", pH]
Print["Is=", Ion]
Print["Bound CiB=", n8 / 3]
```

A.3 Evaluation of Protein Sieving Coefficient

As discussed in Chapters 2 and 5, protein transport is a function of both steric and electrostatic interactions between the protein and the membranes pores. The program written in Mathematica calculates the sieving coefficient S_a of a charged sphere in a charged cylindrical pore using the Smith and Deen (1980) analysis. The electrostatic energy for a protein with radius r_s entering a pore with radius r was calculated. The actual sieving coefficient was then evaluated as the product of the partition coefficient and the convective hindrance factor. The effect of the presence of Cibacron Blue on both protein charge and free solution ionic strength were taken into account. These calculations also took into account the presence of a log-normal pore size distribution for membranes.

```
phi = 0;
Do[
  CibTotal = (8 / 69000) * w; (*in Moles*)
  keq = 4.7 * 100000; (*in Mole inverse*)
  n = 9.8;
  ProteinConc = 8 / 69000; (*in Moles*)
  FreeCib = ( -(1 + n * keq * ProteinConc - CibTotal * keq) +
        √((1 + n * keq * ProteinConc - CibTotal * keq)^2 + 4 * keq * CibTotal)) / (2 * keq); (*in Moles*);
  BoundCib = CibTotal - FreeCib ; (*in Moles*)
  e = 1.6 * 10^-19;
  k = 1.38 * 10^-13;
  T = 298;
  pH = 5.0;
  R = 8.314 * 10^10;
  F = 96500;
  ϵ0 = 8.314 * 10^-32;
  ϵr = 80;
```

$$C_1 = 10 * 10^{-30};$$
$$C_2 = 10 * 10^{-30};$$
$$C_3 = \text{FreeCib} * 10^{-27};$$
$$z_1 = 1;$$
$$z_2 = -1;$$
$$z_3 = -3;$$

$$K = \left(\frac{F^2 * (\sum_{i=1}^{3} z_i^2 * C_i)}{\epsilon_0 * \epsilon_r * R * T} \right)^{0.5};$$

$$\text{Ion} = 0.5 * 10^{27} * \sum_{i=1}^{3} z_i^2 * C_i;$$

$$r_s = 34.8;$$
$$n_1 = 1;$$
$$n_2 = 99;$$
$$n_3 = 16;$$
$$n_4 = 1;$$
$$n_5 = 57;$$
$$n_6 = 19;$$
$$n_7 = 22;$$
$$n_8 = 3 * \text{BoundCib} / \text{ProteinConc};$$

$$pk_1 = 3.75;$$
$$pk_2 = 4.02;$$
$$pk_3 = 6.9;$$
$$pk_4 = 7.75;$$
$$pk_5 = 9.8;$$
$$pk_6 = 10.35;$$
$$pk_7 = 12;$$
$$pk_8 = 1;$$

$m_1 = 1;$
$m_2 = 6;$
$m_3 = 14;$
$K_1 = 530;$
$K_2 = 50;$
$K_3 = 2;$

$$g = 10^{-\frac{0.5\sqrt[3]{0.01/2}}{1+2\sqrt[3]{0.01/2}}};$$

$$AC = \sum_{j=1}^{3} \frac{m_j * K_j * .01 * g * \text{Exp}[\frac{e*\psi}{k*T}]}{1 + K_j * .01 * g * \text{Exp}[\frac{e*\psi}{k*T}]};$$

$$Y = \sum_{i=1}^{8} \frac{n_i}{1 + 10^{pk_i - pH - 0.43 * \frac{e*\psi}{k*T}}};$$

$$\text{ans} = \text{FindRoot}\left[\psi == \frac{e*(96 - Y - AC)}{4*\pi*\epsilon_0*\epsilon_r*r_s*(1 + K*r_s)}, \{\psi, 10000\}\right];$$

$$\text{Charge} = \frac{4*3.14*\epsilon_0*\epsilon_r*r_s*(1 + K*r_s)*\psi}{e} /. \text{ans};$$

```
Do[
  rs = 34.8;

  λ = rs / r;

  qp = -0.01 * 10^-20;
  qs = Charge * e / (4 * 3.14 * rs^2);
```

$$a_1 = -73/60;$$
$$a_2 = 77293/50400;$$
$$a_3 = -22.5083;$$
$$a_4 = -5.6117;$$
$$a_5 = -0.3363;$$
$$a_6 = -1.216;$$
$$a_7 = 1.647;$$
$$b_1 = 7/60;$$
$$b_2 = -2277/50400;$$
$$b_3 = 4.0180;$$
$$b_4 = -3.9788;$$
$$b_5 = -1.9215;$$
$$b_6 = 4.392;$$
$$b_7 = 5.006;$$

$$K_s = \frac{9}{4} * \pi^2 * (2)^{0.5} * (1-\lambda)^{-2.5} * \left(1 + \sum_{k=1}^{2} b_k (1-\lambda)^k \right) + \sum_{k=3}^{7} (b_k) * (\lambda)^{k-3};$$

$$K_t = \frac{9}{4} * \pi^2 * (2)^{0.5} * (1-\lambda)^{-2.5} * \left(1 + \sum_{k=1}^{2} a_k (1-\lambda)^k \right) + \sum_{k=3}^{7} (a_k) * (\lambda)^{k-3};$$

$$p[r\_] = \left(\frac{r^4}{r * (2*\pi)^{0.5}} (\text{Log}[1 + (z)^2])^{-0.5} * \text{Exp}\left[\frac{-\left(\text{Log}[\frac{r}{54}] + \frac{\text{Log}[1+(z)^2]}{2}\right)^2}{2 * \text{Log}[1 + (z)^2]} \right] \right); \text{(*Pore size distribution*)}$$

$$m[r\_] = \text{NIntegrate}\left[\left(\frac{\text{BesselK}[1, ((\kappa * r)^2 + x^2)^{0.5}]}{\text{BesselI}[1, ((\kappa * r)^2 + x^2)^{0.5}]} \right), \{x, 0, 1.25\} \right]; \text{(*Function M0*)}$$

$$h[r\_] = (1 + \kappa * r * \lambda) * e^{-\kappa * r * \lambda} - (1 - \kappa * r * \lambda) * e^{\kappa * r * \lambda}; \text{(*Function h*)}$$

$$\sigma_s = \frac{F * r * q_s}{\epsilon_0 * \epsilon_r * R * T};$$

$$\sigma_p = \frac{F * r * q_p}{\epsilon_0 * \epsilon_r * R * T};$$

$$A_s = \frac{4 * \pi * K * r * \lambda^4 * e^{(K*r*\lambda)} * m[r]}{(1 + K * r * \lambda)};$$

$$A_{sp} = \frac{4 * \pi^2 * \lambda^2}{\text{BesselI}[1, K * r]};$$

$$A_p = \frac{\pi^2 * h[r]}{(K * r)^2 * (\text{BesselI}[1, K * r])^2};$$

$$v[r\_] = (A_s * \sigma_s^2 + A_{sp} * \sigma_s * \sigma_p + A_p * \sigma_p^2) / (\pi * K * r\,(1 + K * r * \lambda) * e^{(-K*r*\lambda)} - m[r] * h[r]);\ (*\text{Vsigma}*)$$

$$c[r\_] = \frac{r * \epsilon_0 * \epsilon_r * R^2 * T^2 * v[r]}{F^2};$$

$$j[r\_] = \left(\frac{K_s * (1 - \lambda)^2 * \text{Exp}[\frac{-c[r]}{k*T}]}{2 * K_t}\right);\ (*\text{phiKc}*)$$

```
phi1 = j[r] * p[r];
phi = phi1 + phi, {r, 36.5, 250}];
```

DenR =

$$\text{NIntegrate}\Big[\frac{r^4}{r * (2 * \pi)^{0.5}}\ (\text{Log}[1 + (z)^2])^{-0.5} * \text{Exp}\Big[\frac{-\left(\text{Log}[\frac{r}{54}] + \frac{\text{Log}[1+(z)^2]}{2}\right)^2}{2 * \text{Log}[1 + (z)^2]}\Big], \{r, 1, 250\}\Big];$$

```
Sieve = phi / DenR;

Print[Sieve], {w, 0, 150, 0.5}]
```

VITA
Suma Rao

EDUCATION

Ph.D., Chemical Engineering May 2007, Advisor: Dr. Andrew L. Zydney
The Pennsylvania State University, University Park, Pennsylvania
Bachelor of Engineering, Chemical Engineering, September 2000
R.V. College of Engineering, Bangalore, India

EXPERIENCE

RESEARCH EXPERIENCE

Doctoral Research Jan. 2002 – May 2007
Advisor: Dr. Andrew Zydney, Pennsylvania State University
Thesis Title: Protein Separations by Affinity Ultrafiltration using Small Charged Ligands

Undergraduate Research Jan. 2000 – Sept. 2000
Advisor: Dr. Ganesan, R.V.C.E., Bangalore, India
Studied effluent treatment of metallic wastes using a membrane electrode process to selectively remove cations from an effluent stream.

WORK EXPERIENCE

Internship at Amgen Inc. Seattle, Washington May 2006 – Aug. 2006
Supervisor: Dr. Ganesh Vedantham

- Studied the fouling behavior of various monoclonal antibodies on virus filtration membranes
- Studied protein-protein interactions using self-interaction chromatography

TEACHING EXPERIENCE

Teaching Assistant, Pennsylvania State University

- Chemical Reaction Engineering Jan. 2005 – May 2005
- Chemical Engineering Thermodynamics Jan. 2004 – May 2004

PRESENTATIONS AND PUBLICATIONS

- Rao S. and Zydney A. L., High Performance Tangential Flow Filtration Using Affinity Ligands, North American Membrane Society (NAMS), Chicago, IL (2006)
- Rao S. and Zydney A. L., Protein Separations using HPTFF with affinity ligands (Submitted to Journal of Separation Science and Technology)
- Rao, S. and A. L. Zydney., "High resolution protein separations using affinity ultrafiltration with small charged ligands." Journal of Membrane Science 280: 781,2006
- Rao S. and Zydney A. L., Protein Separations by Ultrafiltration: Exploiting Small Charged Ligands, AIChE Annual Meeting, Cincinnati, OH (2005)
- Rao S. and Zydney A. L., Controlling Protein Transport in Ultrafiltration using Small Charged Ligands, Medical and Biological Applications, Camogli, Italy (2005)
- Rao S. and Zydney A. L., Controlling Protein Transport in Ultrafiltration Using Small Charged Ligands, Biotechnology and Bioengineering 91: 733-742, 2005
- Rao S. and Zydney A.L., Use of Small Affinity Ligands to Control Protein Transport during Ultrafiltration, North American Membrane Society (NAMS), Honolulu, Hawaii (2004)

AWARDS

- NAMS 2006 student poster award
- Elias Klein travel award 2006, conferred by NAMS
- Lee S. Gaumer Scholarship (2004) in Chemical Engineering
- NAMS Travel Award (2003)